Papers of Ship Research Institute, Supplement No.15 (September 1993)

COMPARATIVE CALCULATIONS OF PROPELLERS BY SURFACE PANEL METHOD —— WORKSHOP ORGANIZED BY 20th ITTC PROPULSOR COMMITTEE ——

by

Koichi KOYAMA *

ABSTRACT

Comparative calculations of marine propellers by surface panel method are presented. The plan was organized by 20th ITTC Propulsor committee. Calculation results from 15 organizations are included in the comparison. Results are shown for thrust, torque and pressure distribution on blades. The results of the comparative calculation show the state of the art of surface panel method for marine propellers. The numerical results are useful as the database for marine propellers.

CONTENTS

* Arctic Vessel and Low Temperature Engineering Division

1 INTRODUCTION

It goes without saying that analysis method for hydrodynamic characteristics of propellers is very important for the development of technology of marine propellers. Today lifting surface theory plays an important role in analysis or design of marine propellers. Recently the application of panel methods to the hydrodynamic analysis of marine propellers becomes active.

20th ITTC Propulsor Committee carried out comparative calculations of marine propeller performance by the surface panel method and a workshop for the discussion of the comparison as Task2 of the committee in order to make clear the accuracy of the panel method for the analysis of marine propellers and to review the applicability of the method. The author was in charge of the task. The intent of the task was to evaluate and promote the use of surface panel methods. This can be accomplished through the comparison of extensive numerical results by many panel methods. The purpose of the comparison is not as a competition but rather as a method to assess the various numerical issues that may be important.

Results of the comparative calculations and workshop are presented in 20th ITTC Report of the propulsor committee [1]. However only the summary of the workshop activities is shown in the report, although many useful data were collected in the project. Many valuable papers were also presented in the workshop. The author wanted to make the extensive valuable data and papers by the contributors open to the public. Almost all results of the comparative calculations are presented in this report. Some papers by the contributors in the workshop are inserted in the appendices of this report by permission of the contributors. They show the state of the art of the surface panel method for marine propellers

2 SURFACE PANEL METHOD

Surface panel method analyzes numerically the potential flow around the lifting body as exactly as possible. The geometry of the lifting body can be treated as accurately as wanted with a very fine panel arrangement on the surface of the lifting body.

We consider a propeller (with duct, stator etc. in case of need) operating in an unbounded flow field. It is assumed that the vortex wake emanating from the trailing edge of the blades is infinitesimally thin and that the flow field except vortex wake is incompressible, inviscid and irrotational. Then there exists a velocity potential in the flow field.

The velocity potential in the flow field is expressed using Green's identity formula and boundary values as

$$\phi = -\frac{1}{4\pi}\iint \frac{\partial \phi}{\partial n'}\frac{1}{r}dS + \frac{1}{4\pi}\iint \phi \frac{\partial}{\partial n'}\left(\frac{1}{r}\right)dS \qquad (1)$$

Equation (1) is the basic starting formula for panel methods [2]. The velocity is expressed as

$$V = \nabla\phi = -\frac{1}{4\pi}\iint \frac{\partial \phi}{\partial n'}\nabla\frac{1}{r}dS + \frac{1}{4\pi}\iint \phi \nabla\frac{\partial}{\partial n'}\left(\frac{1}{r}\right)dS \qquad (2)$$

The velocity field produced by the doublet distribution on panels is given by the second term of equation (2). This term can be integrated by parts to obtain

$$V_D = \nabla\phi_D = \frac{1}{4\pi}\iint \gamma \times \nabla\left(\frac{1}{r}\right)dS - \frac{1}{4\pi}\int \phi \nabla\left(\frac{1}{r}\right) \times tds \qquad (3)$$

The surface panel method employs one of the above equations(1) through (3). Singularities such as source, doublet (potential itself), or vorticity are distributed on the body surface which is a boundary of the flow field. The problem is solved using an integral equation with a boundary condition. The equation is discretised for numerical calculation. The variety of surface panel methods is due to the choice of the integral equations, singularities, and the method of discretisation. For instance potential based panel method employs Eq.(1). Surface vortex lattice method employs Eq.(3).

3 WORKSHOP

20th ITTC Propulsor Committee distributed a questionnaire outlining the plan of the comparative calculation and called for contributions to 98 organizations on June 24,1991. 16 organizations signified their

intention to perform the comparative calculation.

The committee furnished them with the calculation documents (Appendix A) on Feb.4,1992. 15 organizations sent the committee the results of their calculations. The workshop was held in Seoul, Korea on August 23, 1992.

In the workshop 19 participants attended, 10 participants presented the results of their calculations and the use of the surface panel method for marine propellers was discussed. Organizations of the participants are listed in Table 1. Papers contributed by the participants to the comparative calculation are listed in Tables 2(a),2(b). Some of them are printed in Appendices of this report (Appendix B, C, D, E, F).

Table 1 List of Organizations Contributing to Workshop on Surface Panel Method for Marine Propellers

Massachusetts Institute of Technology, USA
Analytical Methods,Inc., USA
Chungnam National University, Korea
Korean Research Institute of Ships and Ocean Engineering, Korea
Hyundai Heavy Industries, Korea
Samsung Heavy Industries, Korea
Mitsubishi Heavy Industries,Ltd. Nagasaki R&D Center, Japan
Nippon Kaiji Kyokai, Research Institute, Japan
Yokohama National University, Japan
Ship Research Institute, Japan
Cento per gli Studi di Tecnica Navale CETENA, Italy
Bassin d'Essais des Carenes, France
Maritime Research Institute Netherlands, The Netherlands
Delft University of Technology, The Netherlands
Versuchsanstalt fur Wasserbau & Schiffbau, Germany
Canal Experiencias Hidrodinamicas, Spain

Table 2(a) Distributed Materials for the workshop

1) K.Koyama: Comparative Calculation of Propellers by Surface Panel Method from All Participants
2) Cheng-I Yang: Prediction of Hydrodynamic Performance of DTMB Propellers 4119 and 4842 with a Panel Method
3) Ching-Yeh Hsin and Justin E.Kerwin: Steady Performance Analysis for Two Propellers using MIT-PSF-10
4) B.Maskew, J.S.Fraser, J.B.Murray and J.M.Summa: Calculations for the DTRC 4119 and DTRC 4842 Propellers Using VSAERO/MPROP and USAERO Panel Codes
5) J.-T.Lee,Y.-G.Kim,J.-C.Suh, and C.-S.Lee: Calculation of the Propeller Performance by a Surface Panel Method
6) T.Hoshino: Results of Comparative Calculation of Propellers by Surface Panel Method
7) S.Ryo: Calculation results of DTRC4119 and DTRC4842 by NK's computer code based on Boundary Element Method (Panel Method)
8) S.Ryo,Y.Sasaki and late M.Takahashi: Analysis of Three Dimensional Flow around Marine Propeller by Direct Formulation of Boundary Element Method,ISPC92,China
9) H.Yamasaki: Calculation by Surface Vortex Lattice Method
10) K.Koyama: Calculation of Propellers DTRC4119 and DTRC4842 by Surface Panel Method
11) G.Caprino, L.Sebastiani, M.Caponnetto, and M.De Benedetti: Propanel: A Surface Panel Method for the Steady Analysis of Naval Propellers
12) R.Baubeau: Comparative Calculation of Propellers by Surface Panel Method
13) P.Sander: Calculation of the pressure distribution on a propeller blade with a continue Method
14) H.Streckwall: Calculations for the 20th ITTC Propulsor Committee

Table 2(b) Supplementary Materials for the workshop

1) 20th ITTC Propulsor Committe, Comparative Calculation of Propellers by Surface Panel Method; Calculation Document, February 4,1992
2) J.-C.Suh: Analytical Evaluation of the Surface Integral in the Singularity Methods, Transactions of SNAK, Vol.29, No.1, March 1992
3) T.Hoshino: A Surface Panel Method with a Deformed Wake Model to Analyze Hydrodynamic Characteristics of Propellers in Steady Flow, Mitsubishi Technical Bulletin MTB195 April 1991
4) K.Koyama: Application of a Panel Method to the Unsteady Hydrodynamic Analysis of Marine Propellers, 19th ONR, Aug.1992
5) N.Kroll, D.Lohmann, and J.Schone: Numerical Methods for Propeller Aerodynamics and Acoustics at DFVLR, AGARD Paper69-24,May 1987
6) F.Genoux, R.Baubeau, A.Bruere, and M.DuPont: Steady and Unsteady Characteristics of a Propeller Operating in a Non-Uniform Wake: Comparisons Between Theory and Experiments, 18th ONR, 1990
7) K.Yossifov,BSHC: Propeller Comparative Calculations with Application of the Surface Panel Method
8) A.Haimov,D.Minchev, and T.Videv: Off-Design Propeller Performance Prediction Based on a Deformed Slipstream Model, 5th Int. Congress on Marine Tech., Athens,1990
9) Dang Jie and Tang Denghai : ITTC Comparative Calculation of Propellers
10) S.D.Jessup : An Experimental Investigation of Viscous Aspects of Propeller Blade Flow, The Catholic Univ. of America,1989

4 SAMPLE PROPELLERS AND CALCULATION CONDITIONS

Experimental data are very important for the evaluation of the surface panel method. S.D.Jessup presented detailed measurement for flow around propellers in his dissertation [3]. One of his propellers DTRC4119 is used in the comparative experiments on viscous effects for Task 1 of the 20th ITTC Propulsor Committee.

Two propellers DTRC4119 and DTRC4842 were selected as the propellers for the comparative calculation. DTRC4119 is a three bladed propeller with neither rake nor skew. DTRC4842 is a five bladed propeller with high skew. Their geometries are shown in Table 3(a),(b),(c). Detail of their geometry is presented in the calculation document (Appendix A). Photographs of the propellers are shown in Fig.1.1.1 of Appendix A.

At the workshop the comparative calculations were discussed for the fictitious propeller DTRC4842I instead of DTRC4842 because of confusion over the rake distribution of DTRC4842. Propeller DTRC4842I, which is shown as DTRC4842 in the calculation document, has different rake distribution i_T/D from DTRC4842. Rake distribution i_T/D of DTRC4842 is shown in Table 3(b), whereas that of DTRC4842I is shown in Table 1.1.2(a) of Appendix A. After the workshop many participants reperformed the calculation for DTRC4842. The results for DTRC4842 and DTRC4842I are presented in this report.

Table 3(a) Geometry of DTRC 4119

Diameter, D: 1.00 ft. (0.305 m)
Rotation: Right Hand
Number of Blades: 3
Hub-Diameter Ratio: 0.20
Skew, θ_s,Rake,i_T: none
Design Advance Coefficient, J: 0.833
Section Thickness Form: NACA66(DTRC Modified)
Section Meanline: NACA, a=0.8
Design Thrust Coefficient, K_T: 0.150

r/R	C/D	P/D	θ_s (degree)	i_T/D	t_M/C	f_M/C
0.2	0.320	1.105	0	0	0.2055	0.01429
0.3	0.3635	1.102	0	0	0.1553	0.02318
0.4	0.4048	1.098	0	0	0.1180	0.02303
0.5	0.4392	1.093	0	0	0.09016	0.02182
0.6	0.4610	1.088	0	0	0.06960	0.02072
0.7	0.4622	1.084	0	0	0.05418	0.02003
0.8	0.4347	1.081	0	0	0.04206	0.01967
0.9	0.3613	1.079	0	0	0.03321	0.01817
0.95	0.2775	1.077	0	0	0.03228	0.01631
1.0	0.0	1.075	0	0	0.03160	0.01175

Table 3(b) Geometry of DTRC 4842

Diameter, D: 1.219 ft. (0.3717 m)
Rotation: Right Hand
Number of Blades: 5
Hub-Diameter Ratio: 0.323
Design Advance Coefficient, J: 0.905
Section Thickness Form: NACA66(DTRC Modified)
Section Meanline: Specified
Design Thrust Coefficient, K_T: 0.306

r/R	C/D	P/D	θ_s (deg.)	i_T/D	t_M/C	f_M/C
0.323	0.2015	0.9321	0.38	0.0010	0.2179	0.0100
0.35	0.2181	1.0790	-3.07	-0.0090	0.1871	0.0158
0.4	0.2494	1.2361	-6.82	-0.0229	0.1415	0.0253
0.5	0.3113	1.4194	-9.02	-0.0369	0.0854	0.0365
0.6	0.3664	1.4892	-7.57	-0.0325	0.0581	0.0390
0.7	0.4031	1.488	-3.24	-0.0136	0.0444	0.0371
0.8	0.4090	1.329	4.34	0.0165	0.0379	0.0319
0.9	0.3651	1.0759	13.75	0.0423	0.0356	0.0264
0.95	0.3106	0.9012	19.25	0.0509	0.0363	0.0247
1.0	0.0700	0.6981	25.42	0.0561	0.0880	0.0243

Table 3(c) Thickness and Camber Distributions for DTRC 4119 and 4842

X c	t/C	f/C,4119	f/C,4842
0.0000	0.0000	0.0000	0.0000
0.0125	0.2088	0.0907	0.0875
0.0250	0.2932	0.1586	0.1530
0.0500	0.4132	0.2712	0.2625
0.0750	0.5050	0.3657	0.3585
0.1000	0.5814	0.4482	0.4415
0.1500	0.7042	0.5869	0.5803
0.2000	0.8000	0.6993	0.6955
0.3000	0.9274	0.8635	0.8630
0.4000	0.9904	0.9615	0.9630
0.4500	1.0000	0.9881	0.9907
0.5000	0.9924	1.0000	1.0000
0.6000	0.9306	0.9786	0.9750
0.7000	0.8070	0.8892	0.8777
0.8000	0.6220	0.7027	0.6760
0.9000	0.3754	0.3586	0.3613
0.9500	0.2286	0.1713	0.1785
1.0000	0.0666	0.0000	0.0000

Table 4 Standard Calculation Cases

A)	DTRC4119 without hub	J=0.833	recomended paneling linear wake
B)	DTRC4119 without hub	J=0.833	reference paneling linear wake
C)	DTRC4119 with hub	J=0.833	recomended paneling linear wake
D)	DTRC4119 without hub	J=0.833	recomended paneling devised wake
E)	DTRC4119 with hub	J=0.833	recomended paneling devised wake
F)	DTRC4119 without hub	J=1.100	recomended paneling linear wake
G)	DTRC4119 without hub	J=1.100	recomended paneling devised wake
H)	DTRC4842 with hub	J=0.905	recomended paneling devised wake
I)	DTRC4842I with hub	J=0.905	recomended paneling devised wake

recommended paneling :
paneling participants recommend or use
reference paneling :
fine or course or lower order or higher order paneling which shows the validation of the paneling participants recommend
linear wake :
blade vortex wake remains its location at the point it has emanated in spite of induced velocity
devised wake :
modeled wake or calculated wake

The advance coefficients J=0.833 and J=1.100 are for DTRC4119, and J=0.905 for DTRC4842 and DTRC4842I. Details of the calculation conditions are shown in Table 4.

5 COMPARATIVE CALCULATION

The list of contributors from the 15 organizations who sent the calculation results is shown in Table 5.

The calculation methods and their characteristics are shown in Table 6. Many researchers use a potential based panel method and employ plane panels or hyperboloidal panels. Many researchers use the pressure Kutta condition. The coarsest paneling in the table is NR×NC = 7×8. The finest paneling is NR×NC = 30×20 and 15×30.

Some calculations based on lifting surface theory were contributed to the workshop and were included for reference.

Table 5 List of Participants to Comparative Calculation

1) Dr.Cheng-I. Yang
David Taylor Model Basin (DTMB), USA
2) Prof.J.E.Kerwin,Dr.C.Y.Hsin,Dr.S.Kinnas
Massachusetts Institute of Technology (MIT), USA
3) Dr.B.Maskew
Analytical Methods,Inc. (AMI), USA
4) Dr.J.T.Lee,Mr.Y.G.Kim,Dr.J.C.Suh,Prof.C.S.Lee
Korean Research Institute of Ships and Ocean Engineering (KRISO), and Chungnam National University (CNU), Korea
5) Dr.T.Hoshino
Mitsubishi Heavy Industries,Ltd. Nagasaki R&D Center (MHI), Japan
6) Dr.S.Ryo
Research Institute, Nippon Kaiji Kyokai (NK), Japan
7) Mr.H.Yamasaki
Yokohama National University (YNU), Japan
8) Dr.K.Koyama
Ship Research Institute (SRI), Japan
9) Dr.G.Caprino
Cento per gli Studi di Tecnica Navale (CETENA), Italy
10) Dr.Dieter Lohmann
Deutsche Forschungsanstalt fur Luft und Raumfahrt (DLR), Germany
11) Prof.P.Bogdanov,
Bulgarian Ship Hydrodynamics Centre (BSHC), Bulgaria
12) Dr.R.Baubeau
Bassin d'Essais des Carenes (DGA), France
13) Dr.P.Sander
Institut fur Schiffbau Universitat Hamburg (Hamburg), Germany
14) Dr.H.Streckwall
Hamburgische Schiffbau-Versuchsanstalt GmbH (HSVA), Germany
15) Mr.Dang Jie, and Mr.Tang Denghai
China Ship Scientific Research Center (CSSRC), China

6 CALCULATION RESULTS

Standard calculation conditions are case A, case B,,, case I as shown in Table 4. Some

Table 6 (a) Calculation Method

		Calculation Method	Panel Type	NR × NC	Kutta Condition
1)	DTMB	Potential based P.M. (DTMB ver. of VSAERO)	Quadrilateral plane panel	10 × 29	
2)	MIT	Potential based P.M. (MIT-PSF-10)	Hyperboloidal	30 × 20	Iterative Pressure Kutta Condition
3)	AMI	Potential based P.M. (VSAERO, USAERO)		15 × 30	
4)	KRISO/ CNU	Potential based P.M. (KPA11)	Hyperboloidal panel	10 × 20	Pressure Kutta Condition
5)	MHI	Potential based P.M.	Hyperboloidal quadrilateral panel	12 × 12	Pressure Kutta Condition
6)	NK	Direct Formulation of BEM (Potential based P.M.)	Triangular element	8 × 13	Pressure Kutta Condition
7)	YNU	Surface Vortex Lattice M.	Horse-shoe	10 × 12	Nothing
8)	SRI	Potential based P.M. Time-Stepping code	Quadrilateral plane panel	7 × 8	Modified Morino Kutta Condition
9)	CETENA	Potential based P.M.	Quadrilateral plane panel	17 × 12	Trial And Error technique based on linear interpolation
10)	DLR	Lifting Surface Theory based on FW-H equation	plane panel	10 × 15	Geometric Kutta Condition (bisector, 2% of chord)
11)	BSHC	Lifting Surface Theory		15 × 9	
12)	DGA	Lifting Surface Theory Quasi-Continuous Method		12 × 12	
13)	Hamburg	Lifting Surface Theory Continue Method(Mode Function Method)			
14)	HSVA	Lifting Surface Theory Vortex-Lattice Method		10 × 10	
15)	CSSRC	Potential Based P.M. (MBPM-V1.0)	Hyperboloidal quadrilateral panel	10 × 16	Pressure Kutta Condition

NR : number of panels in radial direction
NC : number of panels in chordwise direction

Table 6 (b) Calculation Method

		Cal. of Velocity	Viscous Correction
1)	DTMB		Sectional drag coefficient (empirical correction)
2)	MIT	2nd Oder Finite Difference Scheme	Sectional drag coefficient
3)	AMI		Boundary layer calculation
4)	KRISO/ CNU	Numerical Differentiation Piecewise Quadratic Inter.	Viscous friction coefficient C_F=0.004
5)	MHI		Empirically determined formula for frictional drag
6)	NK	Numerical Differentiation 1st order shape function	drag coefficient
7)	YNU	Numerical cal.by Biot-Savart Low	Prandtl-Schlichting formula for drag
8)	SRI	Numerical Differentiation Quadric curved surface	Exp. data for section drag and circulation reduction Abbot and Von Doenhoff
9)	CETENA	Numerical Differentiation Pot. expressed by parabola	Van Oossanen $Cr = Cf\ (1+1.2t/c+70(t/c)^4)$
10)	DLR		Transpiration method - boundary layer calculation from previous pressure distribution
11)	BSHC		drag coefficient and circulation reduction
12)	DGA		integrating local flat plate friction coefficient
13)	Hamburg		
14)	HSVA	Biot-Savart	Sectional drag coefficient
15)	CSSRC	Numerical Differentiation	Viscous friction coefficient $Cf=0.026Res^{-1/7}$

participants carried out calculations for all cases. Others carried out some parts of the cases. Results of all the calculations were discussed in the workshop.

Examples of paneling for the propellers are seen in Figs.1,8 of Appendix B, Figs.1,2 of Appendix C, or Figs.4.1,4.8 of Appendix D.

6.1 THRUST AND TORQUE

Calculation results for thrust coefficient K_T and torque coefficient K_Q are shown in Fig.1.1.1 - Fig.1.6.2.

The case A (DTRC4119, J=0.833, without hub, linear wake) without viscous correction is the most basic case. The case is suitable for the validation of numerical results. K_T, K_Q values for the case are shown in Fig.1.1.1(a),(c). Correlation between calculation and experiment is reasonable. However the scatter of the calculation results is somewhat unexpected. A possible reason for the scatter may be that some calculations modify the pitch of the vortex wake in spite of linear calculation.

Calculation results for the case A with viscous correction are shown in Fig.1.1.1(b),(d). Improvement of the correlation with experiment is shown.

Calculation results for the case C (DTRC4119, J=0.833, with hub, linear wake) are shown in Fig.1.2.1(a),(b),(c),(d). Comparison between case C and case A shows the effect of hub. The effect is not so large in this case. Detailed survey of the effect is discussed in materials presented by MIT (Appendix C) . In order to understand the effect of the hub geometries, they have calculated the forces on propeller DTRC4119 by using three different hub geometries, along with the no hub results. Besides the hub model suggested by ITTC, they also used hub geometries with constant radii downstream and upstream.This corresponds to the real experiments in which the propellers may be driven either from upstream, or from downstream. Fig.5 of Appendix C shows these three different hub models. Results of their calculation are shown in Fig.6 of Appendix C.

Calculation results for the case D (DTRC4119, J=0.833, without hub, devised wake) are shown in Fig.1.3.1(a),(b),(c),(d). Comparison between case D and case A shows the effect of devised wake.

The case E (DTRC4119, J=0.833, with hub, devised wake) with viscous correction is most realistic case. The case is suitable for comparison with experiment. K_T, K_Q values for the case are shown in Fig.1.4.1(b),(d). Correlation between calculation and experiment is good which demonstrates the value of the surface panel method. The correlation for K_Q is not as good as that for K_T. Although viscous effect, devised wake effect and hub effect are included in case E, the viscous effect is dominant for K_Q.

Calculation results of the case H for DTRC4842 are shown in Fig.1.5.1(b),(d). The correlation between calculation and experiment has the same tendency as the case for DTRC4119.

Calculation results of the case I for DTRC4842I are shown in Fig.1.6.1. The comparison between case I and case H shows the effect of rake.

Calculation results by the lifting surface theory are shown in Fig.1.1.2, 1.2.2, 1.3.2, 1.4.2, 1.6.2.

6.2 PRESSURE DISTRIBUTION

Calculation results for pressure coefficient C_P are shown in Fig.2.1.1 - Fig.2.7.1.

Pressure coefficients C_P for the case A for DTRC4119 are shown in Fig.2.1.1 (a),(b),(c),(d),(e),(f). The small scatter shows the merit of surface panel methods. It becomes clear when we compare these results with 15th ITTC Comparative Calculations of Propeller Blade Pressure Distributions [4]. On the whole the results for C_P on the blade are considered to be satisfactory although there is considerable scatter near the root, tip, leading edge, and trailing edge.

Calculation results for the case C are shown in Fig.2.2.1. The effect of the hub makes pressure low at 0.3R back and face.

Calculation results for the case D are shown in Fig.2.3.1. Discrepancies between the case D and the case A seems not to be large.

Pressure coefficients C_P for the case E are shown in Fig.2.4.1(a),(b),(c),(d),(e),(f). Correlation between calculations and experiment in general, is good although many calculations for $-C_P$ near the root r/R=0.3 is higher than the experiment.

Calculation results for the case F and the case G are shown in Fig.2.5.1.

Pressure coefficients C_P for the case H for DTRC4842 are shown in Fig.2.6.1 (a),(b),(c),(d),(e),(f). There seems to be more scatter in the results.

Calculation results for the case I for

DTRC4842I are shown in Fig.2.7.1. Comparison between the case I and the case H shows the effect of rake.

Calculation results for DTRC4119 by lifting surface theory are shown in Fig.2.1.2.

7 DISCUSSIONS

Detailed comparison between case A through case G reveals the viscous effect, the effect of hub and the effect of devised wake on the thrust, torque, and the pressure distribution.

Viscous effect on K_T,K_Q values is shown in Fig.2 and Fig.9 of Appendix B (DTMB). Viscous drag correction is essential to the correct prediction of the torque. Its effect on the prediction of the thrust is marginal.

The effect of hub appears as a low pressure on the blade near hub. The effect of hub on thrust and torque is small in these calculation cases.

Although the effect of the devised wake does not seem to be completely clear, the devised wake is very different from that of classical propeller theory. Examples of the devised wake are shown in Fig.3 (cited from the materials presented by MHI, No.6 in Table 2(a) of this report). Further study on the deformation of the vortex wake is expected.

8 CONCLUSION

The results of the comparative calculation show the state of the art of surface panel method for marine propellers. The numerical results are useful as the database for marine propellers. Conclusions of the comparative calculations and workshop are as follows,

1. The results of comparative calculations demonstrate the value of panel methods for propeller analysis. Most of the methods are potential based, rather than velocity based.

2. The predictions of performance for propellers are generally in good agreement with the experimental data.

3. Panel methods predict the pressure distribution well except near the root, tip, leading edge and trailing edge. Further investigation on the arrangements of panels close to the root, tip, leading edge and trailing edge is required in order to improve the accuracy of predictions.

4. For further development, the treatment of viscous corrections and the slipstream wake model must be studied.

ACKNOWLEDGEMENT

These comparative calculations and the workshop were accomplished through the considerable effort of all participants. Participants in the comparative calculations are listed in Table 5 and the participants in the workshop are listed in Table 1. Korean colleague, Dr.H.S.Lee contributed in the preparation for the workshop and KTTC supported the workshop with the conference room and many conveniences. The author would like to express his sincere gratitude to all participants, Dr.H.S.Lee and KTTC.

The author also wishes to express his indebtedness to the members of 20th ITTC Propulsor Committee

Dr. Frank B. Peterson, NSWC, USA
(Chairman)
Prof. Shi- Tang Dong, CSSRC, China
Dr. A. Gorschkov, KSRI, Russia
Dr. Alfred M. Kracht, VWS, Germany
Dr. Ramon Quereda Lavina, PARDO TANK, Spain
Dr. Giovanni Caprino, CETENA, Italy
Dr. Jaakko Pylkkanen, VTT, Finland
Mr. Colin Wills, DRA, UK

for their support and cooperation.

Furthermore the author is grateful to Mr.K.Awai for drawing the figures.

The author also wishes to express his indebtedness to the editorial committee of Ship Research Institute.

REFERENCES

[1] 20th ITTC Report of Propulsor Committee, Sept.1993, SanFrancisco

[2] Koyama,K. et al., "Experimental Investigation of Flow Around a Marine Propeller and Application of Panel Method to the Propeller Theory," 16th Symposium on Naval Hydrodynamics,1986, Berkeley

[3] Jessup,S.D., "An Experimental Investigation of Viscous Aspects of Propeller Blade Flow," The Catholic University of America, PHD Thesis, 1989

[4] 15th ITTC Report of Propeller Committee, Sept. 1978, the Hague, page 266

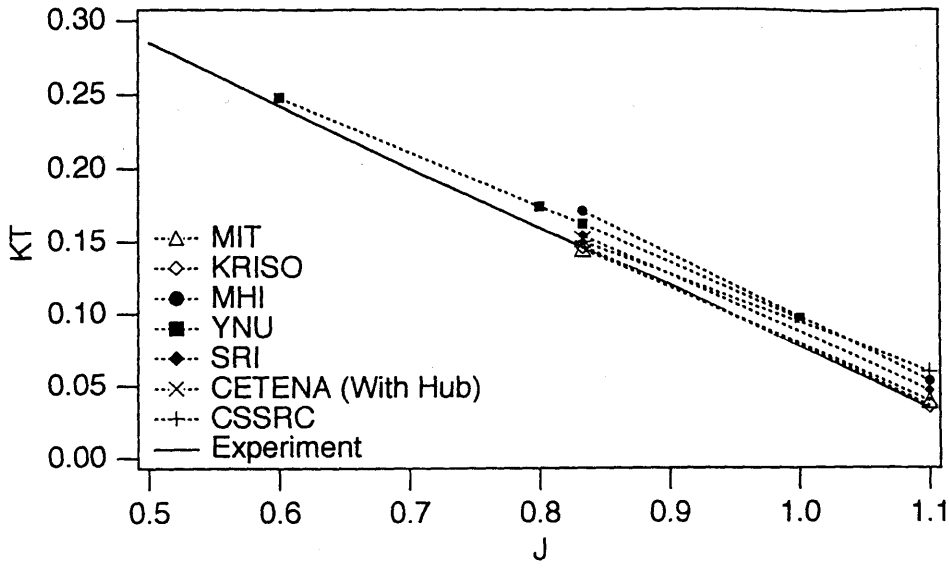

Fig.1.1.1(a) Case A , DTRC4119 , Without Hub , Linear Wake
KT Without Viscous Correction

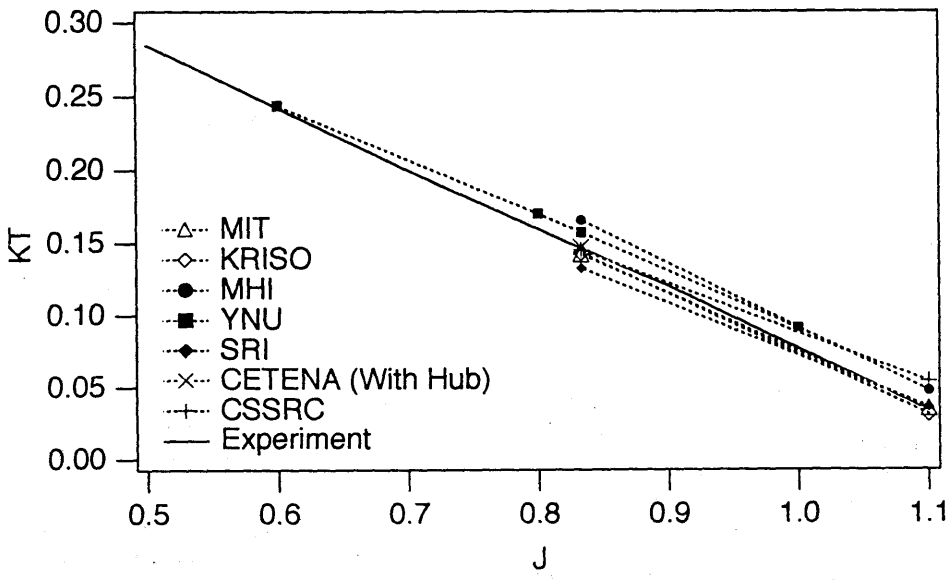

Fig.1.1.1(b) Case A , DTRC4119 , Without Hub , Linear Wake
KT With Viscous Correction

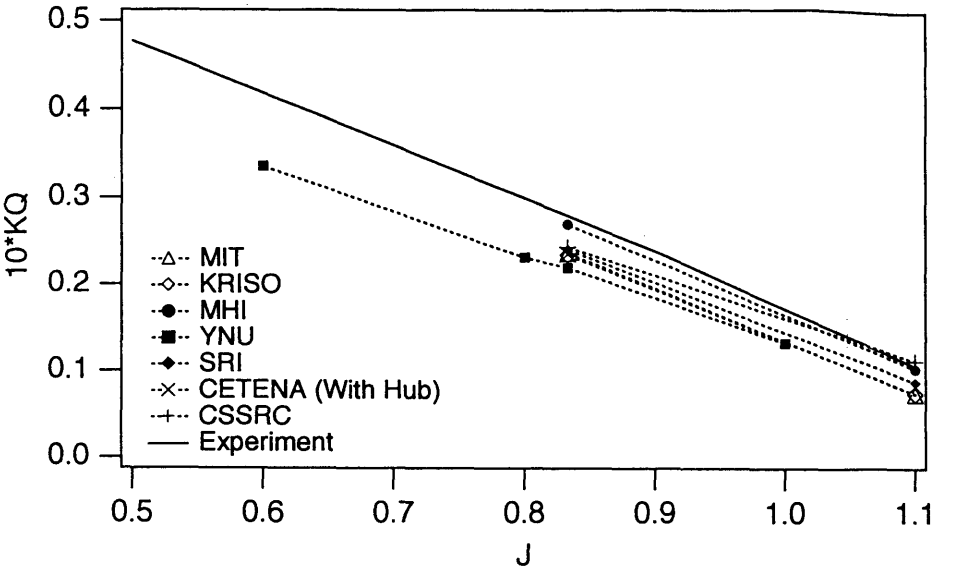

Fig.1.1.1(c) Case A , DTRC4119 , Without Hub , Linear Wake
KQ Without Viscous Correction

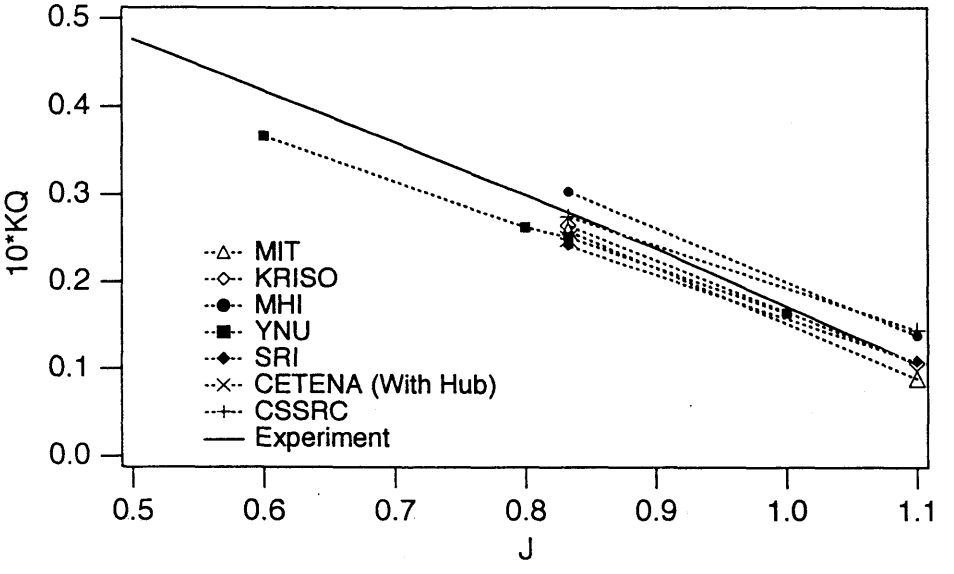

Fig.1.1.1(d) Case A , DTRC4119 , Without Hub , Linear Wake
KQ With Viscous Correction

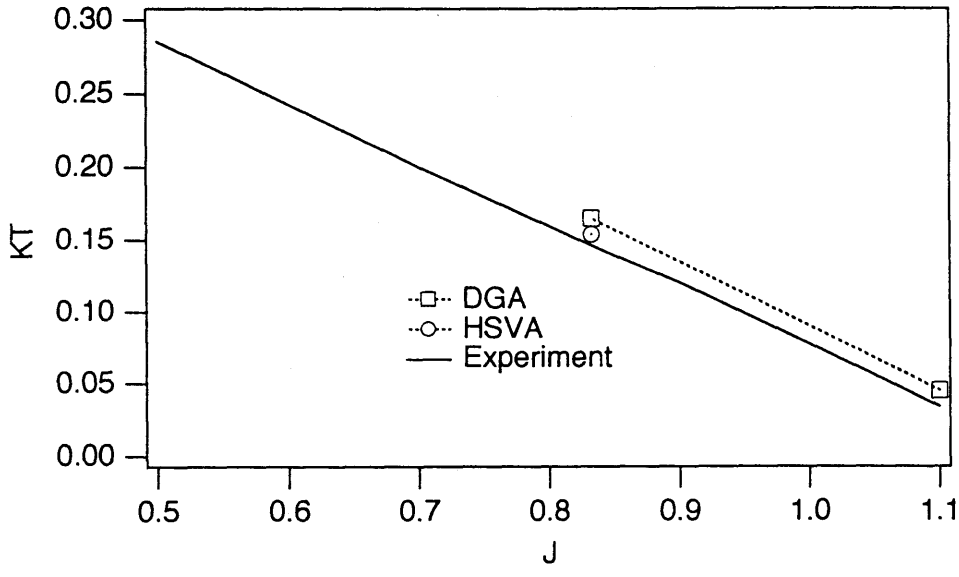

Fig.1.1.2(a) Case A , DTRC4119 , Without Hub , Linear Wake
KT Without Viscous Correction

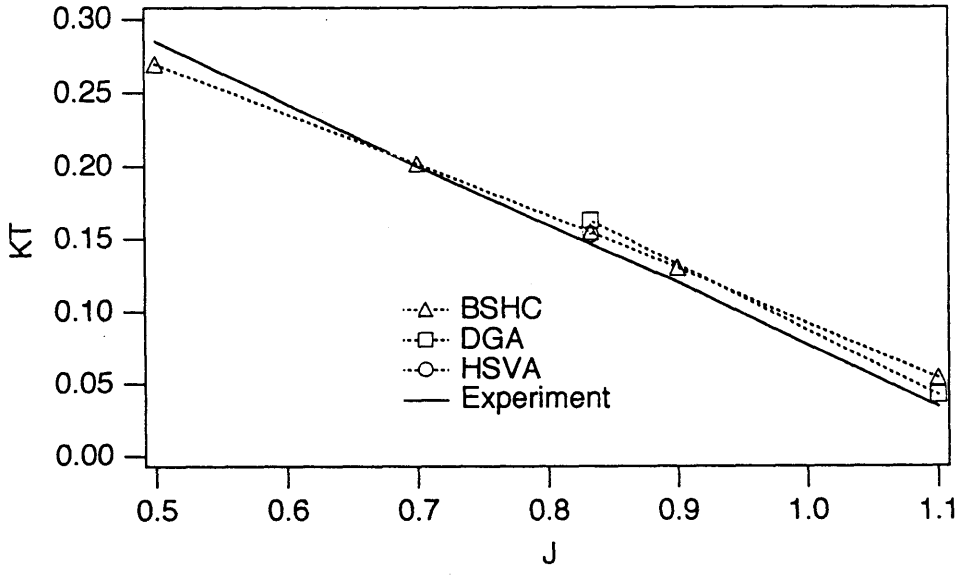

Fig.1.1.2(b) Case A , DTRC4119 , Without Hub , Linear Wake
KT With Viscous Correction

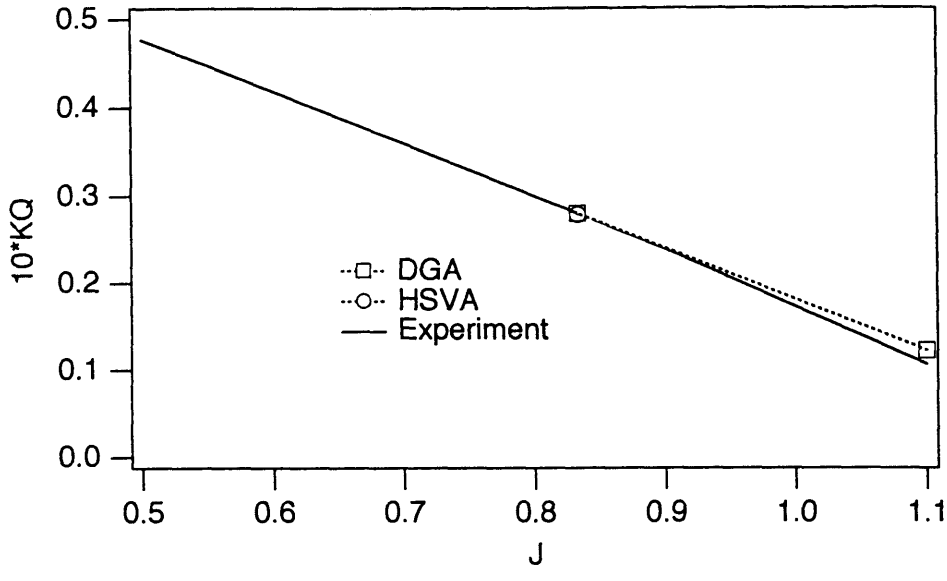

Fig.1.1.2(c) Case A , DTRC4119 , Without Hub , Linear Wake
KQ Without Viscous Correction

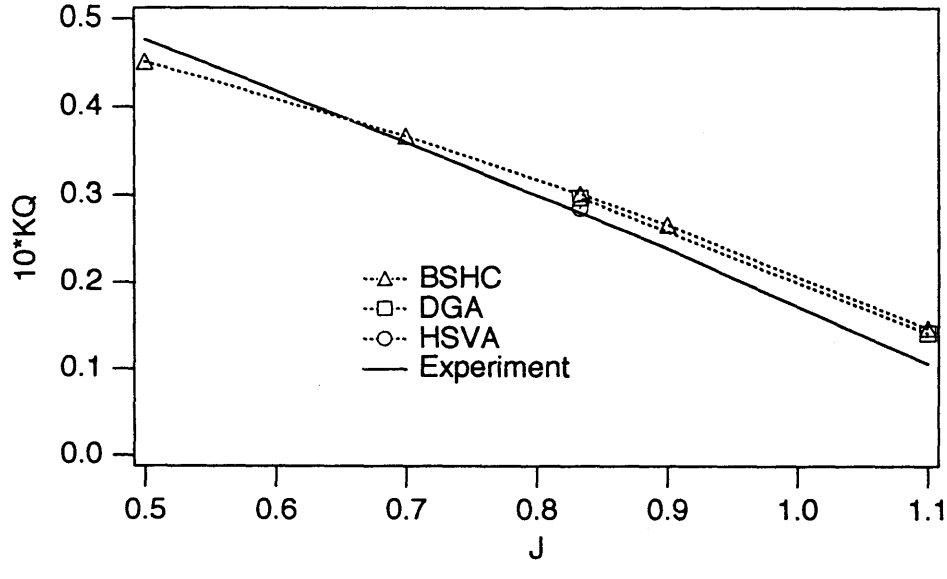

Fig.1.1.2(d) Case A , DTRC4119 , Without Hub , Linear Wake
KQ With Viscous Correction

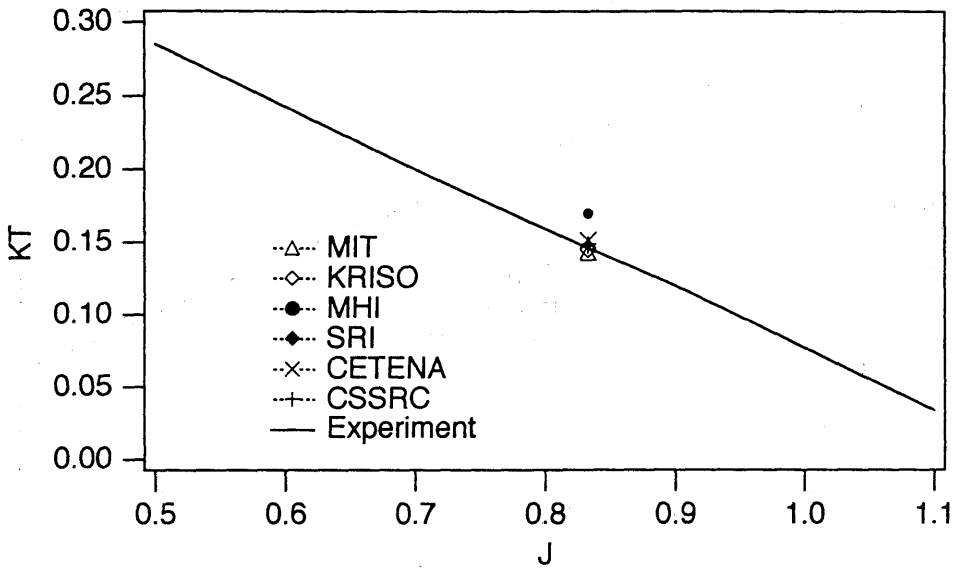

Fig.1.2.1(a) Case C , DTRC4119 , With Hub , Linear Wake
KT Without Viscous Correction

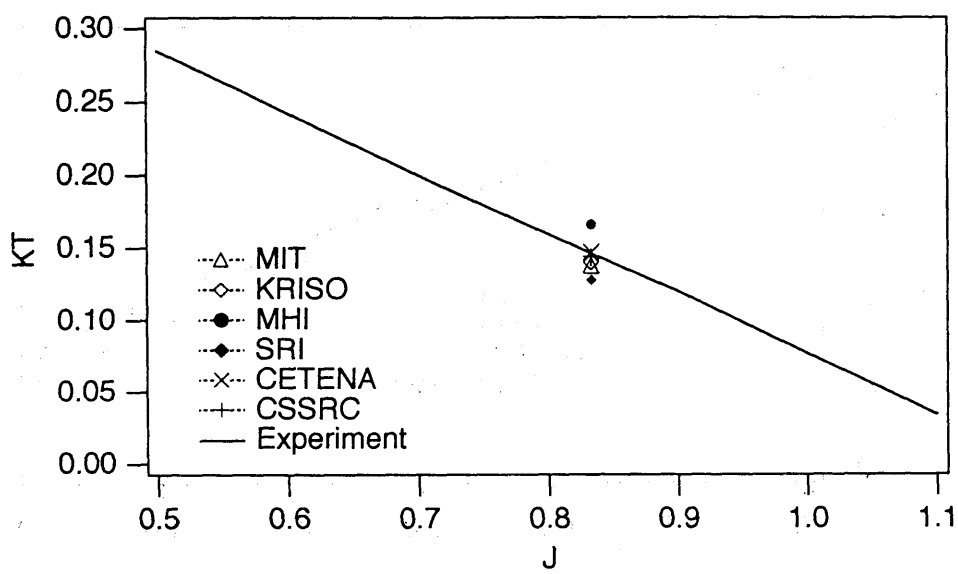

Fig.1.2.1(b) Case C , DTRC4119 , With Hub , Linear Wake
KT With Viscous Correction

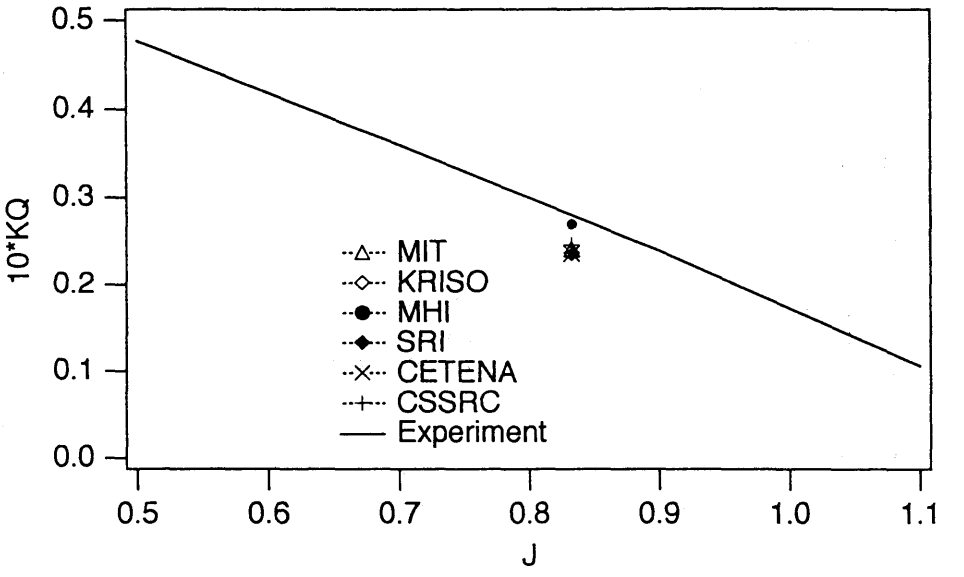

Fig.1.2.1(c) Case C , DTRC4119 , With Hub , Linear Wake
KQ Without Viscous Correction

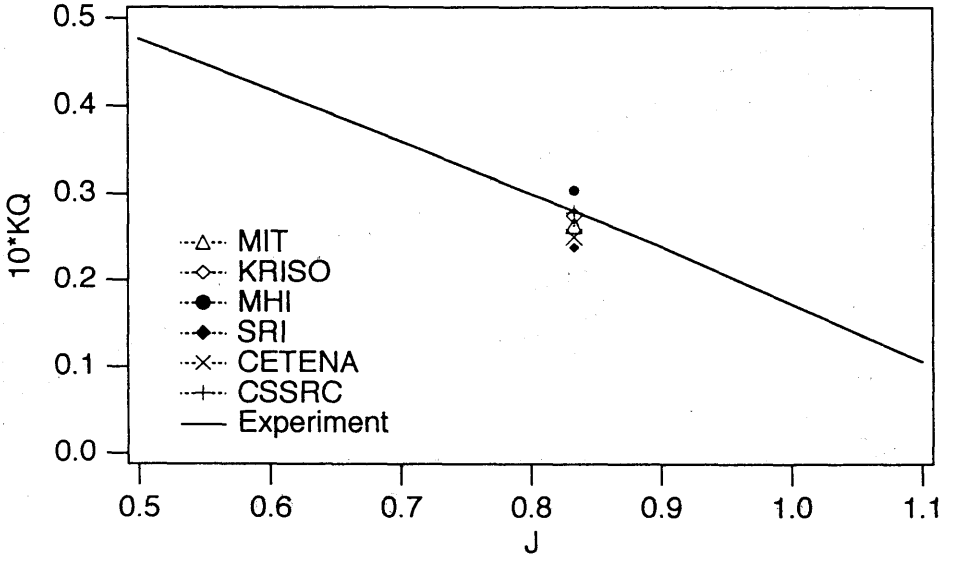

Fig.1.2.1(d) Case C , DTRC4119 , With Hub , Linear Wake
KQ With Viscous Correction

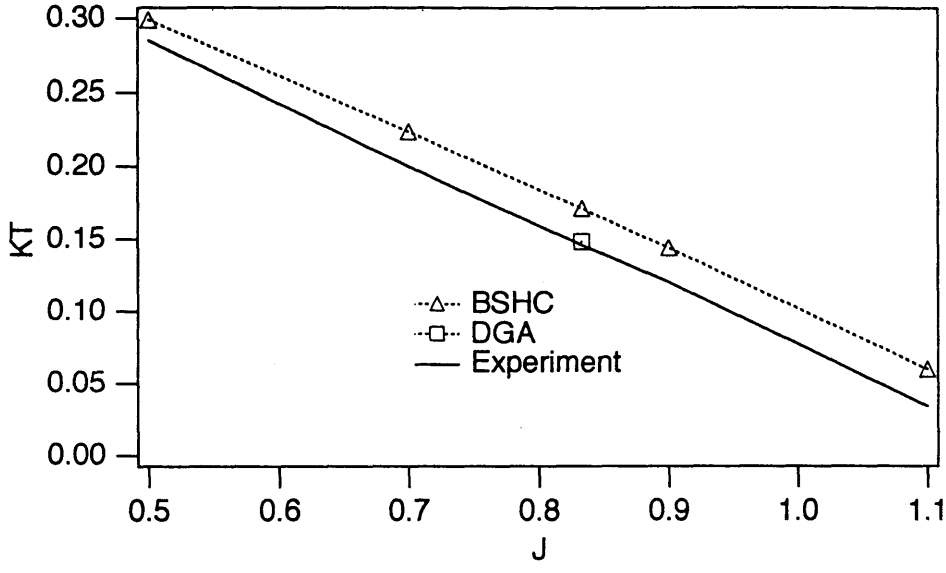

Fig.1.2.2(a) Case C , DTRC4119 , With Hub , Linear Wake
KT Without Viscous Correction

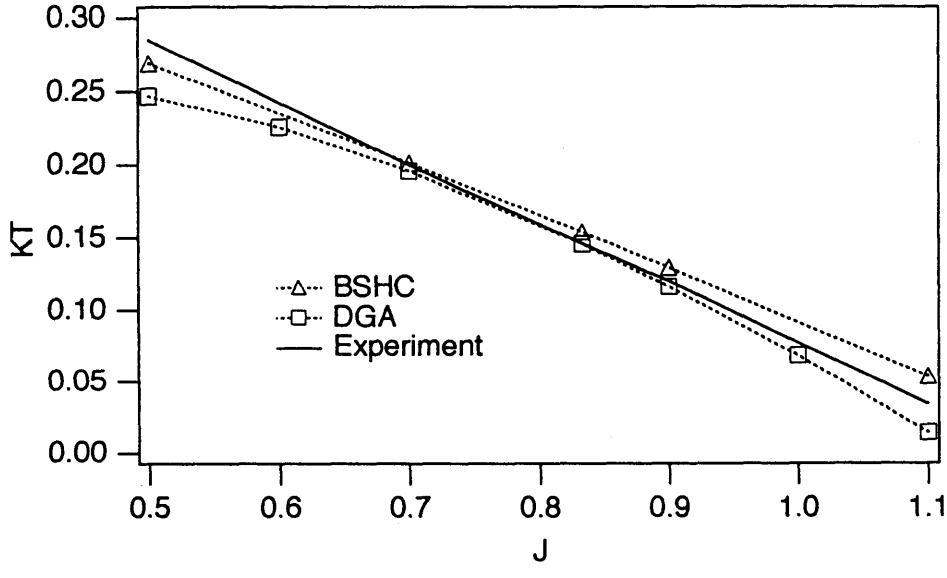

Fig.1.2.2 (b) Case C , DTRC4119 , With Hub , Linear Wake
KT With Viscous Correction

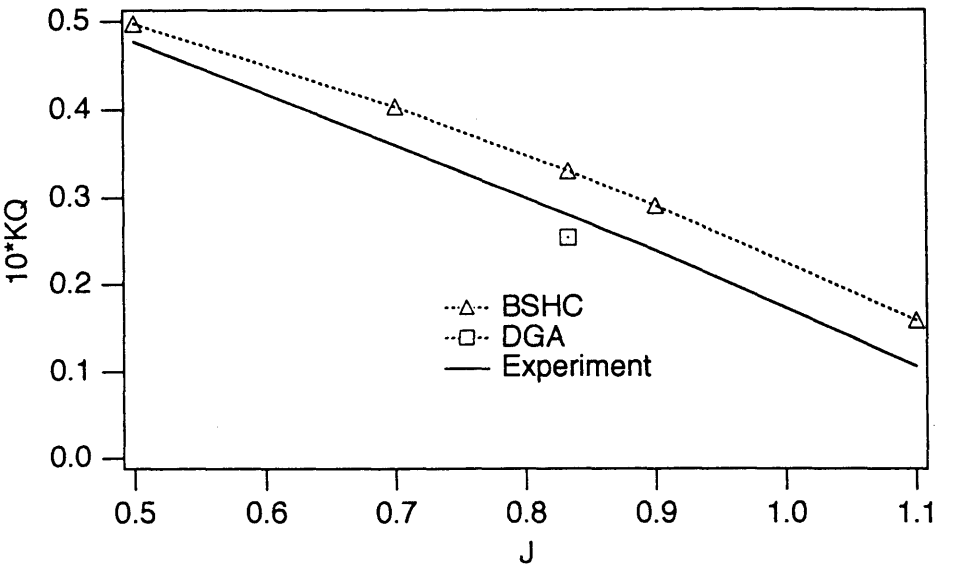

Fig.1.2.2(c) Case C , DTRC4119 , With Hub , Linear Wake
KQ Without Viscous Correction

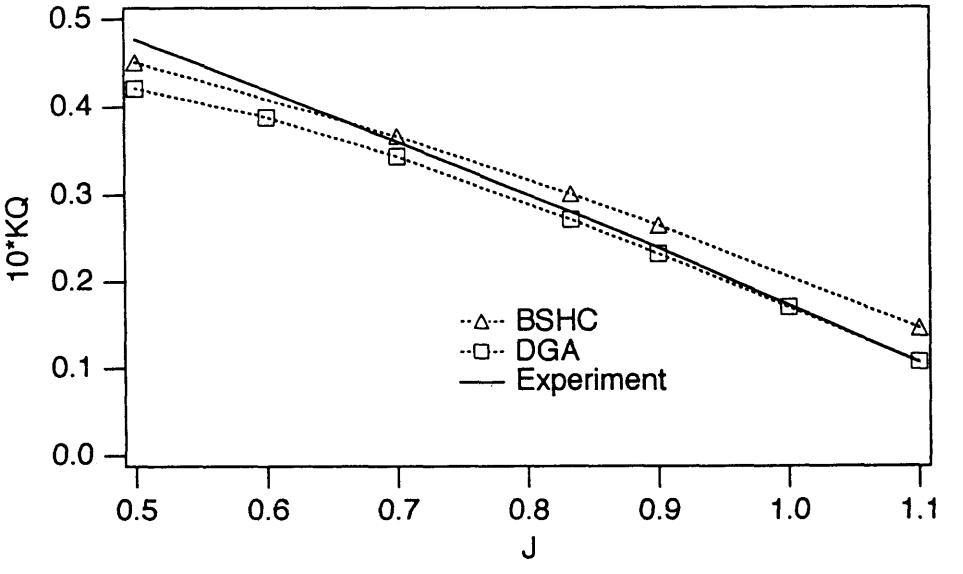

Fig.1.2.2 (d) Case C , DTRC4119 , With Hub , Linear Wake
KQ With Viscous Correction

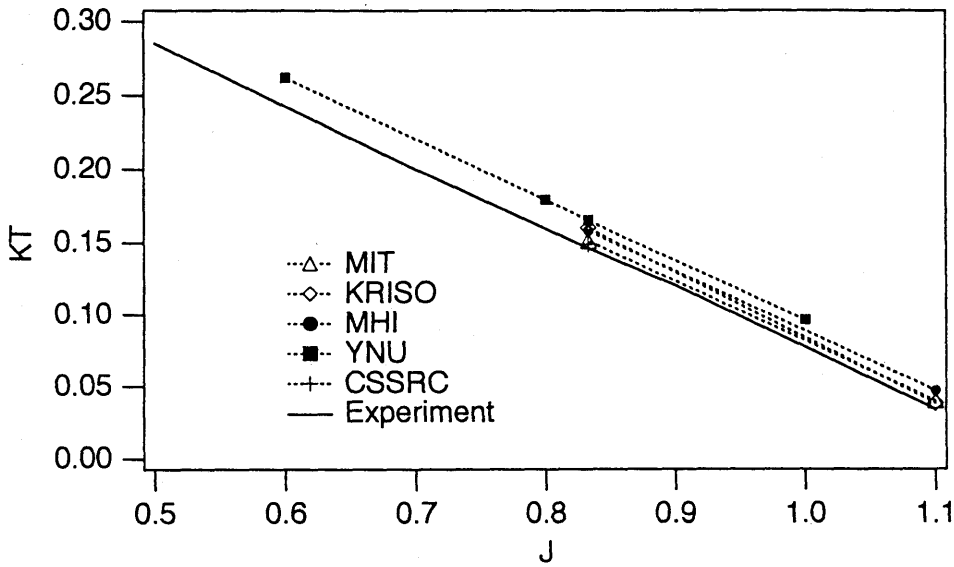

Fig.1.3.1(a) Case D , DTRC4119 , Without Hub , Devised Wake
KT Without Viscous Correction

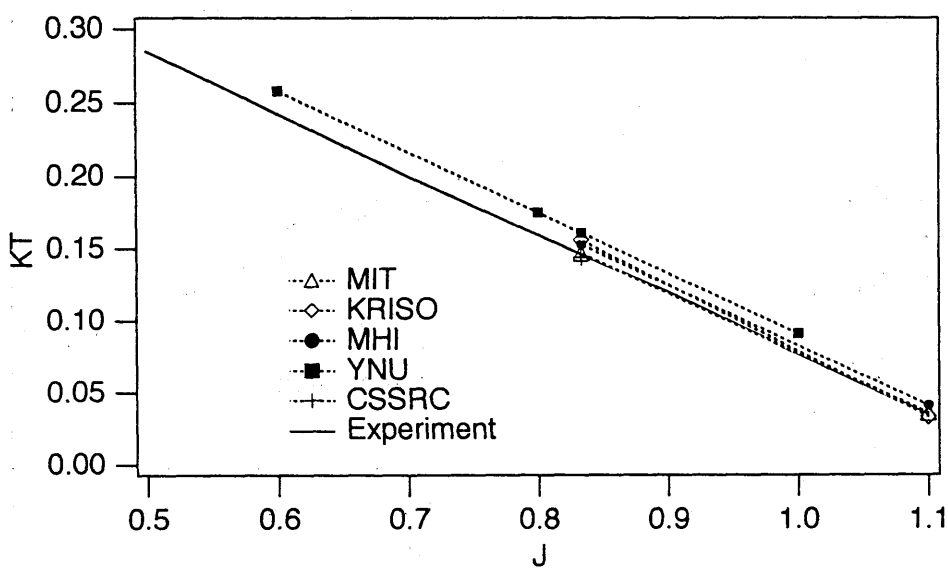

Fig.1.3.1(b) Case D, DTRC4119 , Without Hub , Devised Wake
KT With Viscous Correction

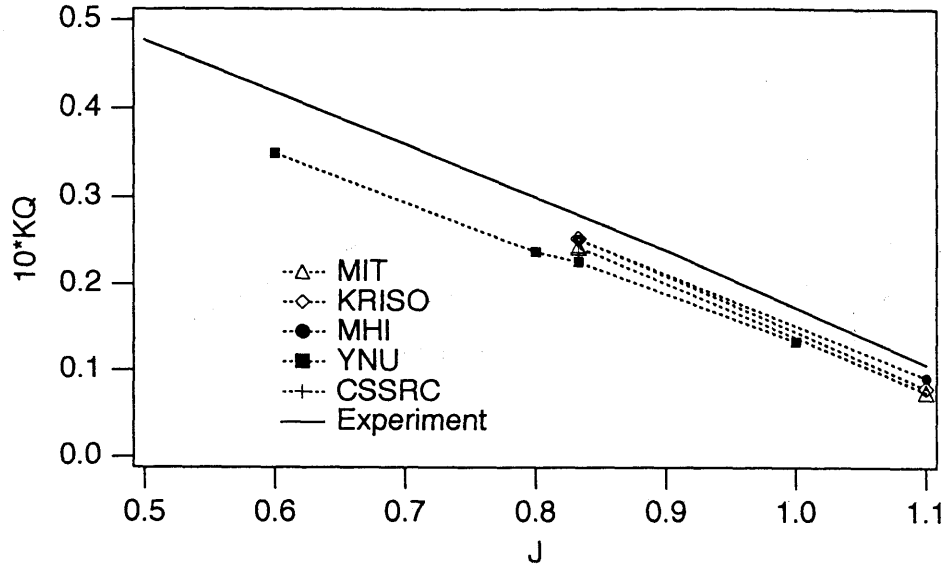

Fig.1.3.1(c) Case D , DTRC4119 , Without Hub , Devised Wake
KQ Without Viscous Correction

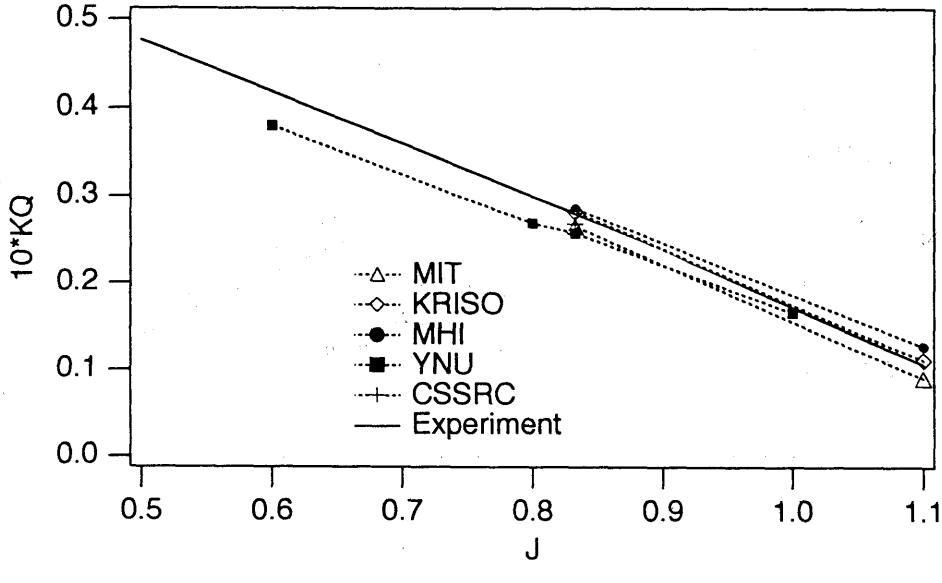

Fig.1.3.1(d) Case D , DTRC4119 , Without Hub , Devised Wake
KQ With Viscous Correction

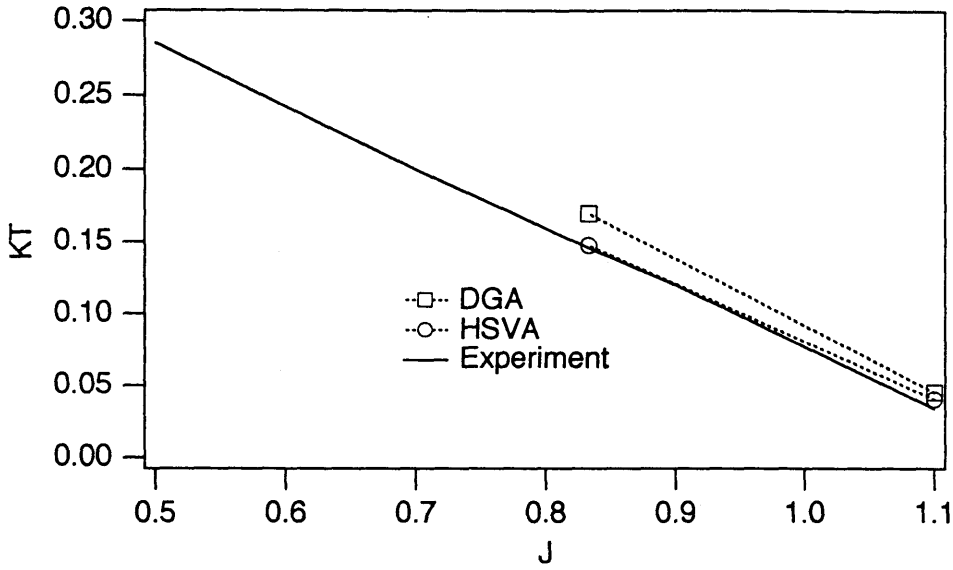

Fig.1.3.2(a) Case D, DTRC4119 , Without Hub , Devised Wake
KT Without Viscous Correction

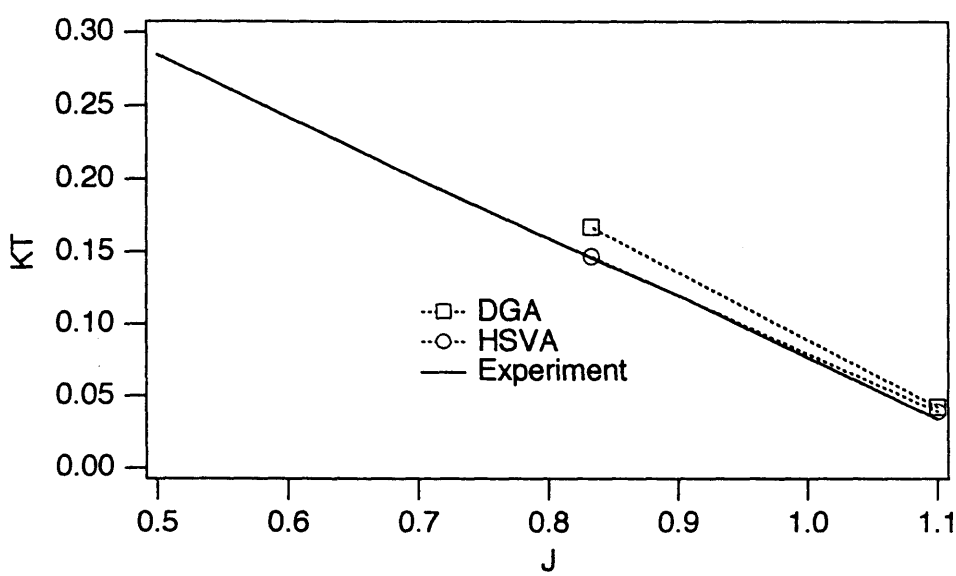

Fig.1.3.2(b) Case D , DTRC4119 , Without Hub , Devised Wake
KT With Viscous Correction

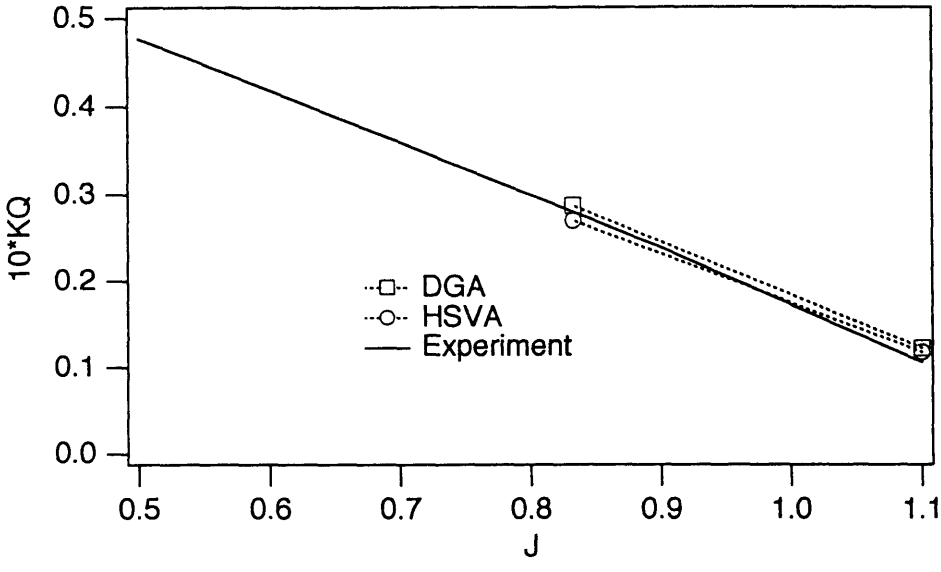

Fig.1.3.2(c) Case D, DTRC4119 , Without Hub , Devised Wake
KQ Without Viscous Correction

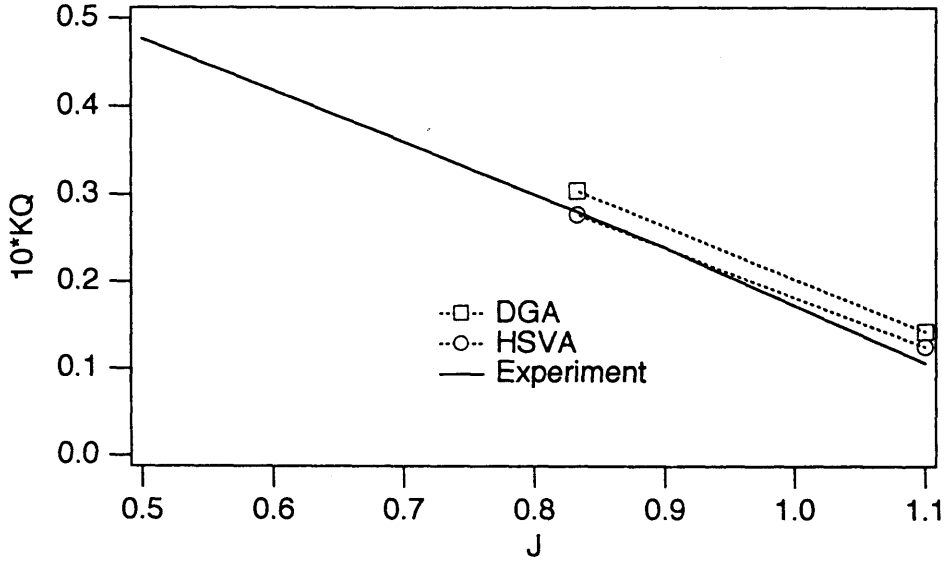

Fig.1.3.2(d) Case D , DTRC4119 , Without Hub , Devised Wake
KQ With Viscous Correction

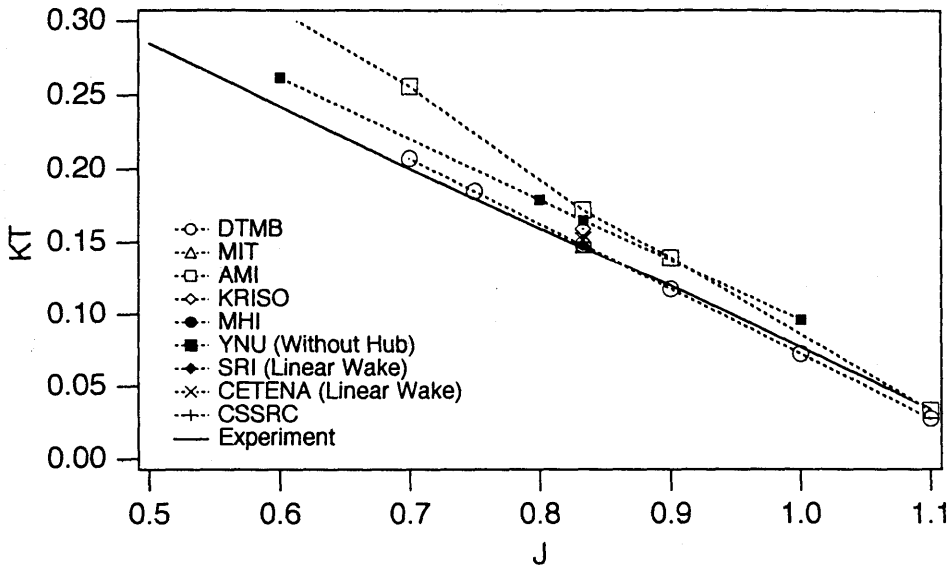

Fig. 1.4.1 (a) Case E , DTRC4119 , With Hub , Devised Wake
KT Without Viscous Correction

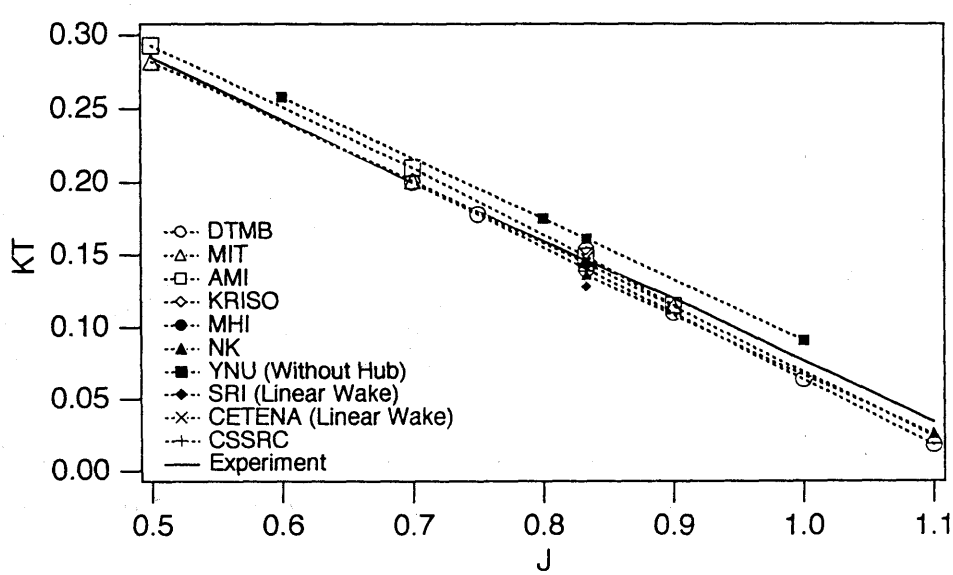

Fig. 1.4.1 (b) Case E , DTRC4119 , With Hub , Devised Wake
KT With Viscous Correction

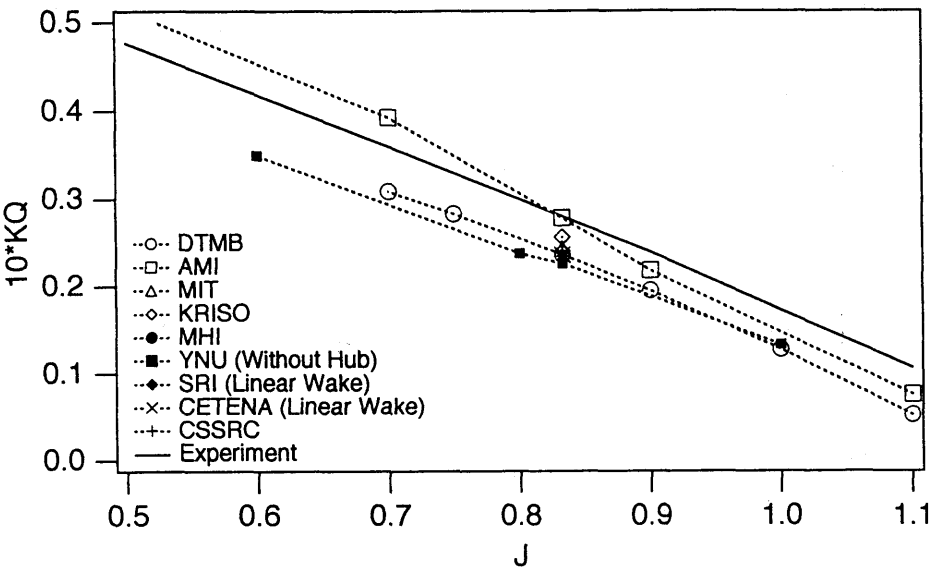

Fig. 1.4.1 (c) Case E , DTRC4119 , With Hub , Devised Wake
KQ Without Viscous Correction

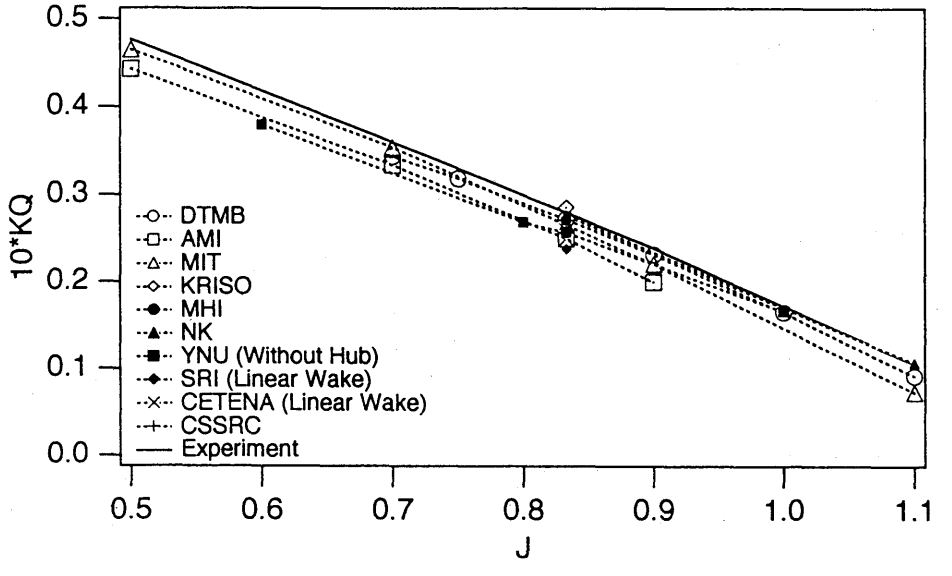

Fig. 1.4.1 (d) Case E , DTRC4119 , With Hub , Devised Wake
KQ With Viscous Correction

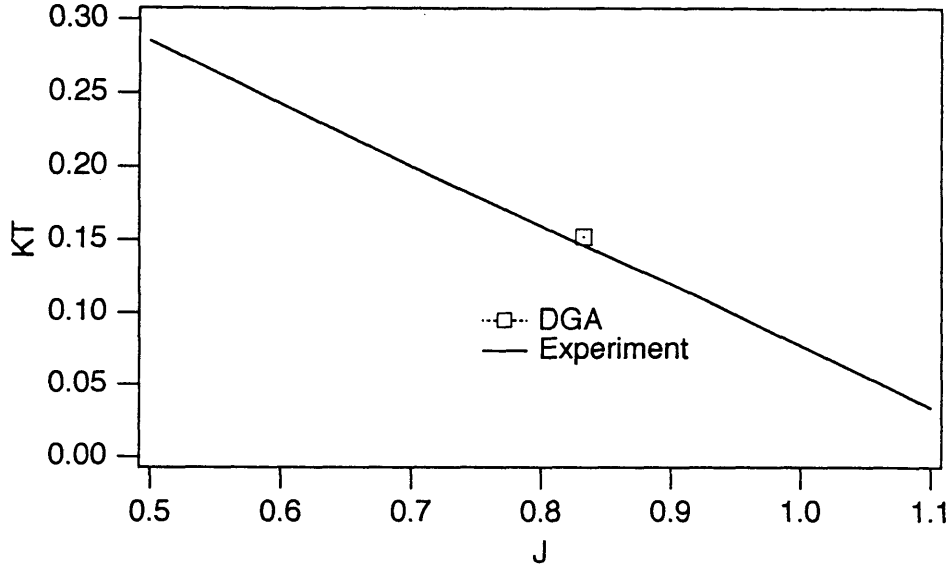

Fig.1.4.2 (a) Case E , DTRC4119 , With Hub , Devised Wake
KT Without Viscous Correction

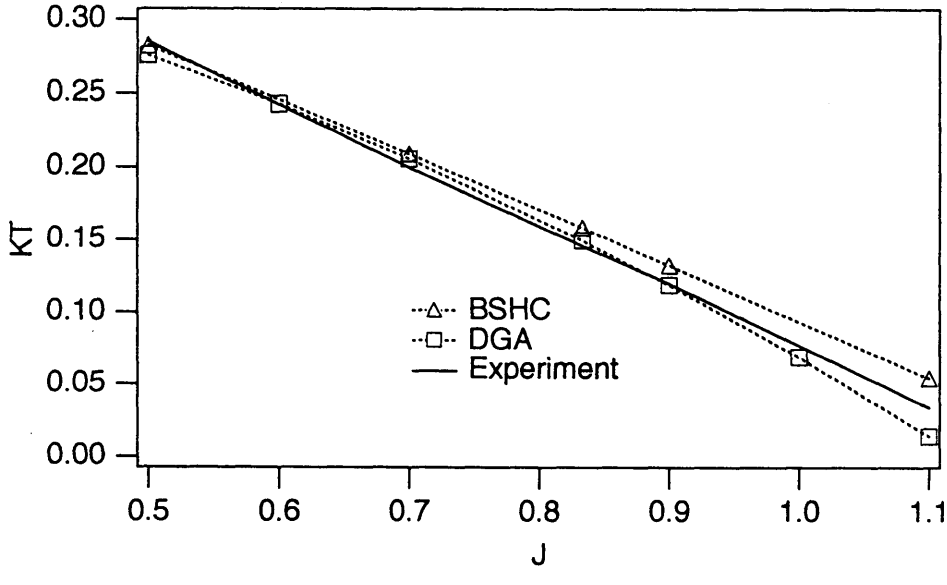

Fig.1.4.2 (b) Case E , DTRC4119 , With Hub , Devised Wake
KT With viscous Correction

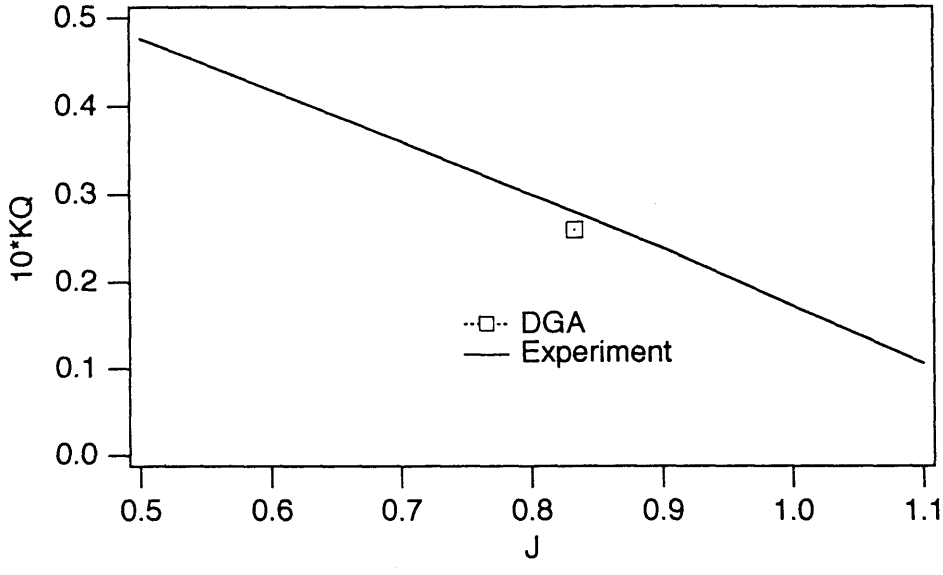

Fig.1.4.2 (c) Case E , DTRC4119 , With Hub , Devised Wake
KQ Without Viscous Correction

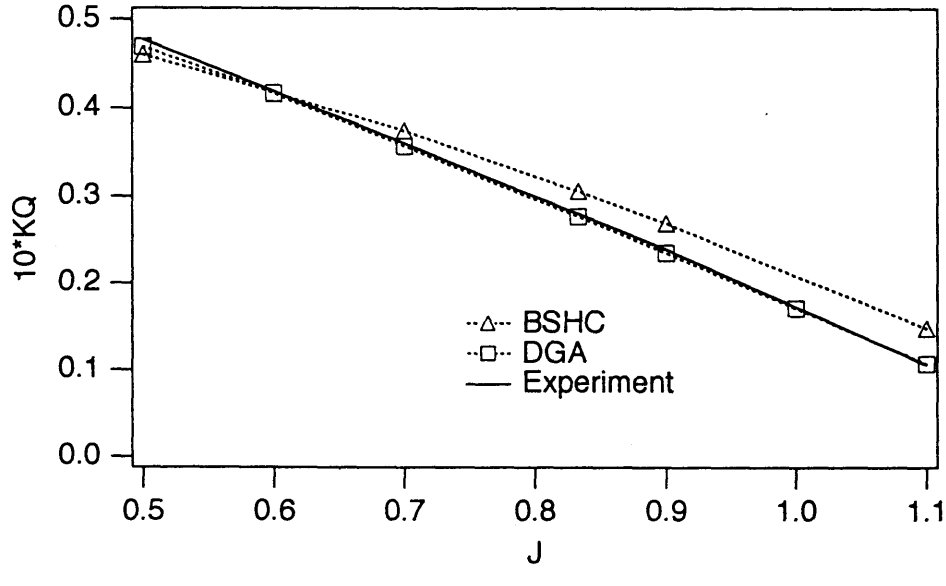

Fig.1.4.2 (d) Case E , DTRC4119 , With Hub , Devised Wake
KQ With Viscous Correction

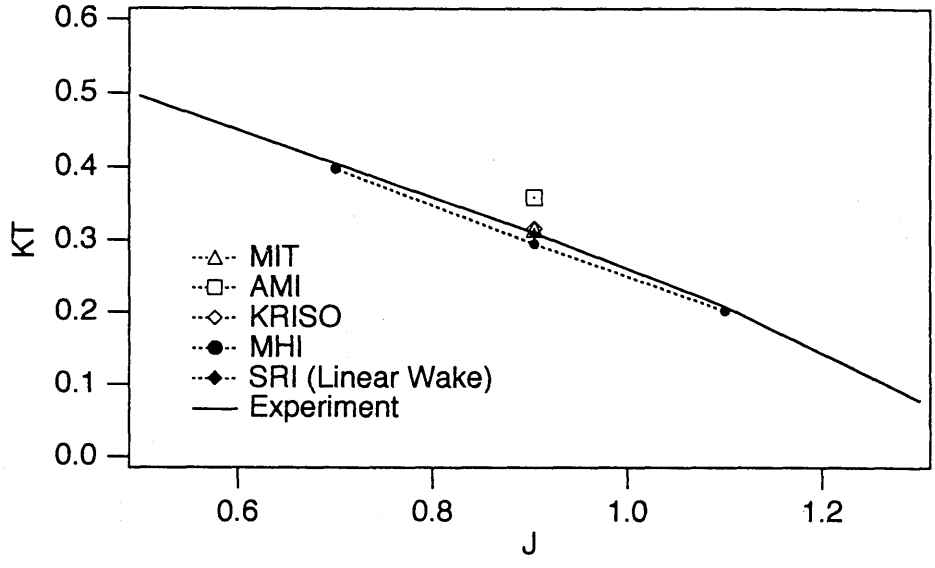

Fig. 1.5.1 (a) Case H , DTRC4842 , With Hub , Devised Wake
KT Without Viscous Correction

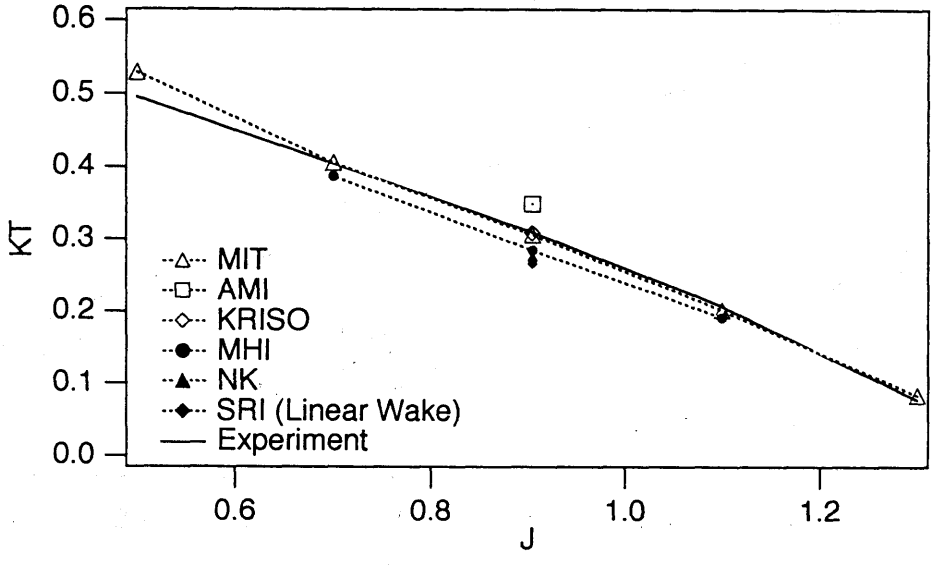

Fig. 1.5.1 (b) Case H , DTRC4842 , With Hub , Devised Wake
KT With Viscous Correction

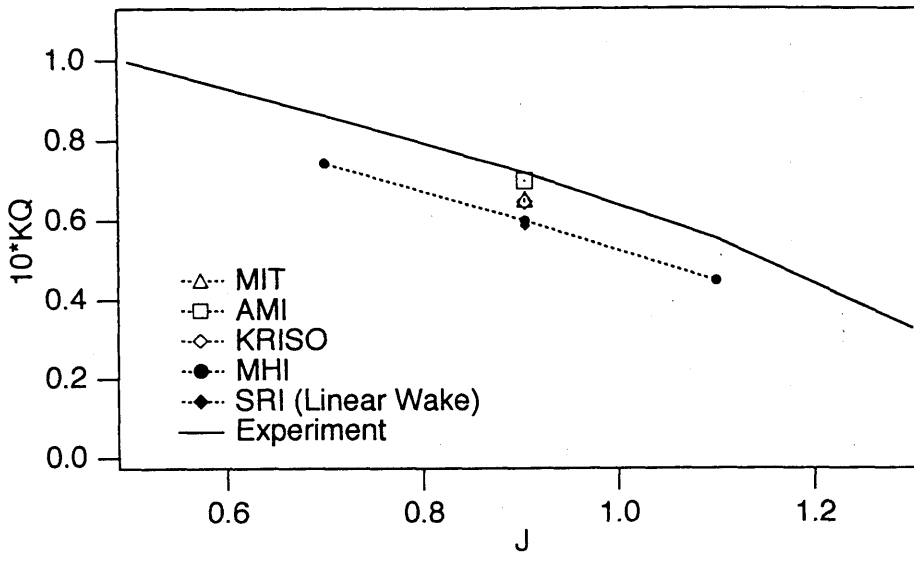

Fig. 1.5.1 (c) Case H , DTRC4842 , With Hub , Devised Wake
KQ Without Viscous Correction

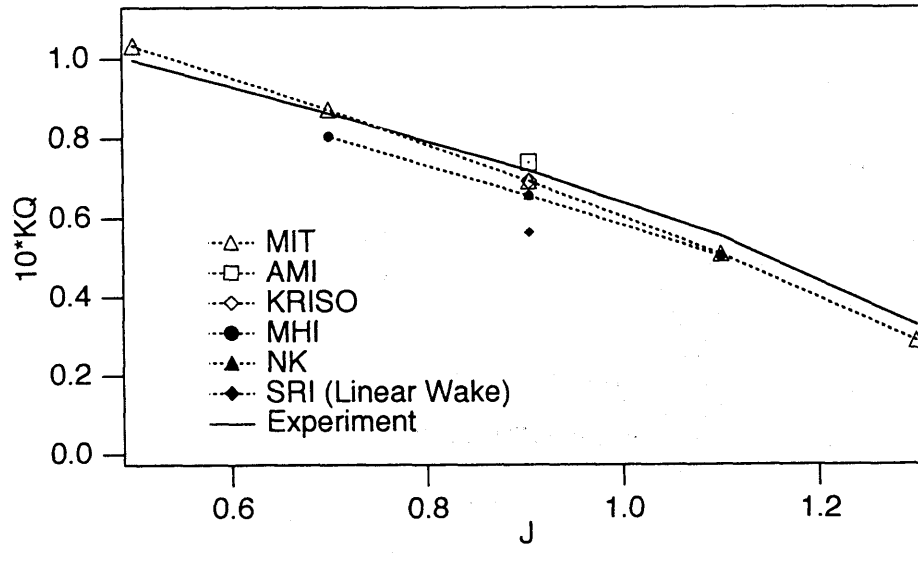

Fig.1.5.1(d) Case H , DTRC4842 , With Hub , Devised Wake
KQ With Viscous Correction

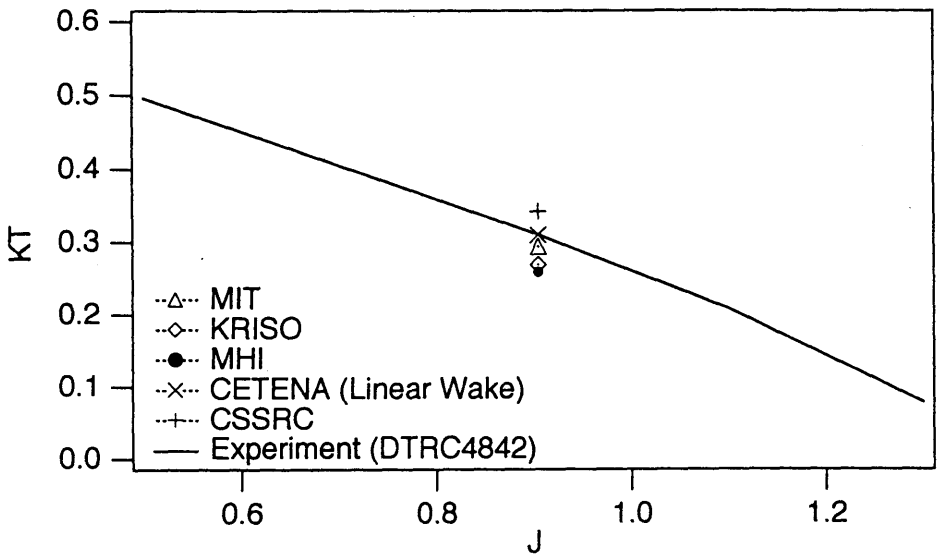

Fig.1.6.1(a) Case I , DTRC4842I , With Hub , Devised Wake
KT Without Viscous Correction

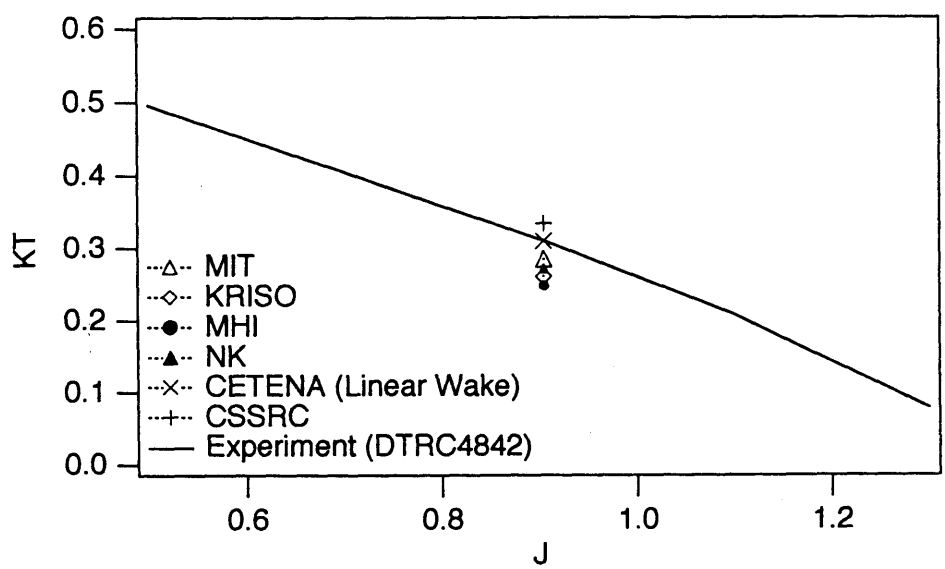

Fig.1.6.1(b) Case I , DTRC4842I , With Hub , Devised Wake
KT With Viscous Correction

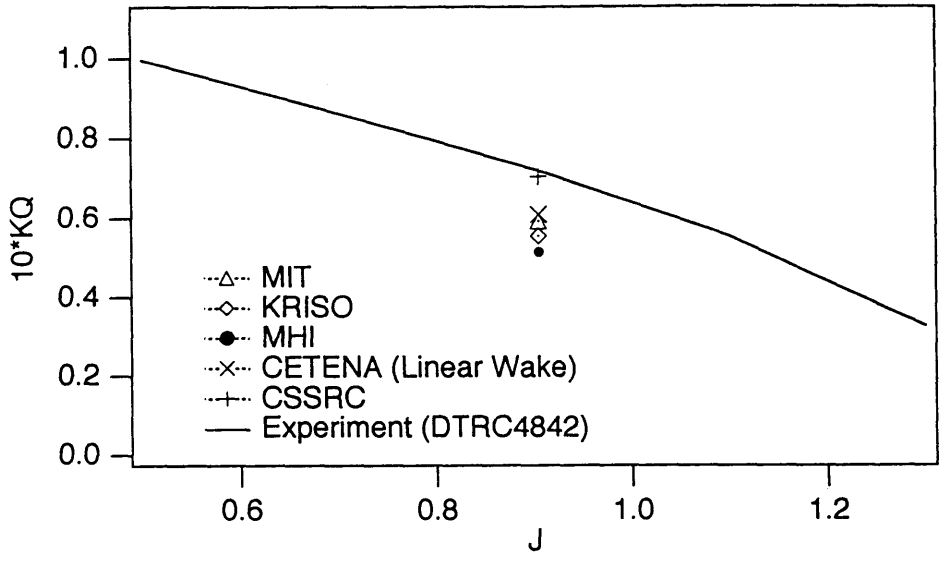

Fig.1.6.1(c) Case I , DTRC4842I , With Hub , Devised Wake
KQ Without Viscous Correction

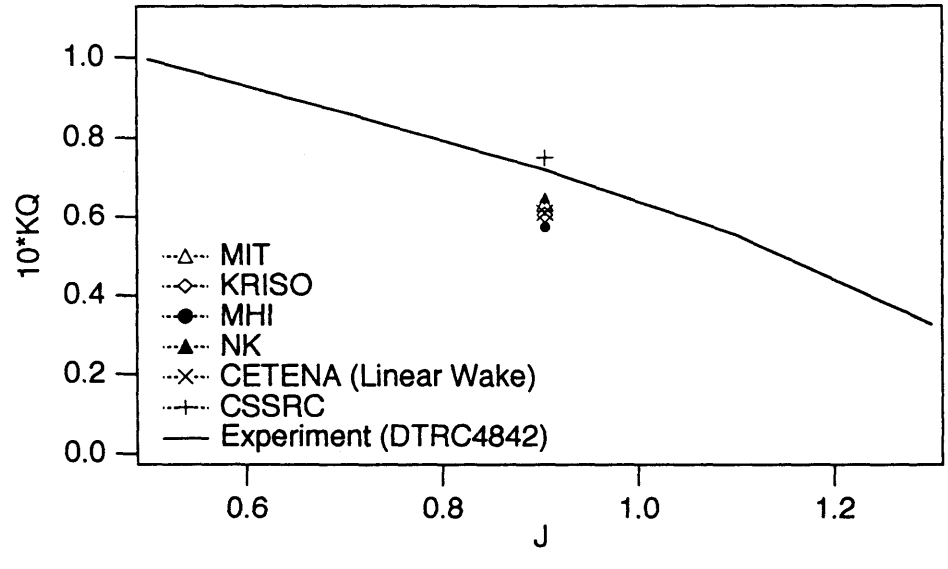

Fig.1.6.1(d) Case I , DTRC4842I , With Hub , Devised Wake
KQ With Viscous Correction

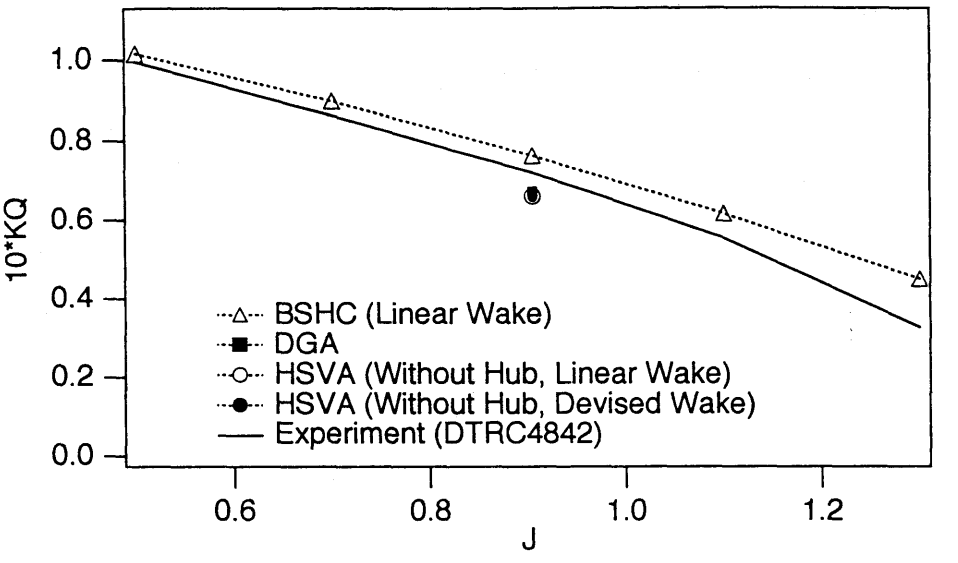

Fig.1.6.2(c) Case I , DTRC4842I , With Hub , Devised Wake
KQ Without Viscous Correction

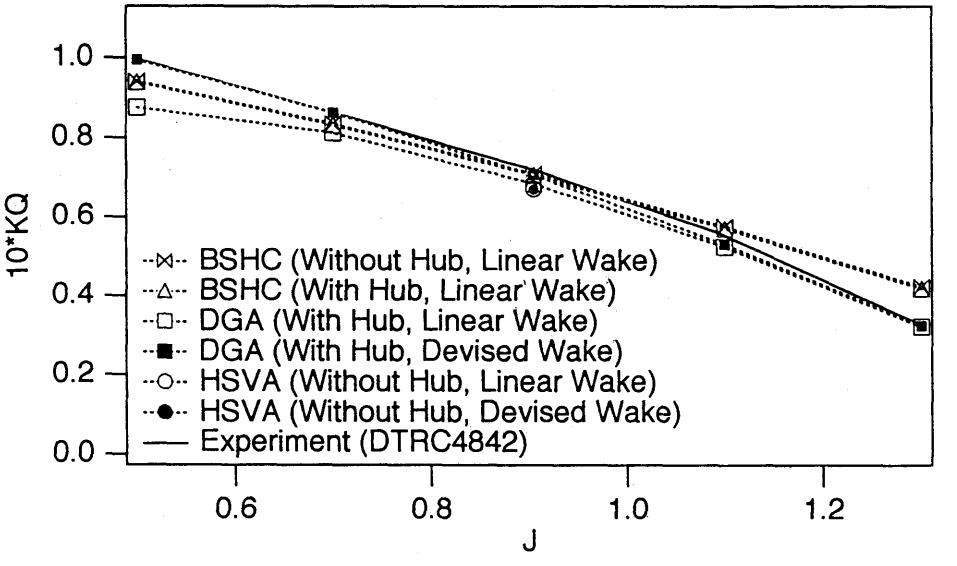

Fig.1.6.2 (d) Case I , DTRC4842I , With Hub , Devised Wake
KQ With Viscous Correction

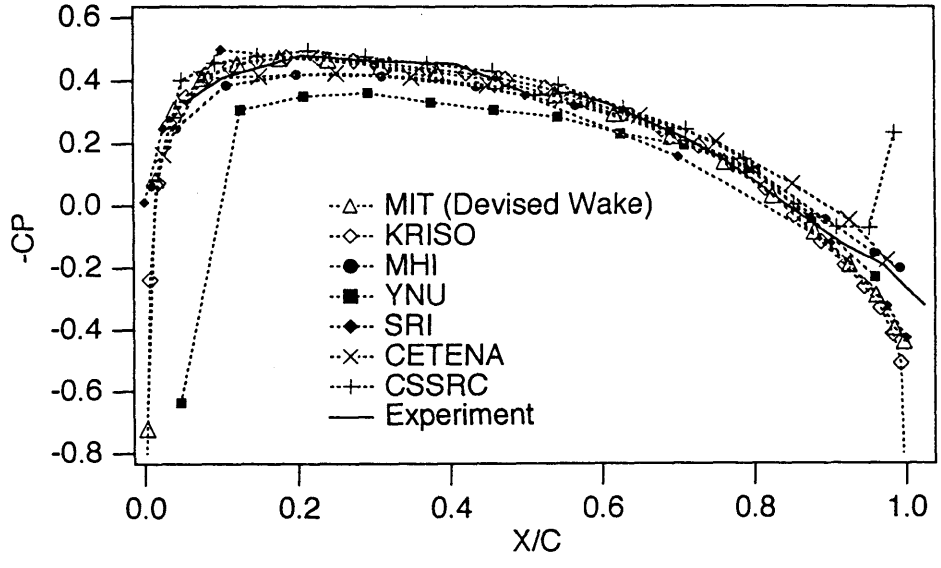

Fig.2.1.1(a) CP for Case A (DTRC4119 , J=0.833 , Without Hub , Linear Wake) on 0.3R Back

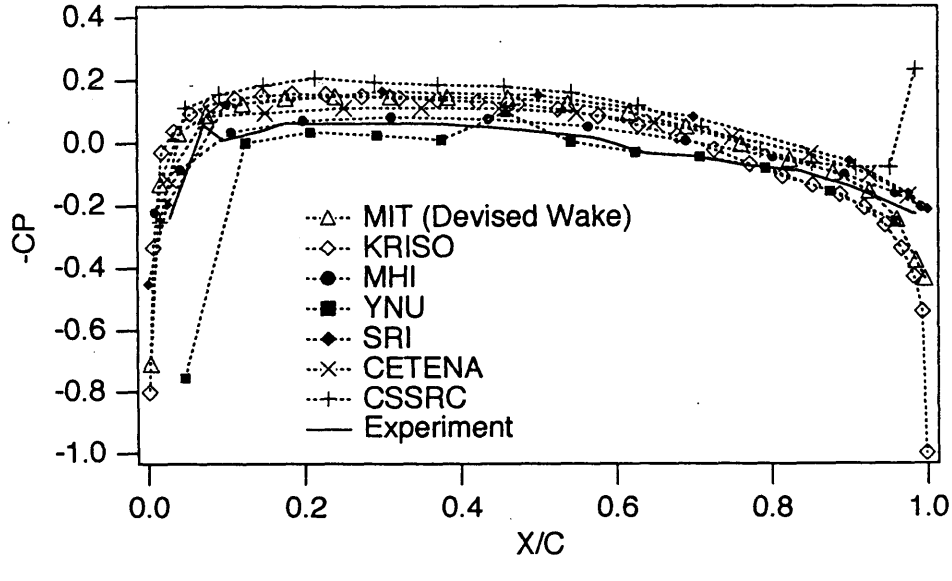

Fig.2.1.1(d) CP for Case A (DTRC4119 , J=0.833 , Without Hub , Linear Wake) on 0.3R Face

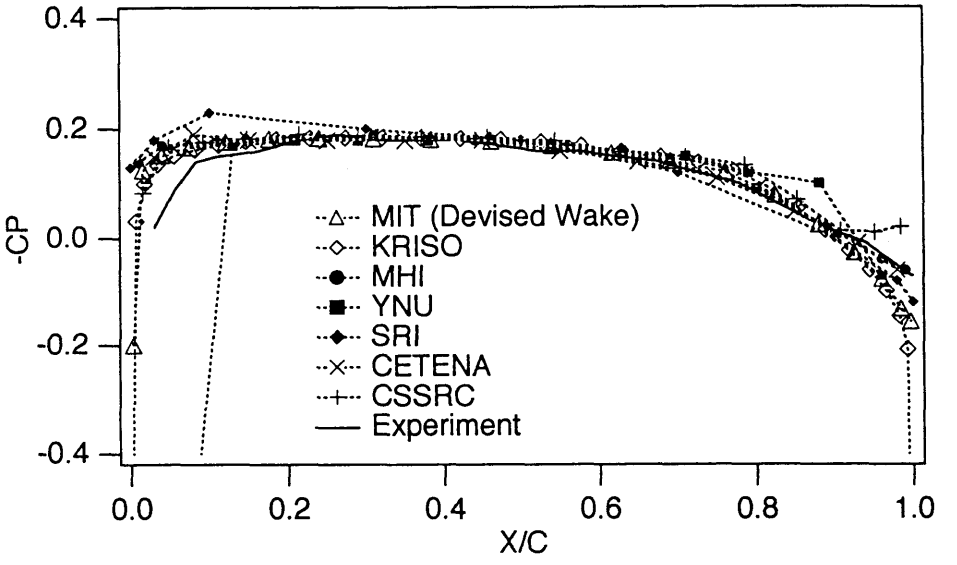

Fig.2.1.1(b) CP for Case A (DTRC4119 , J=0.833 , Without Hub , Linear Wake) on 0.7R Back

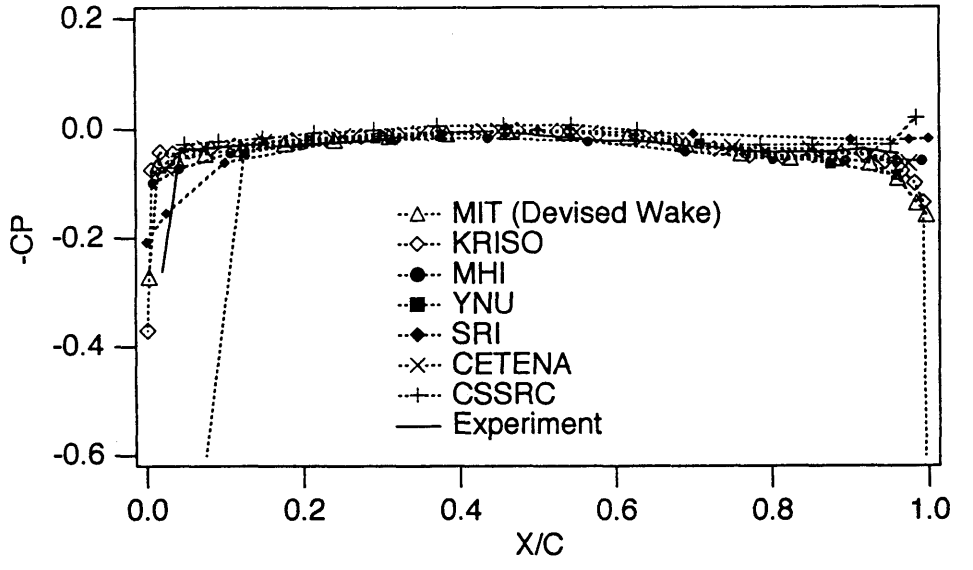

Fig.2.1.1(e) CP for Case A (DTRC4119 , J=0.833 , Without Hub , Linear Wake) on 0.7R Face

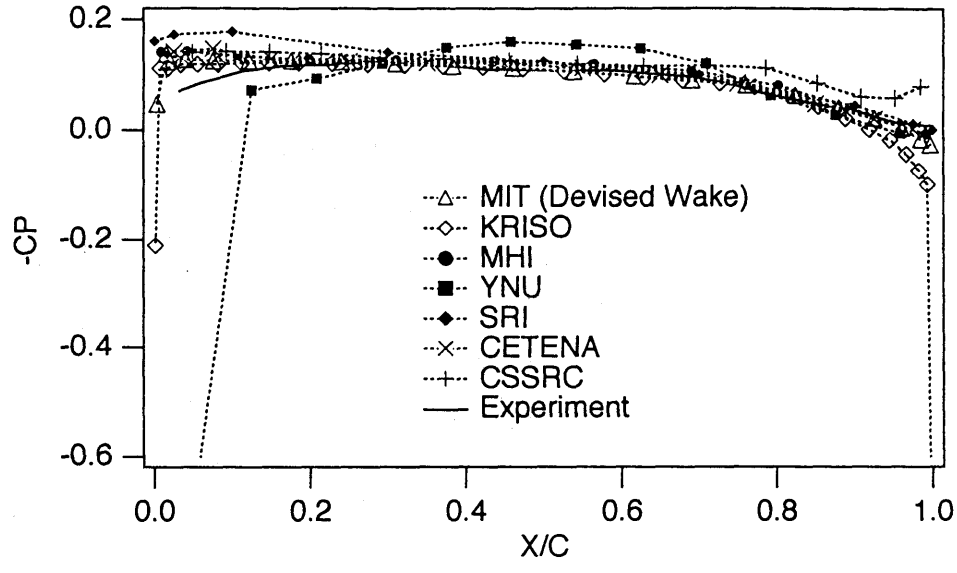

Fig.2.1.1(c) CP for Case A (DTRC4119 , J=0.833 , Without Hub , Linear Wake) on 0.9R Back

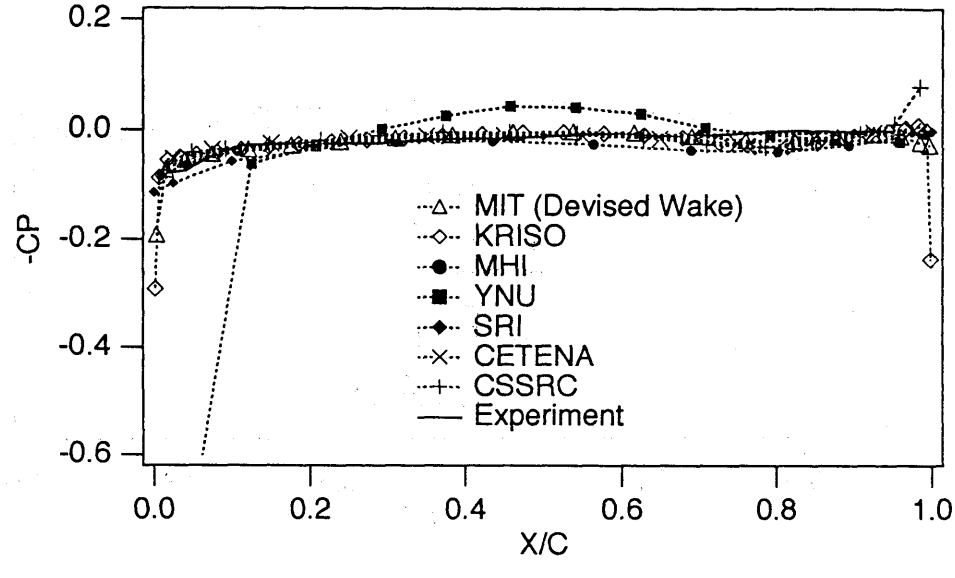

Fig.2.1.1(f) CP for Case A (DTRC4119 , J=0.833 , Without Hub , Linear Wake) on 0.9R Face

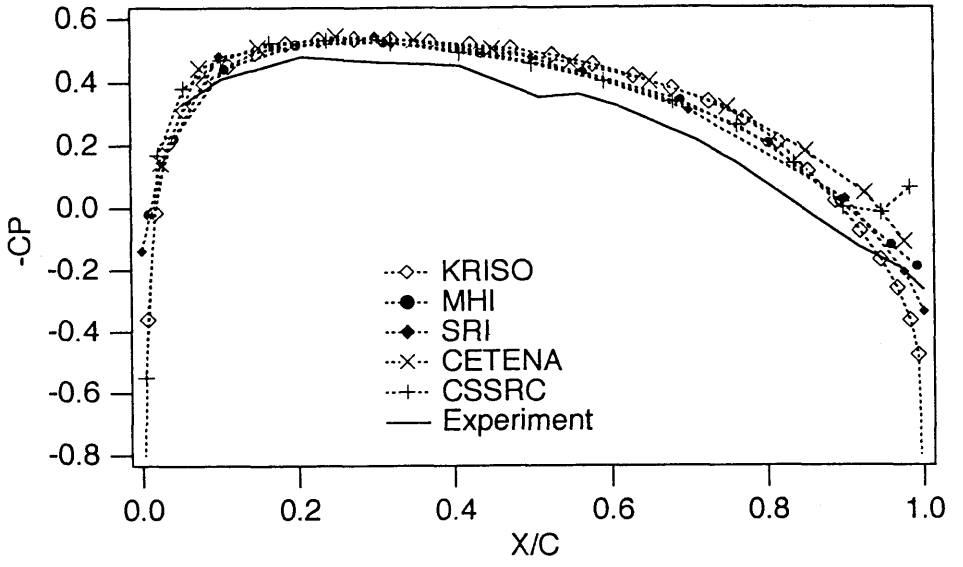

Fig.2.2.1(a) CP for Case C (DTRC4119, J=0.833, With Hub, Linear Wake) on 0.3R Back

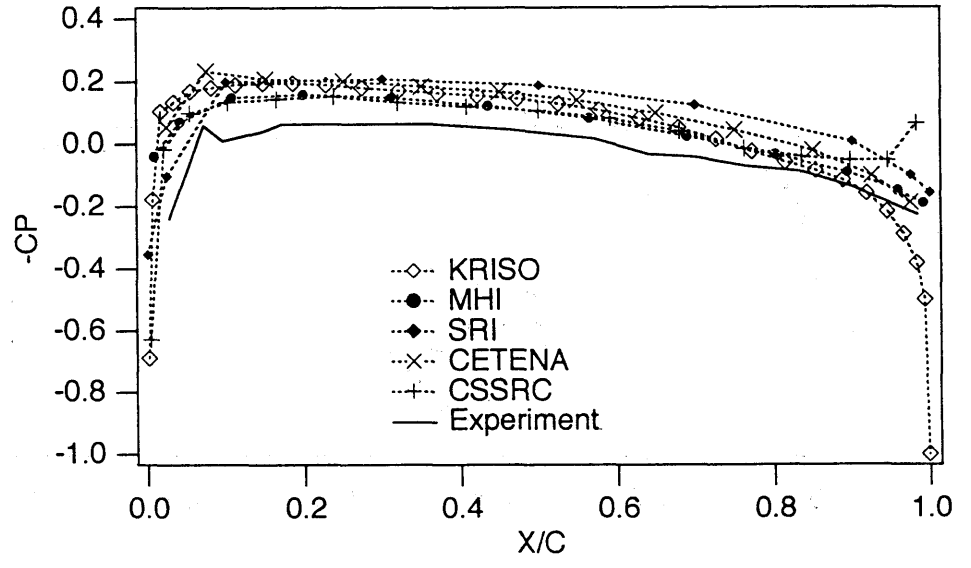

Fig.2.2.1(d) CP for Case C (DTRC4119, J=0.833, With Hub, Linear Wake) on 0.3R Face

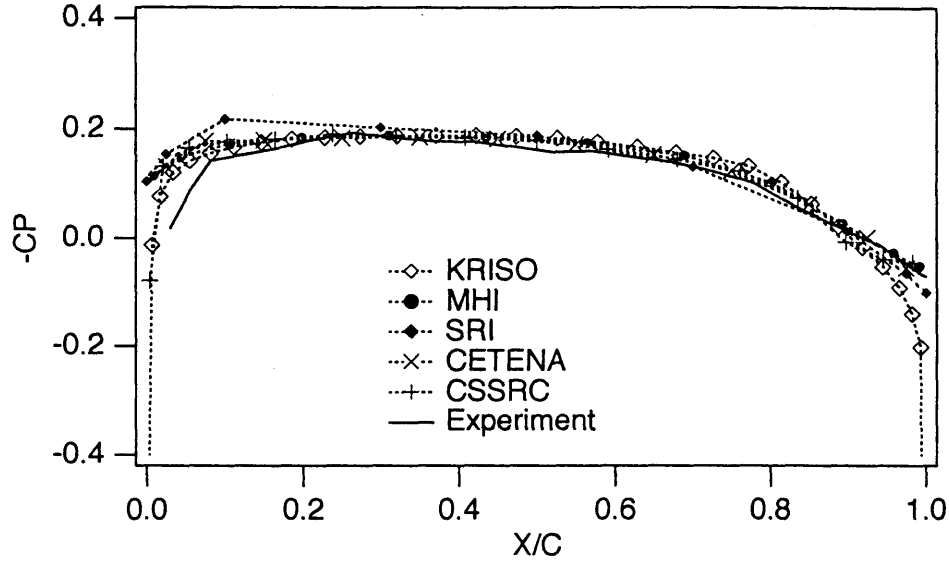

Fig.2.2.1(b) CP for Case C (DTRC4119, J=0.833, With Hub, Linear Wake) on 0.7R Back

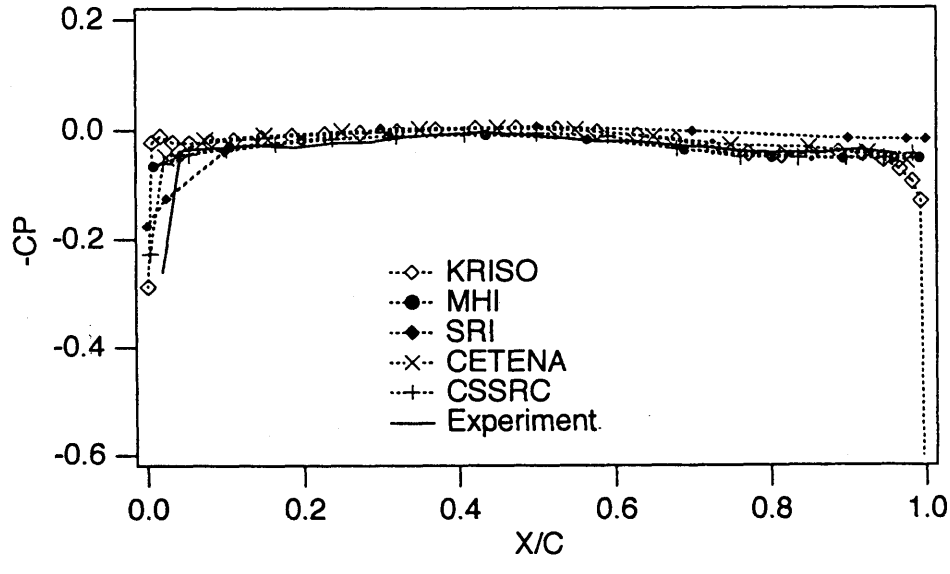

Fig.2.2.1(e) CP for Case C (DTRC4119, J=0.833, With Hub, Linear Wake) on 0.7R Face

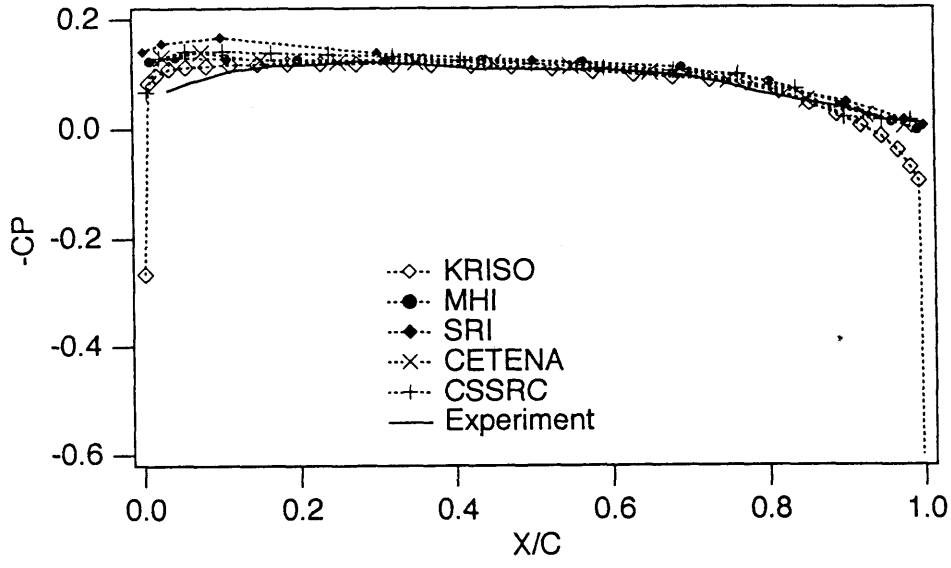

Fig.2.2.1(c) CP for Case C (DTRC4119, J=0.833, With Hub, Linear Wake) on 0.9R Back

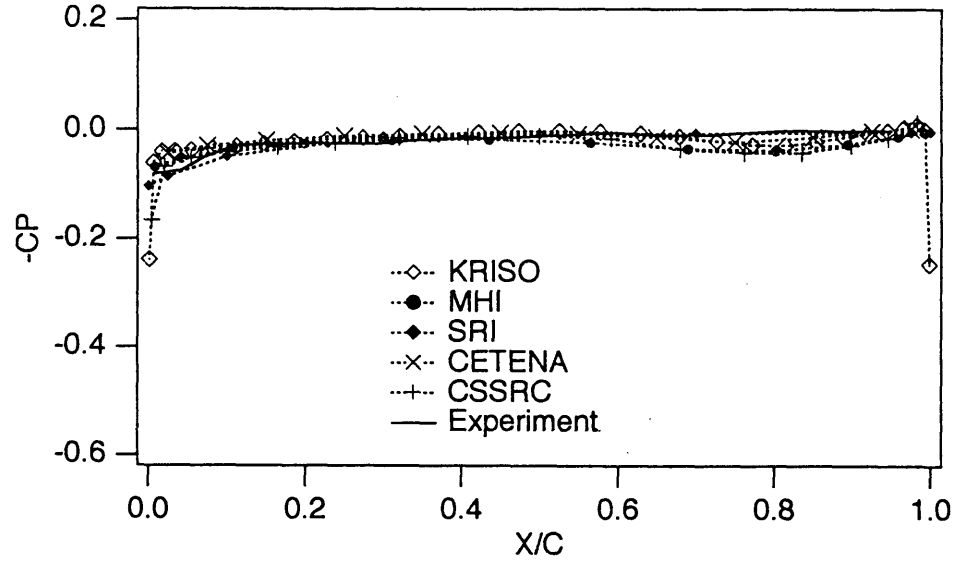

Fig.2.2.1(f) CP for Case C (DTRC4119, J=0.833, With Hub, Linear Wake) on 0.9R Face

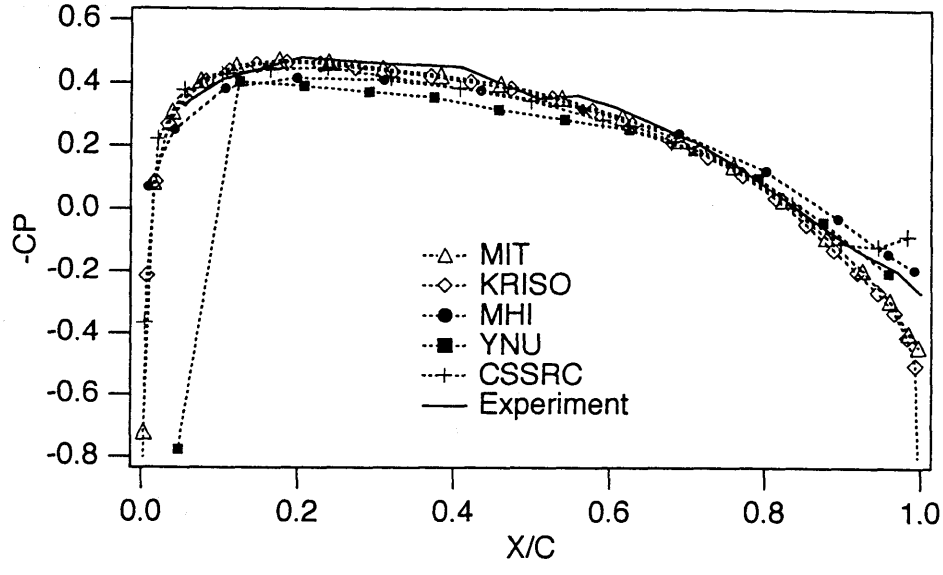

Fig.2.3.1(a) CP for Case D (DTRC4119, J=0.833, Without Hub, Devised Wake) on 0.3R Back

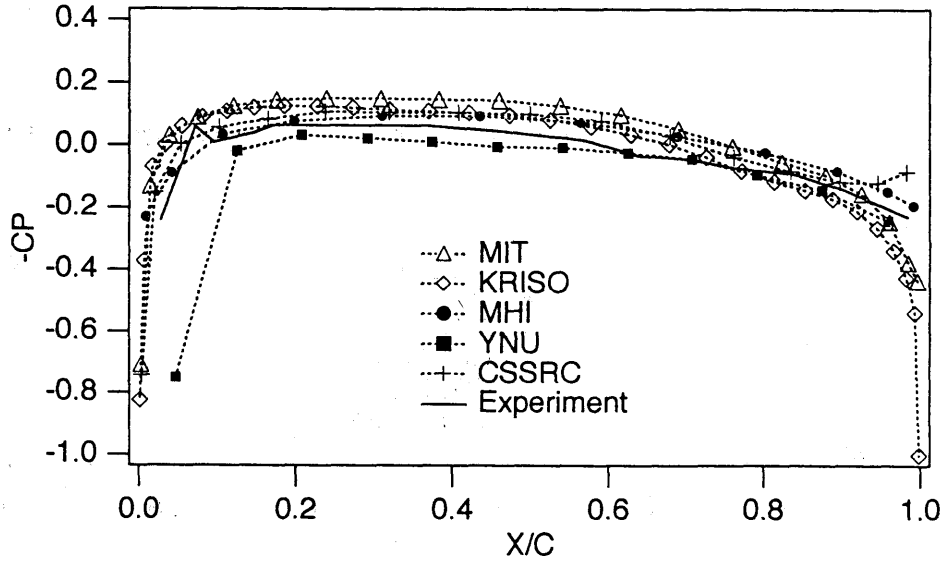

Fig.2.3.1(d) CP for Case D (DTRC4119, J=0.833, Without Hub, Devised Wake) on 0.3R Face

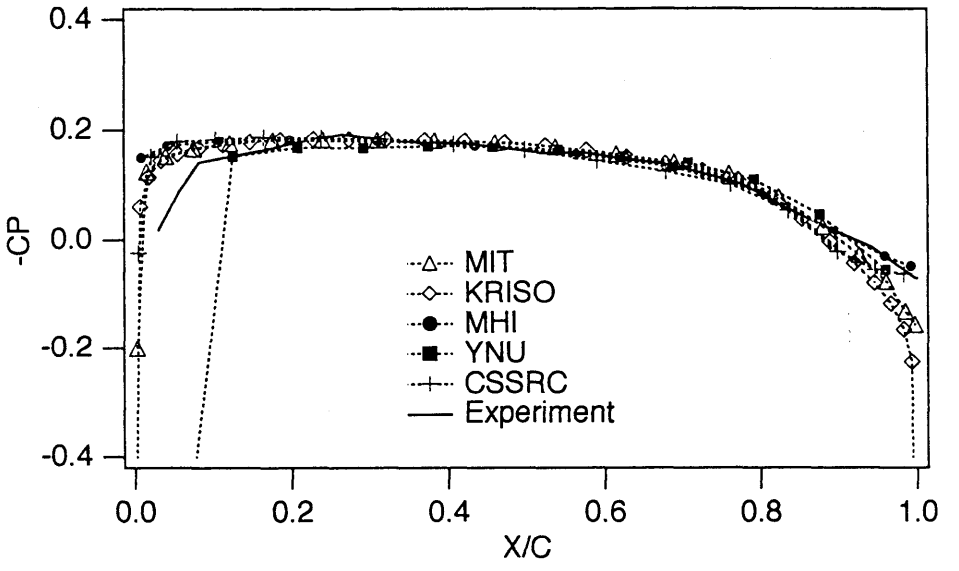

Fig.2.3.1(b) CP for Case D (DTRC4119, J=0.833, Without Hub, Devised Wake) on 0.7R Back

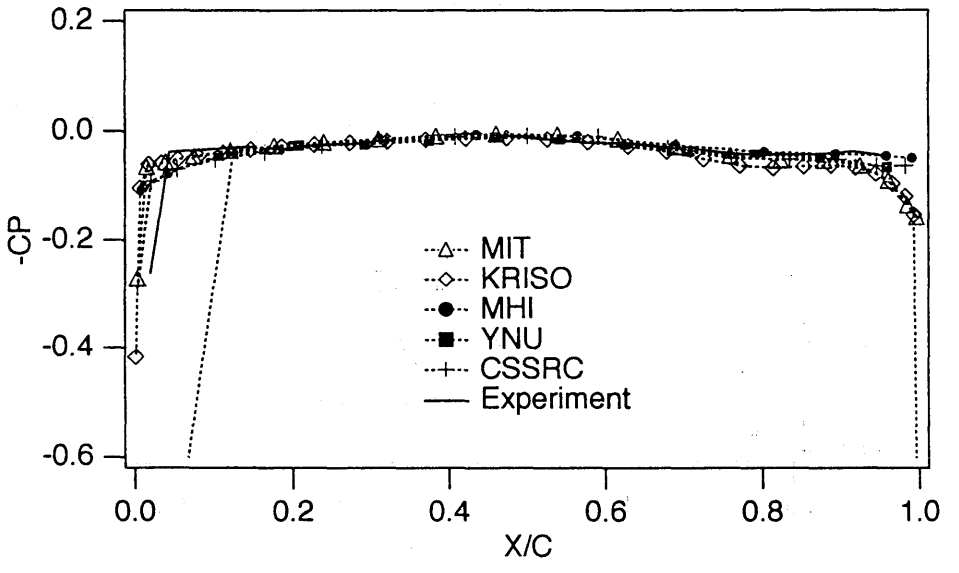

Fig.2.3.1(e) CP for Case D (DTRC4119, J=0.833, Without Hub, Devised Wake) on 0.7R Face

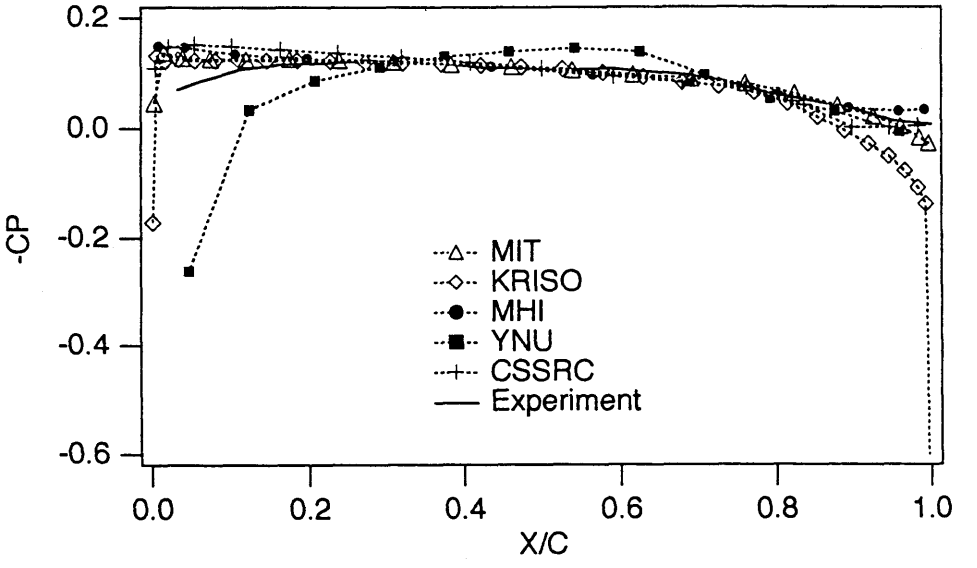

Fig.2.3.1(c) CP for Case D (DTRC4119, J=0.833, Without Hub, Devised Wake) on 0.9R Back

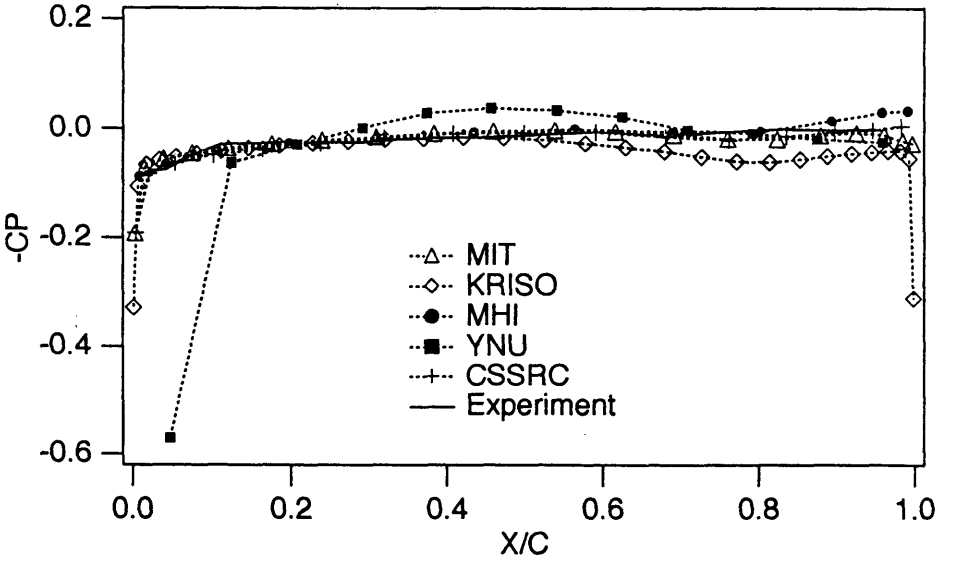

Fig.2.3.1(f) CP for Case D (DTRC4119, J=0.833, Without Hub, Devised Wake) on 0.9R Face

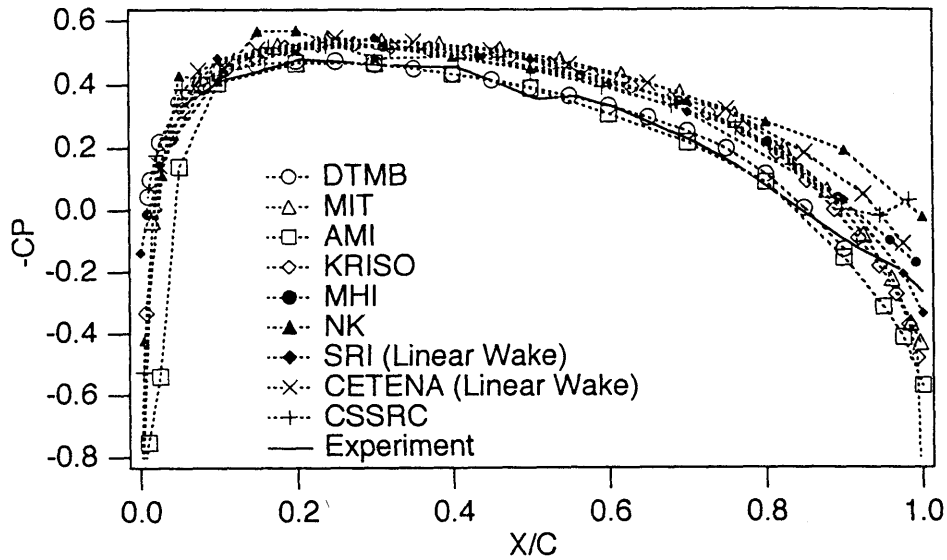

Fig.2.4.1(a) CP for Case E (DTRC4119 , J=0.833 , With Hub , Devised Wake)
0.3R Back

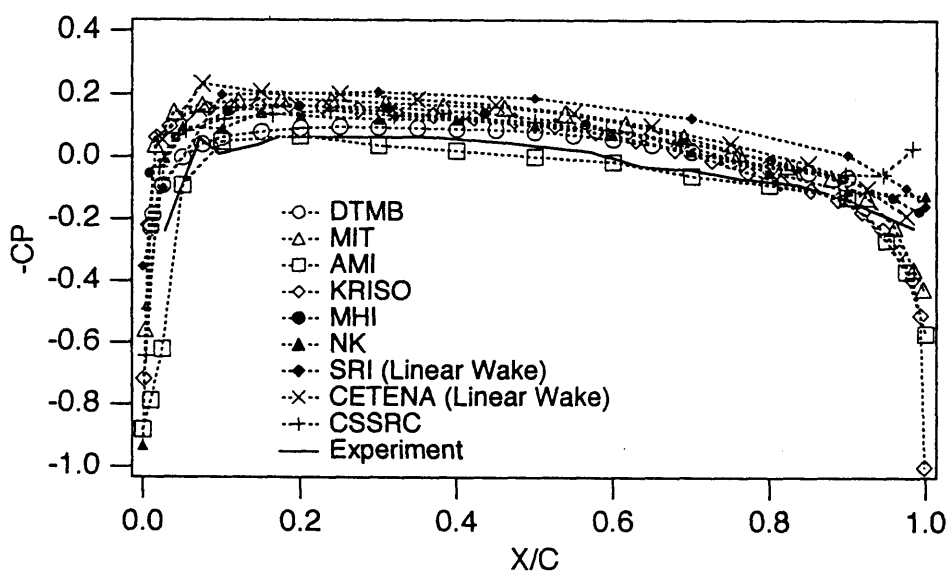

Fig.2.4.1(d) CP for Case E (DTRC4119 , J=0.833 , With Hub , Devised Wake)
on 0.3R Face

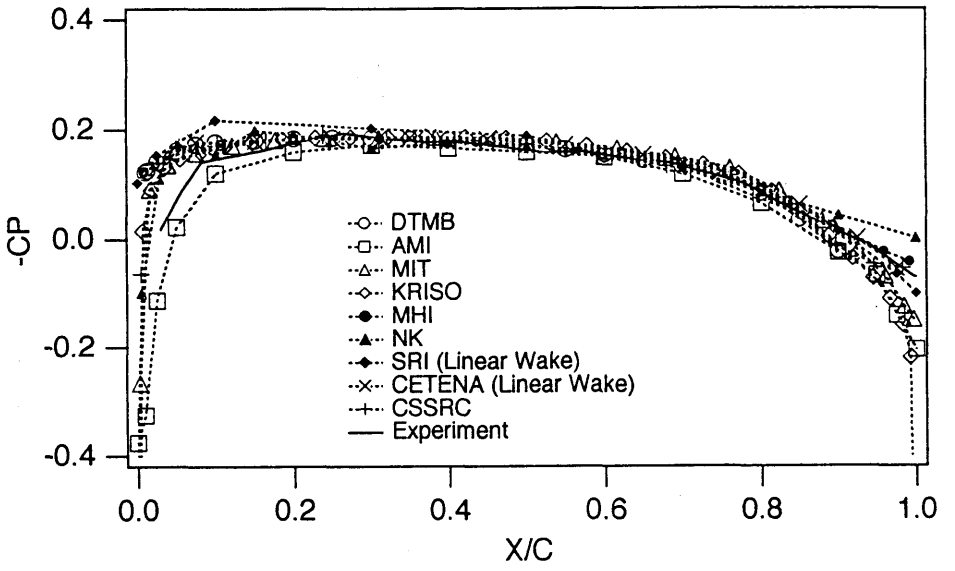

Fig.2.4.1(b) CP for Case E (DTRC4119, J=0.833 , With Hub , Devised Wake) on 0.7R Back

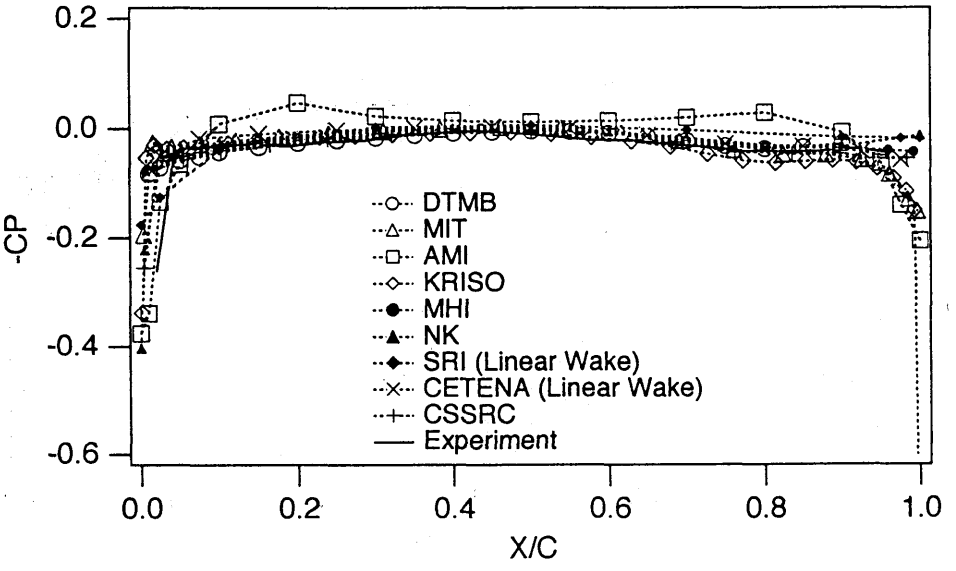

Fig.2.4.1(e) CP for Case E (DTRC4119 , J=0.833 , With Hub , Devised Wake) on 0.7R Face

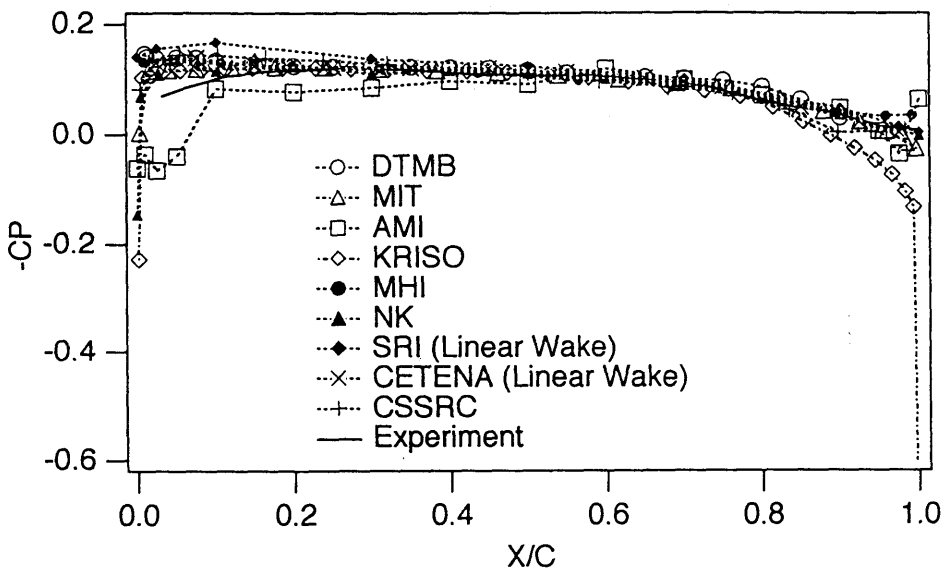

Fig.2.4.1(c) CP for Case E (DTRC4119 , J=0.833 , With Hub , Devised Wake) on 0.9R Back

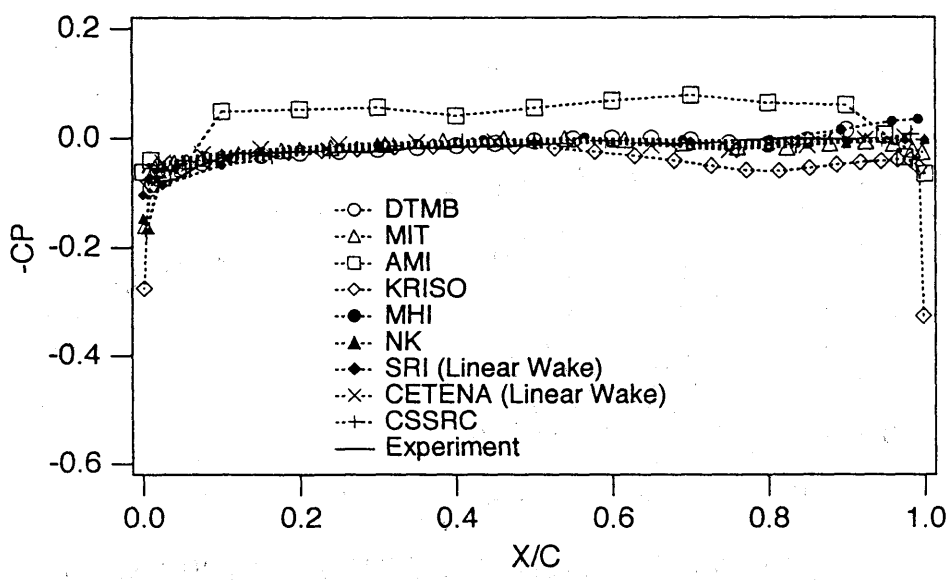

Fig.2.4.1(f) CP for Case E (DTRC4119 , J=0.833 , With Hub , Devised Wake) on 0.9R Face

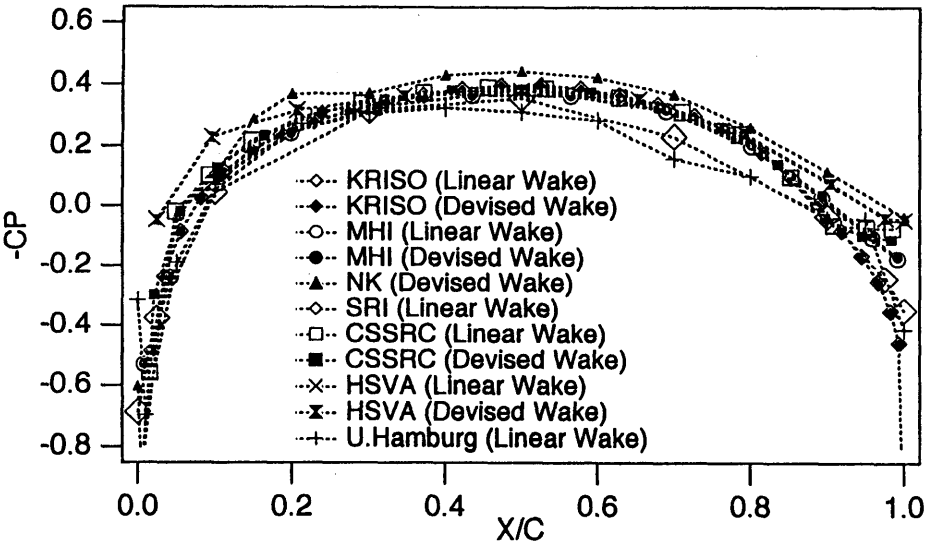

Fig.2.5.1(a) CP for CaseF,G (DTRC4119, J=1.1, Without Hub) on 0.3R Back

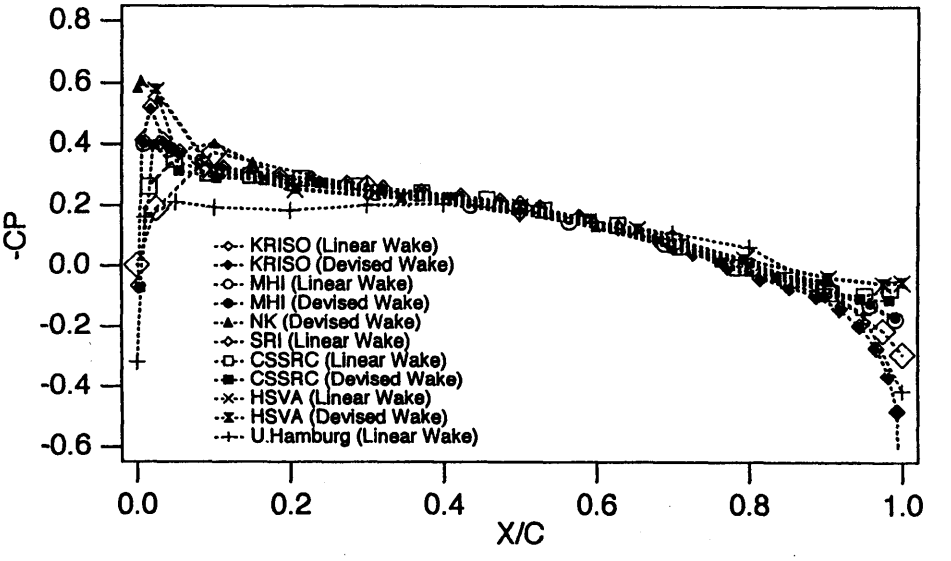

Fig.2.5.1(d) CP for CaseF,G (DTRC4119, J=1.1, Without Hub) on 0.3R Face

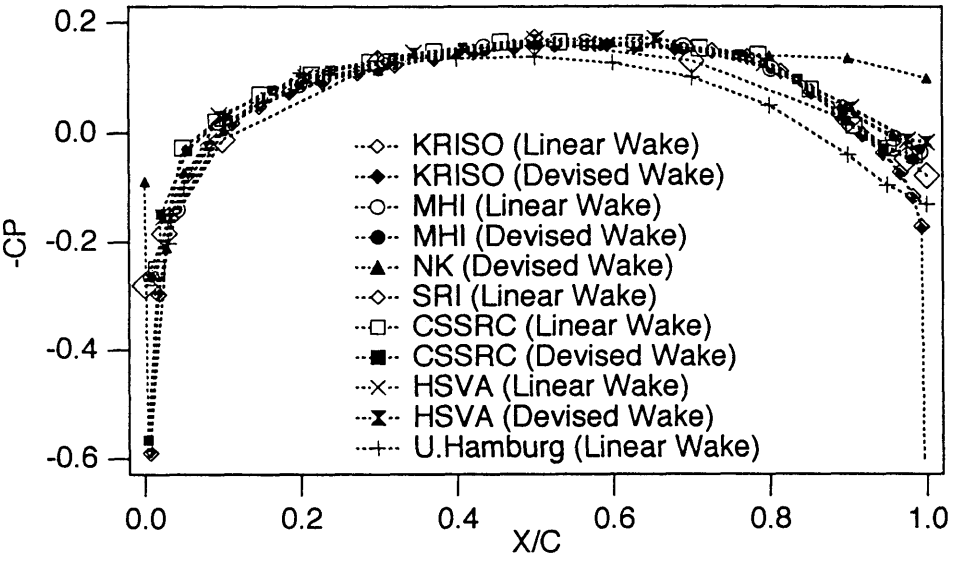

Fig.2.5.1(b) CP for CaseF,G (DTRC4119, J=1.1, Without Hub) on 0.7R Back

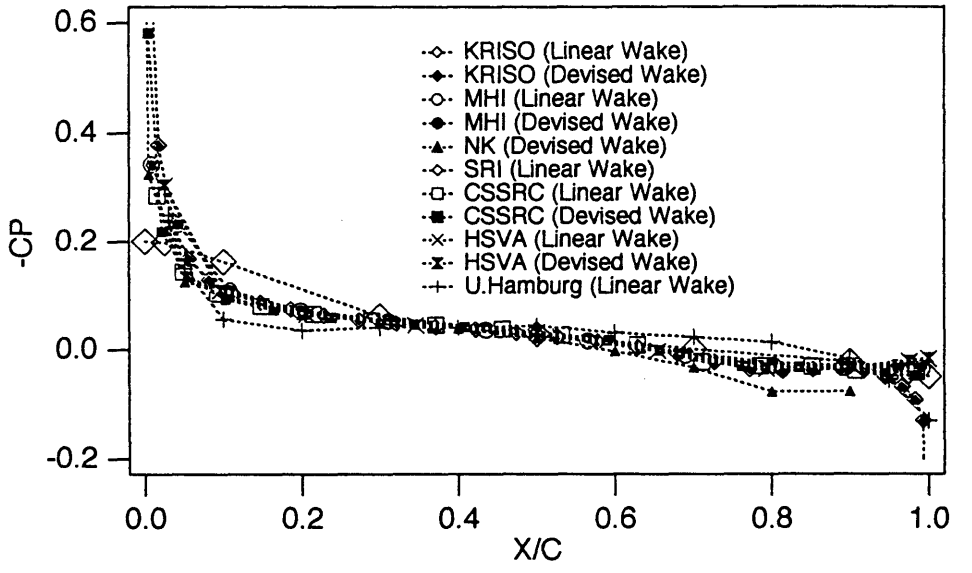

Fig.2.5.1(e) CP for CaseF,G (DTRC4119, J=1.1, Without Hub) on 0.7R Face

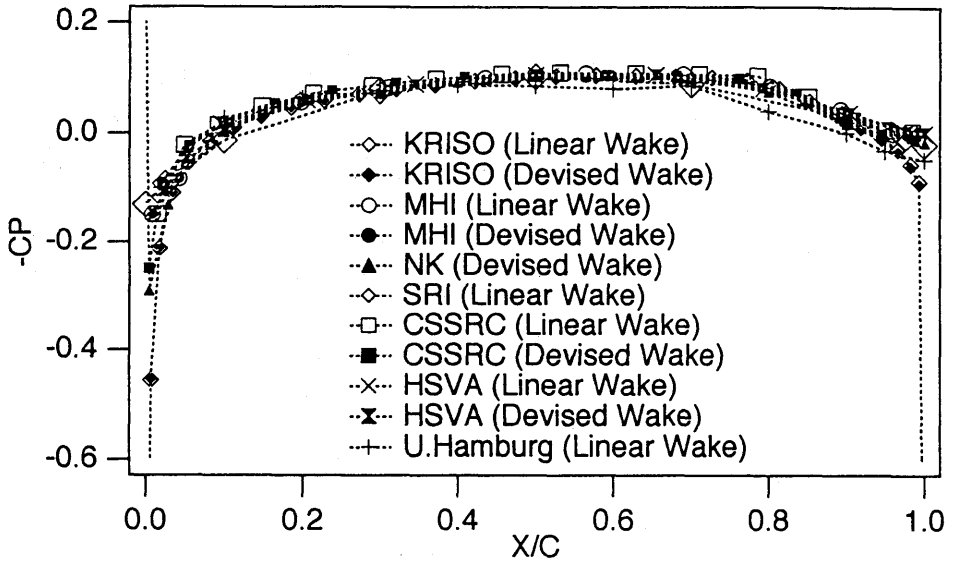

Fig.2.5.1(c) CP for CaseF,G (DTRC4119, J=1.1, Without Hub) on 0.9R Back

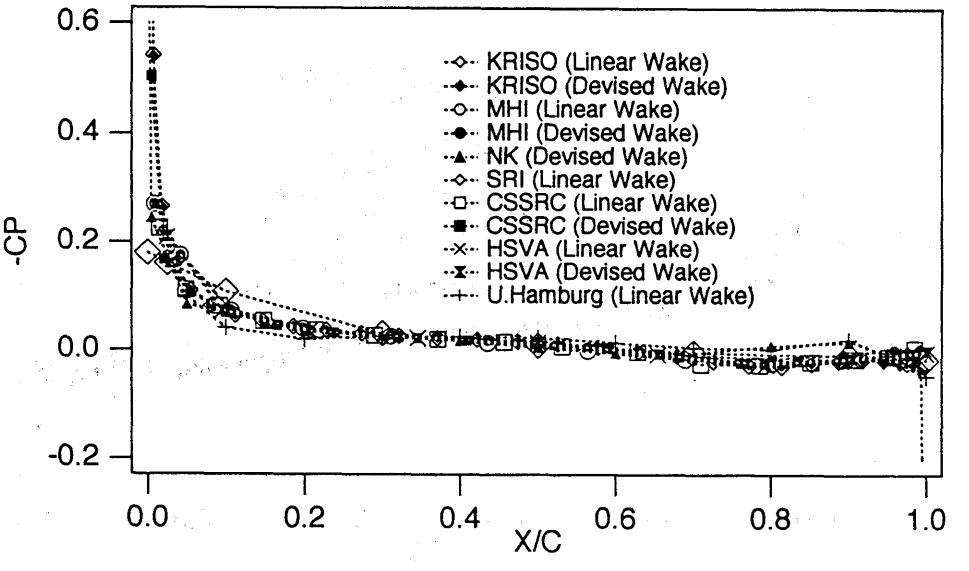

Fig.2.5.1(f) CP for CaseF,G (DTRC4119, J=1.1, Without Hub) on 0.9R Face

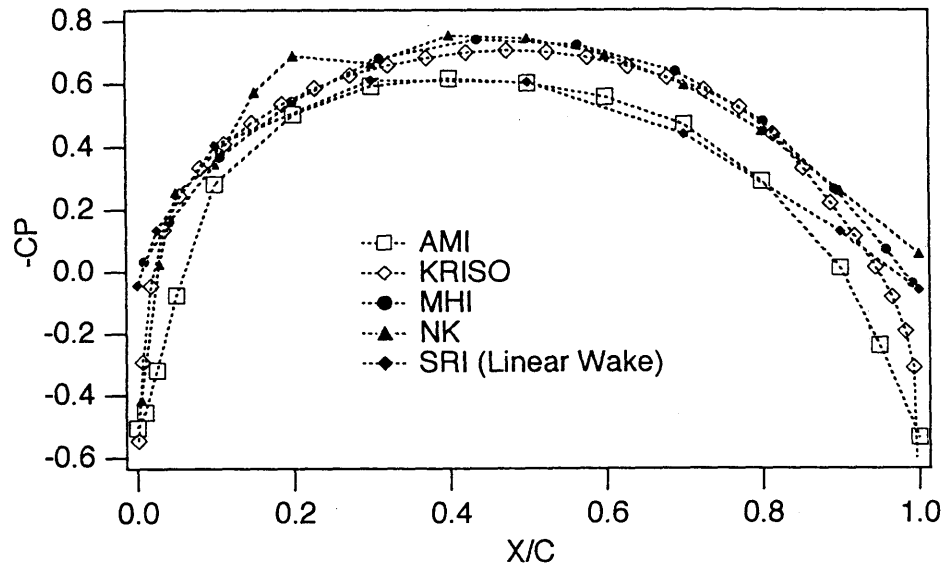

Fig.2.6.1(a) CP for Case H (DTRC4842 , J=0.905 , With Hub , Devised Wake)
0.4R Back

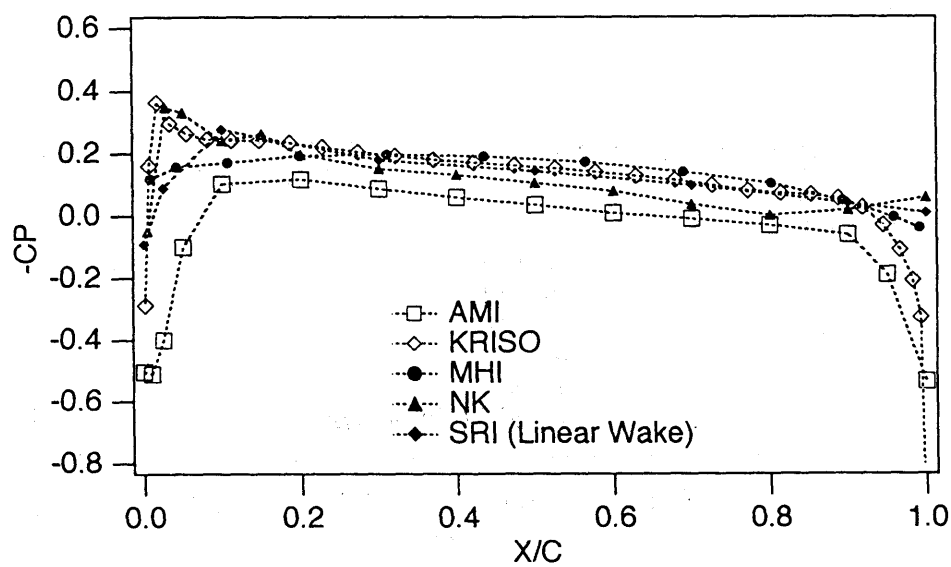

Fig.2.6.1(d) CP for Case H , DTRC4842 , J=0.905 , With Hub , Devised Wake)
0.4R Face

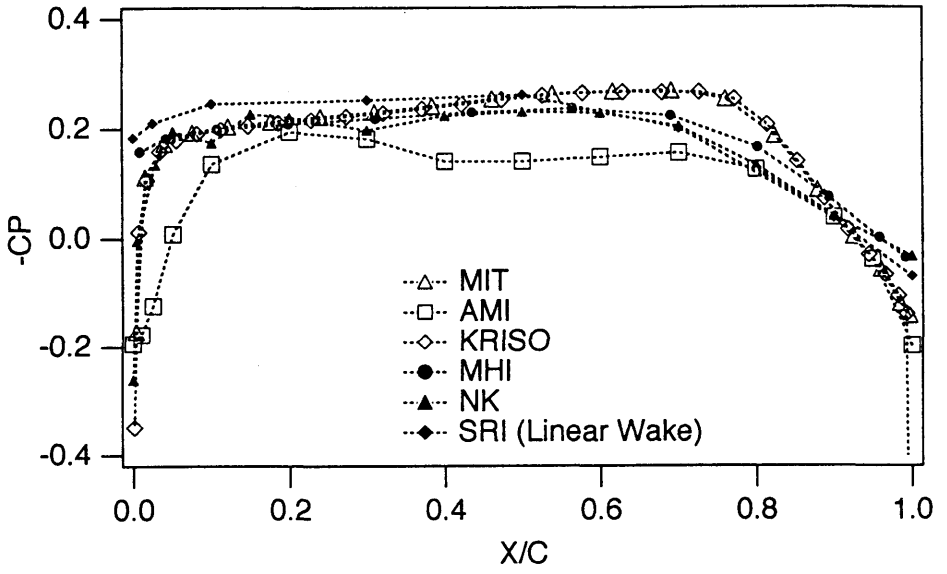

Fig.2.6.1(b) CP for Case H (DTRC4842 , J=0.905 , With Hub , Devised Wake)
0.7R Back

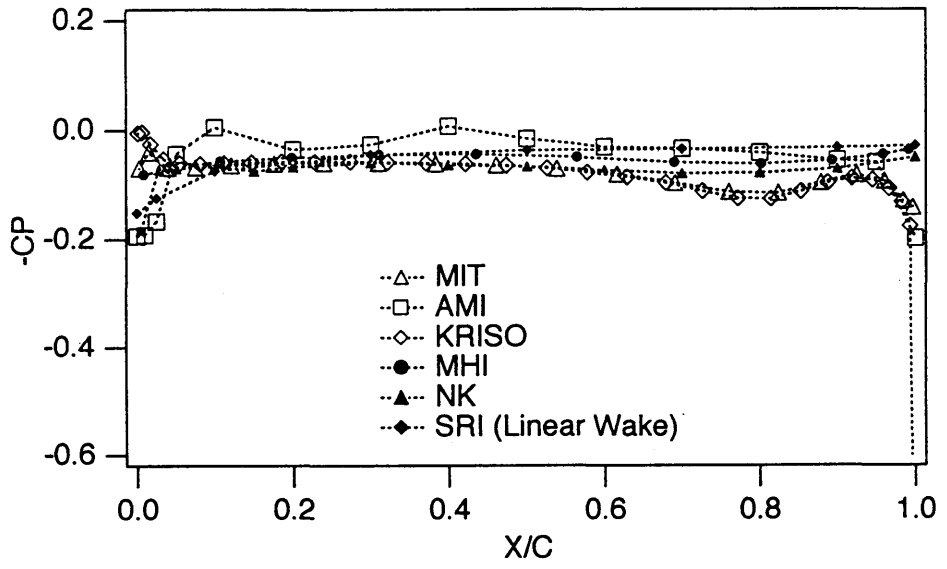

Fig.2.6.1(e) CP for Case H (DTRC4842 , J=0.905 , With Hub , Devised Wake)
0.7R Face

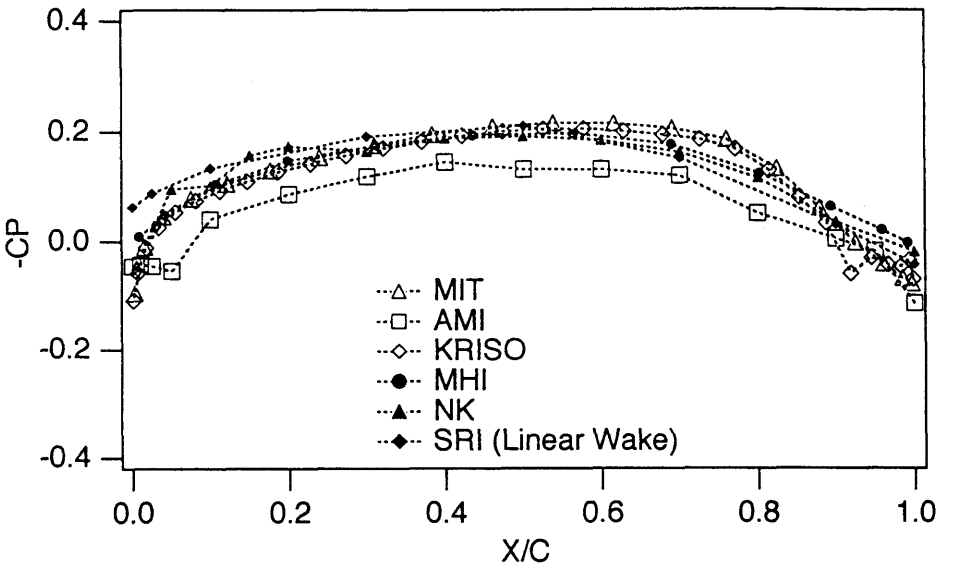

Fig.2.6.1(c) CP for Case H (DTRC4842 , J=0.905 , With Hub , Devised Wake)
0.9R Back

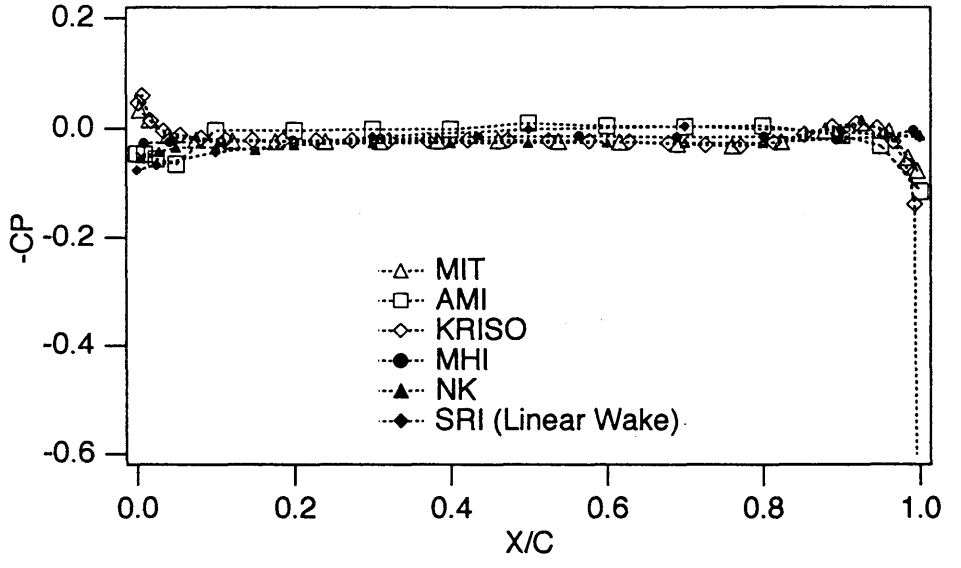

Fig.2.6.1(f)CP for Case H (DTRC4842 , J=0.905 , With Hub , Devised Wake)
0.9R Face

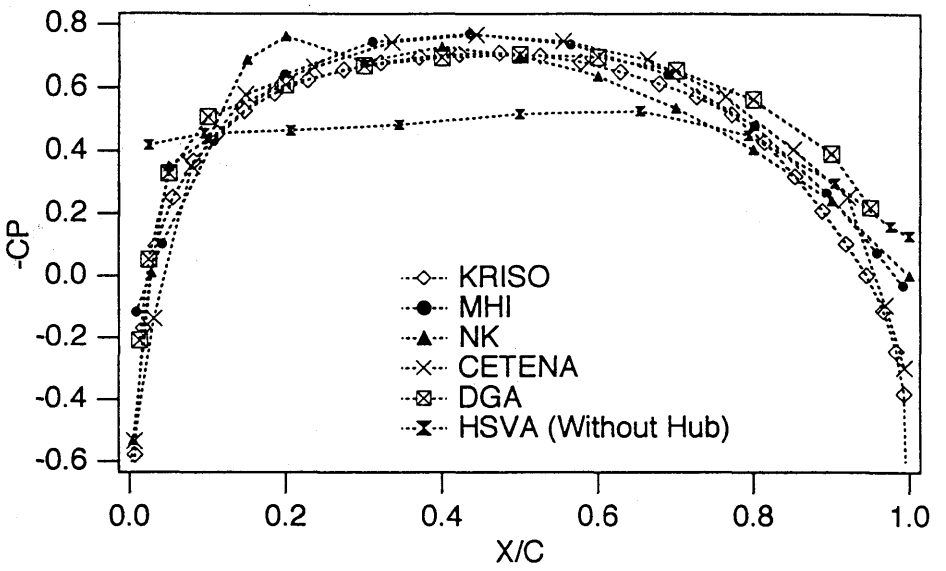

Fig.2.7.1(a) CP for Case I (DTRC4842I , J=0.905 , With Hub , Devised Wake)
0.4R Back

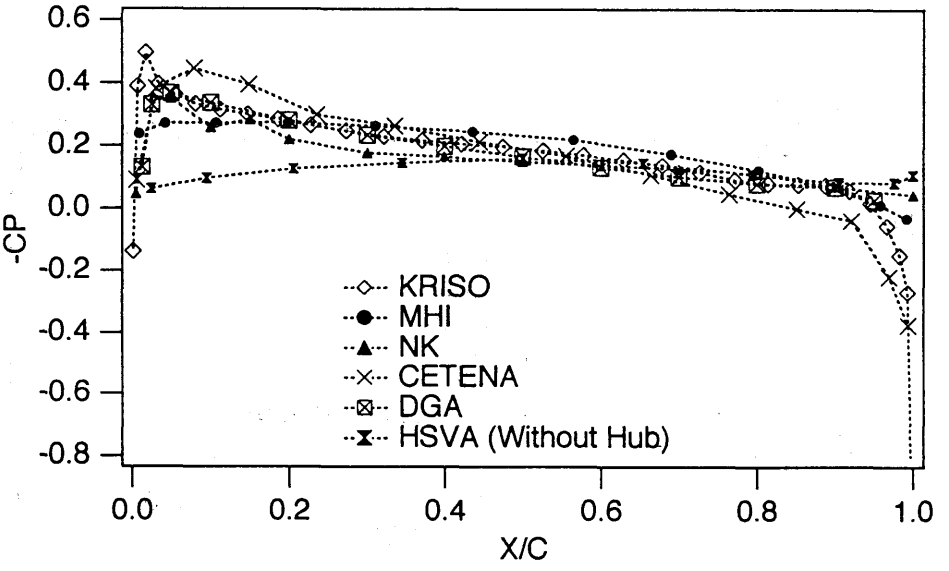

Fig.2.7.1(d) CP for Case I (DTRC4842I , J=0.905 , With Hub , Devised Wake)
0.4R Face

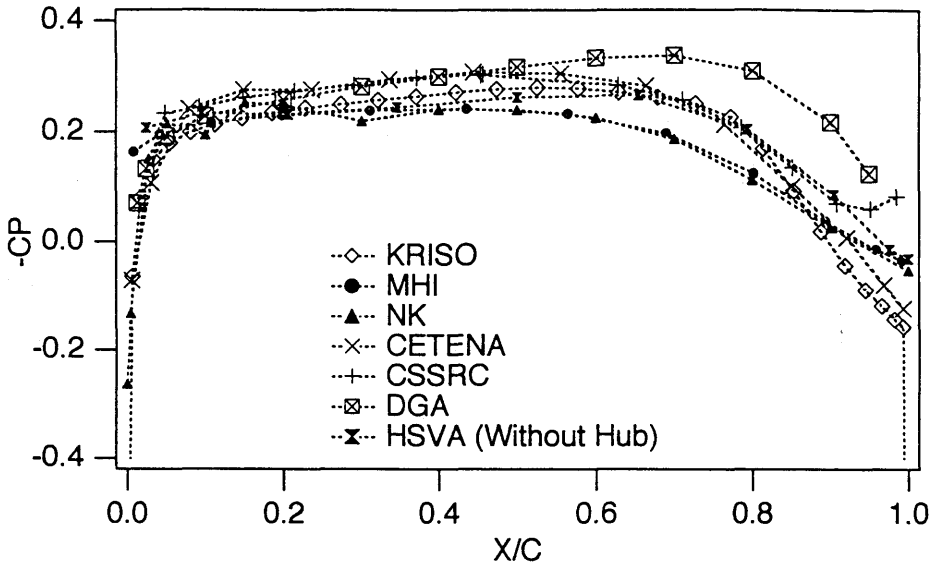

Fig.2.7.1(b) Case I (DTRC4842I , J=0.905 , With Hub , Deviced Wake)
0.7R Back

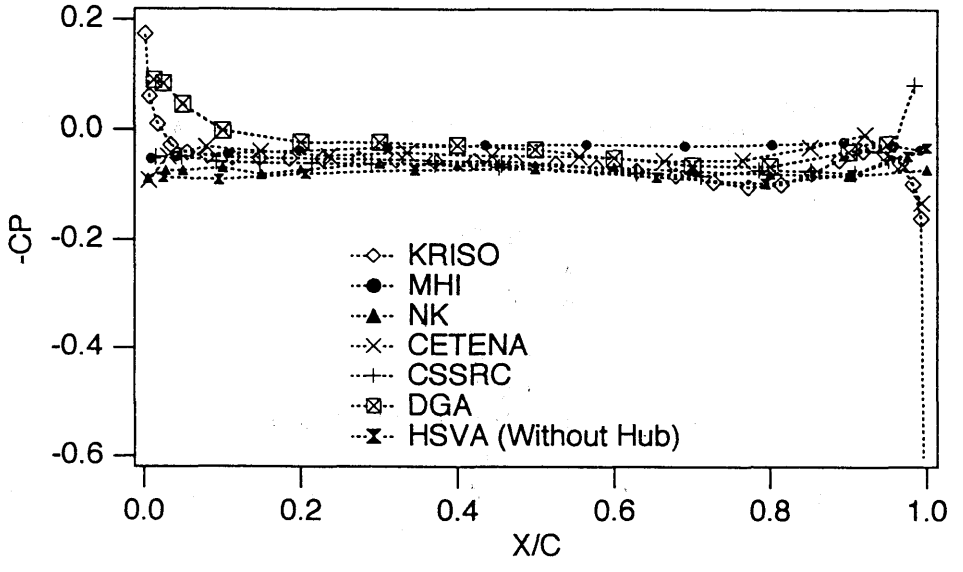

Fig.2.7.1(e) CP for Case I (DTRC4842I , J=0.905 , With Hub , Devised Wake)
0.7R Face

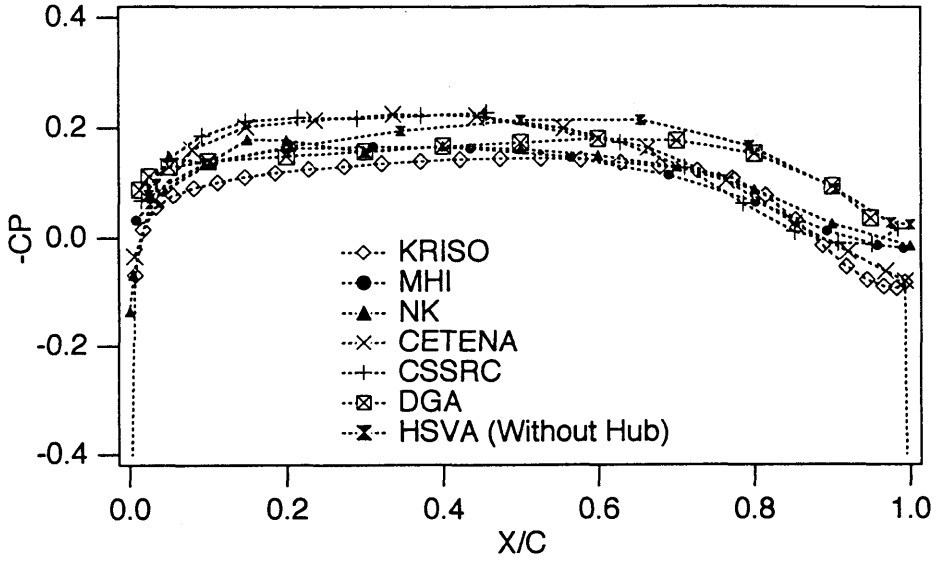

Fig.2.7.1(c) CP for Case I (DTRC4842I , J=0.905 , With Hub , Devised Wake)
0.9R Back

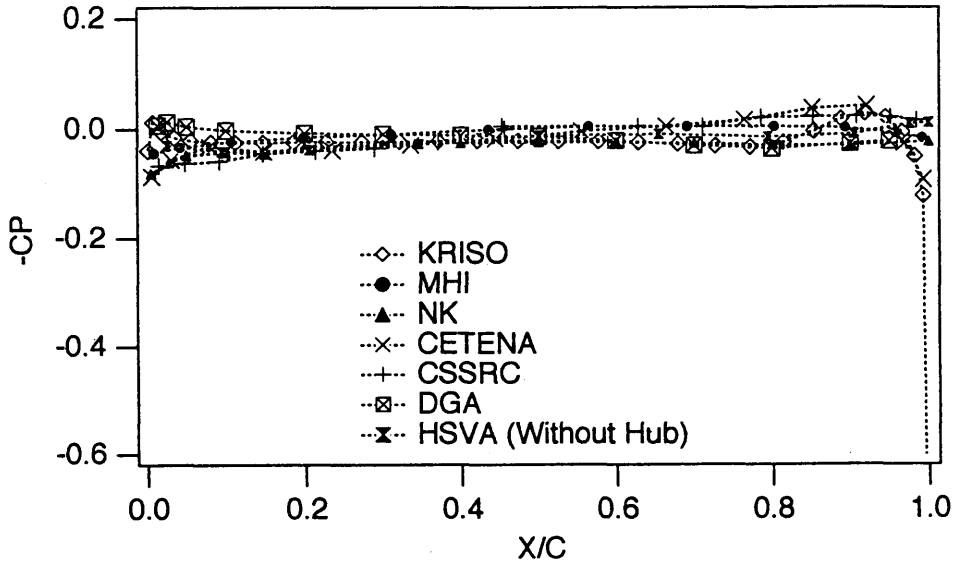

Fig.2.7.1(f) CP for Case I (DTRC4842I , J=0.905 , With Hub , Devised Wake)
0.9R Face

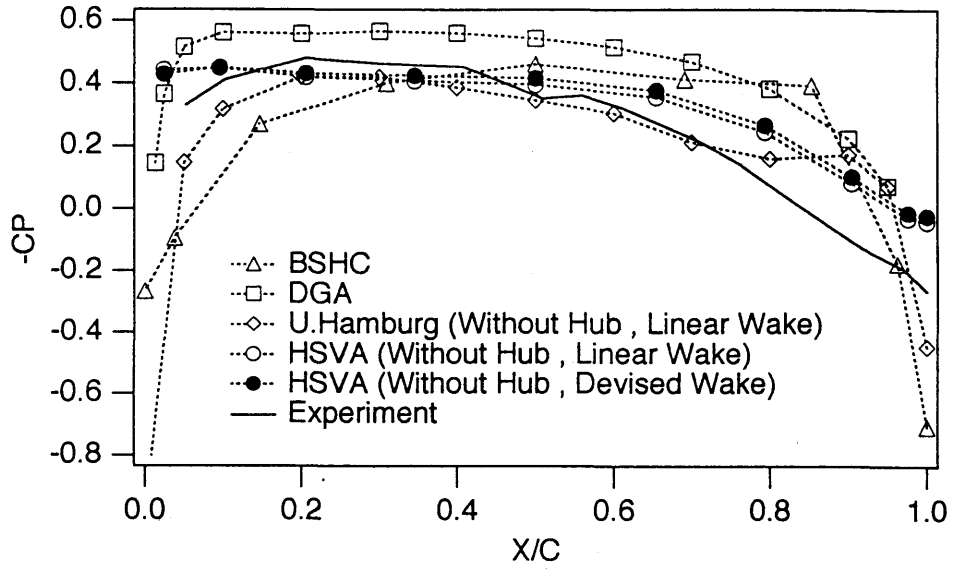

Fig.2.1.2(a) CP for Case E (DTRC4119 , J=0.833 , With Hub , Devised Wake) on 0.3R Back

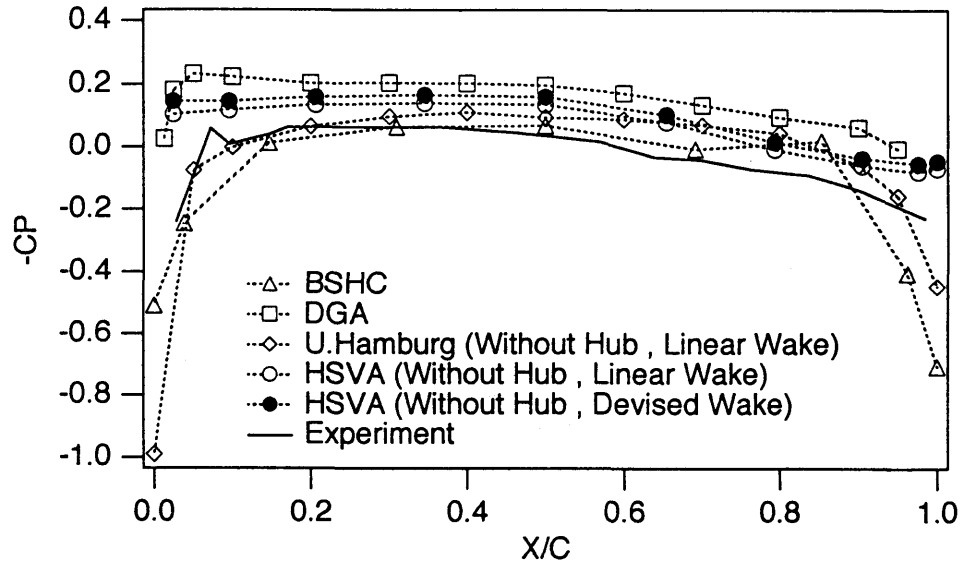

Fig.2.1.2(d) CP for Case E , DTRC4119 , J=0.833 , With Hub , Devised Wake) on 0.3R Face

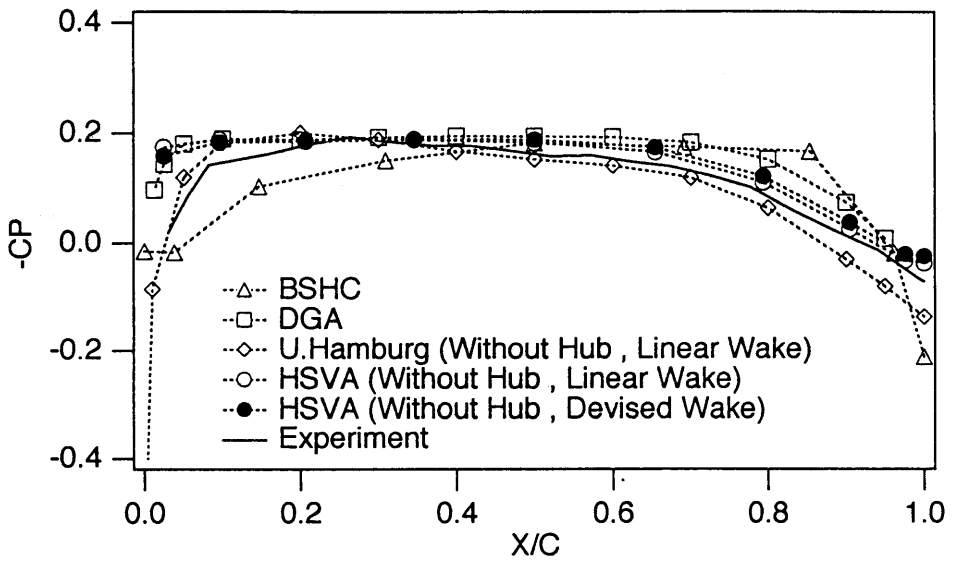

Fig.2.1.2(b) CP for Case E (DTRC4119 , J=0.833 , With Hub , Devised Wake) on 0.7R Back

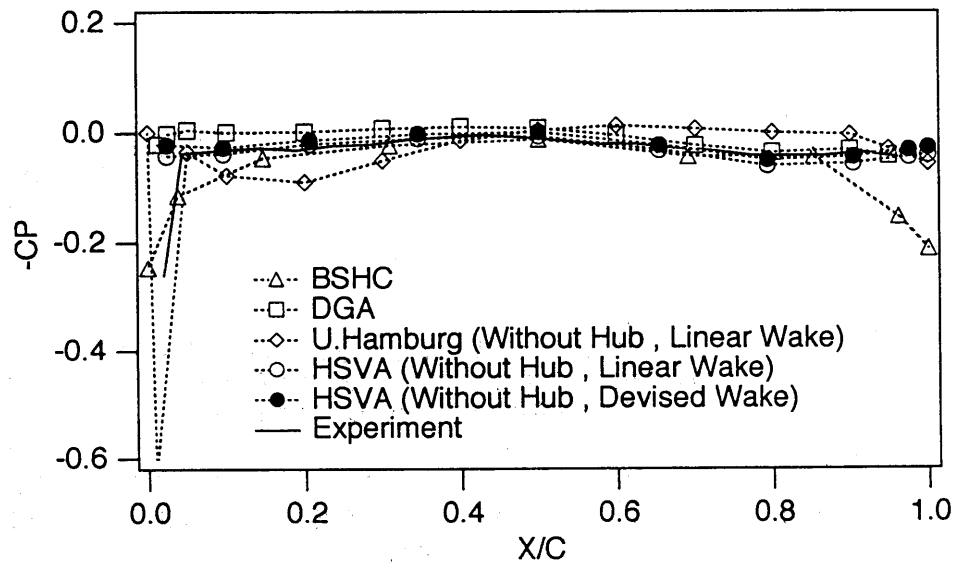

Fig.2.1.2(e) CP for Case E (DTRC4119 , J=0.833 , With Hub , Devised Wake) on 0.7R Face

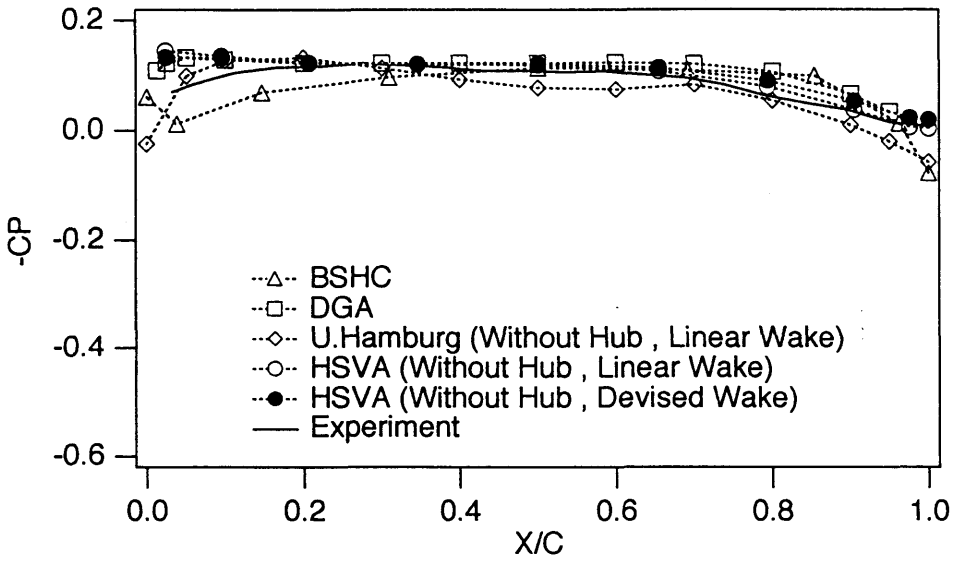

Fig.2.1.2(c) CP for Case E (DTRC4119 , J=0.833 , With Hub , Devised Wake) on 0.9R Back

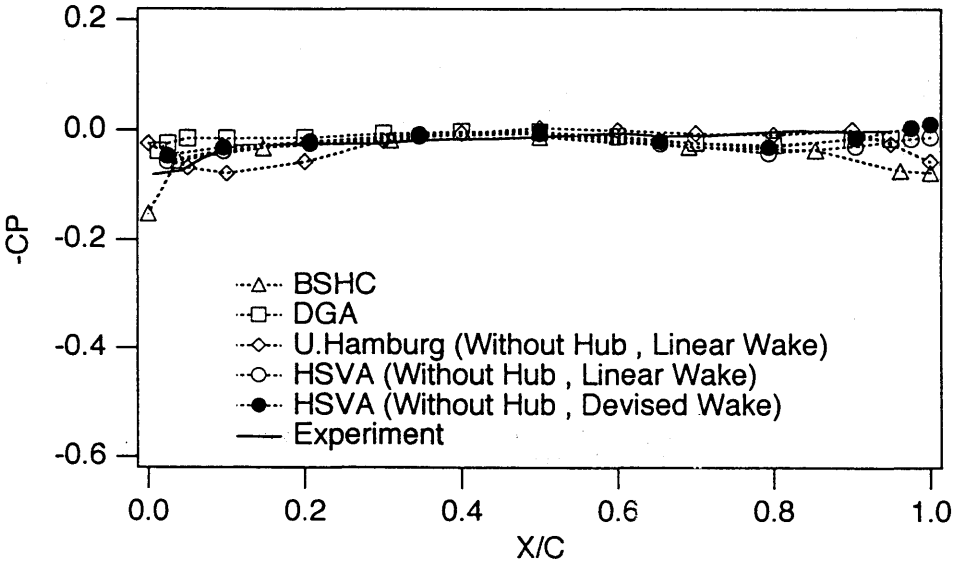

Fig.2.1.2(f) CP for Case E (DTRC4119 , J=0.833 , With Hub , Devised Wake) on 0.9R Face

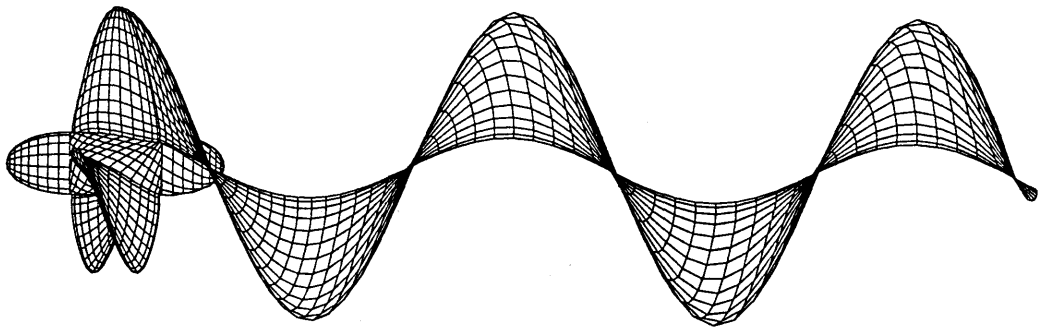

Fig.3(a) Panel Arrangement of Linear Wake for DTRC4119

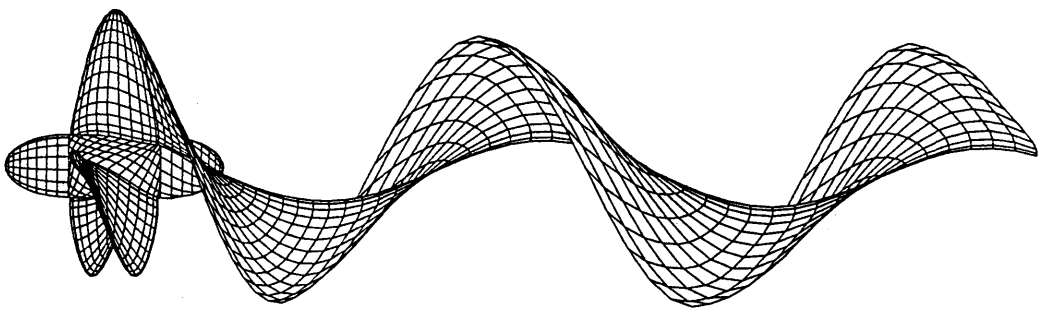

Fig.3(b) Panel Arrangement of Devised Wake for DTRC4119

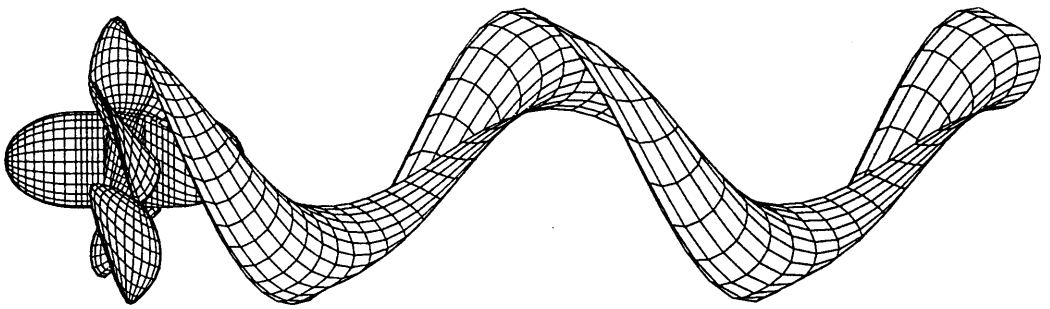

Fig.3(c) Panel Arrangement of Linear Wake for DTRC4842I

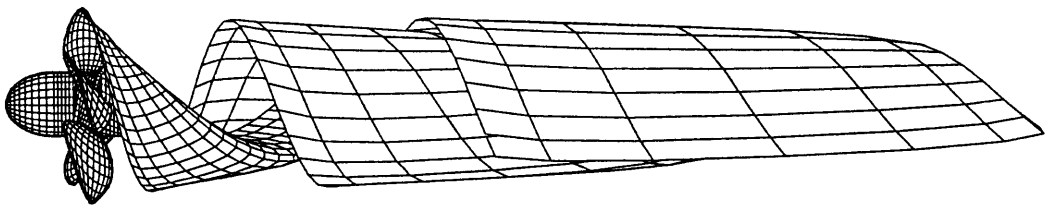

Fig.3(d) Panel Arrangement of Devised Wake for DTRC4842I

APPENDIX A

Calculation Document

20th ITTC Propulsor Committee

Comparative Calculation of Propellers by Surface Panel Method

Comparative calculation of marine propellers by surface panel method and workshop for the discussion of the comparison have been planned in order to make clear the accuracy of the panel method for the analysis of marine propellers and to review the ability of the method. This can be done on the basis of rich numerical results by many panel methods. The purpose of the comparison is not the competition of each method.

As the accuracy of the results depends strongly on the numerical method, the numerical methods should be discussed to the full. Paneling for the geometry is one of the most important factor. Critical number of panels should be clarified for the required accuracy. Benefit of the higher order panel methods should be also found. Effect of the individual paneling method appears near the rapidly deformed surface such as leading edge or tip of the blade.

Using the Surface Panel Method we can get the information for the effect of the existance of the hub, on which we have few informations.

Another important factor is the treatment of the deformation of blade wake. There seems to be many problems to be solved for the treatment of the deformation of blade wake.

Final factor connecting the calculation results by surface panel method and the actual characteristics is the correction for viscous effects. The correction factor for viscous effects is important from the practical point of view.

As was described above there are a lot of factors to be made clear. But there is a limitation of calculation cases. So we would like to make three points. The first is the very simple case without viscous correction. This is useful for the validation of the numerical method. The second is the completed case. This is useful for the evaluation for practical applications. The third is to abstract the important factor existing in the calculation and in the application.

So the priority of the calculation cases is decided as shown in Table 1.2.1. We hope you contribute with as many calculation cases as you can. Of course you can decide your calculation cases in your situation. In all cases both results with/without viscous correction are

desired earnestly. Where the viscous correction means viscous drag and circulation reduction around blade section by the effect of the boundary layer.

It goes without saying that the experimental data are very important for the evaluation of the surface panel method. Dr. Jessup's experimental data presented in his dissertation contributes to our plan. One of the calculation propellers is the same as the one to be used in the comparative experiments for viscous effects, also organized by the 20th ITTC Propulsor Committee.

20th ITTC Propulsor Committee
Comparative Calculation of Propellers by Surface Panel Method

1. Input Data sent here

1.1. Geometry of the propellers

DTRC Prop.4119

Photo	Fig.1.1.1
Blade	Table 1.1.1
Hub	Fig.1.1.2

DTRC Prop.4842

Photo	Fig.1.1.1
Blade	Table 1.1.2
Hub	Fig.1.1.2

1.2. Calculation conditions

in uniform flow

DTRC Prop.4119	Advance Coeficient	J=0.833 , n=10rps
		J=1.100 , n=10rps
DTRC Prop.4842	Advance Coeficient	J=0.905 , n=10rps

* detail and priority of the standard calculation condition are shown in Table 1.2.1

1.3. Experimental data for the reference (Jessup's experiment)

DTRC Prop.4119

KT, KQ	Fig.1.3.1
	Table 1.3.1
CP	Fig.1.3.3
blade wake	Fig.1.3.4
section drag	Fig.1.3.5

DTRC Prop.4842

KT, KQ	Fig.1.3.2
	Table 1.3.1

* If you want Dr.Jessup's dissertation "An Experimental Investigation of Viscous Aspects of Propeller Blade Flow", please ask me for it. I can send you the copy.

2. Output Data required to be sent

2.1. Format of the expression for the calculation results

number, distribution (chordwise and radial) and form of panels

$KT = T / \rho\ n^2\ D^4$

$KQ = Q / \rho\ n^2\ D^5$

$CP = 1 - (VV/VR)^2$ at 0.3, 0.7, 0.9 radius

$VR^2 = V^2 + (2\pi nr)^2$

V = advance speed

VV = flow velocity on the blade

blade wake pitch

viscous correction factors (viscous blade section drag and circulation reduction around blade section)

* Calculation results should be presented in the form of tables and figures
* Please explain any conditions if they are different from the standard calculation condition shown in this document. (for example the hub form)

2.2. Method of calculation (Copy of the paper presenting the method)

Theory

Numerical method

2.3. Comments on the calculation results

paneling

Do you have some standard for the number of panels ?

Do you have some standard for the accuracy of KT or CP ?

effect of hub

deformation of blade wake

viscous effect

How do you make the value of the viscous correction factor?

Table 1.1.1 (a) Blade geometry of DTRC4119

xyzprop blade geometry ofDTRC 4119

NUMBER OF BLADES = 3

PROPELLER DIAMETER = 12.0000 INCHES

INPUT SCALED BY LAMDA = 1.0000

	R/R0	R (INCHES)	CHORD (INCHES)	CHORD/D	TAN PHI	PITCH/D	PITCHAN (RADIANS)
0	0.20000	1.2000	3.8400	0.32000	1.75866	1.10500	1.05377
0	0.25000	1.5000	4.1040	0.34200	1.40527	1.10370	0.95232
0	0.30000	1.8000	4.3620	0.36350	1.16947	1.10220	0.86336
0	0.40000	2.4000	4.8576	0.40480	0.87400	1.09830	0.71826
0	0.50000	3.0000	5.2704	0.43920	0.69595	1.09320	0.60800
0	0.60000	3.6000	5.5320	0.46100	0.57715	1.08790	0.52345
0	0.70000	4.2000	5.5464	0.46220	0.49288	1.08390	0.45794
0	0.80000	4.8000	5.2164	0.43470	0.43016	1.08110	0.40623
0	0.90000	5.4000	4.3356	0.36130	0.38144	1.07850	0.36441
0	0.95000	5.7000	3.3300	0.27750	0.36086	1.07700	0.34632
0	1.00000	6.0000	0.0000	0.00000	0.34218	1.07500	0.32969
0	0.92500	5.5500	3.9145	0.32621	0.37089	1.07779	0.35516
0	0.97500	5.8500	2.4538	0.20449	0.35131	1.07609	0.33784
0	0.99000	5.9400	1.5931	0.13276	0.34579	1.07546	0.33292
0	0.99500	5.9700	1.1375	0.09479	0.34398	1.07523	0.33130

	R/R0	TOTAL RAKE/D	SKEWAN (RADIANS)	T/CHORD	FM/CHORD	TE OFFSET (INCHES)
0	0.20000	0.00000	0.00000	0.20550	0.01429	0.00000
0	0.25000	0.00000	0.00000	0.17870	0.01985	0.00000
0	0.30000	0.00000	0.00000	0.15530	0.02318	0.00000
0	0.40000	0.00000	0.00000	0.11800	0.02303	0.00000
0	0.50000	0.00000	0.00000	0.09016	0.02182	0.00000
0	0.60000	0.00000	0.00000	0.06960	0.02072	0.00000
0	0.70000	0.00000	0.00000	0.05418	0.02003	0.00000
0	0.80000	0.00000	0.00000	0.04206	0.01967	0.00000
0	0.90000	0.00000	0.00000	0.03321	0.01817	0.00000
0	0.95000	0.00000	0.00000	0.03228	0.01631	0.00000
0	1.00000	0.00000	0.00000	0.03160	0.01175	0.00000
0	0.92500	0.00000	0.00000	0.03252	0.01744	0.00000
0	0.97500	0.00000	0.00000	0.03211	0.01450	0.00000
0	0.99000	0.00000	0.00000	0.03187	0.01298	0.00000
0	0.99500	0.00000	0.00000	0.03175	0.01239	0.00000

R/R0 = FRACTION OF PROPELLER RADIUS,R0
R = LOCAL RADIUS
CHORD = TOTAL WIDTH OF BLADE SECTION
D = PROPELLER DIAMETER
TAN PHI = TANGENT OF PITCH ANGLE
LAMDA = ARCTAN((TOT RAKE)/(R'SKEWANGLE))
PITCH = BLADE-SECTION PITCH
PITCHAN = PITCH ANGLE
TOT RAKE = AXIAL DISTANCE OF BLADE-SECTION MID-CHORD POINT FROM PLANE PERPE
NDICULAR TO SHAFT AXIS CONTAINING PROPELLER CENTER AXIS(X=0 PLANE)
SKEWAN = SKEWANGLE = CIRCUMFERENTIAL DISPLACEMENT OF BLADE-SECTION MID-CHORD
POINT FROM PLANE THRU SHAFT AXIS CONTAINING PROPELLER CENTER AXIS (Y=0 PLANE)
T = MAX THICKNESS AT RADIUS R
FM = CAMBER AT RADIUS R

Table 1.1.1 (b) Blade geometry of DTRC4119

SECTION OFFSETS
(IN INCHES)

xyz prop blade geometry of DTRC 4119

ORDINATES (NO TRAILING-EDGE MODIFICATIONS) AT NONDIMENSIONAL RADIUS R/R0

FRACTION OF CHORD		0.2000	0.2500	0.3000	0.4000	0.5000	0.6000	0.7000	0.8000
0.000000	U	0.0000	0.0000	0.0000	0.0000	0.0000	0.0000	0.0000	0.0000
	L	0.0000	0.0000	0.0000	0.0000	0.0000	0.0000	0.0000	0.0000
0.010000	U	0.0780	0.0748	0.0710	0.0621	0.0532	0.0447	0.0365	0.0283
	L	-0.0697	-0.0625	-0.0557	-0.0452	-0.0358	-0.0274	-0.0197	-0.0128
0.025000	U	0.1244	0.1204	0.1153	0.1018	0.0879	0.0746	0.0617	0.0484
	L	-0.1070	-0.0946	-0.0833	-0.0663	-0.0514	-0.0383	-0.0264	-0.0159
0.050000	U	0.1779	0.1736	0.1674	0.1488	0.1294	0.1106	0.0922	0.0732
	L	-0.1482	-0.1294	-0.1125	-0.0881	-0.0670	-0.0485	-0.0320	-0.0175
0.100000	U	0.2540	0.2497	0.2422	0.2168	0.1897	0.1633	0.1371	0.1098
	L	-0.2048	-0.1767	-0.1516	-0.1165	-0.0866	-0.0606	-0.0376	-0.0178
0.200000	U	0.3540	0.3503	0.3417	0.3075	0.2705	0.2342	0.1979	0.1595
	L	-0.2773	-0.2364	-0.2003	-0.1510	-0.1097	-0.0739	-0.0425	-0.0160
0.300000	U	0.4134	0.4105	0.4015	0.3624	0.3197	0.2776	0.2353	0.1904
	L	-0.3186	-0.2698	-0.2269	-0.1692	-0.1211	-0.0796	-0.0434	-0.0132
0.400000	U	0.4435	0.4415	0.4327	0.3914	0.3459	0.3009	0.2556	0.2073
	L	-0.3380	-0.2848	-0.2382	-0.1763	-0.1247	-0.0805	-0.0420	-0.0100
0.500000	U	0.4464	0.4454	0.4372	0.3963	0.3508	0.3057	0.2602	0.2115
	L	-0.3367	-0.2824	-0.2350	-0.1725	-0.1208	-0.0764	-0.0380	-0.0063
0.600000	U	0.4209	0.4210	0.4142	0.3762	0.3336	0.2913	0.2485	0.2025
	L	-0.3135	-0.2615	-0.2163	-0.1572	-0.1086	-0.0670	-0.0311	-0.0017
0.700000	U	0.3672	0.3684	0.3632	0.3308	0.2940	0.2573	0.2200	0.1798
	L	-0.2696	-0.2235	-0.1834	-0.1318	-0.0895	-0.0534	-0.0225	0.0027
0.800000	U	0.2840	0.2853	0.2817	0.2569	0.2286	0.2003	0.1715	0.1403
	L	-0.2069	-0.1708	-0.1396	-0.0997	-0.0670	-0.0392	-0.0154	0.0039
0.900000	U	0.1678	0.1669	0.1634	0.1477	0.1304	0.1134	0.0962	0.0780
	L	-0.1284	-0.1084	-0.0909	-0.0675	-0.0480	-0.0312	-0.0166	-0.0044
0.950000	U	0.0996	0.0978	0.0947	0.0847	0.0740	0.0636	0.0534	0.0427
	L	-0.0808	-0.0699	-0.0601	-0.0464	-0.0346	-0.0244	-0.0153	-0.0075
0.975000	U	0.0635	0.0615	0.0590	0.0520	0.0450	0.0382	0.0316	0.0248
	L	-0.0545	-0.0482	-0.0424	-0.0337	-0.0261	-0.0194	-0.0134	-0.0080
0.990000	U	0.0412	0.0392	0.0370	0.0321	0.0273	0.0228	0.0184	0.0141
	L	-0.0378	-0.0342	-0.0308	-0.0253	-0.0203	-0.0158	-0.0117	-0.0079
1.000000	U	0.0263	0.0244	0.0226	0.0191	0.0158	0.0128	0.0100	0.0073
	L	-0.0263	-0.0244	-0.0226	-0.0191	-0.0158	-0.0128	-0.0100	-0.0073

U = OFFSET OF UPPER SURFACE (SUCTION SIDE, SUCTION FACE, BACK) OF BLADE SECTION MEASURED FROM REFERENCE LINE (NOSE-TAIL LINE)

L = OFFSET OF LOWER SURFACE (PRESSURE SIDE, PRESSURE FACE, FACE) OF BLADE SECTION MEASURED FROM REFERENCE LINE (NOSE-TAIL LINE)

Table 1.1.1 (c) Blade geometry of DTRC4119

xyzprop blade geometry ofDTRC 4119

ORDINATES (NO TRAILING-EDGE MODIFICATIONS) AT NONDIMENSIONAL RADIUS R/RO

FRACTION OF CHORD		0.9000	0.9500	1.0000	0.9250	0.9750	0.9900	0.9950
0.000000	U	0.0000	0.0000	0.0000	0.0000	0.0000	0.0000	0.0000
	L	0.0000	0.0000	0.0000	0.0000	0.0000	0.0000	0.0000
0.010000	U	0.0194	0.0142	0.0000	0.0171	0.0101	0.0063	0.0044
	L	-0.0075	-0.0059	0.0000	-0.0067	-0.0047	-0.0032	-0.0023
0.025000	U	0.0336	0.0244	0.0000	0.0295	0.0172	0.0107	0.0075
	L	-0.0086	-0.0071	0.0000	-0.0078	-0.0059	-0.0042	-0.0031
0.050000	U	0.0511	0.0369	0.0000	0.0448	0.0259	0.0161	0.0113
	L	-0.0084	-0.0075	0.0000	-0.0078	-0.0066	-0.0049	-0.0036
0.100000	U	0.0772	0.0556	0.0000	0.0676	0.0389	0.0240	0.0168
	L	-0.0065	-0.0069	0.0000	-0.0064	-0.0070	-0.0055	-0.0042
0.200000	U	0.1127	0.0810	0.0000	0.0987	0.0564	0.0348	0.0243
	L	-0.0025	-0.0050	0.0000	-0.0032	-0.0066	-0.0058	-0.0046
0.300000	U	0.1348	0.0968	0.0000	0.1180	0.0673	0.0414	0.0289
	L	0.0012	-0.0030	0.0000	-0.0001	-0.0058	-0.0057	-0.0046
0.400000	U	0.1470	0.1055	0.0000	0.1287	0.0732	0.0450	0.0314
	L	0.0044	-0.0010	0.0000	0.0026	-0.0048	-0.0053	-0.0043
0.500000	U	0.1502	0.1077	0.0000	0.1314	0.0747	0.0459	0.0320
	L	0.0073	0.0010	0.0000	0.0051	-0.0035	-0.0045	-0.0038
0.600000	U	0.1441	0.1032	0.0000	0.1260	0.0715	0.0439	0.0306
	L	0.0101	0.0031	0.0000	0.0076	-0.0018	-0.0034	-0.0030
0.700000	U	0.1281	0.0917	0.0000	0.1121	0.0634	0.0389	0.0271
	L	0.0120	0.0049	0.0000	0.0094	-0.0001	-0.0021	-0.0020
0.800000	U	0.1001	0.0716	0.0000	0.0876	0.0495	0.0303	0.0211
	L	0.0106	0.0047	0.0000	0.0084	0.0005	-0.0013	-0.0013
0.900000	U	0.0553	0.0397	0.0000	0.0484	0.0275	0.0169	0.0118
	L	0.0012	-0.0007	0.0000	0.0006	-0.0020	-0.0021	-0.0017
0.950000	U	0.0300	0.0216	0.0000	0.0262	0.0151	0.0093	0.0065
	L	-0.0030	-0.0030	0.0000	-0.0029	-0.0029	-0.0023	-0.0017
0.975000	U	0.0172	0.0125	0.0000	0.0151	0.0088	0.0055	0.0039
	L	-0.0043	-0.0036	0.0000	-0.0039	-0.0030	-0.0021	-0.0015
0.990000	U	0.0096	0.0070	0.0000	0.0084	0.0050	0.0032	0.0022
	L	-0.0048	-0.0037	0.0000	-0.0043	-0.0029	-0.0019	-0.0014
1.000000	U	0.0048	0.0036	0.0000	0.0042	0.0026	0.0017	0.0012
	L	-0.0048	-0.0036	0.0000	-0.0042	-0.0026	-0.0017	-0.0012

U = OFFSET OF UPPER SURFACE (SUCTION SIDE, SUCTION FACE, BACK) OF BLADE SECTION MEASURED FROM REFERENCE LINE (NOSE-TAIL LINE)

L = OFFSET OF LOWER SURFACE (PRESSURE SIDE, PRESSURE FACE, FACE) OF BLADE SECTION MEASURED FROM REFERENCE LINE (NOSE-TAIL LINE)

Table 1.1.2 (a) Blade geometry of DTRC4842

xyz prop blade geometry of DTRC 4842

NUMBER OF BLADES = 5

PROPELLER DIAMETER = 14.6280 INCHES

INPUT SCALED BY LAMDA = 1.0000

	R/R0	R (INCHES)	CHORD (INCHES)	CHORD/D	TAN PHI	PITCH/D	PITCHAN (RADIANS)
0	0.32300	2.3624	2.9475	0.20150	0.91857	0.93210	0.74298
0	0.35000	2.5599	3.1904	0.21810	0.98130	1.07900	0.77596
0	0.40000	2.9256	3.6482	0.24940	0.98366	1.23610	0.77716
0	0.50000	3.6570	4.5537	0.31130	0.90362	1.41940	0.73481
0	0.60000	4.3884	5.3597	0.36640	0.79005	1.48920	0.66864
0	0.70000	5.1198	5.8965	0.40310	0.67664	1.48800	0.59487
0	0.80000	5.8512	5.9829	0.40900	0.52879	1.32900	0.48642
0	0.90000	6.5826	5.3407	0.36510	0.38052	1.07590	0.36360
0	0.95000	6.9483	4.5435	0.31060	0.30196	0.90120	0.29325
0	1.00000	7.3140	1.0240	0.07000	0.22221	0.69810	0.21866
0	0.92500	6.7655	5.0102	0.34251	0.34164	0.99280	0.32921
0	0.97500	7.1312	3.7849	0.25875	0.26199	0.80250	0.25624
0	0.99000	7.2409	2.9400	0.20098	0.23808	0.74046	0.23372
0	0.99500	7.2774	2.4436	0.16705	0.23013	0.71937	0.22619

	R/R0	TOTAL RAKE/D	SKEWAN (RADIANS)	T/CHORD	FM/CHORD	TE OFFSET (INCHES)
0	0.32300	0.00005	0.00663	0.21790	0.01000	0.00000
0	0.35000	0.00020	-0.05358	0.18710	0.01580	0.00000
0	0.40000	0.00053	-0.11903	0.14150	0.02530	0.00000
0	0.50000	-0.00144	-0.15743	0.08540	0.03650	0.00000
0	0.60000	-0.00122	-0.13212	0.05810	0.03900	0.00000
0	0.70000	-0.00021	-0.05655	0.04440	0.03710	0.00000
0	0.80000	0.00040	0.07575	0.03790	0.03190	0.00000
0	0.90000	0.00123	0.23998	0.03560	0.02640	0.00000
0	0.95000	0.00272	0.33598	0.03630	0.02470	0.00000
0	1.00000	0.00684	0.44366	0.08800	0.02430	0.00000
0	0.92500	0.00177	0.28661	0.03325	0.02542	0.00000
0	0.97500	0.00433	0.38827	0.05210	0.02431	0.00000
0	0.99000	0.00571	0.42112	0.07076	0.02425	0.00000
0	0.99500	0.00625	0.43233	0.07886	0.02427	0.00000

R/R0 = FRACTION OF PROPELLER RADIUS,R0
R = LOCAL RADIUS
CHORD = TOTAL WIDTH OF BLADE SECTION
D = PROPELLER DIAMETER
TAN PHI = TANGENT OF PITCH ANGLE
LAMDA = ARCTAN((TOT RAKE)/(R'SKEWANGLE))
PITCH = BLADE-SECTION PITCH
PITCHAN = PITCH ANGLE
TOT RAKE = AXIAL DISTANCE OF BLADE-SECTION MID-CHORD POINT FROM PLANE PERPENDICULAR TO SHAFT AXIS CONTAINING PROPELLER CENTER AXIS(X=0 PLANE)
SKEWAN = SKEWANGLE = CIRCUMFERENTIAL DISPLACEMENT OF BLADE-SECTION MID-CHORD POINT FROM PLANE THRU SHAFT AXIS CONTAINING PROPELLER CENTER AXIS (Y=0 PLANE)
T = MAX THICKNESS AT RADIUS R

Table 1.1.2 (b) Blade geometry of DTRC4842

SECTION OFFSETS
(IN INCHES)

xyz prop blade geometry of DTRC 4842

ORDINATES (NO TRAILING-EDGE MODIFICATIONS) AT NONDIMENSIONAL RADIUS R/R0

FRACTION OF CHORD		0.3230	0.3500	0.4000	0.5000	0.6000	0.7000	0.8000
0.000000	U	0.0000	0.0000	0.0000	0.0000	0.0000	0.0000	0.0000
	L	0.0000	0.0000	0.0000	0.0000	0.0000	0.0000	0.0000
0.010000	U	0.0622	0.0595	0.0550	0.0485	0.0444	0.0404	0.0351
	L	-0.0579	-0.0522	-0.0416	-0.0243	-0.0139	-0.0085	-0.0073
0.025000	U	0.0987	0.0952	0.0898	0.0824	0.0776	0.0719	0.0624
	L	-0.0896	-0.0798	-0.0616	-0.0316	-0.0137	-0.0049	-0.0040
0.050000	U	0.1404	0.1366	0.1309	0.1240	0.1192	0.1115	0.0969
	L	-0.1250	-0.1101	-0.0824	-0.0367	-0.0095	0.0033	0.0033
0.100000	U	0.1997	0.1958	0.1908	0.1864	0.1828	0.1727	0.1502
	L	-0.1737	-0.1513	-0.1093	-0.0397	0.0018	0.0205	0.0183
0.200000	U	0.2774	0.2738	0.2707	0.2712	0.2699	0.2569	0.2234
	L	-0.2364	-0.2037	-0.1423	-0.0400	0.0208	0.0474	0.0420
0.300000	U	0.3233	0.3204	0.3191	0.3238	0.3248	0.3102	0.2699
	L	-0.2724	-0.2333	-0.1598	-0.0369	0.0360	0.0674	0.0595
0.400000	U	0.3464	0.3441	0.3445	0.3526	0.3555	0.3403	0.2961
	L	-0.2897	-0.2471	-0.1667	-0.0325	0.0471	0.0810	0.0715
0.500000	U	0.3482	0.3466	0.3485	0.3592	0.3635	0.3487	0.3034
	L	-0.2892	-0.2458	-0.1639	-0.0268	0.0545	0.0889	0.0783
0.600000	U	0.3276	0.3269	0.3302	0.3430	0.3487	0.3351	0.2916
	L	-0.2701	-0.2286	-0.1502	-0.0189	0.0589	0.0915	0.0806
0.700000	U	0.2850	0.2851	0.2893	0.3028	0.3091	0.2976	0.2590
	L	-0.2333	-0.1966	-0.1273	-0.0110	0.0578	0.0864	0.0760
0.800000	U	0.2197	0.2197	0.2229	0.2333	0.2381	0.2293	0.1995
	L	-0.1798	-0.1516	-0.0982	-0.0086	0.0445	0.0665	0.0585
0.900000	U	0.1312	0.1303	0.1302	0.1330	0.1340	0.1282	0.1115
	L	-0.1099	-0.0938	-0.0635	-0.0129	0.0171	0.0299	0.0264
0.950000	U	0.0787	0.0772	0.0755	0.0741	0.0729	0.0690	0.0600
	L	-0.0682	-0.0592	-0.0425	-0.0148	0.0017	0.0091	0.0081
0.975000	U	0.0505	0.0489	0.0463	0.0430	0.0408	0.0379	0.0329
	L	-0.0456	-0.0404	-0.0309	-0.0152	-0.0058	-0.0013	-0.0010
0.990000	U	0.0329	0.0312	0.0283	0.0240	0.0213	0.0191	0.0165
	L	-0.0313	-0.0285	-0.0233	-0.0149	-0.0099	-0.0071	-0.0061
1.000000	U	0.0214	0.0199	0.0172	0.0129	0.0104	0.0087	0.0076
	L	-0.0214	-0.0199	-0.0172	-0.0129	-0.0104	-0.0087	-0.0076

U = OFFSET OF UPPER SURFACE (SUCTION SIDE, SUCTION FACE, BACK) OF BLADE SECTION MEASURED FROM REFERENCE LINE (NOSE-TAIL LINE)
L = OFFSET OF LOWER SURFACE (PRESSURE SIDE, PRESSURE FACE, FACE) OF BLADE SECTION MEASURED FROM REFERENCE LINE (NOSE-TAIL LINE)

Table 1.1.2 (c) Blade geometry of DTRC4842

xyz prop blade geometry of DTRC 4842

ORDINATES (NO TRAILING-EDGE MODIFICATIONS) AT NONDIMENSIONAL RADIUS R/RO

FRACTION OF CHORD		0.9000	0.9500	1.0000	0.9250	0.9750	0.9900	0.9950
0.000000	U	0.0000	0.0000	0.0000	0.0000	0.0000	0.0000	0.0000
	L	0.0000	0.0000	0.0000	0.0000	0.0000	0.0000	0.0000
0.010000	U	0.0281	0.0236	0.0102	0.0249	0.0252	0.0247	0.0224
	L	-0.0075	-0.0073	-0.0066	-0.0063	-0.0117	-0.0143	-0.0137
0.025000	U	0.0494	0.0413	0.0170	0.0439	0.0430	0.0414	0.0373
	L	-0.0063	-0.0070	-0.0094	-0.0049	-0.0148	-0.0196	-0.0192
0.050000	U	0.0763	0.0635	0.0251	0.0678	0.0649	0.0617	0.0554
	L	-0.0023	-0.0046	-0.0121	-0.0010	-0.0166	-0.0243	-0.0242
0.100000	U	0.1175	0.0975	0.0372	0.1046	0.0980	0.0920	0.0822
	L	0.0070	0.0016	-0.0152	0.0078	-0.0167	-0.0290	-0.0298
0.200000	U	0.1741	0.1440	0.0533	0.1552	0.1429	0.1328	0.1183
	L	0.0220	0.0121	-0.0187	0.0219	-0.0149	-0.0336	-0.0358
0.300000	U	0.2099	0.1733	0.0633	0.1871	0.1709	0.1580	0.1406
	L	0.0335	0.0204	-0.0203	0.0326	-0.0121	-0.0349	-0.0382
0.400000	U	0.2299	0.1897	0.0686	0.2051	0.1863	0.1717	0.1525
	L	0.0416	0.0264	-0.0207	0.0401	-0.0091	-0.0343	-0.0383
0.500000	U	0.2353	0.1941	0.0696	0.2100	0.1899	0.1745	0.1549
	L	0.0467	0.0304	-0.0198	0.0447	-0.0058	-0.0319	-0.0363
0.600000	U	0.2259	0.1862	0.0662	0.2017	0.1815	0.1663	0.1475
	L	0.0490	0.0327	-0.0177	0.0466	-0.0021	-0.0273	-0.0318
0.700000	U	0.2005	0.1650	0.0582	0.1790	0.1603	0.1465	0.1298
	L	0.0470	0.0320	-0.0145	0.0446	0.0012	-0.0214	-0.0257
0.800000	U	0.1544	0.1272	0.0448	0.1379	0.1235	0.1129	0.1000
	L	0.0362	0.0246	-0.0112	0.0343	0.0009	-0.0165	-0.0198
0.900000	U	0.0866	0.0715	0.0259	0.0773	0.0703	0.0648	0.0576
	L	0.0153	0.0096	-0.0079	0.0147	-0.0038	-0.0133	-0.0147
0.950000	U	0.0469	0.0389	0.0147	0.0418	0.0390	0.0365	0.0326
	L	0.0034	0.0012	-0.0059	0.0037	-0.0061	-0.0111	-0.0114
0.975000	U	0.0260	0.0217	0.0088	0.0231	0.0225	0.0215	0.0194
	L	-0.0024	-0.0029	-0.0047	-0.0018	-0.0070	-0.0096	-0.0094
0.990000	U	0.0134	0.0113	0.0052	0.0118	0.0124	0.0124	0.0113
	L	-0.0057	-0.0052	-0.0038	-0.0049	-0.0074	-0.0085	-0.0080
1.000000	U	0.0063	0.0055	0.0030	0.0055	0.0066	0.0069	0.0064
	L	-0.0063	-0.0055	-0.0030	-0.0055	-0.0066	-0.0069	-0.0064

U = OFFSET OF UPPER SURFACE (SUCTION SIDE, SUCTION FACE, BACK) OF BLADE SECTION MEASURED FROM REFERENCE LINE (NOSE-TAIL LINE)
L = OFFSET OF LOWER SURFACE (PRESSURE SIDE, PRESSURE FACE, FACE) OF BLADE SECTION MEASURED FROM REFERENCE LINE (NOSE-TAIL LINE)

Table 1.2.1. Details and priorities of the standard calculation condition

			order of priority
Prop.4119 J=0.833			
recomended paneling	without hub	linear wake	1
reference paneling	without hub	linear wake	4
recomended paneling	with hub	linear wake	5
recomended paneling	without hub	devised wake	6
recomended paneling	with hub	devised wake	2
Prop.4119 J=1.100			
recomended paneling	without hub	linear wake	7
recomended paneling	without hub	devised wake	8
Prop.4842 J=0.905			
recommended paneling	with hub	devised wake	3

recommended paneling	you recommend or you use
reference paneling	fine or course or lower order or higher order paneling which shows the validation of the paneling you recommend
linear wake	blade vortex wake remains its location at the point it has emanated in spite of induced velocity
devised wake	modeled wake calculated wake

Table 1.3.1 Open water test results for DTRC4119 and DTRC4842

Propeller 4119

OPEN WATER RESULTS			
J	K_T	$10K_Q$	η_o
0.5	0.285	0.477	0.489
0.7	0.200	0.360	0.632
0.833	0.146	0.280	0.692
0.9	0.120	0.239	0.725
1.1	0.034	0.106	0.575
DESIGN LOADS			
0.833	0.154	0.290	0.706

Propeller 4842

OPEN WATER RESULTS			
J	K_T	$10K_Q$	η_o
0.5	0.496	0.995	0.397
0.7	0.405	0.863	0.523
0.905	0.310	0.720	0.620
1.1	0.208	0.554	0.658
1.3	0.078	0.326	0.497
DESIGN LOADS			
0.905	0.306	0.689	0.606

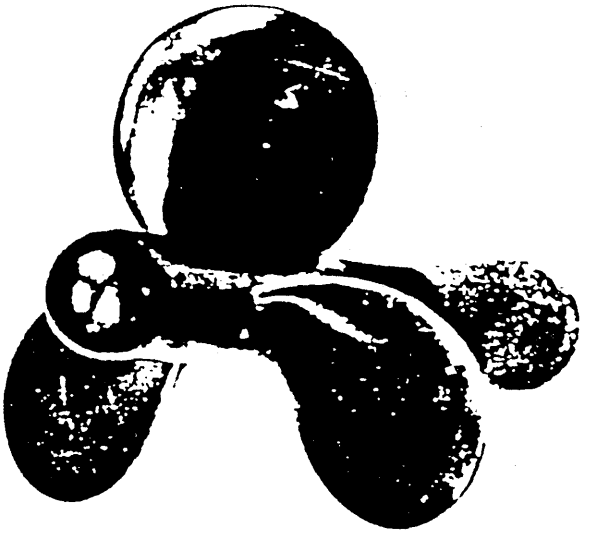

PROPELLER 4119

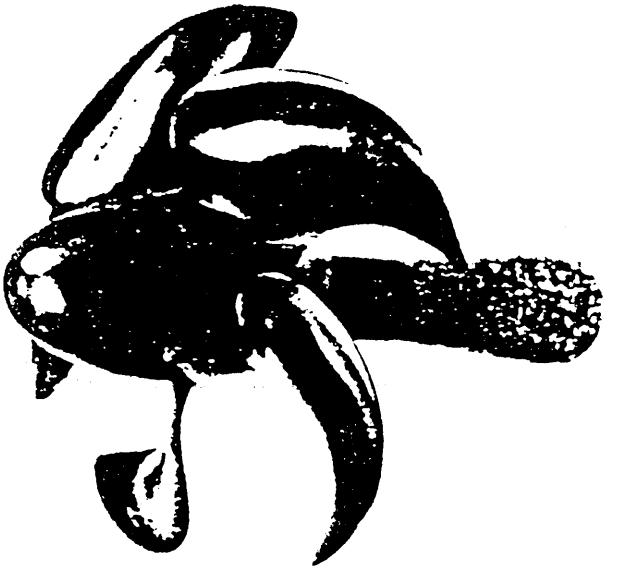

PROPELLER 4842

Fig. 1. 1. 1 Photograph of Proppellers DTRC4119 and DTRC4842

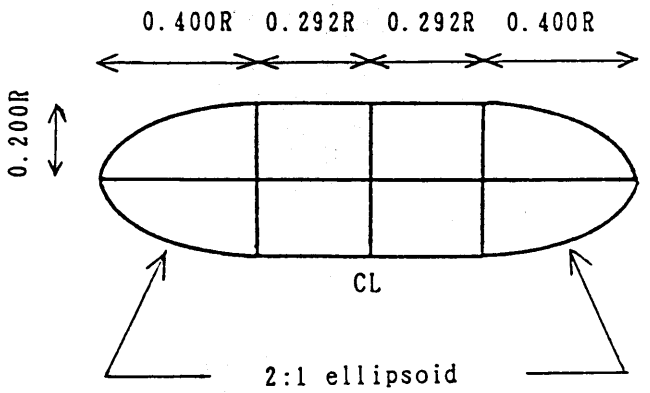

R = propeller radius

DTRC4119

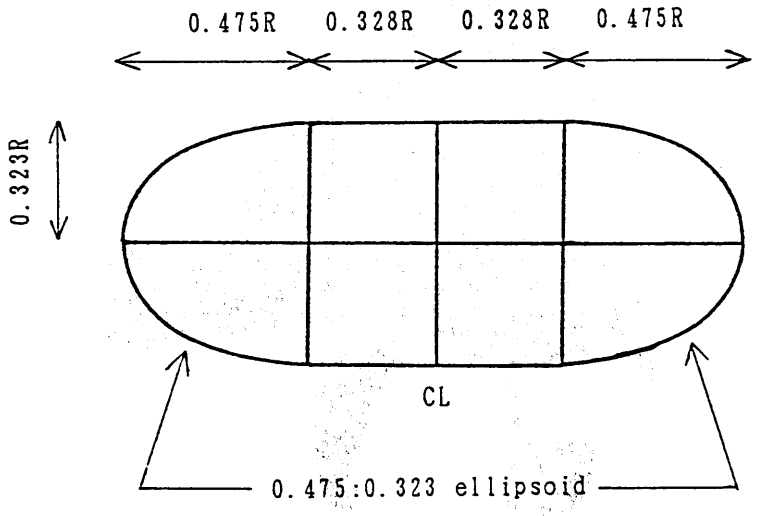

R = propeller radius

DTRC4842

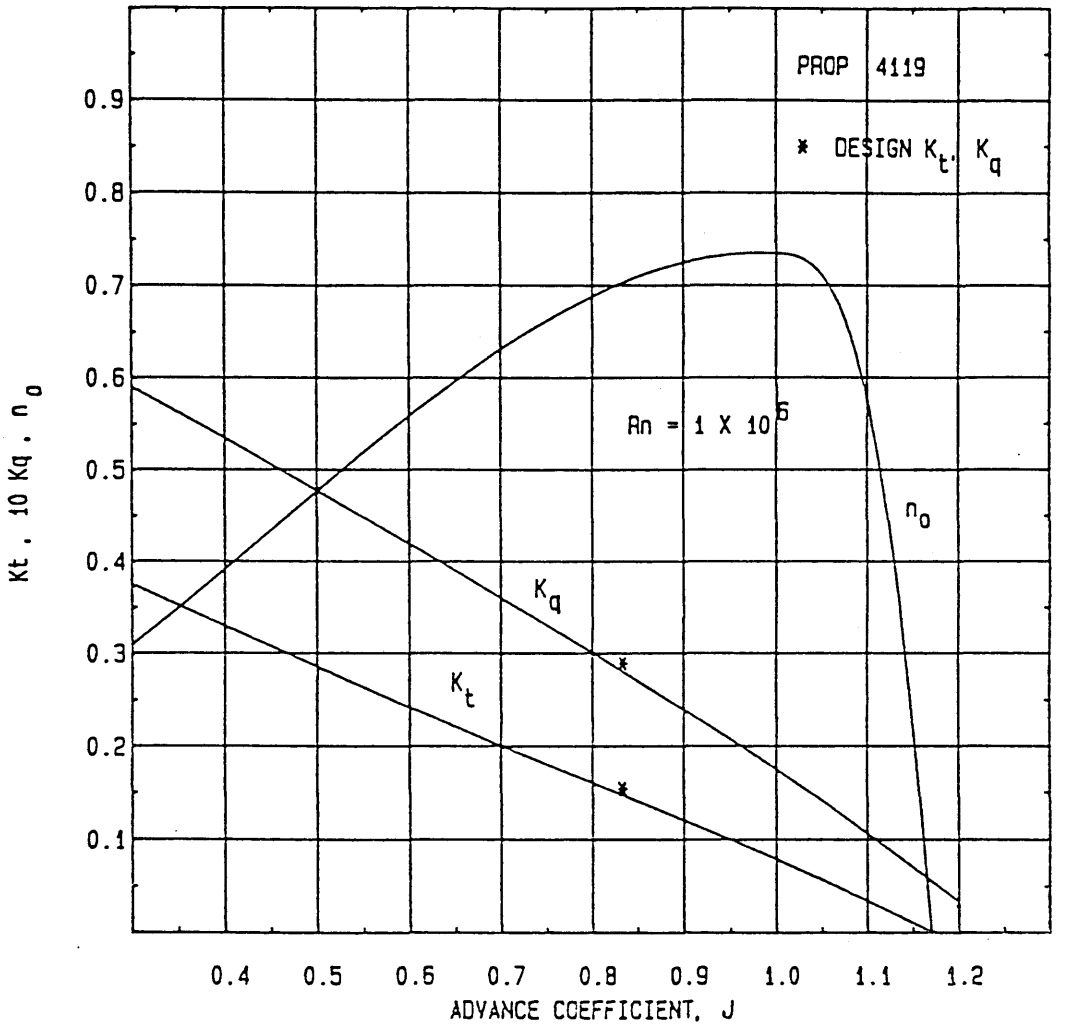

Fig. 1. 3. 1 Open water test results for DTRC4119

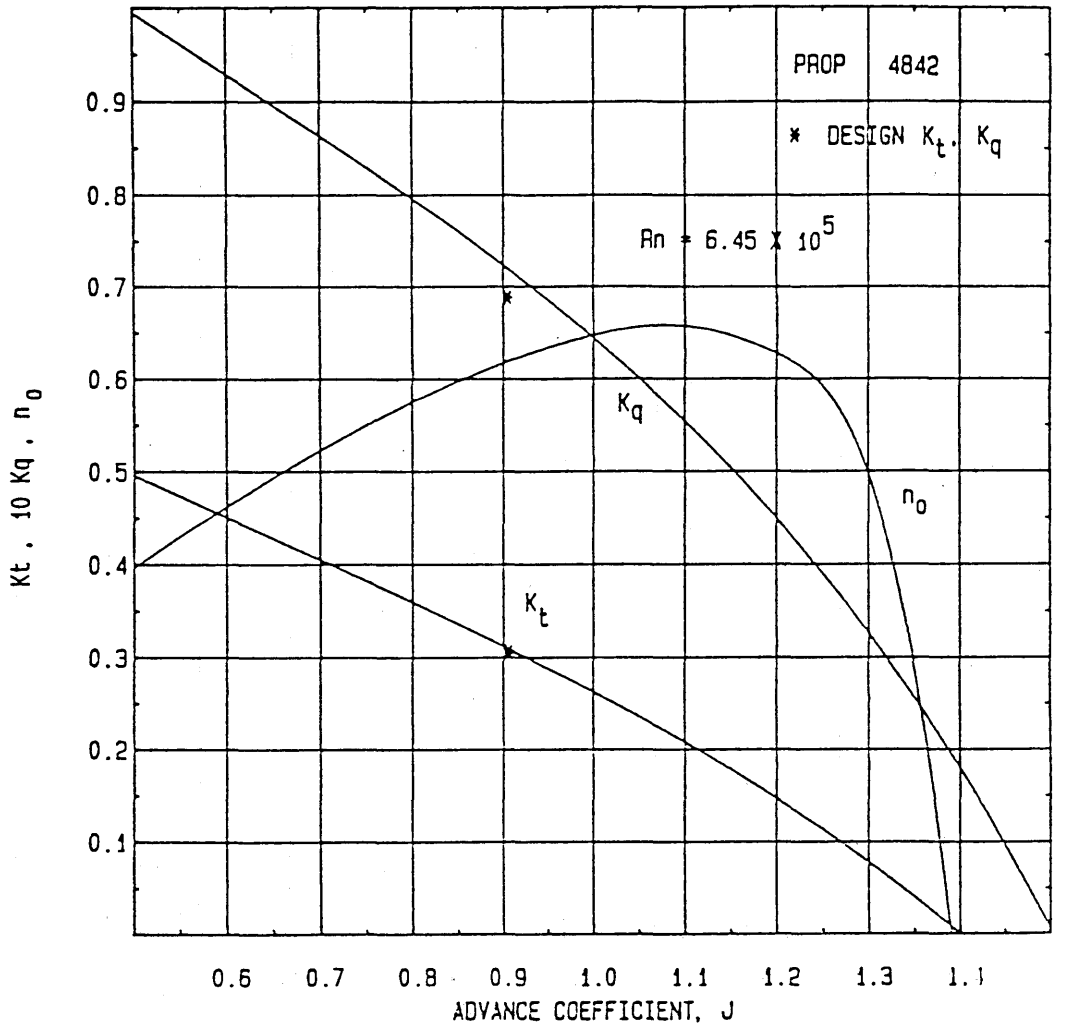

Fig. 1. 3. 2 Open water test results for DTRC4842

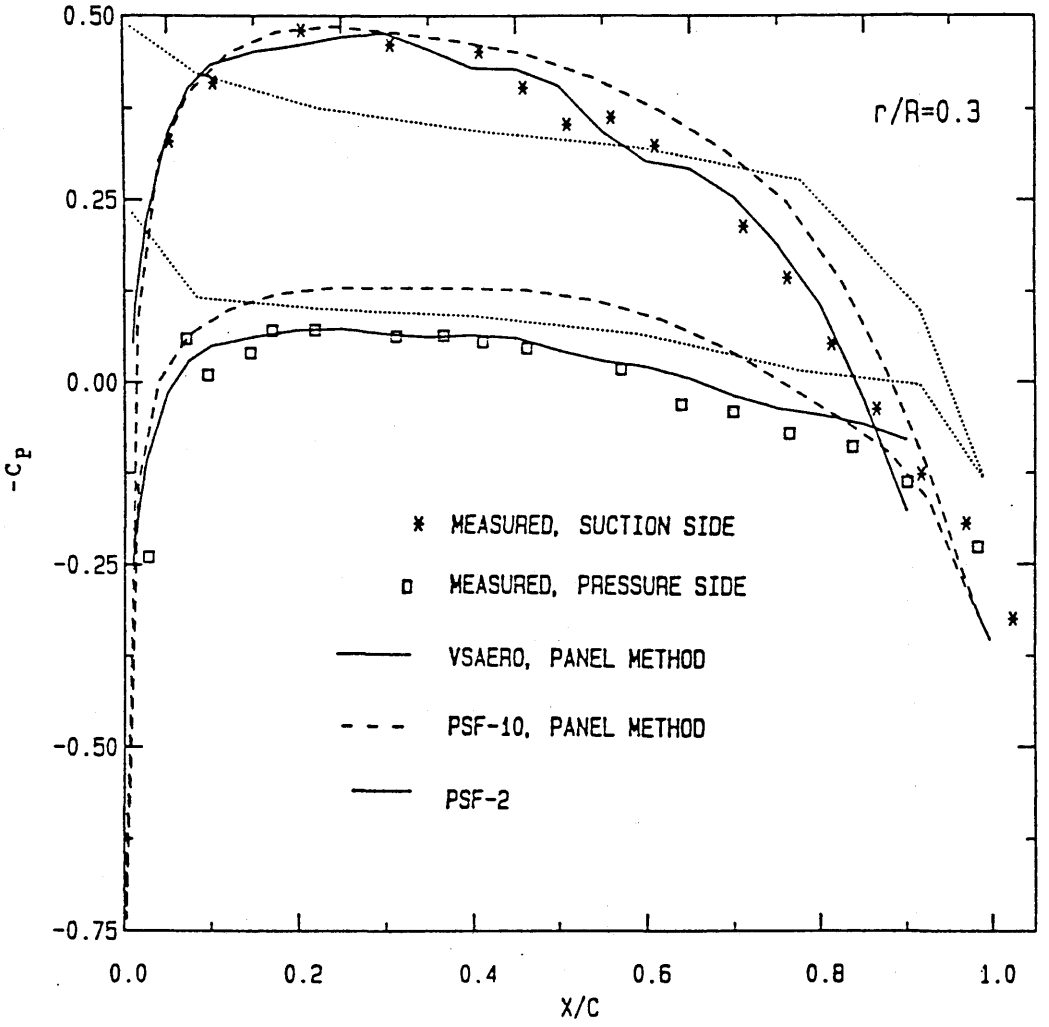

Fig. 1.3.3 (a) Pressure distribution on DTRC4119 (CP at 0.3 radius)

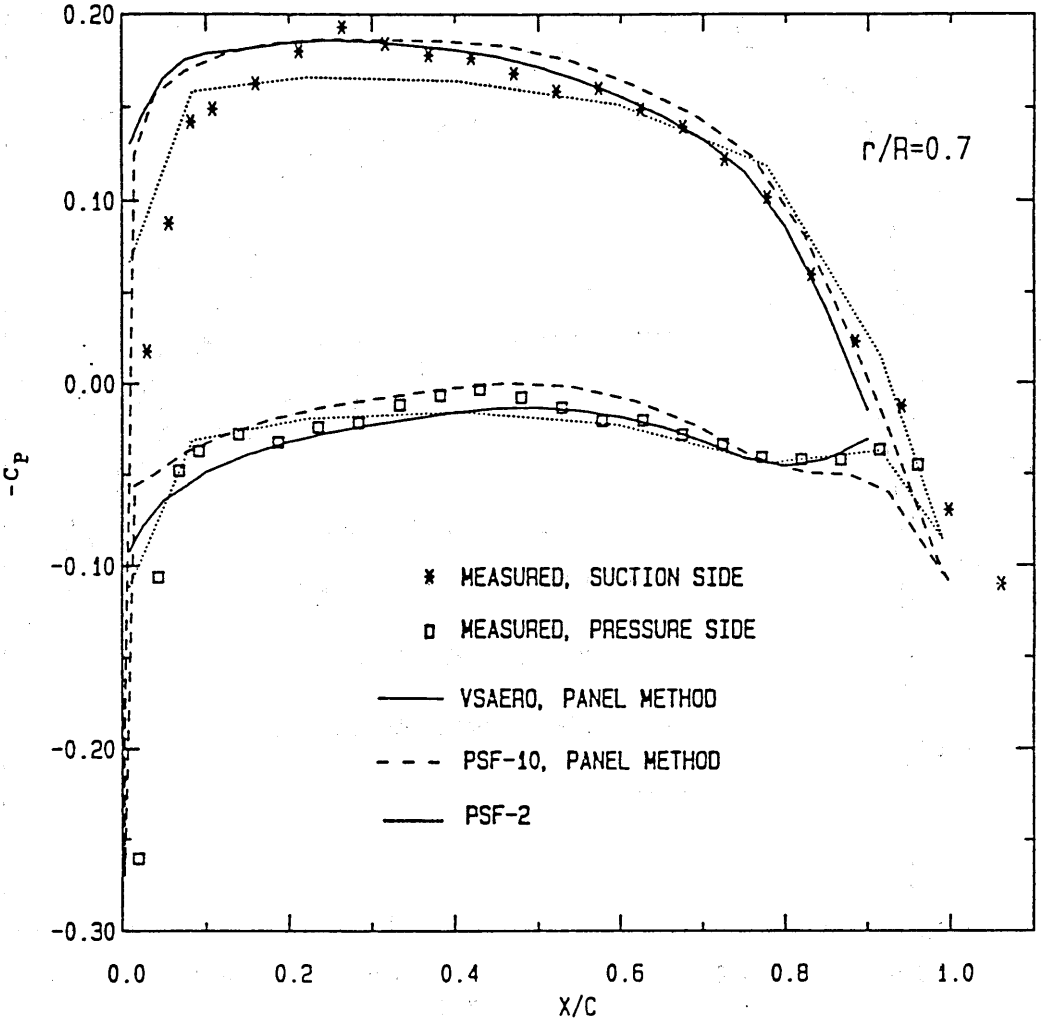

Fig. 1.3.3 (b) Pressure distribution on DTRC4119 (CP at 0.7 radius)

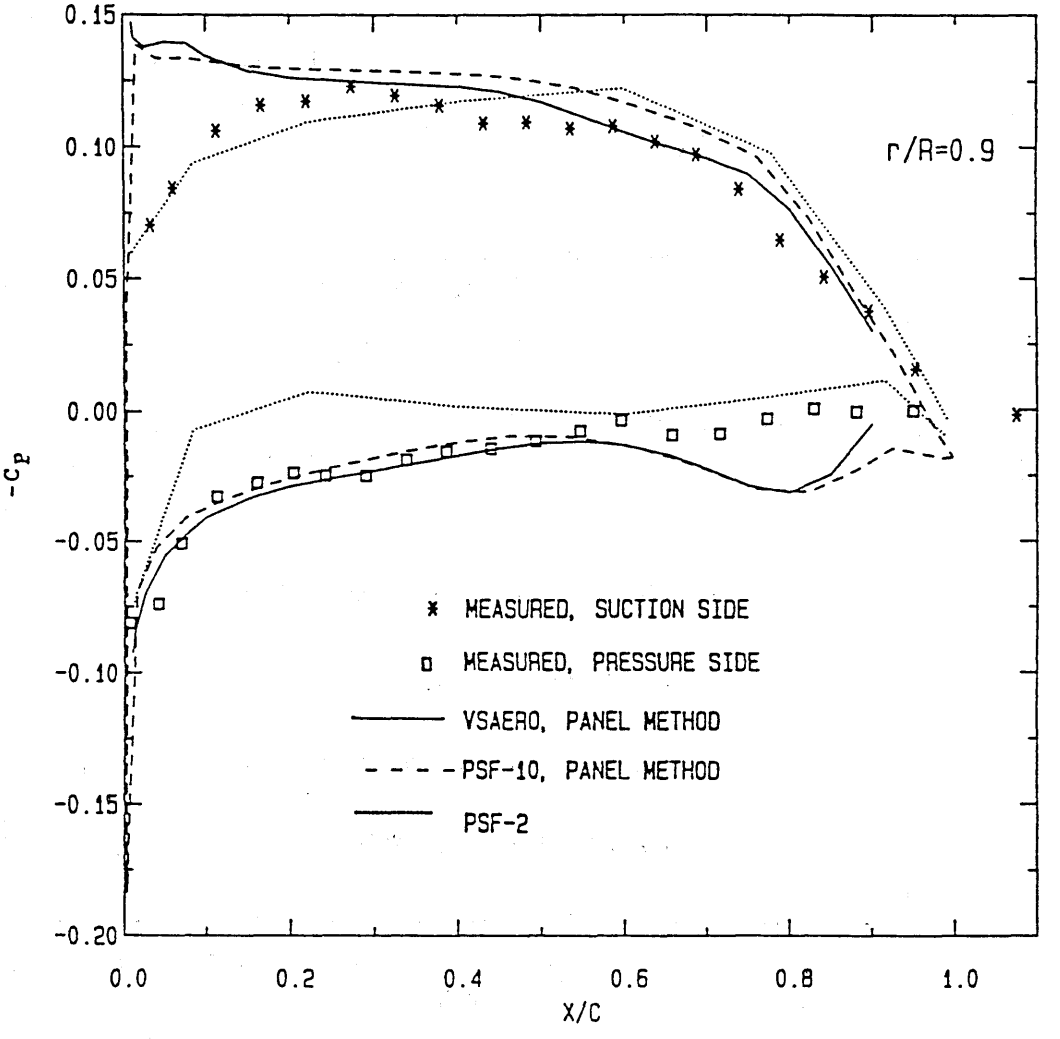

Fig. 1. 3. 3 (c) Pressure distribution on DTRC4119 (CP at 0.9 radius)

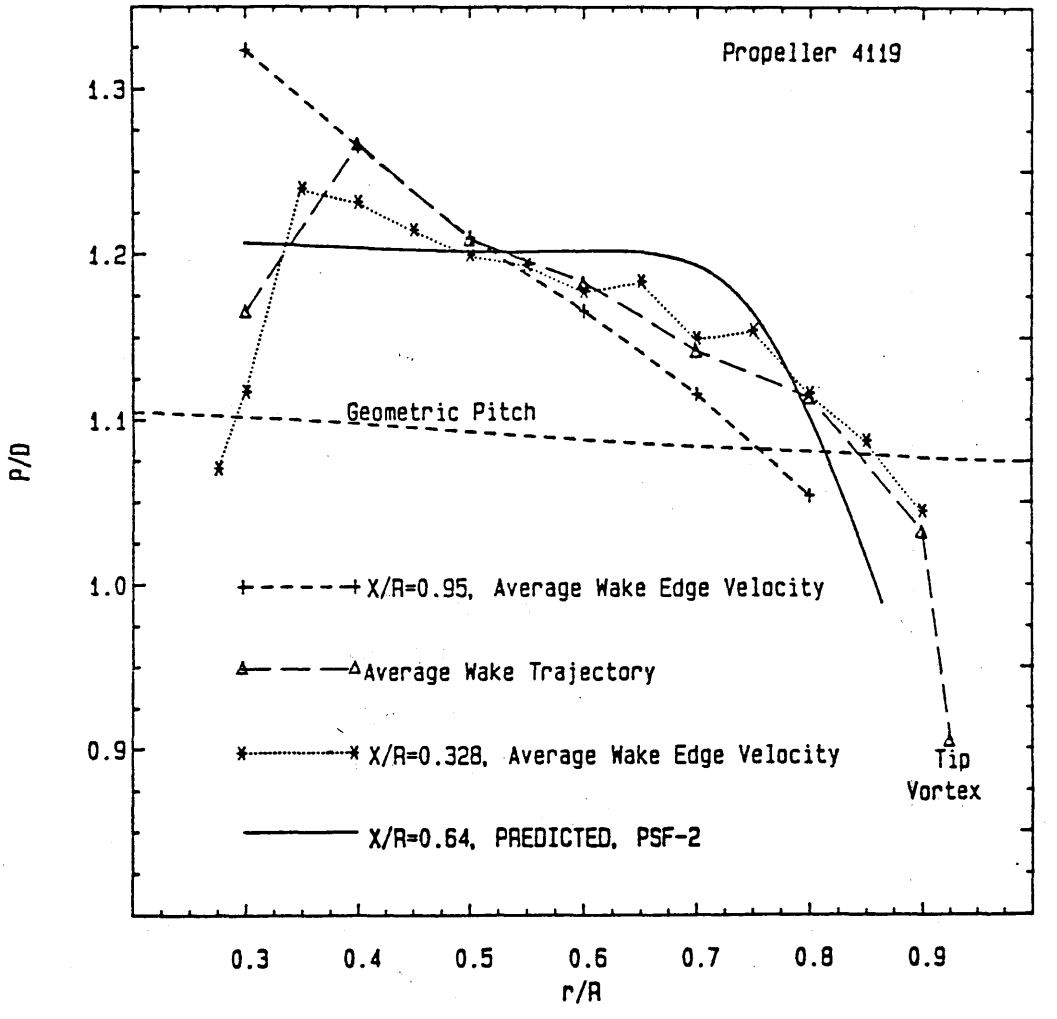

Fig. 1. 3. 4 Distribution of blade wake pitch

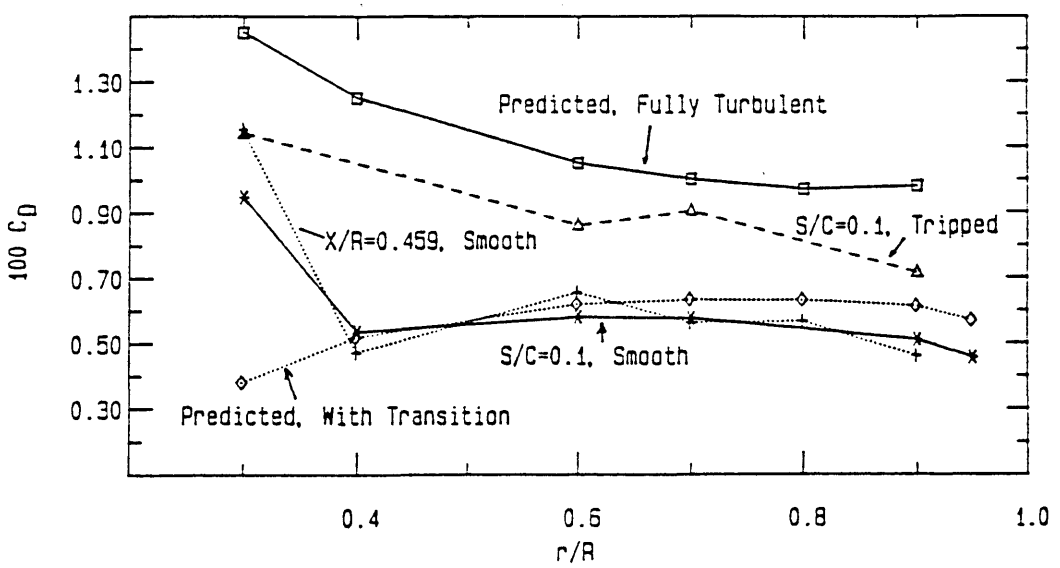

Fig. 1.3.5 Distribution of blade section drag coefficients

The following papers were submitted to the Workshop of ITTC Propulsor Committee. Although these papers contain a lot of valuable and useful information on the panel methods for marine propellers, they are only submitted to the Workshop and they have not been open by any publication. The author believes that it should be very benefitial to researchers of propeller panel methods to publish these papers, and he opens these papers as Appendices of this report with the contributors' permissions. The author would like to thank contributors for permissions.

APPENDIX B

Calculations by DTMB

David Taylor Model Basin
Carderock Division
Naval Surface Warfare Center
carderock, Maryland 20084-5000

Prediction of Hydrodynamic Performance of DTMB Propellers 4119 and 4842 with a Panel Method

Cheng-I Yang

ABSTRACT

This report presents the results of a numerical simulation of the hydrodynamic performance of DTMB Propellers 4119 and 4842. A panel method of analysis is used and the computation code adopted is the DTMB version of the VSAERO code. Numerical prediction includes open water characteristics, pressure distribution on blade surface and velocity at a given plane behind the blade row. Effect of viscous drag correction is also examined. The prediction obtained by panel method agrees reasonably well with the experimental data reported previously by DTMB.

INTRODUCTION

Two open propellers were designed, built and tested extensively in towing basin and water tunnel at DTMB[1]. The physical characteristics of those two propellers are distinctively different. Propeller 4119 is a three bladed propeller with neither rake nor skew. The pitch to diameter ratio of the blade sections remains almost constant from the root to the tip. It has a relatively small hub to diameter ratio (0.2). The design condition of the propeller occurs at advance coefficient , J = 0.833 with a thrust coefficient K_T of 0.154. Propeller 4842 is a five bladed propeller with a moderate degree of rake and skew. The pitch to diameter ratio of blade sections varies significantly from the root to the tip. Its hub to diameter ratio is 0.323. The design advance coefficient is J = 0.905 with a relative high thrust coefficient K_Q of 0.0305. Because of the outlined distinguishing characteristics, the experimental data of these two propellers provide an excellent benchmark for a numerical simulation scheme. The experimental data include; the open water characteristics, surface pressure distribution and the velocity survey behind the propeller. However, because of the obstruction of the optical path by the twisted blade shape of Propeller 4842, information about surface pressure distribution is not available. Comparison of experiment data and computational results obtained by a panel method are presented in following sections.

METHOD OF ANALYSIS

A fluid is incompressible if its particles maintain their density along their paths, i.e., the substantial derivative of mass density ρ is zero:

$$\frac{D\rho}{Dt} = 0 \qquad (1)$$

The principle of mass conservation requires that the net amount of mass flow into a control volume per unit time equal to the rate at which the mass in the control volume is increasing. Thus

$$\frac{\partial \rho}{\partial t} + \nabla \cdot \rho \mathbf{u} = 0. \tag{2}$$

Equation 2 is the differential equation of continuity (the **bold** type denotes a vector quantity). From Eqs. 1 and 2 it follows that for incompressible fluids the equation of continuity is simply

$$\nabla \cdot \mathbf{u} = 0, \tag{3}$$

whether or not the flow is steady and whether or not the fluid is homogeneous. Furthermore, if the density of the fluid is constant and the flow is irrotational, the circulation around a closed circuit is zero,

$$\int \mathbf{u} \cdot d\mathbf{x} = 0. \tag{4}$$

Therefore $\mathbf{u} \cdot d\mathbf{x}$ is an exact differential, which can be denoted by $d\phi$. Thus

$$\mathbf{u} = \nabla \phi. \tag{5}$$

Equations 3 and 5 imply that the function ϕ satisfies the Laplace equation,

$$\nabla^2 \phi = 0 \tag{6}$$

Equation 6 is a kinematics condition; velocity components can be obtained from its solution. The associated pressure, however, can be obtained only from a dynamic condition, that is, the equation of motion. For propeller application, it is more convenient to express the equation of motion with respect to a rotating frame that is fixed to the propeller axis. If the fluid is inviscid and the reference frame is rotating with a constant angular velocity ω about the x axis, Newton's second law governing the flow becomes

$$\frac{D\mathbf{u}}{Dt} + \mathbf{F}_c = -\frac{1}{\rho}\nabla P - \nabla\left(\Omega - \frac{\omega^2 r^2}{2}\right) \tag{7}$$

where $\mathbf{F}_c$ is the Coriolis acceleration vector, Ω is the body force potential, and $r^2 = y^2 + z^2$.

The Coriolis acceleration vector $\mathbf{F}_c$ $(0, -2\omega w, 2\omega v)$ is perpendicular to the velocity vector (u, v, w). Hence its projection onto a streamline is zero. For steady flow of incompressible fluid the density is constant along a streamline S, the equation of motion becomes

$$u_s \frac{\partial u_s}{\partial S} = -\frac{\partial}{\partial S}\left(\frac{P}{\rho} + \Omega - \frac{\omega^2 r^2}{2}\right) \tag{8}$$

Integration of Eq. 8 yields

$$\frac{P}{\rho}+\frac{u_s^2}{2}+\Omega-\frac{\omega^2 r^2}{2}=\text{Constant along a streamline.} \qquad (9)$$

The constant on the right -hand side of Eq.9 can be determined by the upstream condition. It will be invariant throughout the fluid for irrotational flow.

In summary, in deriving Eqs. 6 and 9, it was assumed that (1) the fluid is incompressible and inviscid, the density is constant, and (2) the flow is irrotational and steady. As a consequence, the flow solutions can be obtained from Eqs. 6 and 9, instead of from Eqs. 2 and 7. (Equations 6 and 9 are simplified forms of Eqs.2 and 7.) Equation 6 is linear, with linear boundary condition (without free surface); it can be solved very easily. the velocity components can be determined from Eq. 5 and the associated pressured calculated from Eq. 9. The non linearity of Eq. 7 is reflected only in the non linearity of Eq. 9, and there it presents no difficulty at all because the nonlinear terms are clearly determined and only the pressure is to be evaluated.

Green's theorem is applied to Eq. 6, and then the perturbation velocity potential ϕ_p at a point P on the surface of the propeller can be expressed as follows:

$$2\pi\phi_P=\iint_{S-P}\phi\,\mathbf{n}\cdot\nabla\left(\frac{1}{r}\right)ds+\iint_{W}(\phi_u-\phi_l)\mathbf{n}\cdot\nabla\left(\frac{1}{r}\right)dw$$
$$+\iint_{S}\frac{1}{r}(\mathbf{n}\cdot\mathbf{v}_\infty+\mathbf{n}\cdot\varpi\times\mathbf{R})ds \qquad (10)$$

where
- r =is the length of the vector extended from any other point to the point P and
- S-P =signifies that the point p is excluded from the surface integration;
- **n** =is the normal vector on the surface;
- W =signifies that the surface integration is extended over the wake sheet; and
- ϕ_u, ϕ_l =are the perturbation potentials on the upper and lower sides of the trailing edge, respectively.

The angular velocity of the propeller is ϖ, and **R** is the position vector of point P. The detailed derivation of Eq. 10 is given by Greely and Kerwin[1].

The first term on the right-hand side of Eq. 10 can be interpreted as the potential induced at point P by the distribution of doublets on S-P. their axes lie along the unit normal surface vector **n** and their strength is ϕ on the boundary surface. the same interpretation can be applied to the second term except that the doublet strength is set to $\phi_u - \phi_l$. The third term can be interpreted as the potential induced at point P by the distribution of sources on surface S-P whose strength is determined by the flow condition on the boundary surface. Equation 10 suggests that the strength of the perturbation potential at any given point P on the boundary surface can be considered as a sum of contributions from singularities such as the source and doublet of specified strength placed over the boundary surface of a flow field. Equation 10 can be solved numerically, once the boundary surface is discretized as panels. Therefore, the technique is referred to as a panel method or a singularity method.

The VSAERO code is formulated to solve Eq. 10 numerically to first-order accuracy. It replaces the smooth continuous shape of the body surface with a collection of plane quadrilateral panels and places singularities with constant strengths on the surface

of the plane panels. Some origins of the error associated with the first -order approximation will be outline here.

In general, any four vertices on a curved surface do not determine a plane, that is, the four sides do not rest on a common plane. However, a parallelogram can be formed by joining the four midpoints of the four sides. As a simple approximation, a curved area enclosed by the four vertices can be represented by a plane quadrilateral whose corners are the projections of the vertices onto the plane containing the parallelogram. In order to approximate the continuous physical surface meaningfully with a collection of flat panels, the deviation of the surface points and their projections on the panel plane should be kept as small as possible. The control point of a panel is obtained by taking the algebraic mean of its four corners, but the control point so defined may not lie on the physical surface. the boundary conditions are satisfied only at control points of the panels. Consequently, the velocity components and the potential at the physical surface between the control points are not likely to satisfy the imposed conditions. The difference can be reduced, although it may not be eliminated completely, by a more adaptive panel distribution in which more panels are placed at the region in which the surface normal vector varies rapidly.

The singularities described previously are distributed on the panel surface rather than on the physical surface. For a simple distribution such as the first-order approximation, the influence at a given field point of the singularities of unit strength distributed over a single panel of arbitrary shape can be computed entirely analytically. Such quantities are referred to as influence coefficients. The formation of VSAERO's influence coefficients is described by Newman [2].

When the physical surfaces of the propeller blade are replaced with N flat panels and the wake surface is replaced with M panels, Eq. 10 can be written in a discretized form:

$$2\pi\phi_j = \sum_{\substack{k=1 \\ k\neq j}}^{N}\{C_{jk}\mu_k\} + \sum_{k=1}^{M}\{C_{jk}\mu_k\} + \sum_{k=1}^{N}\{\beta_{jk}\sigma_k\} \qquad (11)$$

where C_{jk} and B_{jk} are the influence coefficients for the constant doublet and source distribution, respectively, on panel k acting on the control point of panel j, and μ_k and σ_k are the strengths of doublet and source on panel k, respective. with σ_k predetermined, Eq. 11 can be written in a matrix form as follow:

$$[\mathbf{A}][\bar{\mu}] = [\mathbf{D}] \qquad (12)$$

where [A] = the influence coefficients matrix,
$[\bar{\mu}]$ = the doublet strength vector, and
[D] = the boundary condition vector.

In actual numerical computation, the assembly of the matrix [A] involves the evaluation of C_{jk} , and the assembly of vector [D] involves the evaluation of B_{jk} . This process is very time consuming. [A] is a full matrix, and the solution of Eq.12 requires a large portion of the total computing effort, especially when the panel number is large.

In VSAERO code, the block Gauss- Seidel method is used for solving the system of equation in Eq.12. Once the potential field is obtained, the velocity components at each control point can be obtained by a finite-differencing scheme. In VSAERO code, the values of the potential at four surrounding control points are used as a base for finite-

differencing, and the method is of first-order accuracy. The pressure distribution on the surface is obtained by applying the steady-state Bernoulli equation.

PROPELLER 4119

The geometrical definition of the blade and the hub is given in reference 3. For numerical modelling, the blade surface is divided into 10 spanwise sections; each section contains 58 panels. The distribution of the panels is nonuniform in order to accommodate the surface curvature variation and to reduce the numerical error. The hub surface between two adjacent blades is modelled by 152 panels, there are 19 panels in axial direction and 8 panels in circumferencial direction. In present model, the corner points of the bounding panels from the blade and the hub match at the intersection. The hub surface in front of the blade row is modelled with 240 panels; there are 10 panels in axial direction and 24 panels in circumferencial direction. The surface behind the blade row is modelled by 240 panels. Over all a total of 2,556 panels are used to model this three bladed propeller. The perspective views of the discretized propeller is shown in Figure 1.

Two wake models are used for computations. The linear wake has no contraction. For a given wake line, its pitch angle is set to equal to the geometrical pitch angle of the blade section from where the wake line emanates. The deformed wake has contraction. The contraction model follows the suggestion by Hoshino [4]. For a given wake line, its pitch angle is aligned with the velocity at the trailing edge of the blade section from where the wake line emanates. To derive the deformed wake , an iteration process is required.

The viscous effect is accounted for through the specified sectional drag coefficient. The frictional coefficient is calculated using the 1957 International Towing Tank Conference Correlation Line. The total drag coefficient is calculated using empirical corrections given by Abbot and Von Doenhoff [5].

OPEN WATER CHARACTERISTICS

The comparison of the computed and the experimental open water characteristics is shown in Figure 2. Two sets of computational results are presented. In both cases, the deformed wake model are used. In one case the viscous correction is applied while in the other it is not. The purpose of this computation is twofold; the first is to examine the ability to predict the thrust and torque over a range of advance coefficient and the second is to examine the effect of the viscous correction. In view of the results presented in Figure 2, it appears that with the viscous drag correction, the thrust and torque can be predicted reasonably well over a wide range of advance coefficient. It also shows that in the absence of the viscous correction, the torque is considerably under predicted.

In order to examine the effect of the hub on the performance prediction, the hub panels are removed and the blade root is patched up with flat panels. The results are shown in Figure 3. Compared with the case with the hub, the differences in predicted thrust and torque are very slight over the range of advance coefficient studied.

The linear wake model has also been used to repeat the computations and it yields practically identical results.

SURFACE PRESSURE DISTRIBUTION

In reference 3, the surface pressure distribution at a given radial position was derived from the velocity components measured near the blade surface with a LDV technique. The derivation followed the inviscid steady-state Bernoulli's equation. In present analysis, the pressure distribution was derived in the similar manner. First, the velocity components were obtained by finite differencing the values of the potential on

blade surface, and then the pressure was obtained by applying the Bernoulli's equation. These approaches adopted in the experiment and in the analysis are compatible and valid under the condition that the blade boundary layer is thin and remains attached. The comparison between the experimental data and the computational results is meaningful only if such condition is fulfilled. Therefore, it is expected that the agreement will be better at the mid-span than at the root or the tip regions.

Surface pressure distributions at several radii are presented in Figure 4. The agreement between the computational results and the experimental data are good The hub effect is significant only at the inner most radius. Both the linear and the deformed wake model were used to perform the computations, the differences in surface pressure distributions are negligible.

VELOCITY COMPONENT BEHIND THE PROPELLER

In order to study the effect of the wake models on the flow field prediction, results from two computations at design advance coefficient are presented. One is obtained with linear wake model and the other is obtained with deformed wake model. Figures 5-6 display the results. The plane on which the velocity components are computed is located at 1.77 inches behind the propeller centerline (x/R = 0.295). Figure 1 shows the relative location of this plane with respective to the blades. The view is from downstream toward upstream and the propeller rotates in clockwise direction. The vortices shed from the blade tips can clearly be identified from the cross flow vector plot. However, different wake models predict different locations for the tip vortices. The deformed wake model predicts tip vortices slightly inboard in the radial direction and further downstream in the circumferencial direction. This is caused by the contraction of the wake lines.

The comparison of the computed and the measured velocity components at axial location x/R = 0.295 and radial location r/R = 0.7 is shown in Figure 7. In present case , the linear wake is used. The advance coefficient is J = 0.806. The agreement between the computed and the measured values is very good except at the regions where the viscous boundary layer is dominating.

PROPELLER 4842

The surface of Propeller 4842 is replaced with panels in the same manner as is described for propeller 4119. A total of 4,260 panels are used to model this five bladed propeller. The perspective views of the discretized propeller are shown in Figure 8 .The after portion of the hub of the test model was truncated and attached to a shaft with a smaller diameter. The panel model reflects this adjustment.

OPEN WATER CHARACTERISTICS

The prediction of open water performance is shown in Figures 9-10. Figure 9 indicates the degree of the viscous effect while Figure 10 shows the degree of the hub effect upon the performance prediction. The hub effect is insignificant at a lower but important at a higher advance coefficient. In all computations the deformed wake model and the viscous correction are implemented.

SURFACE PRESSURE DISTRIBUTION

Figure 11 show the prediction of the surface pressure distribution at various radius positions at the design advance coefficient. It is indicated in the figures that the effect of hub fades rapidly as the radius increases.

VELOCITY COMPONENTS BEHIND THE PROPELLER

Velocity components at a plane behind the propeller were measured [1]. The plane is located at 2.44 inches (x/R = 0.344) from the centerline of the blades. It is about the same axial location where the truncated hub joints the driving shaft. A backward facing step is formed and flow separation is expected. The impact on flow field prediction with a panel method is unclear. The relative location of the velocity measuring plane and the propeller blades is shown in Figure 12. Comparison of computed and measured values at radial position r/R = 0.822 is shown in Figure 13. The agreement is only fair. Cross flow velocity vector and axial velocity contour on that plane are shown in Figure 14-15 respectively. Tip vortices are not as well defined as that of Propeller 4119.

ACCURACY OF THE SIMULATIONS AND THE EXPERIMENT

Numerical simulation is an attempt, with the assistance of mathematics and physics and the resource of modern computers, to predict a physical phenomenon in a discretized manner. At present, one of the most popular approaches involves describing the phenomenon with an equivalent mathematical model and obtaining the solution with a discretization technique. The simulation technique of the panel method presented in this report is an example of this approach. The phenomenon involving fluid dynamics can best be described by the Navier-Stokes equation with an appropriate turbulence model. In formulating the equations various assumptions have been made and the final form is nonlinear. By imposing certain conditions on the flow field, such as those of Eq. 6 and Eq. 9, the non linearity can be removed from the mathematical model. However, the application of the model becomes further restricted and perhaps one more step away from the physical reality. The formulation outlined in the previous sections lead us to expect only first-order accuracy from the results of the panel method code VSAERO. Discretization techniques create yet another source of error. Detailed accounts of the effect of the mathematical accuracy on the physical prediction are discussed in references 6 and 7.

At present simulations, about 852 panels are used to model each blade sector of a propeller. Two sets of paneling with their control points positioned at different locations were modeled. For both sets of paneling, the total number of panels was the same and the panel distributions were nonuniform and curvature-adapted. the difference in computed thrust is approximately 2%.

In experiment, the propeller rotation speed was maintained to within 0.5% while the tunnel speed was maintained to within 1%. The accuracy in which the LDV measuring point was positioned produced errors in the measured results. Overall positioning accuracy was influenced by errors in referencing position, accumulated errors after referencing, and errors occurring when the transmitting beam axis was not perpendicular to the tunnel window. The axial and vertical reference was accurate to within approximately 0.003 inch (0.075 mm)and the y axis reference was accurate to within 0.030 inch (0.75mm). The accumulation of the traverse error was within 0.01 inch (0.25 mm). The calibration of the fiber optic probe was checked by measuring free stream velocity with both optical systems with agreement to within 0.2%.

CONCLUSION

Numerical simulations of the hydrodynamics performance of Propellers 4119 and 4842 with a panel method were performed and the results are presented. It is observed that :

(1) The linear wake model and the deformed wake model predict different locations for the tip vortices.
(2) Wake models have insignificant effect on the thrust and torque prediction.
(3) Viscous drag correction is essential to the correct prediction of the torque. Its effect on the prediction of the thrust is marginal.
(4) The effect of the hub on performance prediction depends not only on its size (hub to diameter ratio) but also the advance coefficient at which the propeller operates.
(5) Panel method predicts the hydrodynamic performance of open propellers well, if the rake and skew are relatively moderate.

REFERENCES

[1] Greely, D.S., Kerwin, J.E."Numerical Method for Propeller Design in Steady Flow," SNAME Transactions, Vol. 90 1982.

[2] Newman, J.N. "distributions of Sources and Normal Dipoles over a Quadrilateral Panel," Journal of Engineering Mathematics Vol 20 1986 pp113-126

[3] Jessup, S.D. "An Experimental Investigation of Viscous Aspects of Propeller Blade Flow," Ph.D. Dissertation. The Catholic University of American. 1989

[4] Hoshino, T. "A Surface Panel Method with a Deformed Wake Model to Analyze Hydrodynamic Characteristics of Propeller in Steady Flow," Mitsubishi Technical Bulletin No.195 April 1991.

[5] Abbot,I.H., von Doenhoff, A.E., "Theory of Wing Sections" Dover Publications Inc., New York (1949)

[6] Maskew, B.," Prediction of Subsonic Aerodynamic Characteristics : a Case of Low-Order Panel Method," J. of aircraft, Vol. 10, No. 2 February 1982

[7] Oskem, B.," Asymptotic convergence of High-Order Accurate Panel Method," NLR MP 85043 U April 1985

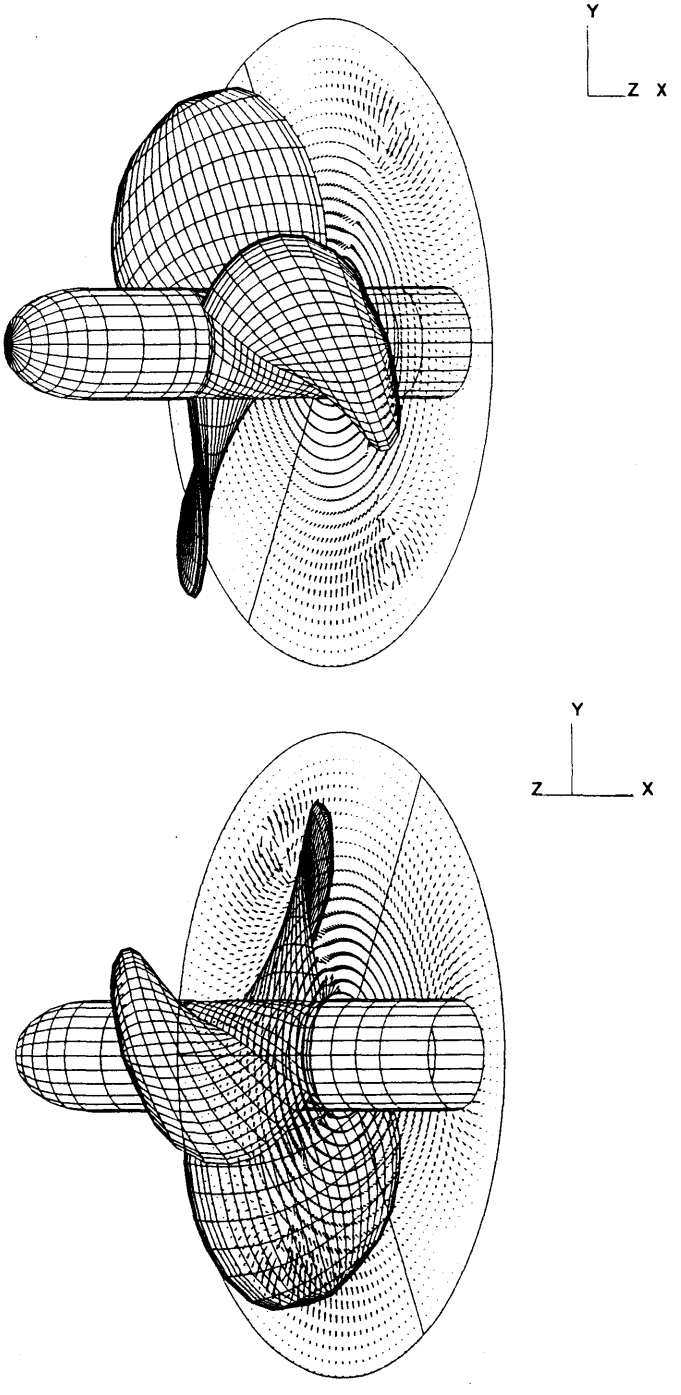

Fig. 1. Perspective Views of Discretized Propeller 4119.

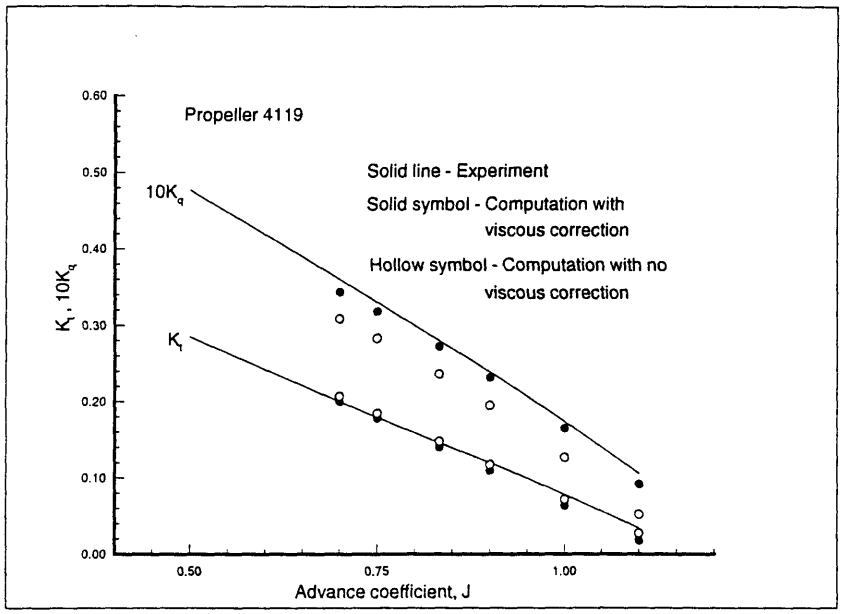

Fig. 2. Open Water Performance Curve, Propeller 4119 - Viscous Effect.

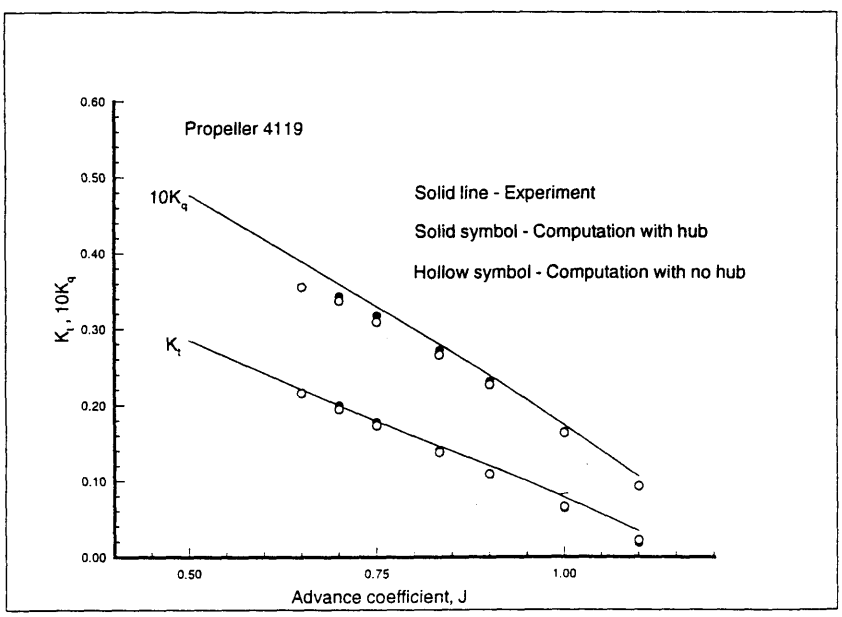

Fig. 3. Open Water Performance Curve, Propeller 4119 - Hub Effect.

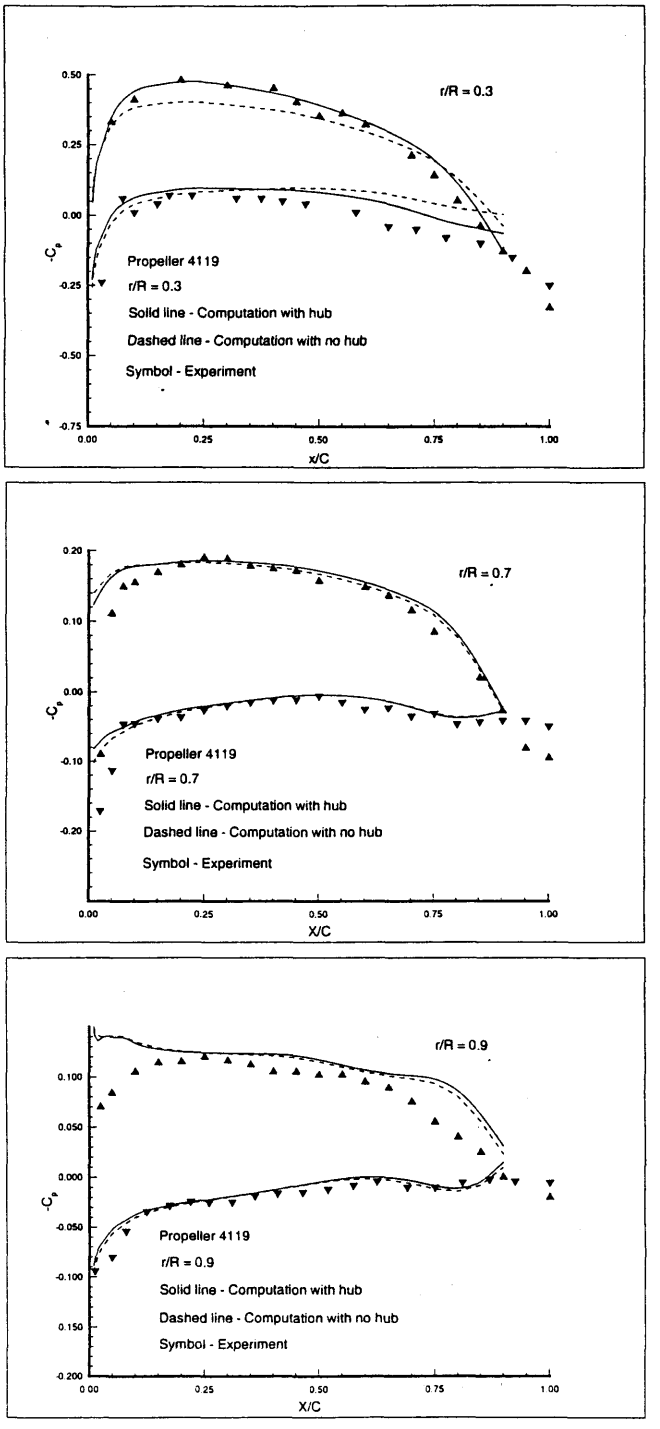

Fig. 4. Measured and Predicted Pressure Distribution on the Blade Surface of Propeller 4119.

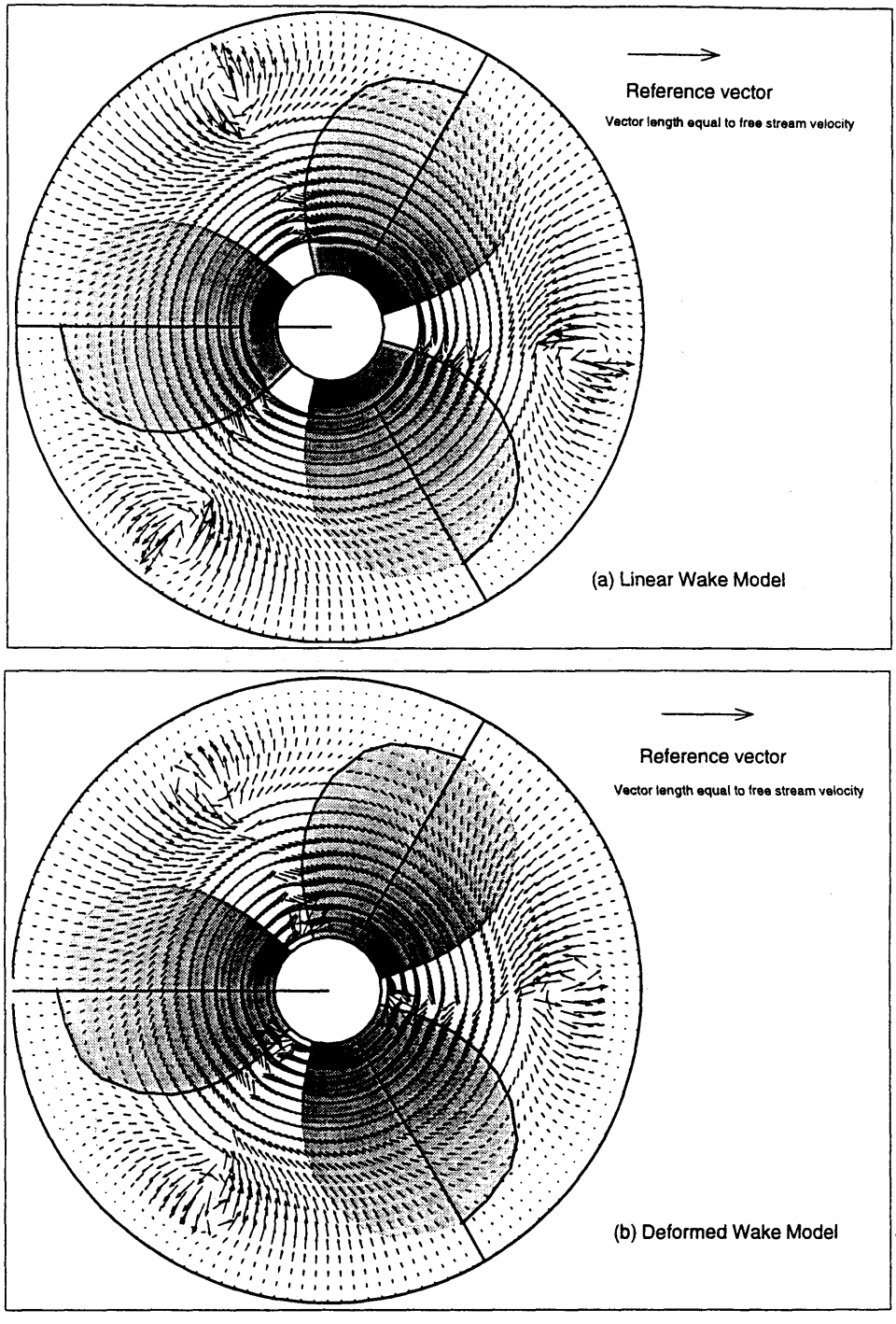

Fig. 5. Predicted Cross Flow Velocity Vectors on a Plane Behind Propeller 4119.

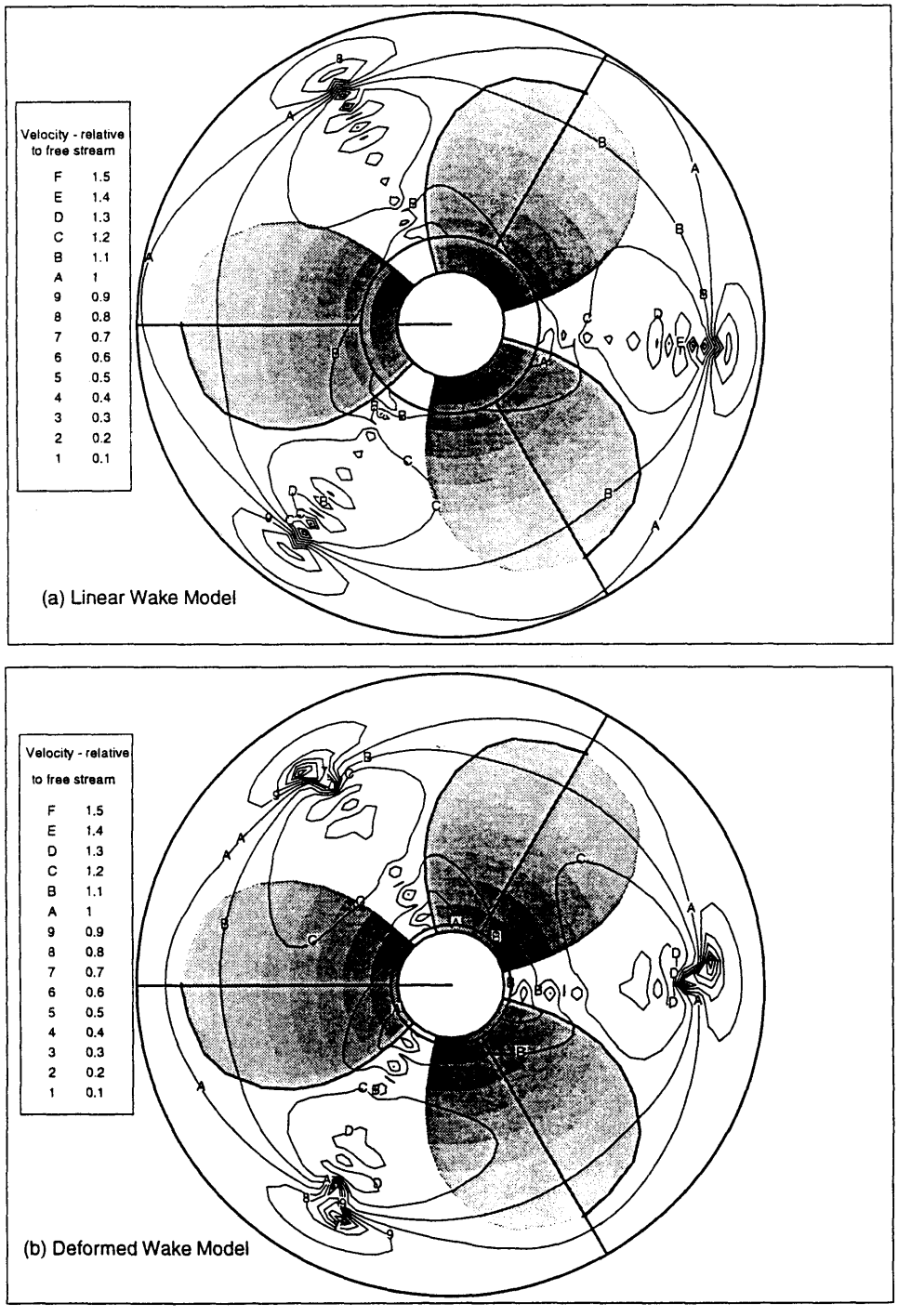

Fig. 6. Predicted Axial Velocity contour on a Plane behind Propeller 4119.

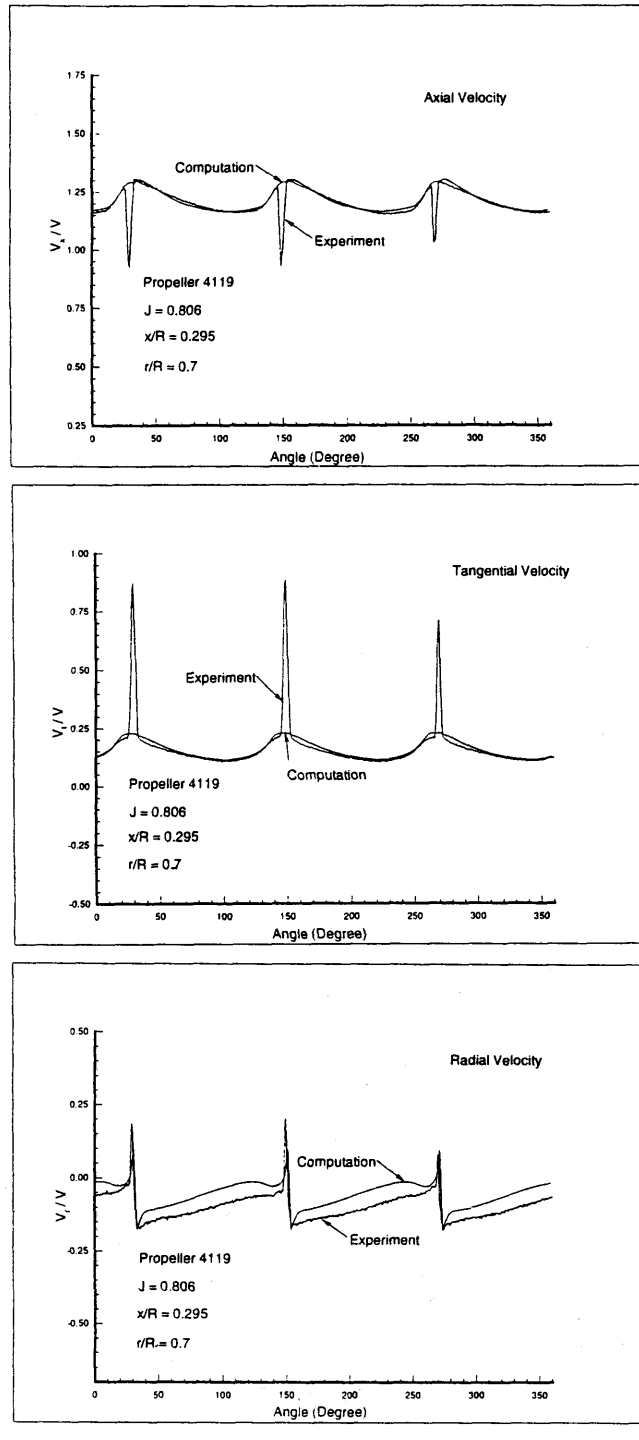

Fig. 7. Measured and Predicted Velocity Components Behind Propeller 4119.

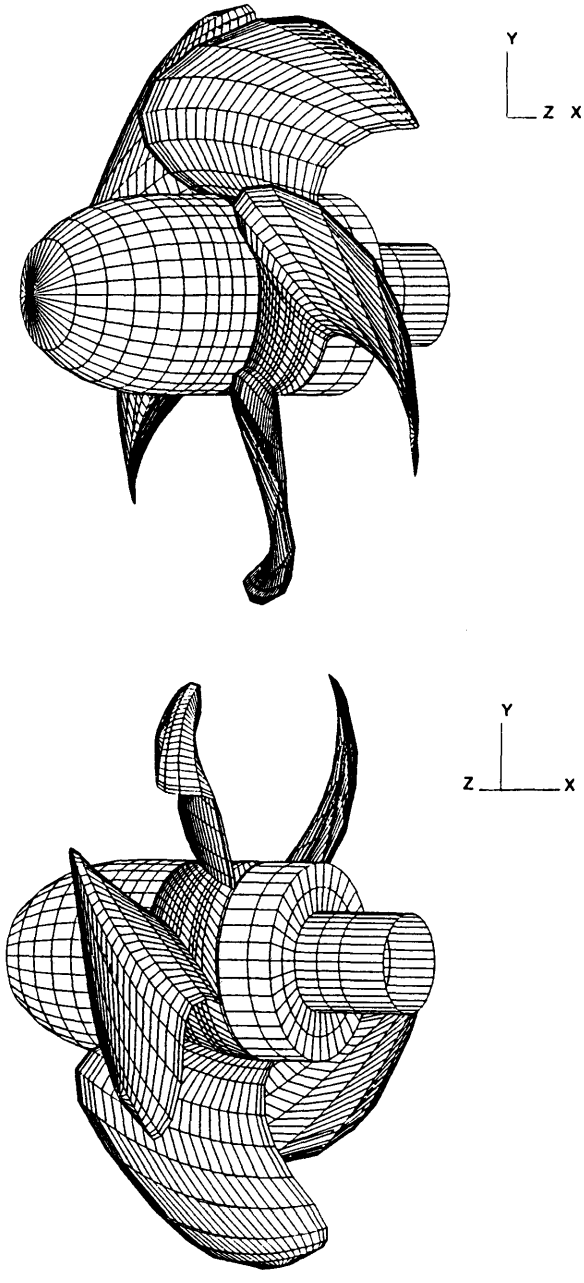

Fig. 8. Perspective Views of Discretized Propeller 4842.

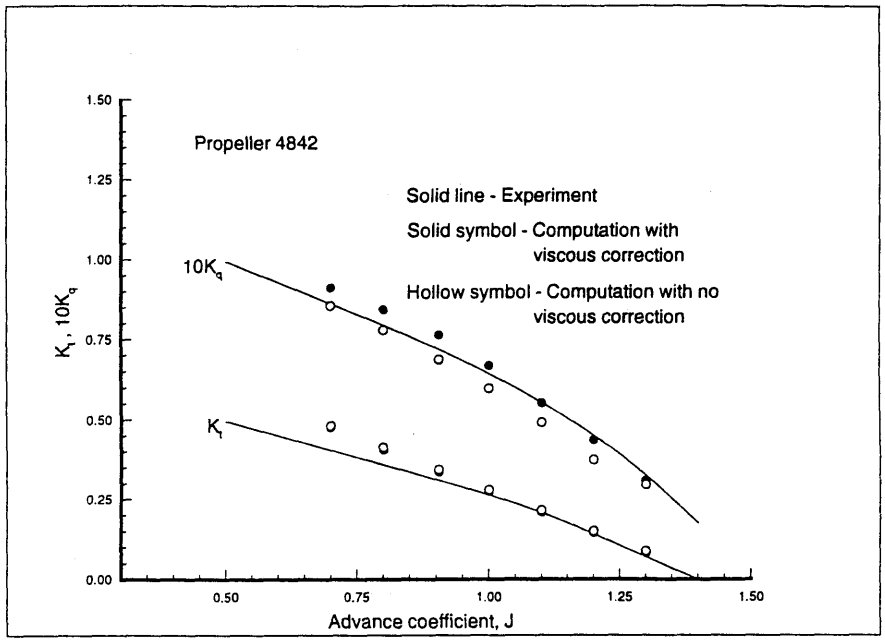

Fig. 9. Open Water Performance Curve, Propeller 4842 - Viscous Effect.

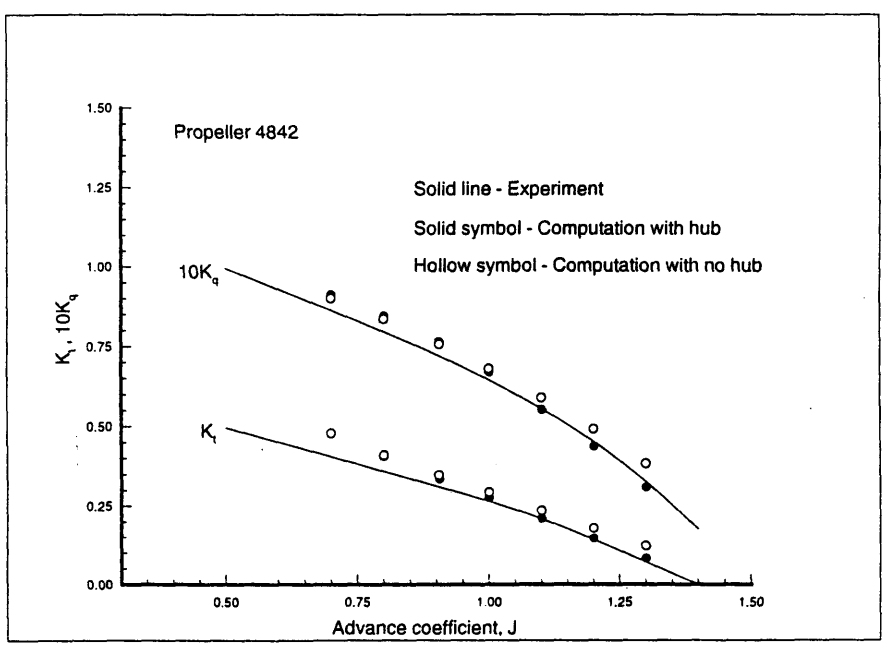

Fig. 10. Open Water Performance Curve, Propeller 4842 - Hub Effect.

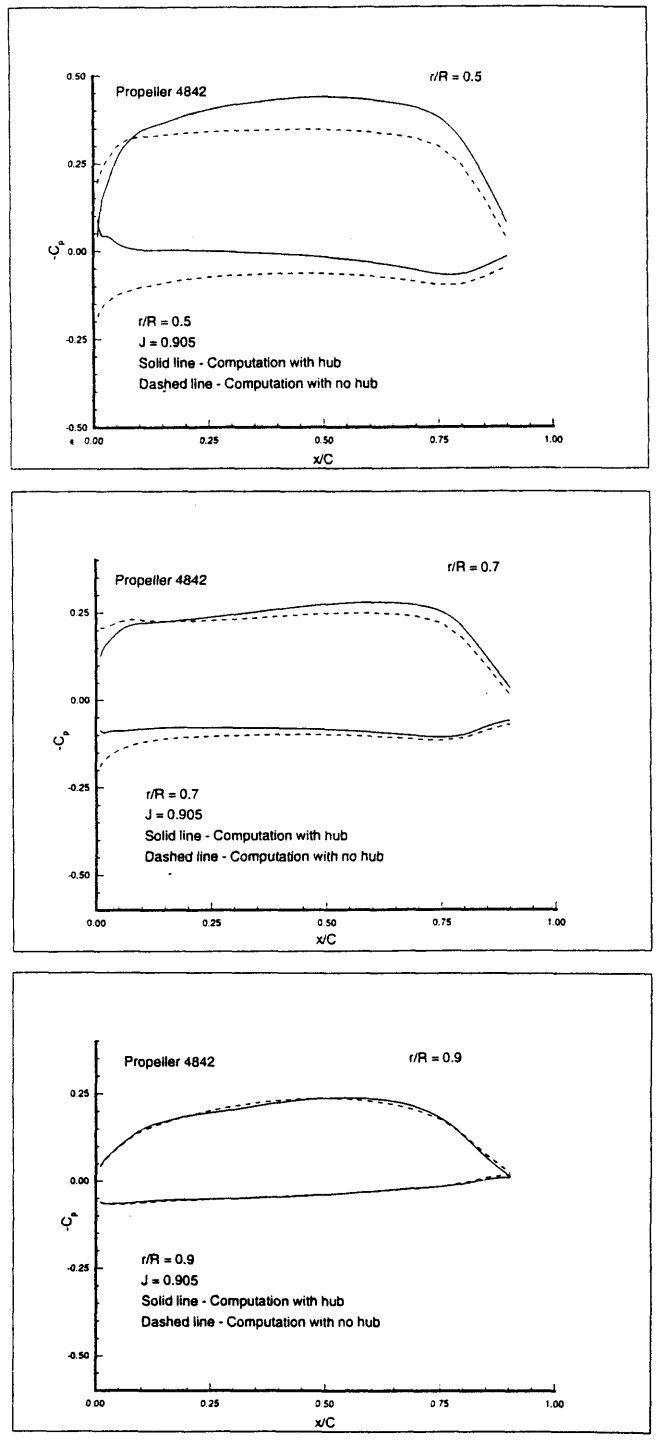

Fig. 11. Predicted Pressure Distribution on the Blade Surface of Propeller 4842.

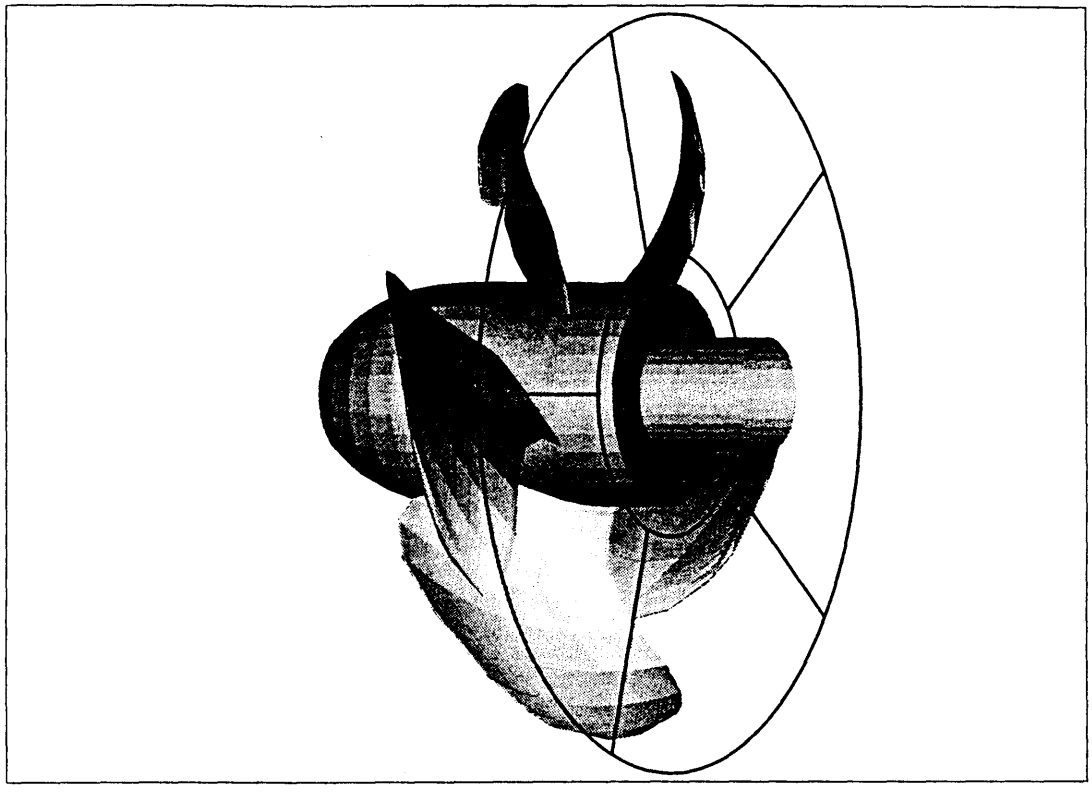

Fig. 12. Location of Velocity Measuring Plane with respect to the Propeller Blades, Propeller 4842

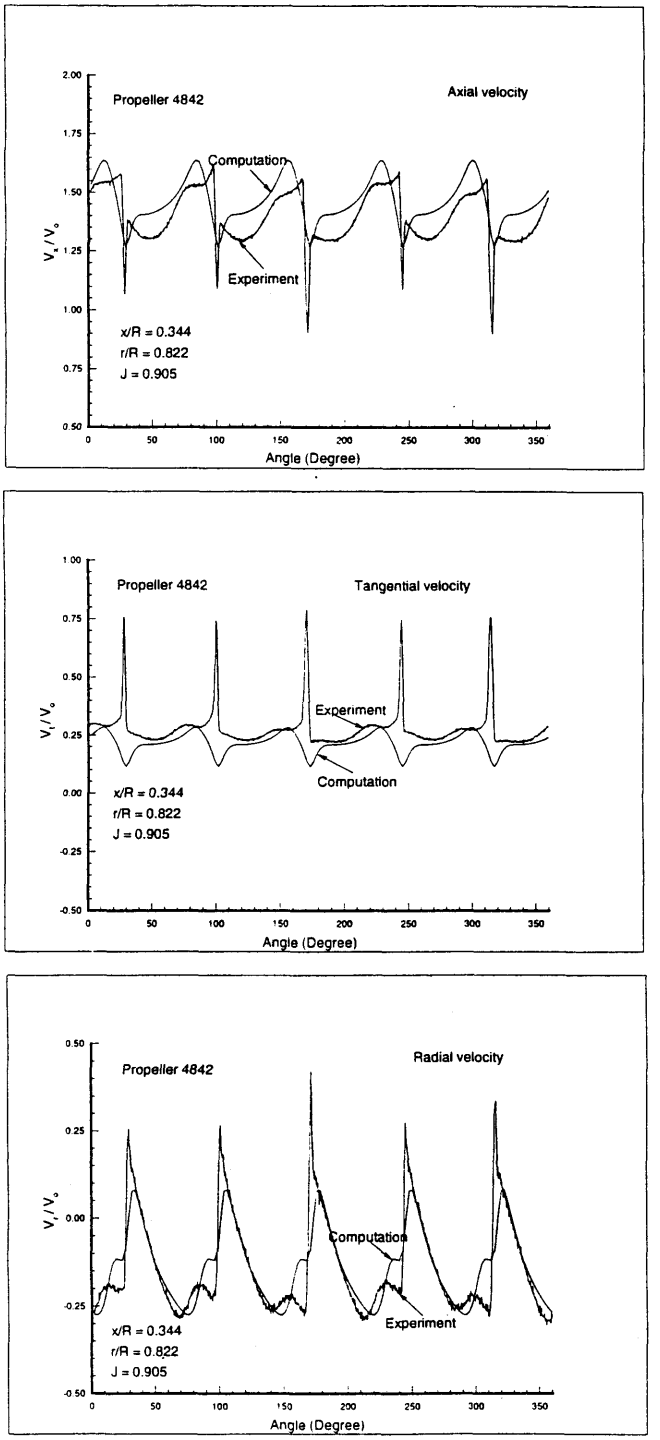

Fig. 13. Measured and Predicted Velocity Components Behind Propeller 4842.

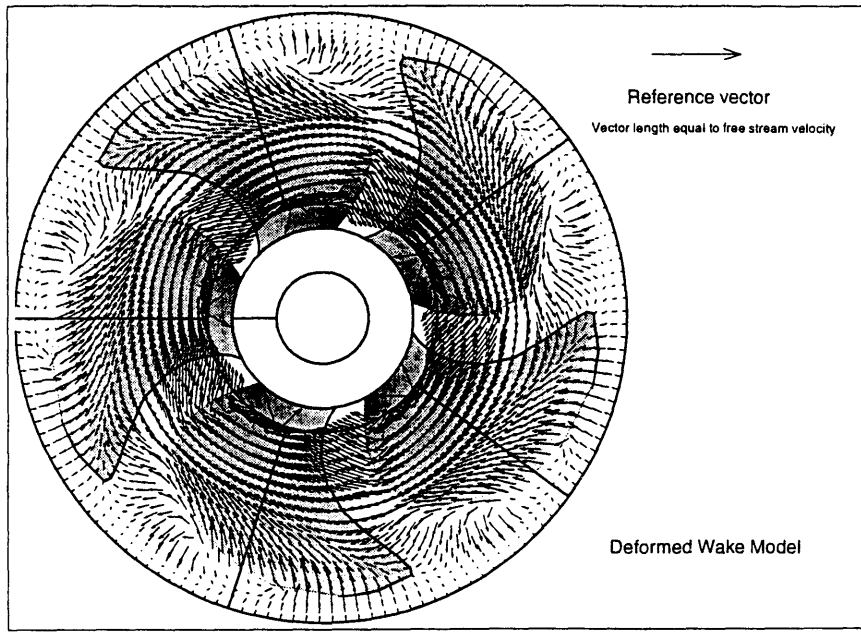

Fig. 14. Predicted Cross Flow Velocity Vectors on a Plane Behind Propeller 4842.

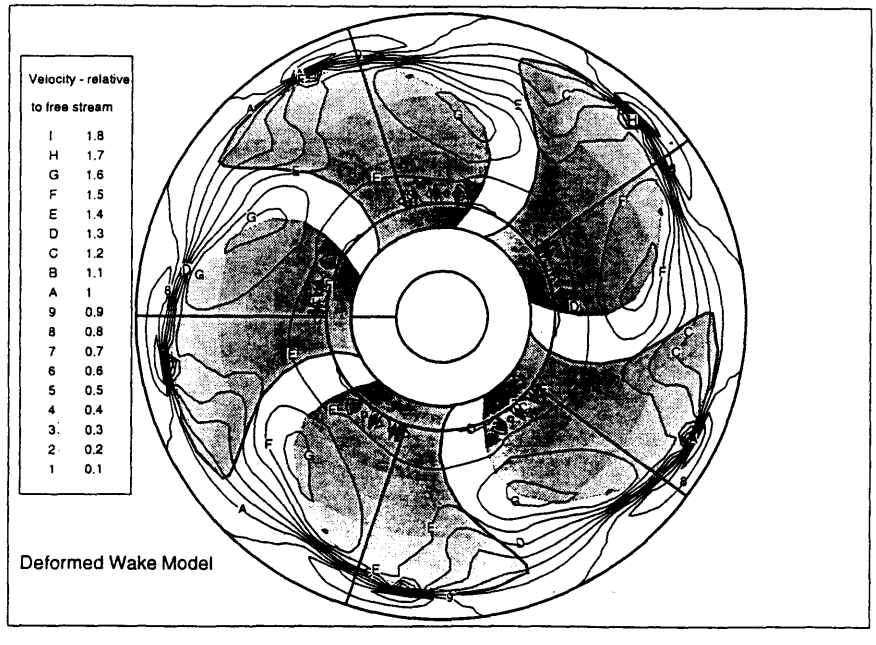

Fig. 15. Predicted Axial Velocity Contour on a Plane Behind Propeller 4842.

APPENDIX C

Calculations by MIT

Steady Performance Analysis for Two Propellers using MIT-PSF-10 prepared for 20^{th} ITTC Propulsor Committee Comparative Calculation of Propellers by Surface Panel Methods

Ching-Yeh Hsin and Justin E. Kerwin
Massachusetts Institute of Technology
Department of Ocean Engineering

July 17, 1992

1 Calculation Results

1.1 Standard-Condition Runs

We will first show the results of the "standard calculation conditions". In Table 1, the results of conditions required by ITTC are tabulated. All the calculations include the potential flow solutions and potential solutions with viscous corrections.

Viscous effects in MIT-PSF-10 are accounted for by a leading edge suction force correction and by the simple addition of tangential stresses derived from a constant frictional drag coefficient. The leading edge suction force correction is based on Polhamus' "leading edge suction analogy" [7], and the detail numerical implementation can been seen in [3]. In the following cases, the frictional drag coefficient is selected as $C_D = D/(\frac{1}{2}\rho V^2 c) = 0.007$, where D is the frictional drag/unit radius, V is the resultant inflow velocity at that radius and c is the expanded chord length.

The devised wake model of MIT-PSF-10 is based on MIT-PSF-2 wake model [1]. In the following cases, the contraction angle of the wake is 30°, and the ultimate tip wake radius is 0.83. The wake induced velocities calculated from MIT-PSF-2 are then used to generate the wake geometries.

The "recommended paneling" is 40 panels chordwise, and 30 panels spanwise. The "reference paneling" results are listed in Table 2. We have both increased and decreased the number of panels to check the convergence. In Table 2, all the results are without the viscous correction, and without the hub. The wake geometry is linear. The symbol $40c \cdot 30s$ indicates the number of panels used is 40 panels chordwise, and 30 panels spanwise.

The results of propeller 4119 at $J = 1.100$ are tabulated in Table 3, and the results of propeller 4842 at $J = 0.905$ are tabulated in Table 4. The calculated results of the propeller 4842 with the wrong rake (originally provided by ITTC) are also included in Table 5.

1.2 Complete runs of Propellers 4119 and 4842

We then calculated the forces of propellers 4119 and 4842 at different advance coefficients. All these calculations used the hub model suggested by ITTC (having fairwaters at both

ends), and used the devised wake model. Viscous corrections are included, and the frictional drag coefficient is selected as 0.007. The number of panels of all the runs is 40 panels chordwise, 30 panels spanwise.

This panel arrangement is illustrated in figures 1 and 2 for the two propellers. These figures also include grey-scale contour of the computed pressure distribution at the design advance coefficient.

Results are first tabulated in Table 6 and Table 7, and then plotted against experimental results in Figure 3 and Figure 4.

1.3 Effect of the Hub Geometries

To understand the effect of the hub geometries, we have calculated the forces on propeller 4119 by using three different hub geometries, along with the no hub results. Besides the hub model suggested by ITTC, we also used hub geometries with constant radii downstream and upstream. This is to simulate the real experiments which the propellers may be driven either from upstream, or from downstream. We named the ITTC hub model as the *hub model 1*, the hub which has a fairwater downstream, and constant radius upstream as the *hub model 2* (driven from upstream), and the hub which has a fairwater upstream, and constant radius downstream as the *hub model 3* (driven from downstream). Figure 5 shows these three different hub models. The calculated forces with hub model 1 have been shown in Table 6, the calculated forces with hub model 2 are shown in Table 8, and the calculated forces with hub model 3 are shown in Table 9. The results without hub are shown in Table 10. We have also plotted theses results against the experimental data in Figure 6.

It should be noted that a singularity will exist at the aft end of a closed hub unless the blade circulation is zero at the hub radius. This can be avoided by introducing a finite core radius to the hub vortex. PSF-10 has a provision for specifying a core radius, and hub forces are then computed assuming constant pressure on all panels that fall within the core. The results for propeller 4119 are shown in Table 11 by using the different core sizes. All the calculations listed before used a core radius of 10% of the hub radius.

2 Comparison with lifting surface methods

The [1] presented panel method is expected to be more accurate than any lifting surface method (linearized about the mean camber surface). The largest differences between the two methods will occur locally, namely at the edges of the blade where the lifting surface assumptions are not valid. However, in some cases (especially for thickness to chord ratios larger than 10%) even the global solutions from the two methods may differ. For example, this may be seen in Figure 7 where the circulation distributions are shown as predicted from the panel method (thick solid line) and from a conventional lifting surface method [1] (thin solid line). The lifting surface theory models the thickness with sources distributed on the mean camber surface. Thus, the effects of the thickness sources on one blade due to the other blades as well as due to the twist of the blade itself are readily included in the solution. However, the thickness/loading coupling, which is present even in the case of the planar wings, is not

[1] The present section has been prepared by Sangwoo Pyo and Spyros Kinnas.

included. A way of including this coupling has been developed recently [5]. The circulation distribution when the thickness/loading coupling is included is also shown in Figure 7 (circles). The agreement with the circulation distribution from the panel method is remarkable. The improved lifting surface method however, is still expected to fail at the blade edge.

3 Method of Calculation

MIT-PSF-10 is a lower order, potential based panel method. It uses hyperboloidal panel geometries and imposes the boundary condition on the panel centroid. The detail of the theory and numerical schemes can be found in [4], [6], [3] and [2].

References

[1] D.S. Greeley and J.E. Kerwin. Numerical methods for propeller design and analysis in steady flow. *Trans. SNAME*, vol 90, 1982.

[2] C-Y. Hsin, J.E. Kerwin, and S.A. Kinnas. A panel method for the analysis of the flow around highly skewed propellers. In *Proceedings of the Propellers/Shafting '91 Symposium*, pages 1–13 (paper No. 11), Virginia Beach, VA, September 1991. Soc. Naval Arch. & Marine Engnrs.

[3] Ching-Yeh Hsin. *Development and Analysis of Panel Method for Propellers in Unsteady Flow*. PhD thesis, Department of Ocean Engineering, MIT, September 1990.

[4] J.E. Kerwin, S.A. Kinnas, J-T Lee, and W-Z Shih. A surface panel method for the hydrodynamic analysis of ducted propellers. *Trans. SNAME*, 95, 1987.

[5] S.A. Kinnas. A general theory for the coupling between thickness and loading for wings and propellers. *Journal of Ship Research*, 36(1):pp. 59–68, March 1992.

[6] Jin-Tae Lee. *A Potential Based Panel Method for the Analysis of Marine Propellers in Steady Flow*. PhD thesis, MIT, Department of Ocean Engineering, 1987.

[7] Edward C. Polhamus. A concept of the vortex lift of sharp-edge delta wings based on a leading-edge-suction analogy. Technical Report NASA TN D-3767, Langley Research Center, 1966.

Without Viscous Correction

paneling	hub	wake	KT	KQ	η
recommended	w/o	linear	0.145	0.0237	0.813
reference	w/o	linear	see	next	table
recommended	w/	linear	0.143	0.0241	0.784
recommended	w/o	devised	0.151	0.0242	0.828
recommended	w/	devised	0.148	0.0243	0.805

With Viscous Correction

paneling	hub	wake	KT	KQ	η
recommended	w/o	linear	0.142	0.0259	0.725
reference	w/o	linear	see	next	table
recommended	w/	linear	0.138	0.0263	0.698
recommended	w/o	devised	0.147	0.0265	0.737
recommended	w/	devised	0.144	0.0266	0.716

Table 1: Propeller 4119, J=0.833

paneling	KT	KQ	η
$20c \cdot 10s$	0.152	0.0245	0.823
$40c \cdot 20s$	0.148	0.0241	0.812
$40c \cdot 30s$	0.145	0.0237	0.813
$60c \cdot 30s$	0.147	0.0241	0.808
$60c \cdot 40s$	0.145	0.0238	0.809
$80c \cdot 30s$	0.147	0.0242	0.806
$80c \cdot 40s$	0.146	0.0240	0.807

Table 2: Propeller 4119 Convergence Test (J=0.833)

Without Viscous Correction

paneling	hub	wake	KT	KQ	η
recommended	w/o	linear	0.0393	0.00734	0.938
recommended	w/o	devised	0.0398	0.00744	0.937

With Viscous Correction

paneling	hub	wake	KT	KQ	η
recommended	w/o	linear	0.0350	0.00890	0.689
recommended	w/o	devised	0.0355	0.00900	0.690

Table 3: Propeller 4119, J=1.100

Without Viscous Correction

paneling	hub	wake	KT	KQ	η
recommended	w/	devised	0.315	0.0653	0.693

With Viscous Correction

paneling	hub	wake	KT	KQ	η
recommended	w/	devised	0.306	0.0693	0.637

Table 4: Propeller 4842, J=0.905

Without Viscous Correction

paneling	hub	wake	KT	KQ	η
recommended	w/	devised	0.294	0.0593	0.714

With Viscous Correction

paneling	hub	wake	KT	KQ	η
recommended	w/	devised	0.285	0.0634	0.648

Table 5: Propeller 4842 with wrong rake, J=0.905

J	KT	KQ	η
0.500	0.282	0.0465	0.483
0.700	0.201	0.0354	0.633
0.833	0.144	0.0266	0.716
0.900	0.114	0.0221	0.740
1.100	0.024	0.0073	0.586

Table 6: Propeller 4119 with ITTC hub (hub model 1)

J	KT	KQ	η
0.500	0.530	0.1032	0.408
0.700	0.406	0.0872	0.518
0.905	0.306	0.0693	0.637
1.100	0.202	0.0509	0.695
1.300	0.084	0.0287	0.609

Table 7: Propeller 4842 with ITTC hub (hub model 1)

J	KT	KQ	η
0.500	0.282	0.0467	0.481
0.700	0.202	0.0358	0.630
0.833	0.146	0.0267	0.727
0.900	0.117	0.0226	0.739
1.100	0.028	0.0080	0.624

Table 8: Propeller 4119 with hub model 2

J	KT	KQ	η
0.500	0.296	0.0469	0.503
0.700	0.211	0.0361	0.652
0.833	0.151	0.0274	0.729
0.900	0.121	0.0230	0.753
1.100	0.031	0.0084	0.638

Table 9: Propeller 4119 with hub model 3

J	KT	KQ	η
0.500	0.273	0.0424	0.513
0.700	0.201	0.0338	0.661
0.833	0.147	0.0265	0.737
0.900	0.120	0.0225	0.765
1.100	0.035	0.0089	0.689

Table 10: Propeller 4119 without hub

core radius	KT	KQ
0.00	0.142	0.0266
0.02 (10%)	0.144	0.0266
0.04 (20%)	0.144	0.0266

Table 11: The results for propeller 4119 by using the different hub vortex core radius

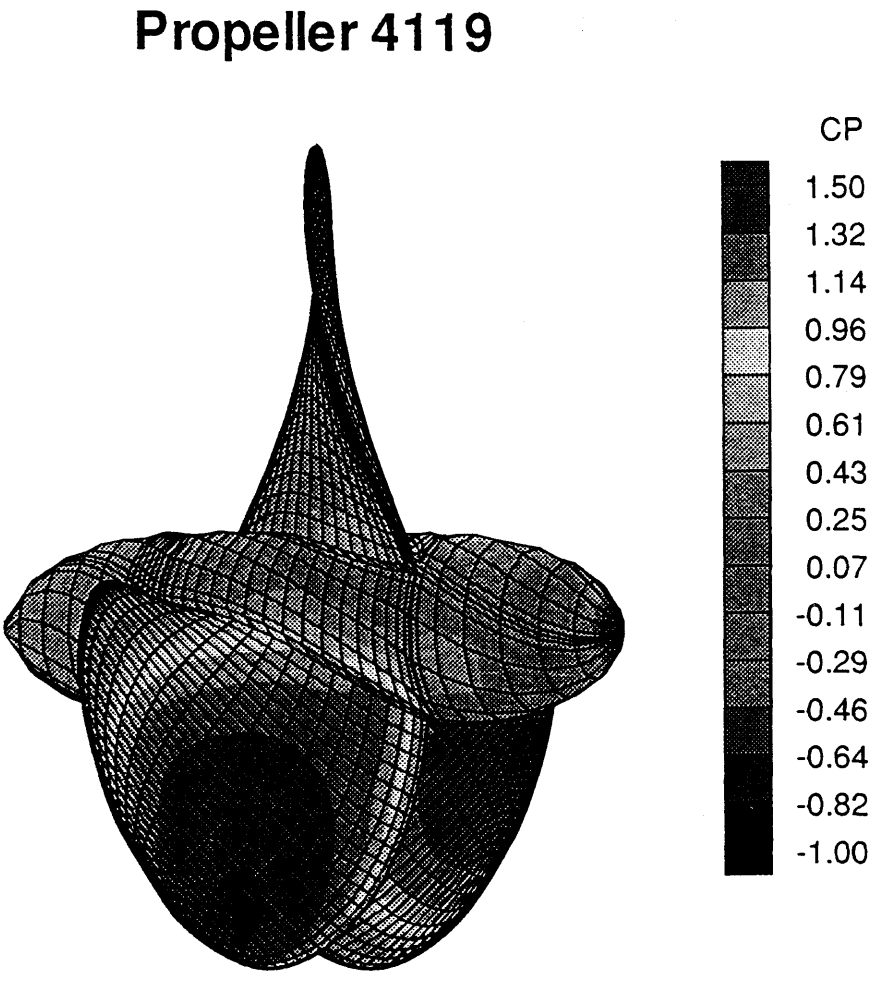

Figure 1: The panel arrangement and pressure distribution on propeller 4119 at the design advance coefficient. The paneling used here is the recommended paneling (40 panels chordwise, 30 panels spanwise).

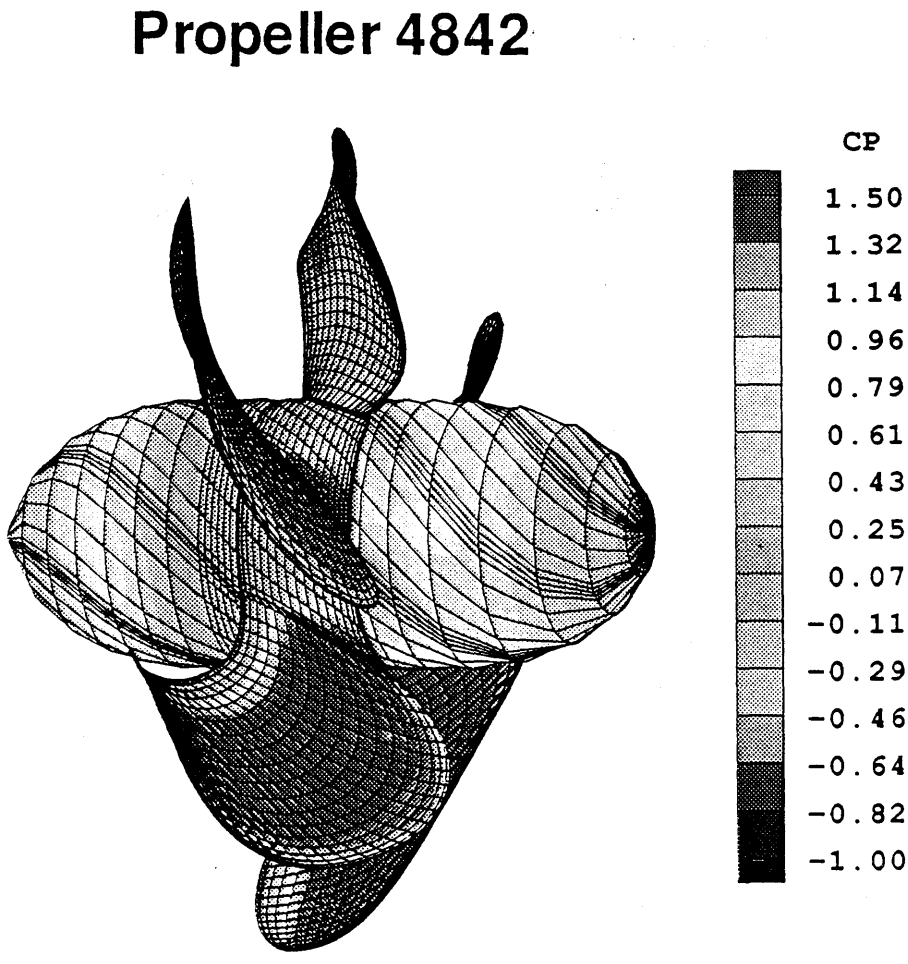

Figure 2: The panel arrangement and pressure distribution on propeller 4842 at the design advance coefficient. The paneling used here is the recommended paneling (40 panels chordwise, 30 panels spanwise).

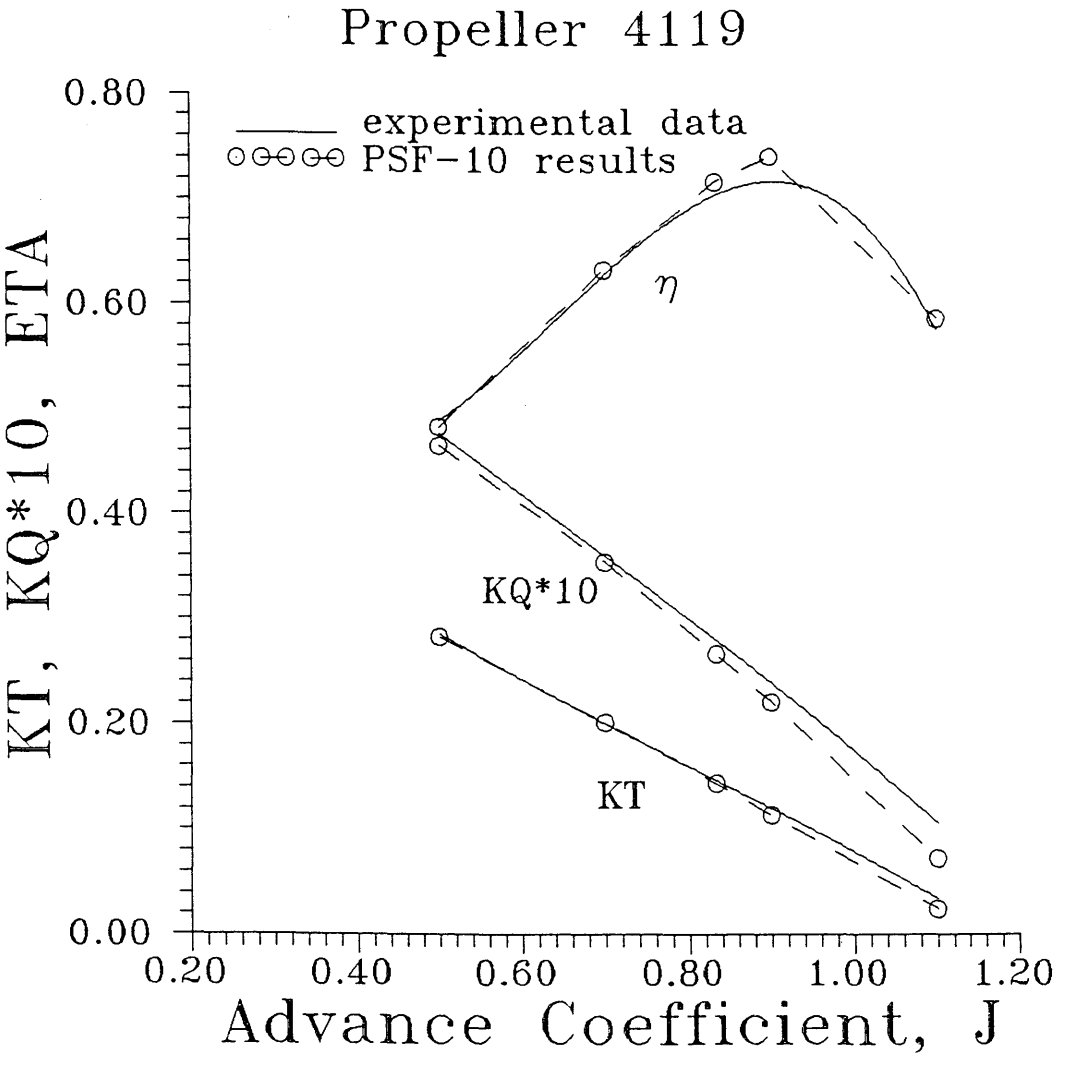

Figure 3: Computational results vs. experimental data of propeller 4119. All the computational results used ITTC hub model, and a drag coefficient 0.007.

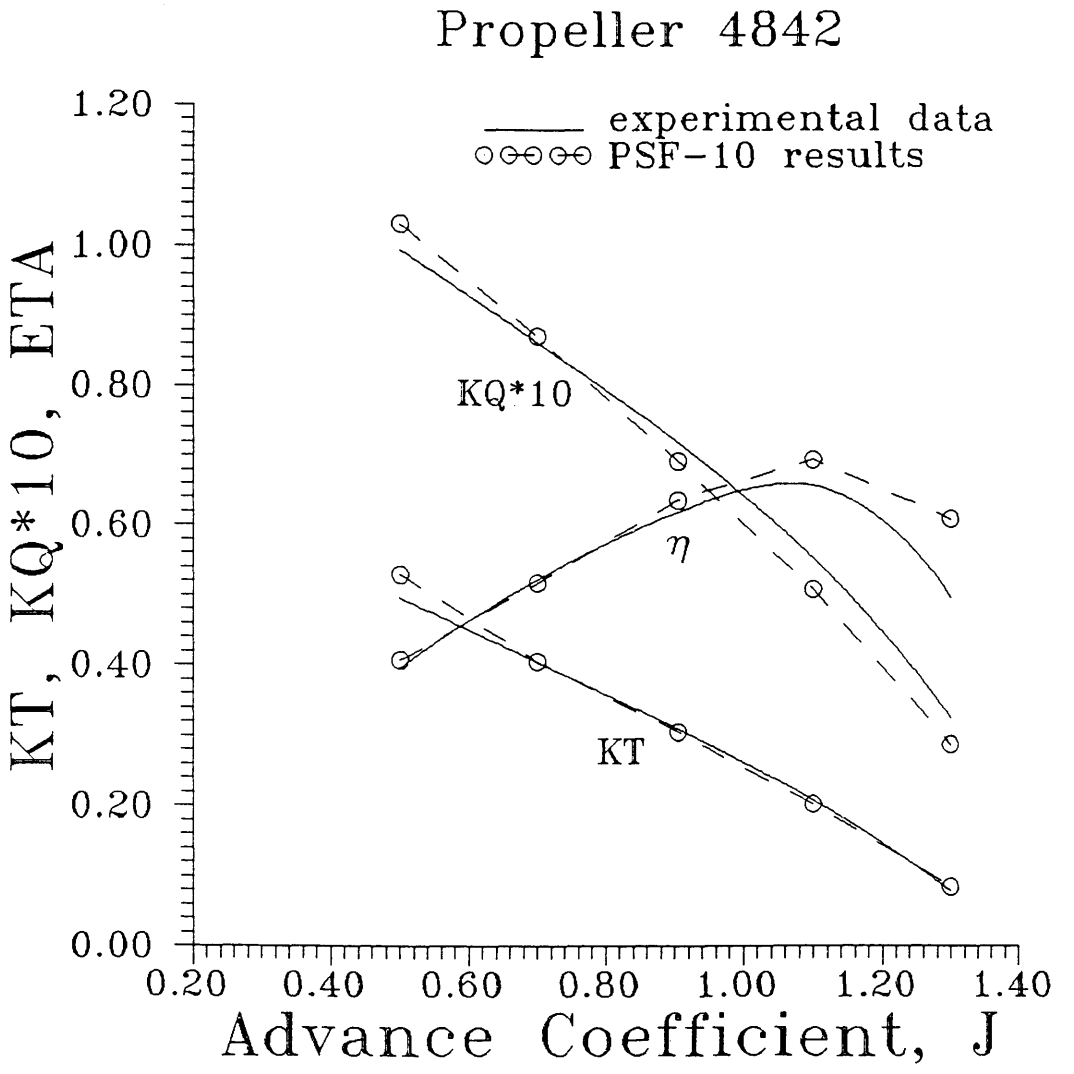

Figure 4: Computational results vs. experimental data of propeller 4842. All the computational results used ITTC hub model, and a frictional drag coefficient 0.007.

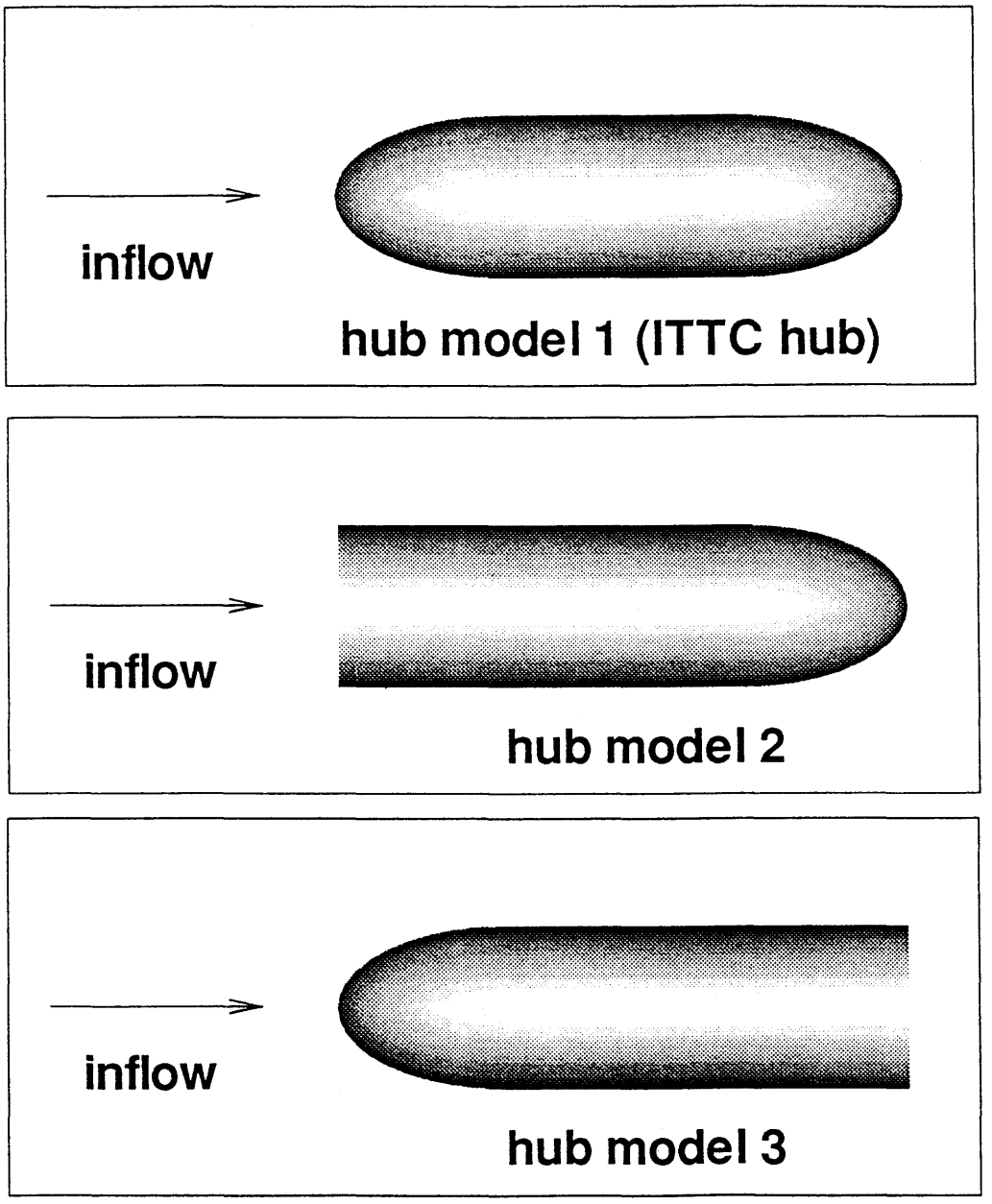

Figure 5: Different hub models used to investigate the hub effect.

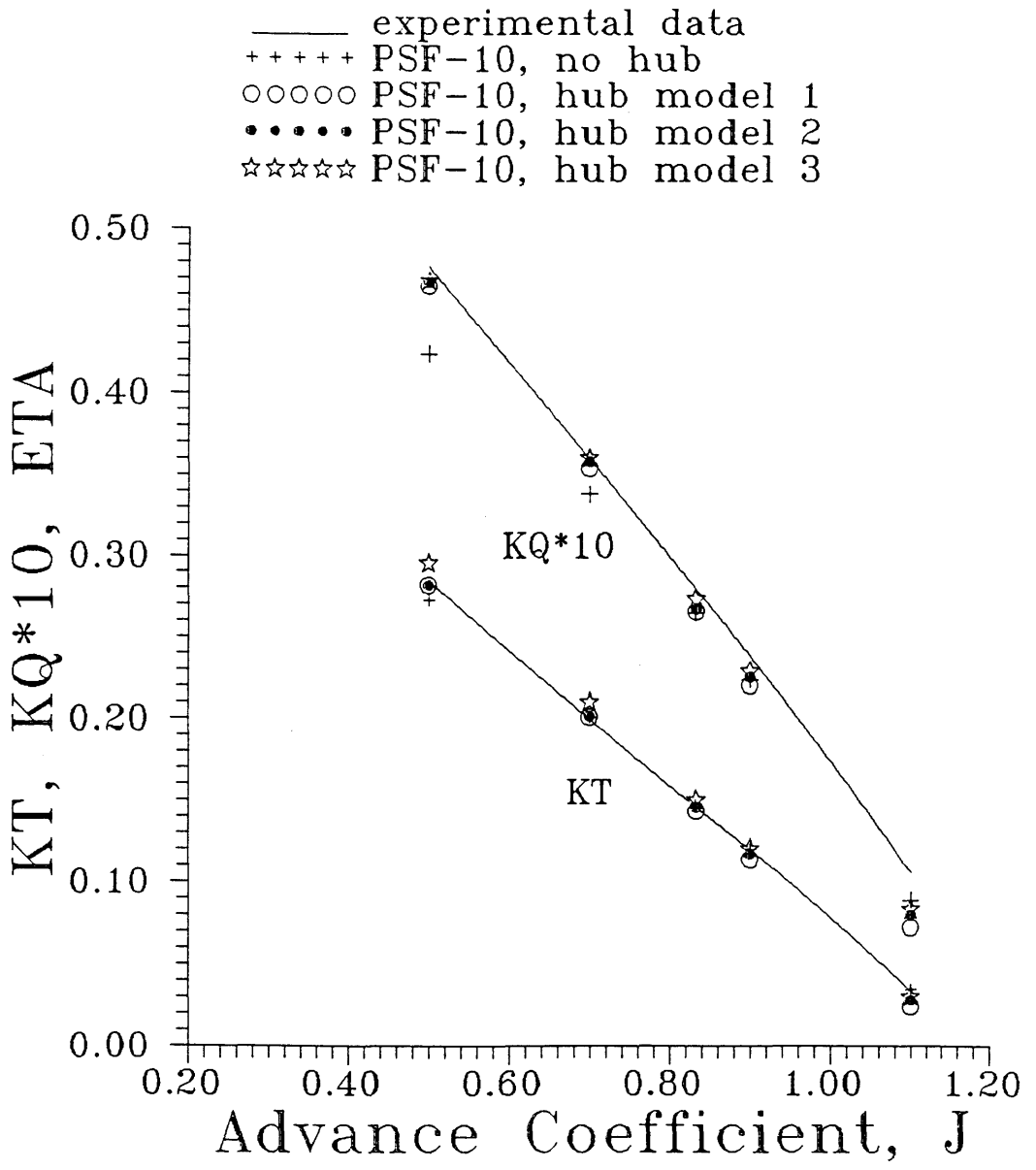

Figure 6: Computation results of different hub models of propeller 4119.

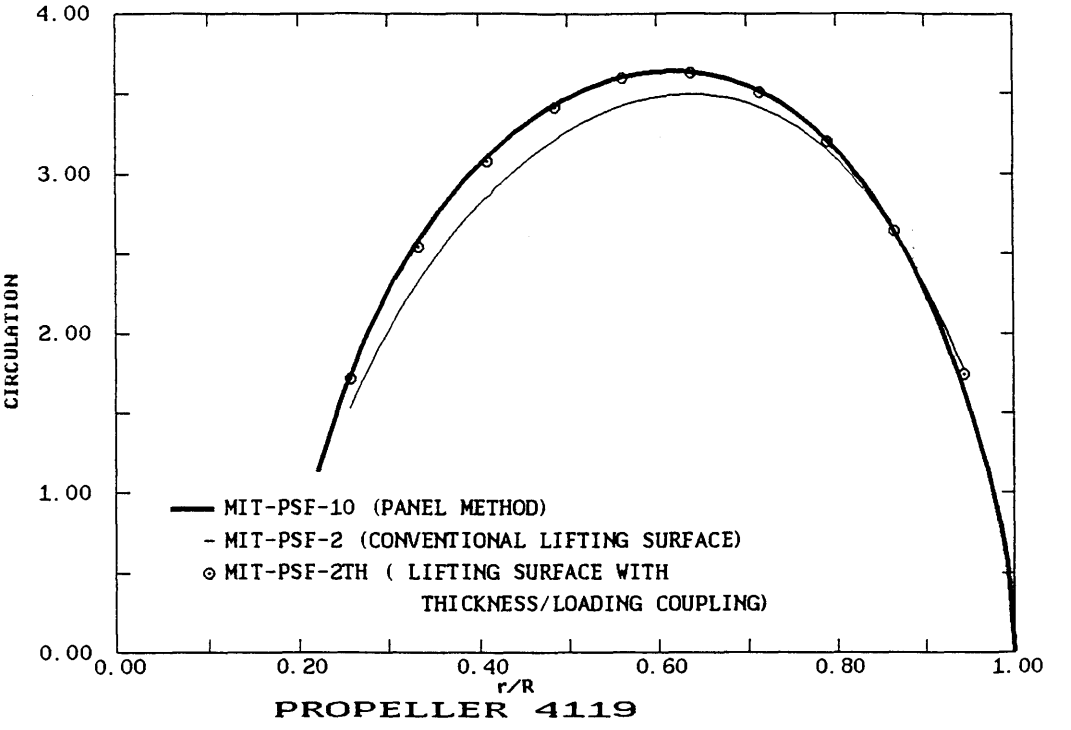

Figure 7: Circulation distribution (made non-dimensional on $2\pi RV_S$, where R is the radius of propeller, and V_S is the ship speed) for the 4119 propeller predicted from different methods (the effect of hub is not included).

APPENDIX D

Calculations by AMI

Calculations for the DTRC 4119 and DTRC 4842 Propellers Using VSAERO/MPROP and USAERO Panel Codes

Prepared by:

Analytical Methods

B. Maskew, J.S. Fraser, J.B. Murray and M.J. Summa

Prepared for the 20th ITTC Propulsor Committee Workshop

Korea, August 1992

July 31, 1992

Introduction

Analytical Methods, Inc. (AMI) analyzed the two workshop propeller configurations, DTRC 4119 and DTRC 4842, using the VSAERO/MPROP and USAERO panel codes. VSAERO/ MPROP is a Marine Propeller version of AMI's widely used VSAERO program, the MPROP extension providing certain features for propeller applications in steady axisymmetric conditions. USAERO is a time-stepping panel code with a very general capability. Although it was developed primarily for aircraft maneuver and store release calculations, its general options for multiple moving frames of reference allow a very broad scope of application covering complete vehicles, helicopter, automobiles, trains, ships, etc. Even though no specific development has been undertaken for marine propeller applications, the general capability of USAERO allows such configurations to be treated, and in fact, a propeller in non-uniform flow, a counter-rotating propulsor, a propeller with cyclical pitch variation and a propeller near a free surface, have been briefly studied. USAERO was, therefore, included in the current study, the time-stepping calculations proceeding until essentially steady state conditions were reached.

The wake models used in the present calculations were different; the VSAERO cases used a simple helical wake with the pitch determined by the local advance coefficient. In the USAERO calculations, a new set of wake panels is created along the shedding lines at each time step, and all the existing wake panels are convected with the local flow for the duration of the time step. The calculations normally start impulsively from rest with no initial wake. With the present range of advance coefficients, the calculations reach essentially steady state conditions within about 20 steps. In the present axisymmetric flow conditions, the number of unknowns in USAERO can be reduced to the number of panels on a single blade (plus corresponding strips of panels along the hub, if present) using an "SSCOPY" option (for same solution copy) when generating the configuration geometry. A similar option, "RSCOPY" provides a "Repeat Solution" capability for treating the cyclical conditions encountered in non-uniform flows.

Both VSAERO/MPROP and USAERO include coupled integral boundary layer calculations, which provide the skin friction distribution over the surfaces as well as boundary layer displacement effect, which is modelled in the codes, using a transpiration technique. The VSAERO boundary layer coupling has been in use for over 12 years and has been extensively tested and refined. The USAERO unsteady boundary layer coupling has been in active use only over the past two years and is less robust in application; some minor problems occurred in the boundary layer displacement effect coupling with the panel boundary conditions in the present cases.

A brief outline of the method formulation and numerical procedure for the two codes is given in the following two sections before discussion of the actual calculations.

2.0 MATHEMATICAL MODEL

2.1 General

The mathematical foundation for VSAERO and USAERO are very similar. The mathematical models for the two codes are therefore outlined together here before discussing the numerical procedures in Section 3.

2.2 Basic Equations

Consider the *configuration* moving with velocity, $\vec{V}_B$, through an unbounded fluid initially at rest, Fig. 2.1. The basic assumptions are that the effects of viscosity are largely confined to thin boundary layers on the *configuration* surface and that wake vorticity is essentially concentrated in thin, free-shear layers and discrete vortex filaments. The majority of the flow is, therefore, regarded as inviscid, irrotational and incompressible. Laplace's equation can then be applied:

$$\nabla^2\phi = 0 \tag{2.1}$$

The convention adopted here is that the perturbation velocity is the *negative* gradient of ϕ:

$$\vec{v} = -\nabla\phi \tag{2.2}$$

Green's Theorem is applied next; note that with $\nabla^2\phi = 0$, the volume integral disappears. The flow is therefore uniquely determined by surface integrals of ϕ and its normal derivative over the surface of the *configuration* and its *wake*. Thus the velocity potential, ϕ_p, for a point, P, on the wetted side of the surface is

$$\phi_p = \frac{1}{4\pi}\iint_{S-P} \phi\,\vec{n}\cdot\nabla\left(\frac{1}{r}\right)dS + \frac{\phi_p}{2} - \frac{1}{4\pi}\iint_S \frac{1}{r}\vec{n}\cdot\nabla\phi\,dS + \frac{1}{4\pi}\iint_W (\phi_U - \phi_L)\,\vec{n}\cdot\nabla\left(\frac{1}{r}\right)dW \tag{2.3}$$

where $\vec{n}$ is the outward normal from the surface and r is the length of the vector from the surface element, dS, to the point, P. S-P signifies that the point, P, is excluded from the surface integral--the limiting process for the singular point when $r \to 0$ yields the local contribution, $\phi_p/2$.

The first integral in Eq. (2.3) is the contribution from a surface distribution of normal doublets of strength,

$$\mu = \frac{\phi}{4\pi} \tag{2.4}$$

The second integral is the contribution from a surface distribution of sources of strength,

$$\sigma = -\frac{\vec{n}\cdot\nabla\phi}{4\pi} \tag{2.5}$$

The third integral in Eq. (2.3) is the contribution from the wake surface. Here, the upper and lower surfaces have been combined, taking the upward facing normal. The upper and lower potentials have been combined, yielding a wake doublet distribution of strength,

$$\mu_W = \frac{(\phi_U - \phi_L)}{4\pi} \tag{2.6}$$

This is the potential jump across the wake. In combining the upper and lower surfaces, the source term has been discarded, implying that there is no normal flow relative to the wake--the wake points, in fact, convect with the flow and so the wake surface is always aligned with the local flow. (The entrainment effect due to turbulent mixing is neglected for the moment.) Thus, Eq. (2.3) becomes

$$\iint_{S-P} \mu\, \vec{n} \cdot \nabla\left(\frac{1}{r}\right) dS - 2\pi\mu_p + \iint_S \frac{\sigma}{r}\, dS + \iint_W \mu_W \vec{n} \cdot \nabla\left(\frac{1}{r}\right) dW = 0 \tag{2.7}$$

In the general case of analyzing the flow about a given configuration, the doublet distribution on the surface is unknown, while the source distribution is determined directly by the external Neumann boundary condition specifying the resultant normal velocity at the boundary. The flow velocity relative to the surface is

$$\vec{V} = \vec{v} - \vec{V}_s \tag{2.8}$$

where $\vec{v}$ is the perturbation velocity (eq. (2.2)), and

$$\vec{V}_s = \vec{V}_B + \vec{\Omega} \times \vec{R} - \vec{V}_\infty \tag{2.9}$$

is the surface velocity relative to the undisturbed fluid. V_B is now measured in an inertial frame which may have a uniform flow, V_∞. $\vec{\Omega}$ is the velocity of rotation of the body, and $\vec{R}$ the position of a surface point relative to the rotational axis. The normal component of $\vec{V}$ is, from Eq. (2.8),

$$\vec{V} \cdot \vec{n} = \vec{v} \cdot \vec{n} - \vec{V}_s \cdot \vec{n} = V_N \tag{2.10}$$

V_N is the resultant normal velocity at the surface. This is usually zero (solid boundary), but it can have a number of nonzero parts, e.g.,

$$V_N = VNORM + V_{BL} \tag{2.11}$$

where VNORM is the user-specified inflow/outflow representing an engine inlet/exhaust modeling, and V_{BL} is the boundary layer displacement effect using the transpiration technique,

$$V_{BL} = \frac{\partial}{\partial s}(V_e \delta^*) \tag{2.12}$$

where V_e is the local speed at the edge of the boundary layer and δ^* is the displacement thickness. The derivative is taken in the direction of the local external flow.

Using Eqs. (2.2), (2.5) and (2.10), the source term is,

$$\sigma = \frac{\left(\vec{n} \cdot \vec{V}_B + \vec{\Omega} \cdot \vec{R} \wedge \vec{n} - \vec{n} \cdot \vec{V}_\infty + VNORM + V_{BL}\right)}{4\pi} \tag{2.13}$$

The wake doublet distribution, μ_w, in Eq. 2.7, is treated differently in the two codes: in VSAERO, μ_w, is constant along streamlines in the wake surface. The value of μ_w on each streamline takes the difference in strength between the upper and lower solid surface doublet values where the streamline leaves the trailing edge. In this case, μ_w becomes involved with the *unknown* surface-doublet distribution. In USAERO, the wake doublet distribution is essentially *known* from earlier time steps: as each new wake element is created, it carries with it the instantaneous doublet jump at the local trailing edge, and holds this constant for the rest of the calculation.

2.4 Surface Pressure

With the solution known, the surface velocities and pressures can be evaluated. The tangential component of perturbation velocity is obtained from the surface gradient of the potential. The normal component comes from the source term. The pressure is evaluated using the Bernoulli equation for a moving frame,

$$C_p = V_s^2 - V^2 + 2\left(\frac{\partial \phi}{\partial \tau}\right). \tag{2.14}$$

In VSAERO, the $\frac{\partial \phi}{\partial \tau}$ term is zero. The velocities V_s, V, are normalized by the reference speed; this may be the blade tip speed or it may be the local speed due to rotation at the local radius.

2.5 Kutta Condition

In VSAERO, the (steady state) Kutta condition is usually satisfied implicitly by shedding the doublet jump across the trailing edge into the local wake column,

$$\mu_W = \mu_U - \mu_L \tag{2.15}$$

This essentially states that there is zero load at the trailing edge.

An iterative loop is available in the code for explicitly satisfying a zero pressure jump condition at the trailing edge; however, it was not applied in the present cases.

In USAERO, an *unsteady* Kutta condition is obtained after equating the unsteady upper and lower trailing edge pressures using the C_P expression in Eq. (2.14):

$$\left(\frac{\partial \mu_W}{\partial \tau}\right) + V_M\left(\frac{\partial \mu_W}{\partial s}\right) = 0 \tag{2.16}$$

V_M is the mean convection speed and the s direction follows the local mean flow at the trailing edge. μ_W is the jump in doublet strength across the trailing edge, i.e., μ_W is the newly emerging wake strength. Equation (2.16) essentially states that the rate of change of circulation at the trailing edge must match the transport of circulation into the wake.

2.6 Force and Moment

The forces and moments are obtained by integrating the pressure over the surface.

The force coefficient is,

$$\vec{C}_F = -\iint_S C_p \vec{n} - C_f \vec{V}_R |\vec{V}R| dS \tag{2.17}$$

The moment coefficient is,

$$\vec{C}_M = \iint_S \left(Cp\vec{n} - C_f \vec{V}_R |\vec{V}_R|\right) \times \vec{r}\, dS \tag{2.18}$$

The axial components of these quantities provide the thrust and torque values, respectively, for a propellar configuration.

3.0 NUMERICAL PROCEDURE

3.1 General

The numerical procedure flow diagrams for VSAERO and USAERO are shown in Fig. 3.1. The main difference is that the separate iteration loops for spatial wake relaxation and steady boundary layer effects in VSAERO become a single in-line time-step loop in USAERO with time-domain wake convection and unsteady integral boundary layer treatment.

The *initial set-up* is very similar in the two codes and involves the specifications of *basic data* such as onset conditions, reference quantities, program controls, etc. VSAERO uses fixed format for this input, whereas USAERO now has a *namelist* style of input format; the namelist scheme was written specifically for the code in standard Fortran 77 and is therefore portable to a wide range of computers.

The *geometry definition* involves the description of the *configuration* surfaces. Both VSAERO and USAERO provide the option to break the configuration into a number of convenient parts. USAERO, in addition, allows the user to specify multiple moving frames of reference. Configuration modeling aspects are discussed below in Section 3.2. The smallest subdivision of a configuration surface is a quadrildial *panel*. Panels are arranged in a structured mesh of rows and columns and are the basic elements used to discretize Eq. (2.7). These aspects and the formation of the *matrix of influence coefficient* are discussed in 3.3; *matrix solution* options are given in 3.4. *Analysis* of the surface velocities and pressures, and the treatment of the surface streamlines, boundary layers and wakes, are outlined in 3.5, 3.6., 3.7 and 3.8, respectively.

3.2 Configuration Modeling

Configuration refers to the vehicle, bodies, etc. and their wakes about which the flow is to be calculated. It includes all solid boundaries in the flow problem; for example, a *configuration* may include the wind tunnel walls or water tank walls in cases where model test measurements are being used to validate calculations. The present section is concerned with creating a panel model, which represents the *configuration surfaces* in the flow calculations. Treatment of a *configuration* in USAERO is basically similar to that in VSAERO, except there is now an additional breakdown level, i.e., *frames*. These provide a convenient way of describing arbitrary movements of multiple parts of the vehicle.

Fig. 3.2 shows the breakdown of a *configuration* into a number of convenient parts, i.e., *frames, components, patches, panels,* and *wakes*. The first step in breaking down a *configuration* into manageable pieces is to identify the individual motions of its various parts. This establishes the *frames* of reference required to describe the various motions. *Configuration* parts associated with each *frame* may consist of one or more *components*. The *component* breakdown is chosen by the user on the basis of convenient parts for separate force and moment information; for example, a hull, a blade stator or duct, etc. In USAERO, each *component* is assigned to a *frame*--this is its local reference frame in which its basic geometry is first described. If the *component* has no motion, it may be assigned directly to the ground-fixed frame.

A *component* is further subdivided into one or more *patches*. The *patch* breakdown is selected with a view to paneling convenience, or available section geometry information. A surface *patch* consists of a set of ***panels*** arranged in a structured network of rows and columns.

Careful attention to the details of panel arrangement over the configuration surface helps ensure a good quality solution, particularly in regard to the evaluation of doublet gradients (i.e., tangential velocity components). Both programs provide various automatic paneling options to help the user distribute the panels over each patch.

Lines of wake separation are identified on the configuration surfaces. Each wake is assigned to the patch where it leaves the surface. Multiple wake/patch assignments are allowed to cover the case where a wake separation line extends over more than one patch.

3.3 Matrix Equations

The surface integrals in Eq. (2.7) are evaluated in a piecewise manner over each panel assuming the doublet and source are locally uniform. In USAERO, the doublet distribution on each wake panel is assumed to be linear in the streamwise direction and the integration is performed over a pair of triangles in order to treat the possibly highly warped quadrilaterals in a strong wake roll-up situation. The piecewise integration yields influence coefficients for source and doublet singularities (1) and Eq. (2.7) becomes,

$$\sum_{K=1,K\neq J}^{N_e} (\mu_K C_{JK}) - 2\pi\mu_J + E_J = 0 \qquad J=1,N \tag{3.1}$$

where μ_K is the doublet value for panel K and C_{JK} (1) is the doublet influence coefficient for panel K acting at the control point of panel J.

$$E_J = \sum_{K=1}^{N_s} \sigma_K B_{JK} + \sum_{K=1}^{N_W} \mu_{WK} C_{JK} \tag{3.2}$$

N_s is the number of surface panels and N_w the number of wake panels.

B_{JK} is the source influence coefficient for panel K acting at the central point of panel J.

C_{JK} and B_{JK} are given in Ref. 1 and include symmetry terms for configurations having geometrical and aerodynamic symmetries.

In USAERO, surface panels involved with wake shedding have a small contribution from the newly formed wake panel. Basically, the doublet value at the downstream edge is the value propagated at the last time step. At the upstream edge, i.e., at the shedding line, the doublet strength is unknown. The influence coefficient for these wake panels, therefore, goes partly into the known right-hand side of the equations and partly into the matrix of influence coefficients to contribute to the "upper" and "lower" wake-shedding panels, see Fig. 3.3.

In VSAERO, the influence coefficient for a complete streamline set of wake panels is combined with the influence coefficients of the wake-shedding panels, being added to the "upper" and subtracted from the "lower" term.

3.4 Matrix Solution

Both codes offer a number of matrix solver options which may be selected at the input stage. A blocked Gauss-Seidel iterative method and the direct Purcell vector method (for smaller problems) are the basic solvers in each code. An alternative special solver was developed in USAERO to deal with problems having *relative* motions. This method reorders the matrix at each time-step if necessary, based on a panel proximity criterion; this condenses the major terms towards the matrix diagonal. A direct solution is then obtained for the banded matrix using a band width of the order of 100. A Jacobi iteration on the complete matrix with further banded matrix treatment of the residuals provides a fairly robust iterative solver for complex configurations.

Other solver options point to various in-core solvers that have been optimized for specific computers. For example, the LAPACK (direct) solver on the Silicon Graphics workstation has shown a 3:1 speedup over the Purcell vector method. *Direct* solutions for 10,000 panels have been executed in a reasonable time scale using a Convex C.3 in-core solver.

3.5 Surface Pressure Analysis

The surface gradient of the potential is evaluated at the center of each panel by differentiating a two-way parabolic curve fit through the values on the panel and its four immediate neighbors. At certain lines on the surface where there is a jump in conditions, e.g., a wake separation line, the code uses forward or backward differencing using information from a neighbor of a neighbor if available. The surface gradient of the potential provides the tangential perturbation velocity while the normal perturbation velocity comes from the source term. There are combined with the local "body" velocity to provide the total fluid velocity relative to the surface point, Eq. (2.8). The pressure coefficient is then evaluated at each panel center (Eq. (2.14)). The $\partial\phi/\partial\Upsilon$ term for USAERO is evaluated using second order differencing based on the two previous time steps.

3.6 Surface Streamlines

With the surface flow velocities known, families of streamlines (instantaneous in the case of USAERO) are traced over the configuration by an automatic integration process. These provide a basis for 2-D integral boundary layer calculations (outlined below). This approach has been successfully applied to a wide range of very complex problems and provides a more versatile and robust alternative to fully 3-D boundary layer methods.

3.7 Boundary Layer Analysis

In the VSAERO boundary layer routines, the laminar calculation is based on Curle's method (2). Once transition or laminar separation is detected (by a modified Granville approach), or boundary layer tripping is prescribed, the turbulent boundary layer development is determined by a modified Nash and Hicks method (3).

In USAERO laminar boundary layer calculations follow Curle's original Method (2) with modification to solve the unsteady momentum integral equation using a Runge-Kutta method. The turbulent boundary layer method is also based on the unsteady momentum integral equation. Cousteix's entrainment relation (4) and Lyrio/Ferziger's skin friction relationship (5) are used for closure. The details of the method are described in Ref. 6.

The calculations provide the boundary layer displacement source term and skin friction distribution along each of the instantaneous streamlines. These quantities are then redistributed onto the surface panels in the attached flow regions. The skin friction force contribution is included in the analysis of forces and moments. The calculations also provide the location of separation on each streamline, based on a vanishingly small skin friction coefficient. The locus of such points defines a separation line on the body surface. At this time there is no automatic coupling of these data with the wake shedding routine. Simple cases of separated flow can be treated, but the user must specify the separation line at this time, based on the boundary layer prediction.

3.8 Wake Treatment

In VSAERO, there is an option to iteratively relax the wake surfaces into a force-free condition by aligning each individual wake longitudinal segment (Fig. 3.3) into the local flow direction. The latter is computed by summing the velocity influences of all the source and doublet singularity panels on the configuration and its wake, including *image* contributions if planes of symmetry are being used or if anisymmetric conditions for multiple propeller blades exist.

The force-free wake condition in USAERO is satisfied by convecting each free wake point along the instantaneous local computed velocity vector for the duration of the time step. A new set of wake points is therefore created along the wake-shedding lines at each time step. Each new wake point is given a doublet value equal to the difference in doublet strength between the local upper and lower wake shedding panels. This value remains constant for each wake point as it convects downstream. In this way, the *vorticity* on the wake varies in time and space according to the local stretching or contraction of the wake surface as the wake points convect at different rates and in different directions.

4.0 CALCULATIONS

4.1 Three-Bladed Propeller, DTRC 42119

4.1.1 Panelling

The panelling used for the DTRC 4119 propeller is shown in Fig. 4.1. The total number of unknowns is 1755 with 900 on the blade in a 60 (around the chord) x 15 (radial) array and 855 on the hub. The computing time for VSAERO/MPROP with rigid wake was 388 seconds on an SGI 4D/35 personal IRIS workstation. The time-stepping calculations in USAERO with free wake analysis "converged" to steady state in about 13 steps in a time of 4725 seconds.

4.1.2 Pressure Distribution

Fig. 4.2(a) shows the pressure coefficient contours computed by VSAERO/MPROP at J = 0.833.

$$(Cp = p - p\infty) / 1/2\rho V_{TIP}^2)$$

Fig. 4.2 (b) shows the "converged" Cp contours predicted by USAERO. Also shown are the computed wake panels, generated in 20 time steps.

Fig. 4.3 shows the USAERO pressure distribution at three radial stations compared with measured data. Here the Cp was reduced (outside the code) to the required form

$$C_p = 1 - (VV/VR)^2$$

The comparison is good at the two inner stations but not at the outer station. The latter problem is being examined further, but it is thought to arise from the form of the panelling in the tip region which has extremely skewed triangular panels.

The corresponding VSAERO Cp plots were not reduced to this form, but a comparative constant radius Cp plot between USAERO and VSAERO indicates very similar solutions (Fig. 4.4). The strange behavior near the trailing edge is partly due to the way the blunt trailing edge region was modified to make it sharp. Fig. 4.5 shows the modified contour detail--this should have been carried over a broader region.

4.1.3 Thrust and Torque

Fig. 4.6(a) shows the KT, KQ curves computed by VSAERO/MPROP. These are for the inviscid case, but no significant change was seen with the boundary layer calculation included. The KT is in very close agreement with experiment while KQ is somewhat low compared with experiment. Computed values at the 0.5 advance coefficient were omitted because of inconsistent behavior in the tip region. Repanelling to avoid the highly skewed triangular tip panels needs to be done before reexamining the lower advance coefficients. This would also allow a more non-linear tip wake model to be examined for possible tip leading edge separation treatment.

The corresponding KT, KQ comparisons for USAERO are shown in Fig. 4.6 (b). The boundary layer effects here are quite significant and in view of the VSAERO/MPROP solutions - need further investigation. The final KT curve is in close agreement with measurement while the total viscous correction to the KQ curve has tended to undershoot the measurement. A large part of the shift probably comes from a reduction in the induced torque due to the large shift in KT at the lower advance coefficients.

4.1.4 Skin Friction Distribution

Fig. 4.7(a) shows the computed skin friction coefficient distribution along streamlines predicted by VSAERO/MPROP for the J = 0.833 case. A significant amount of laminar flow is indicated across the chord at all radial stations. The corresponding calculation in USAERO Fig. 4.7 (b) gives similar behavior in the inner region but indicates earlier transition in the tip region. This solution may have been affected by the unsatisfactory tip panelling noted above.

4.2 Five-Bladed Propeller, DTRC 4842

4.2.1 Panelling

The panelling used for the DTRC 4842 propeller is shown in Fig. 4.8. This has 1550 unknowns with 950 on a blade and 600 in the hub. Computing times for VSAERO/MPROP with rigid wake was 482 seconds on the SGI 4D/35 personal IRIS workstation. USAERO, with free wake calculation converged in about 17 steps in a time of 7320 seconds.

4.2.2 Pressure Distribution

Fig. 4.9(a) shows the pressure coefficient contours $(Cp = p - p_\infty)/1/2\rho V_{TIP}^2)$ computed by VSAERO/MPROP at J = .905. The USAERO solution is shown in Fig. 4.9(b) and includes the computed wake panels for 29 steps.

Fig. 4.10 shows the USAERO pressure distributions at three radial stations. The problems seen in the tip region of DTRC 4119 are not evident here, the panelling form at the tip being less severe on the 5 blader. Also, the behavior near the trailing edge appears much smoother - in this case the modification to sharpen the otherwise blunt trailing edge is taken over a wider region (Fig. 4.11).

4.2.3 Thrust and Torque

Fig. 4.12 shows the KT, KQ curves computed by VSAERO/MPROP compared with experiment and indicate about a 10% difference. Again, no significant viscous correction was shown by VSAERO for this case. USAERO was run only at J = .905 for this case and gave the following results:

	KT	10 x KQ
Experiment	.310	.720
No BL	.359	.6993
With BL	.349	.7397
With BL/No Hub	.352	.7465

Again, USAERO indicates a larger viscous correction than VSAERO. In the present case, this is just due to skin friction. The source term for displacement effect gave a problem on this configuration and was temporarily deactivated.

4.2.4 Skin Friction Distribution

Fig. 4.13(a) shows the VSAERO/MPROP computed skin friction distribution along streamlines for DTRC 4842 at J = .905. Again, VSAERO indicates a significant extent of laminar flow extending right out to the tip. The corresponding calculation in USAERO, Fig. 4.13(b) indicates a region of earlier transition in the middle of the blade. This is more clearly seen in Fig. 4.13(c) which gives the same information transferred to the panels and displayed as contours.

5.0 CONCLUSION

The (steady) VSAERO/MPROP and (unsteady) USAERO codes were applied to the DTRC 4119 and DTRC 4842 propellers with very encouraging results on the whole. Some additional investigation is needed for the panelling details in the tip region of DTRC 4119; USAERO did not behave well near the tip and the VSAERO solution gave spurious results at the lower advance coefficient. The viscous effects also need further examination: whereas the VSAERO calculations showed very small viscous corrections the USAERO calculation indicated significant effects when the boundary layer was activated.

Application of an *unsteady* code to a steady axisymmetric propeller condition in one sense is overkill; the computer time to convergence is about 15 times that required for the steady code. (Even so, the times were not unreasonable, i.e., two hours on an SGI personal IRIS.) The calculations were included here primarily with a view to the more general options provided by the unsteady formulation--viz, non-uniform flows, propeller/hull interaction, variable pitch propellers, etc.

6.0 REFERENCES

1. Maskew, B., "Program VSAERO Theory Document", NASA CR-4023, 1985.
2. Curle, H., "A Two-Parameter Method for Calculating the Two-Dimensional Incompressible Laminar Boundary Layer", J. R. Aero. Soc., Vol. 71, 1967.
3. Nash, J.F. and Hicks, J.G., "An Integral Method Including the Effect of Upstream History on the Turbulent Shear Stress", Proc. Computation of Turbulent Boundary Layers--1968, AFOSR-IFP-Stanford Conference, Vol. 1, 1968.
4. Cousteix, J., and Houdeville, R., "Singularities in Three-Dimensional Turbulent Boundary Layer Calculation and Separation Phenomena", *AIAA J.*, Vol. 21, No. 4, April 1983.
5. Lyrio, A.A., and Ferziger, J.H., "A Method for Predicting Unsteady Turbulent Flows and its Application to Diffusers with Unsteady Inlet Conditions", *AIAA J.*, Vol. 21, No. 4, April 1983.
6. Maskew, B. and Dvorak, F.A., "Prediction of Dynamic Stall Characteristics Using Advanced Nonlinear Panel Methods", presented at AFOSR/FJSRL Workshop on Unsteady Separated Flows, USAF Academy, Colorado Springs, CO, August 1983.

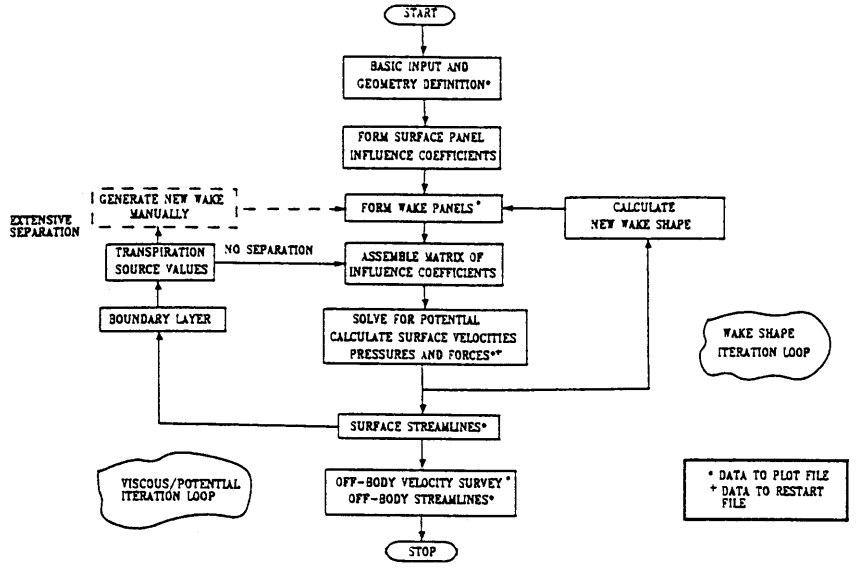

VSAERO

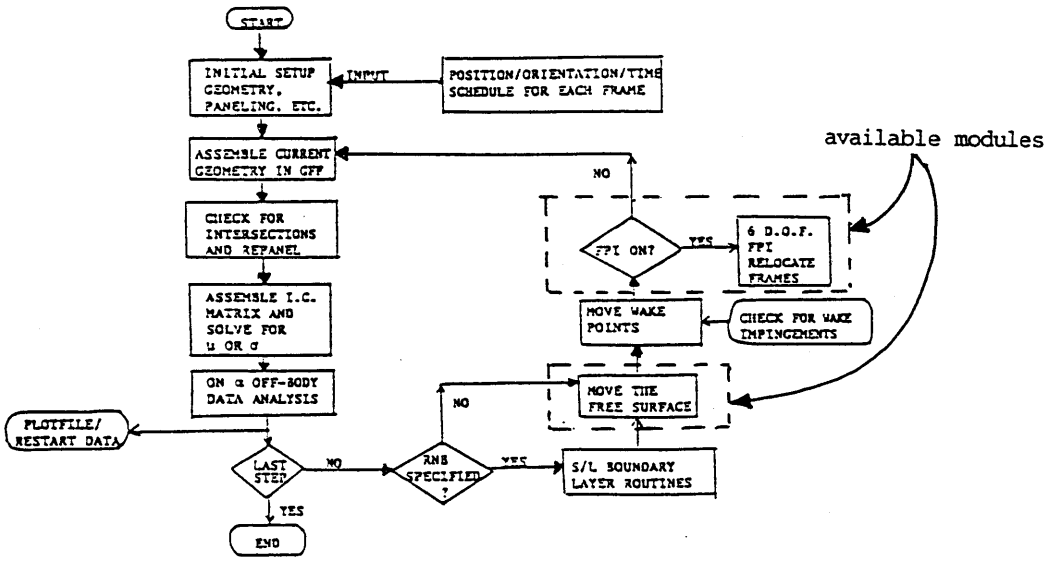

USAERO

Fig. 3.1. Numerical Procedure Flow Diagrams for VSAERO and USAERO

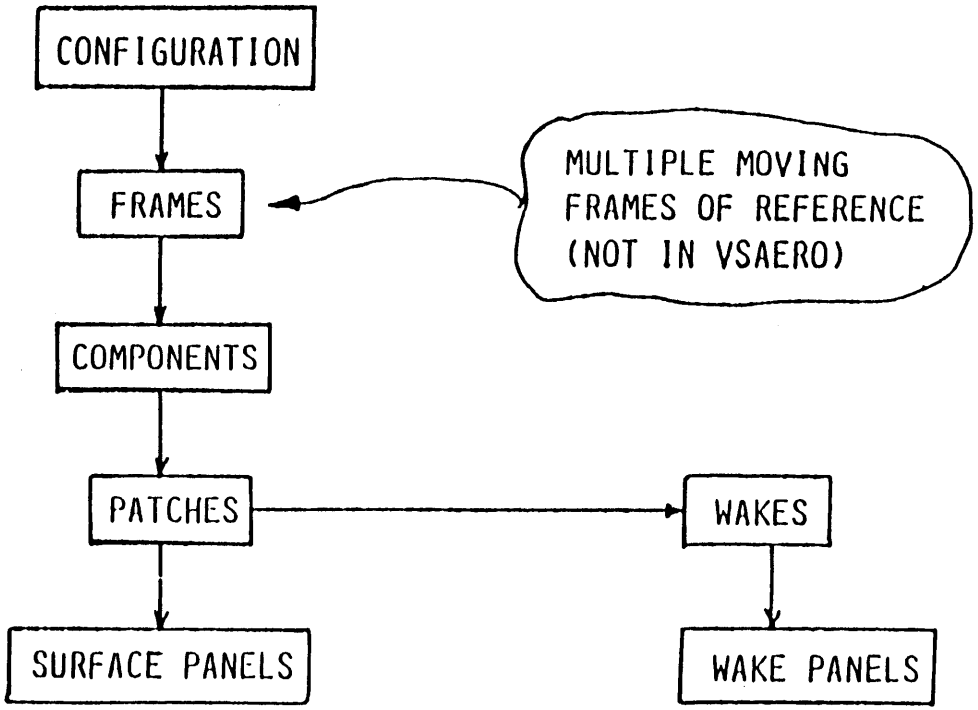

Fig. 3.2. Configuration Breakdown.

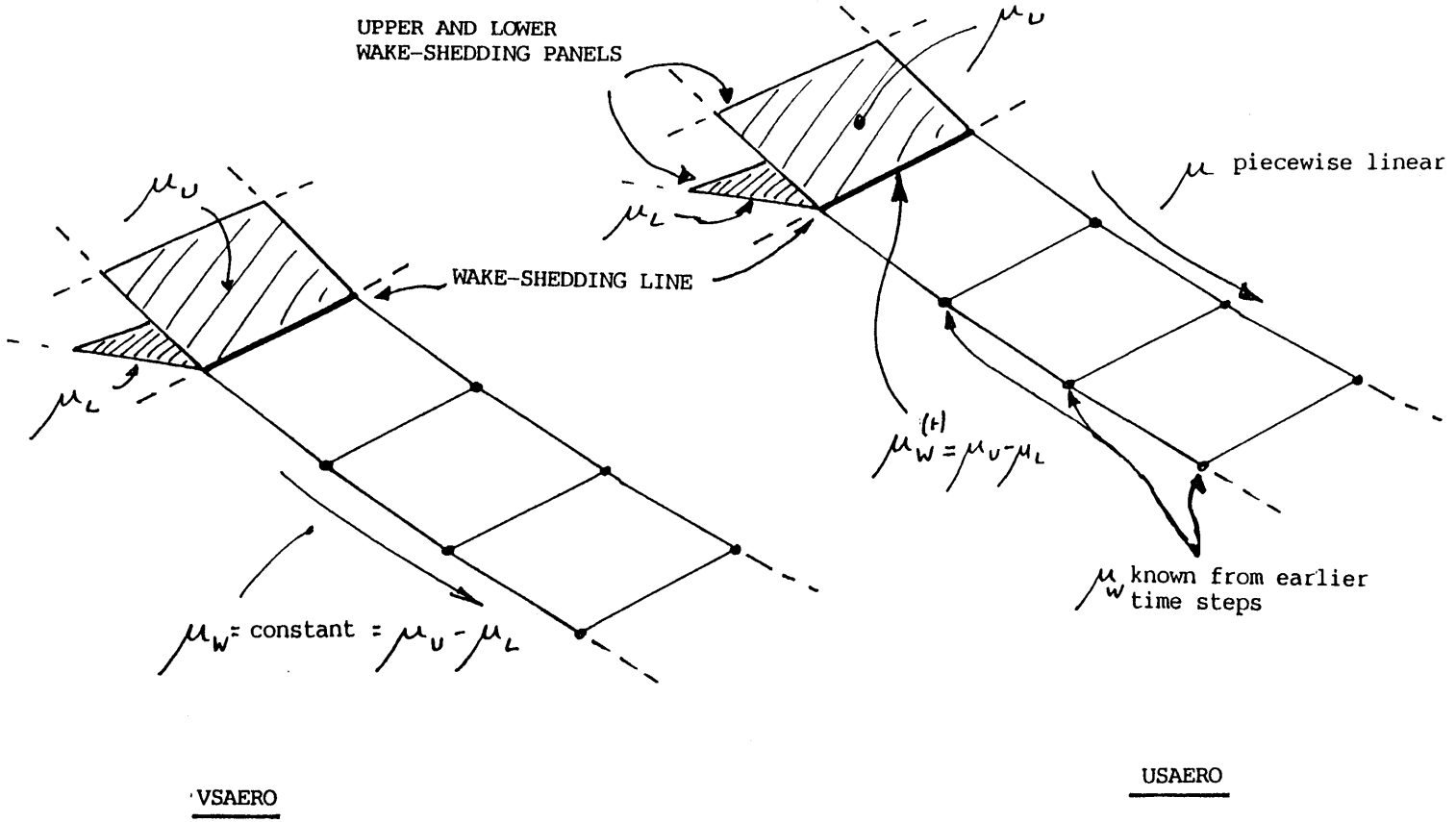

Fig. 3.3. Comparison of Basic Wake Models in VSAERO and USAERO

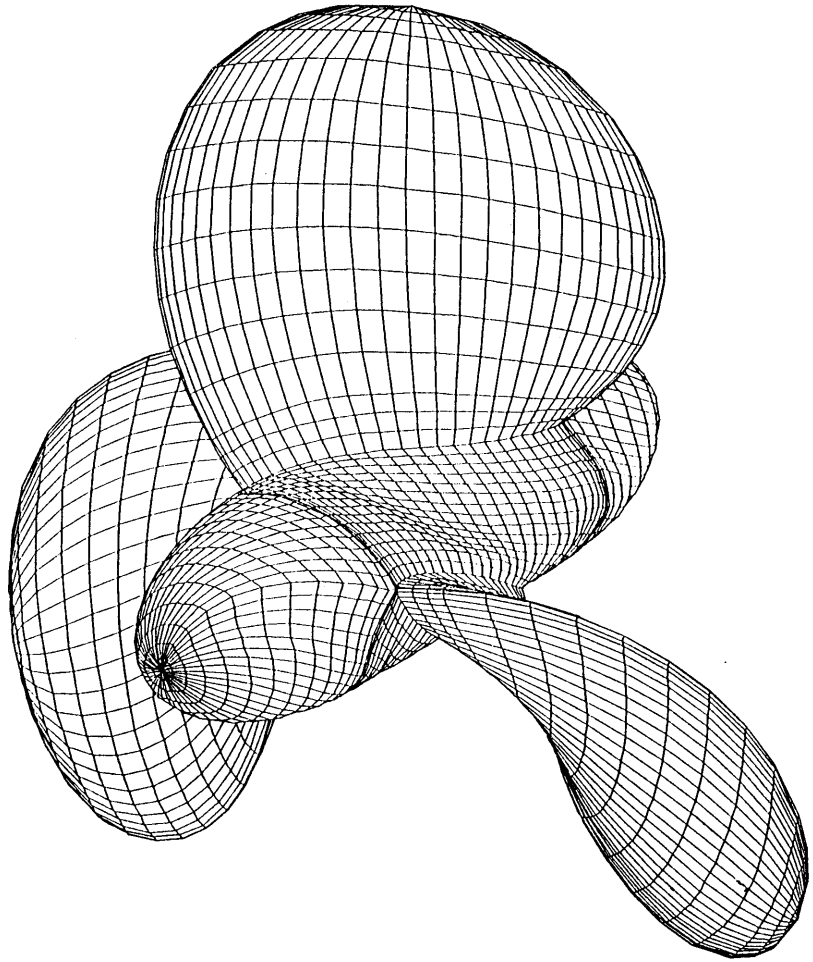

3 BLADE OPEN PROP, DTRC 4119

Fig. 4.1. General View of Panelling

Fig. 4.2. Calculated Pressure Contours at J = .833
(a) VSAERO/MPROP

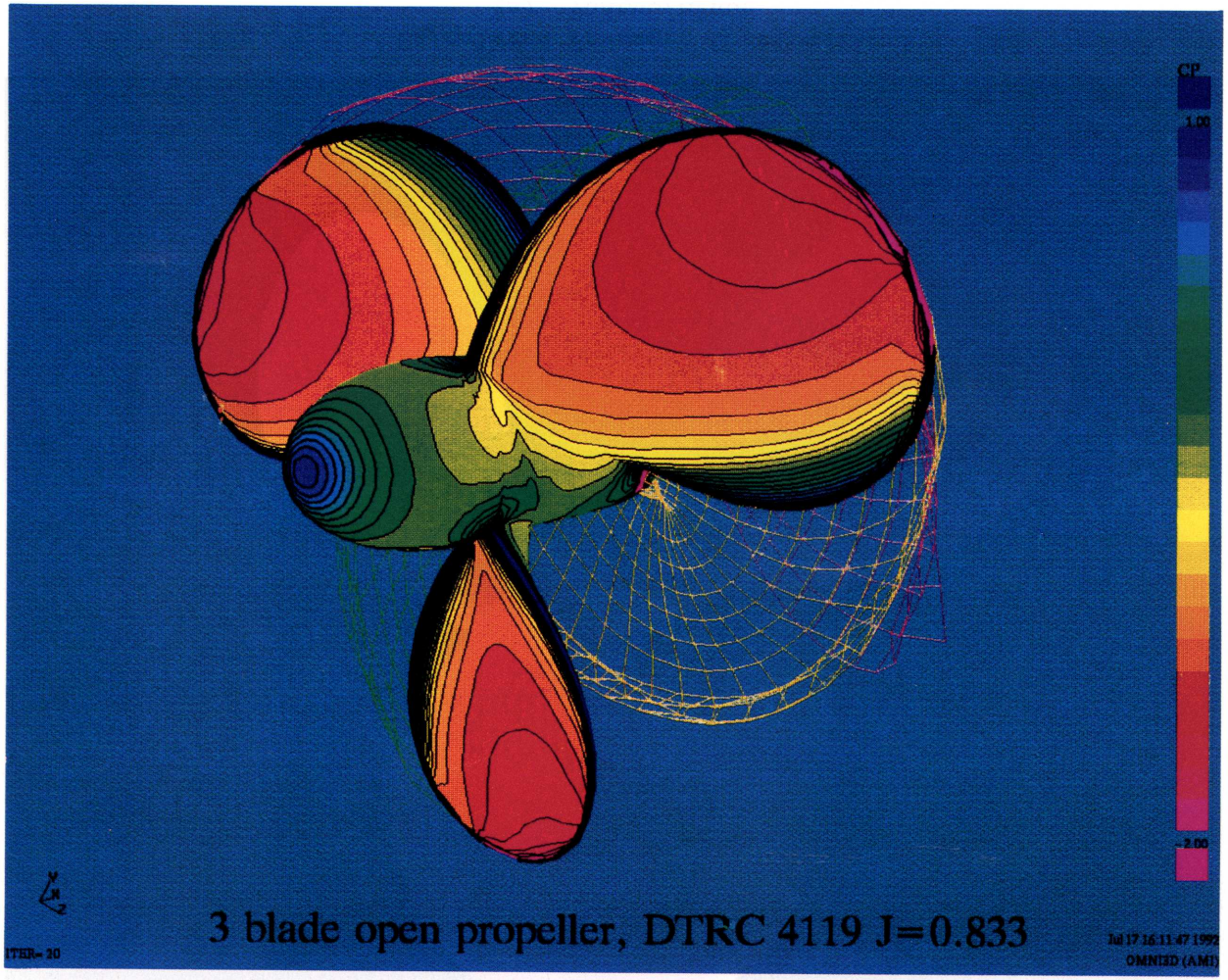

Fig. 4.2. Concluded
(b) USAERO

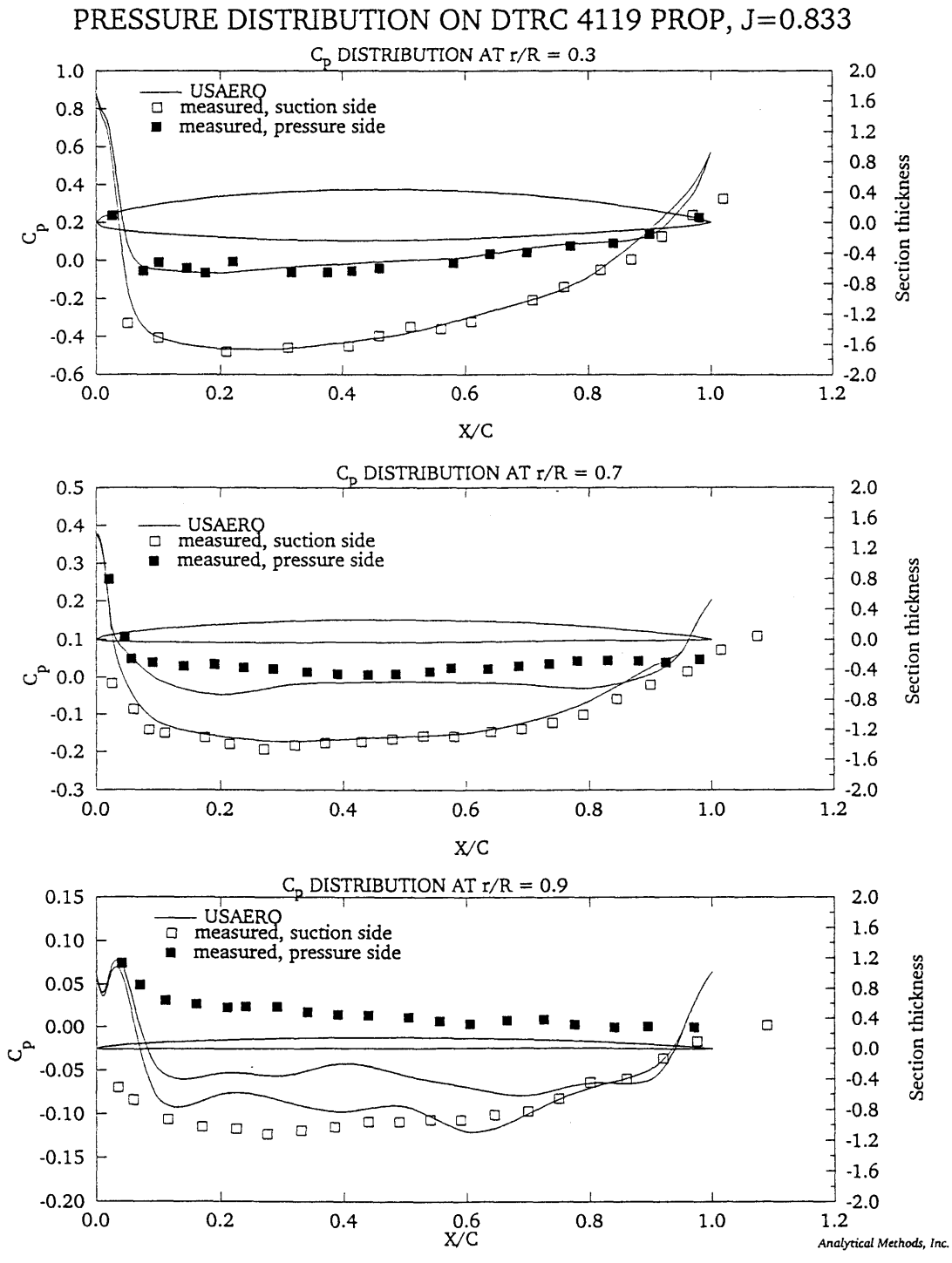

Fig. 4.3. Comparison of USAERO Calculated and Measured Pressure Distributions at Three Radial Stations.

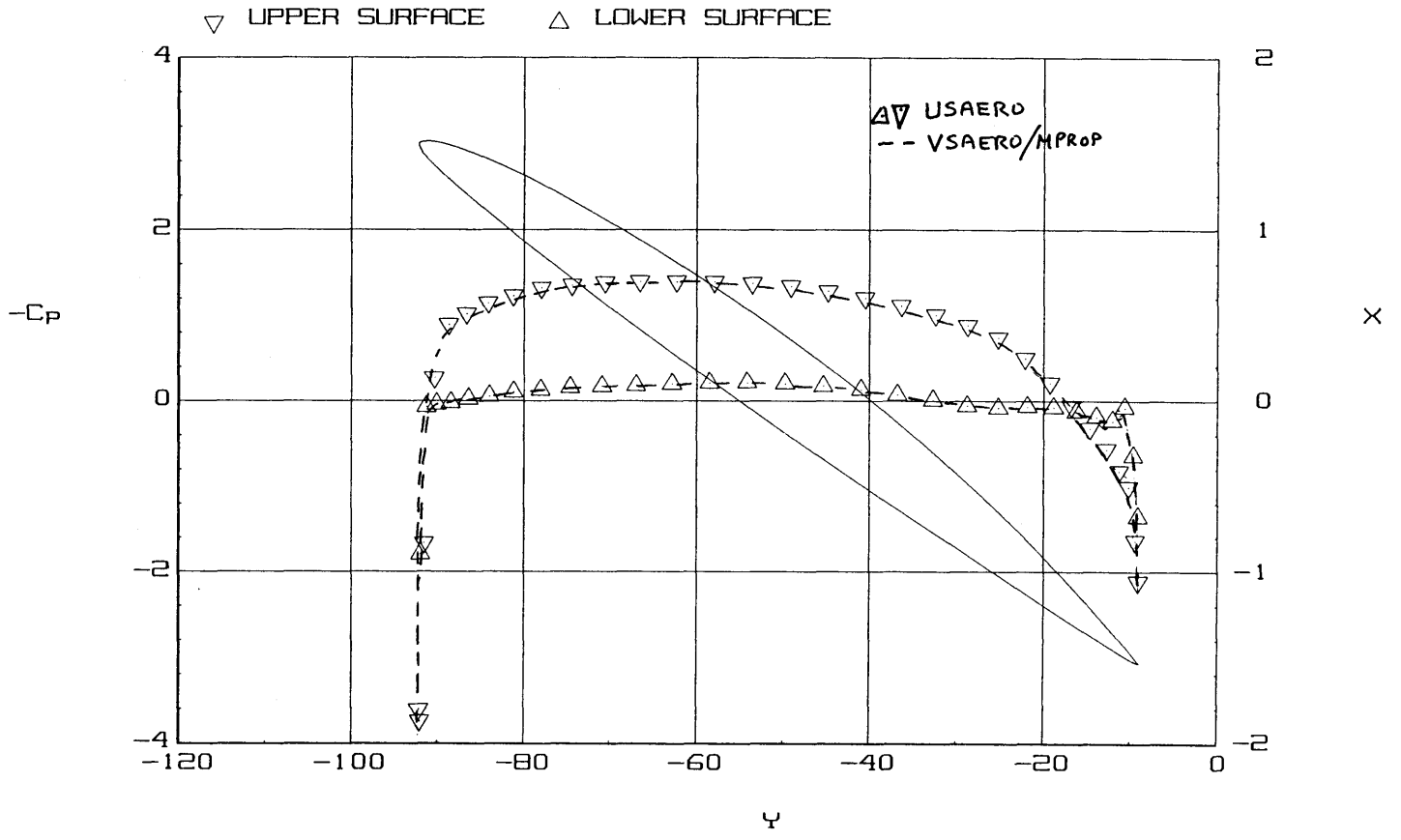

Fig. 4.4. Comparison of VSAERO/MPROP and USAERO Chordwise Pressure Distribution.

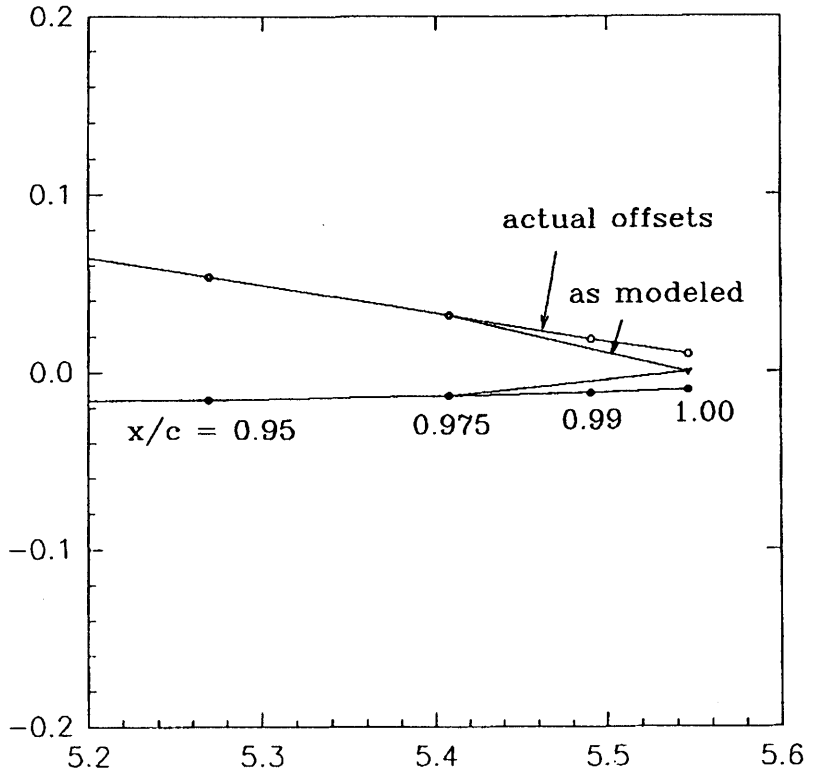

Fig. 4.5. Details of Trailing Edge Modification to Achieve Sharpe Edge.

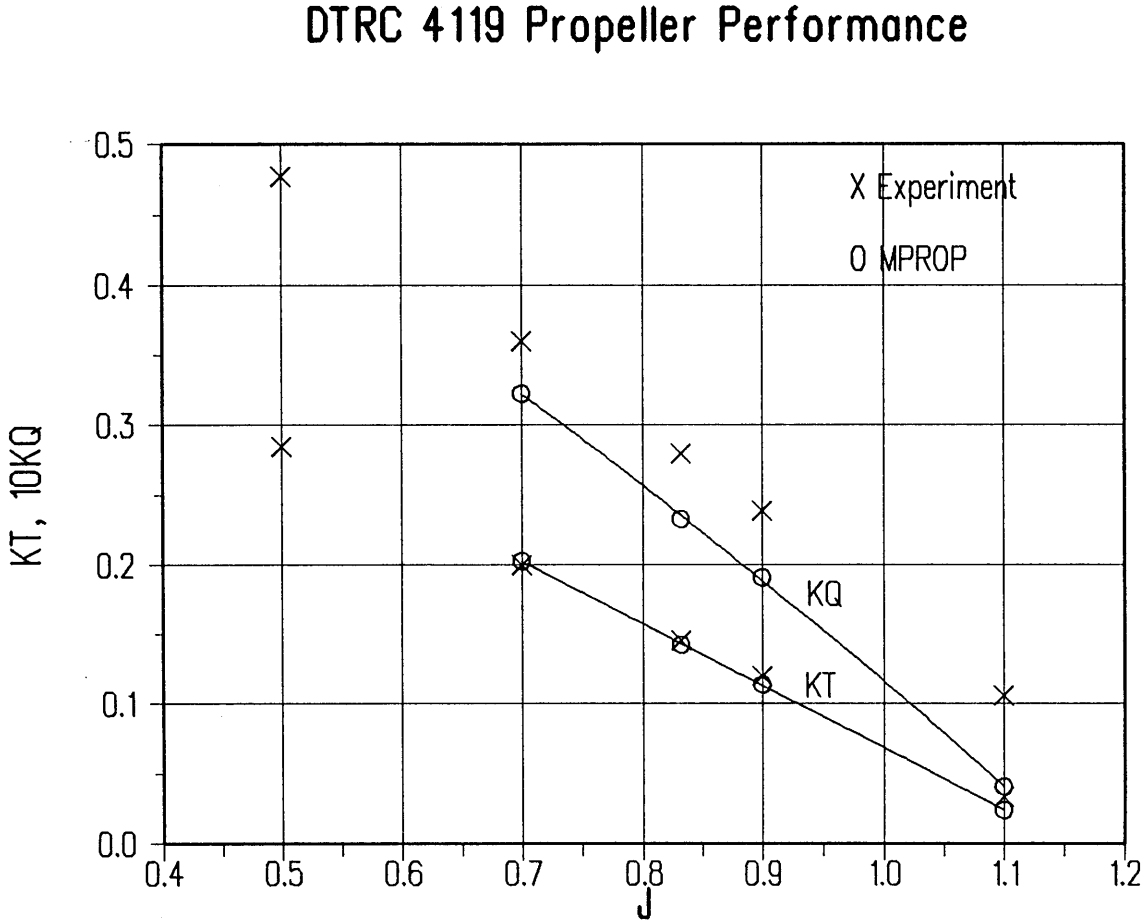

Fig. 4.6. Comparison of Calculated and Measured KT, KQ Characteristics
(a) VSAERO/MPROP

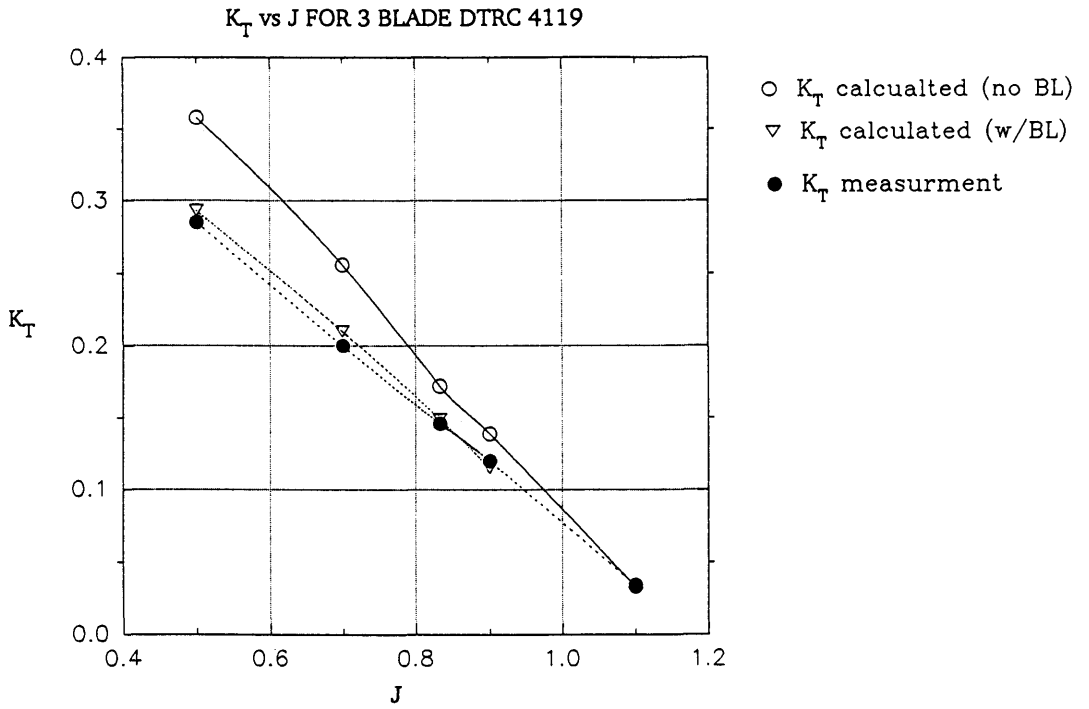

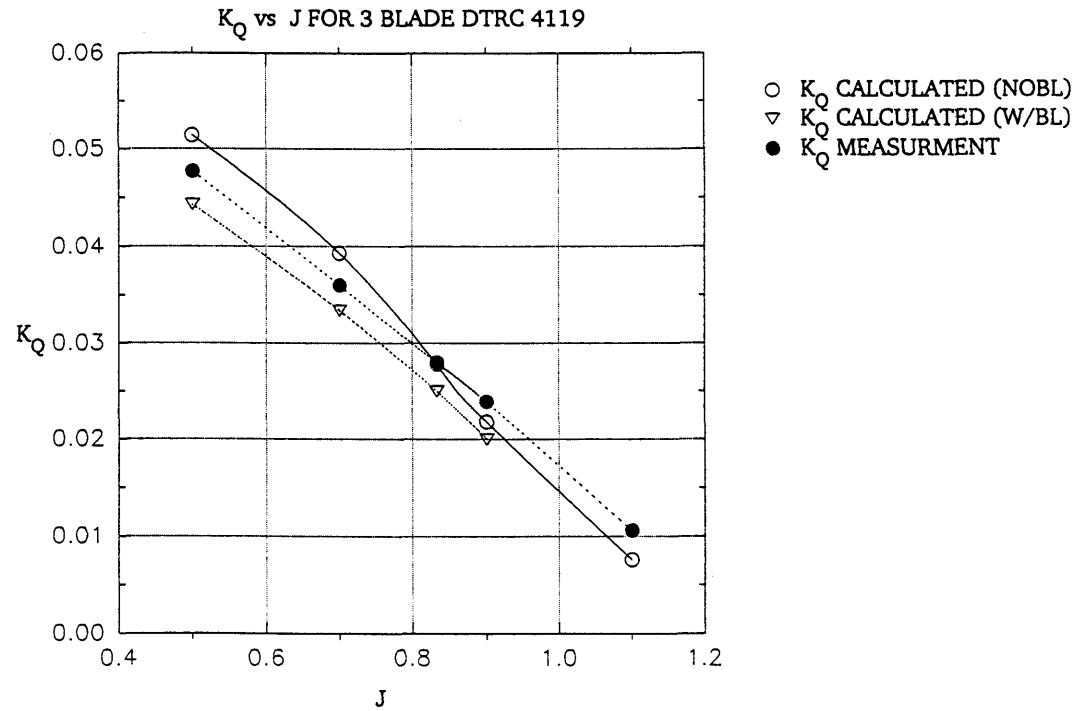

Fig. 4.6. Concluded.
(b) USAERO

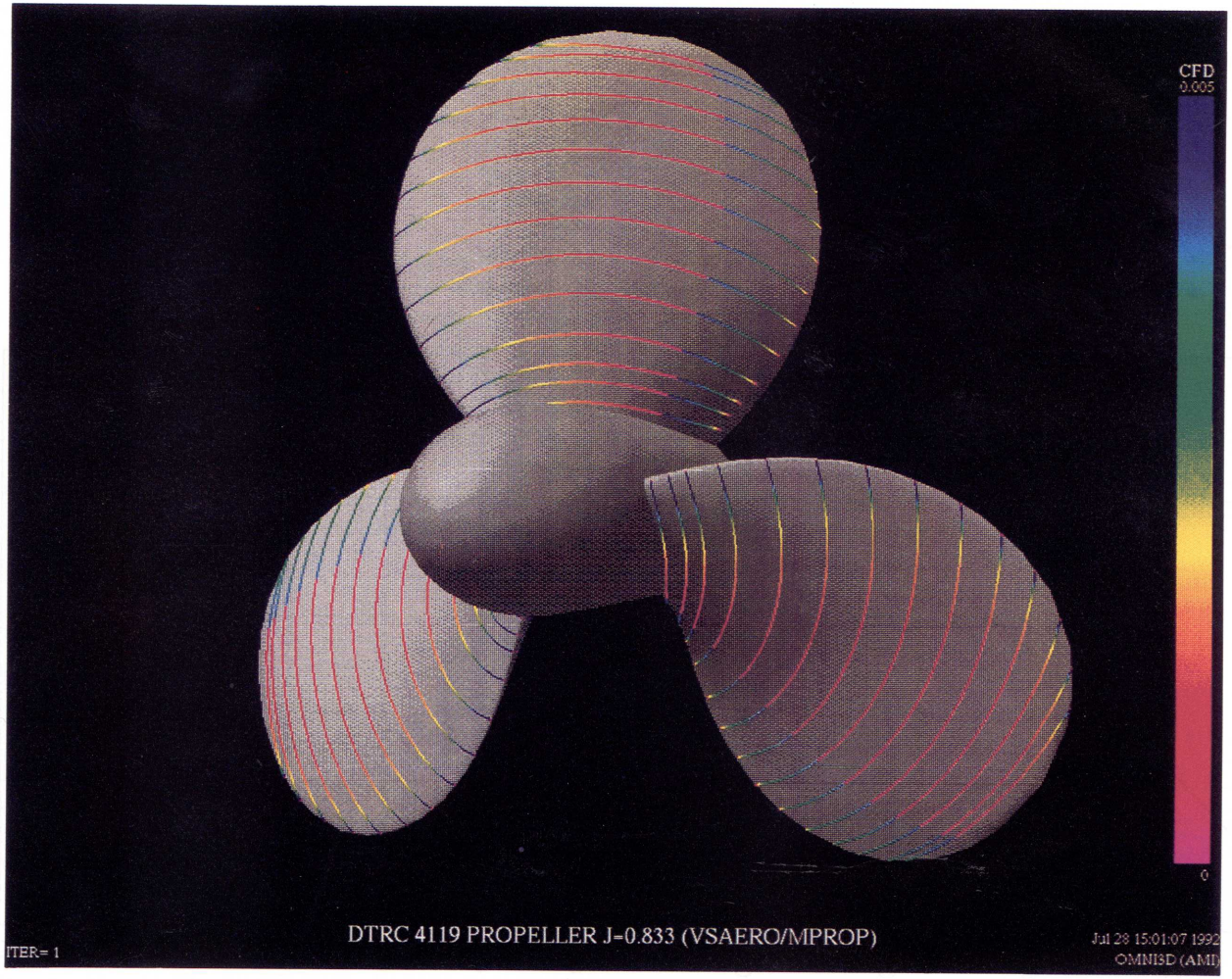

Fig. 4.7. Calculated Skin Friction Distribution Along Streamlines at J = 0.833
(a) VSAERO/MPROP

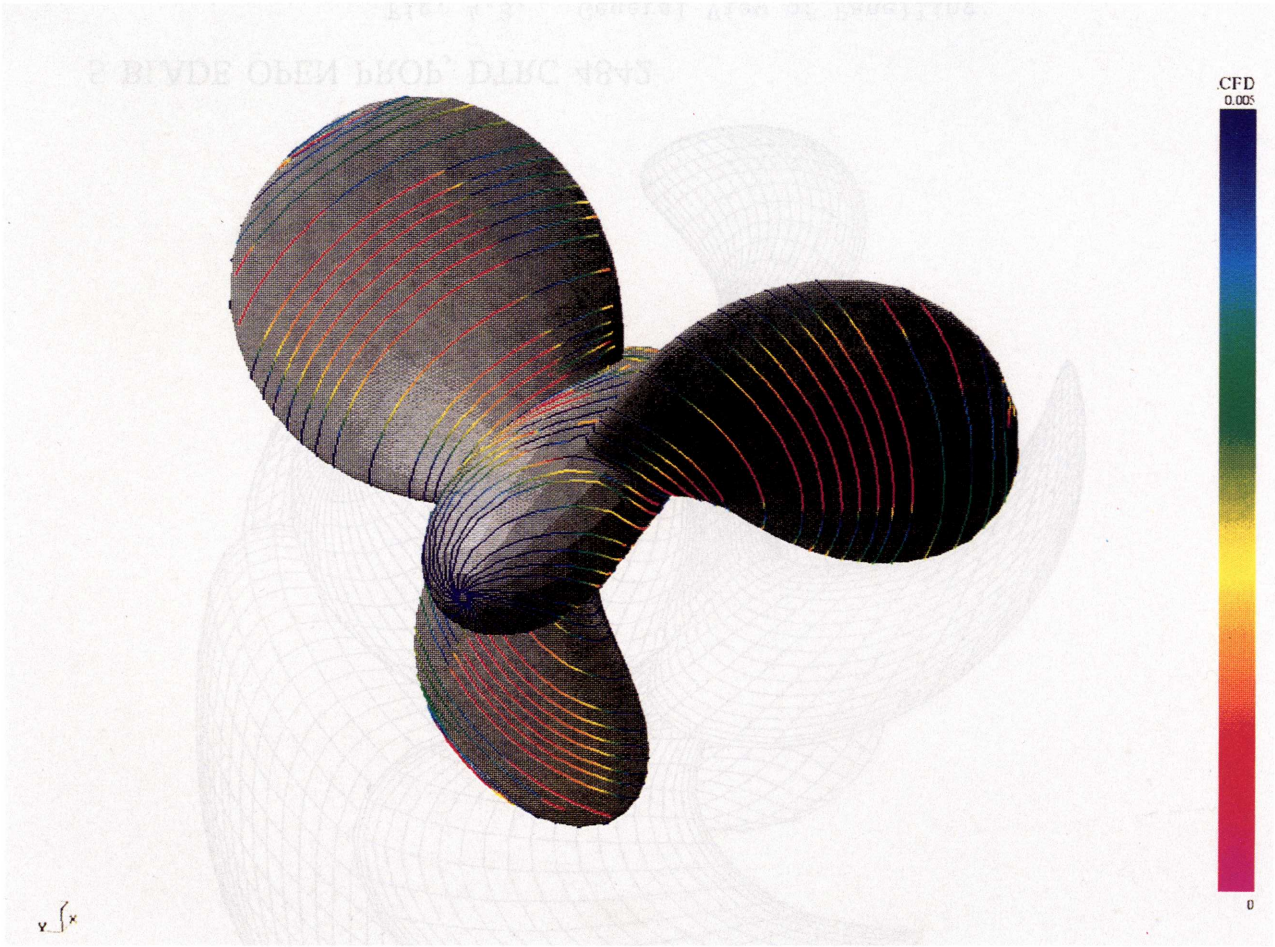

Fig. 4.7. Concluded.
(b) USAERO

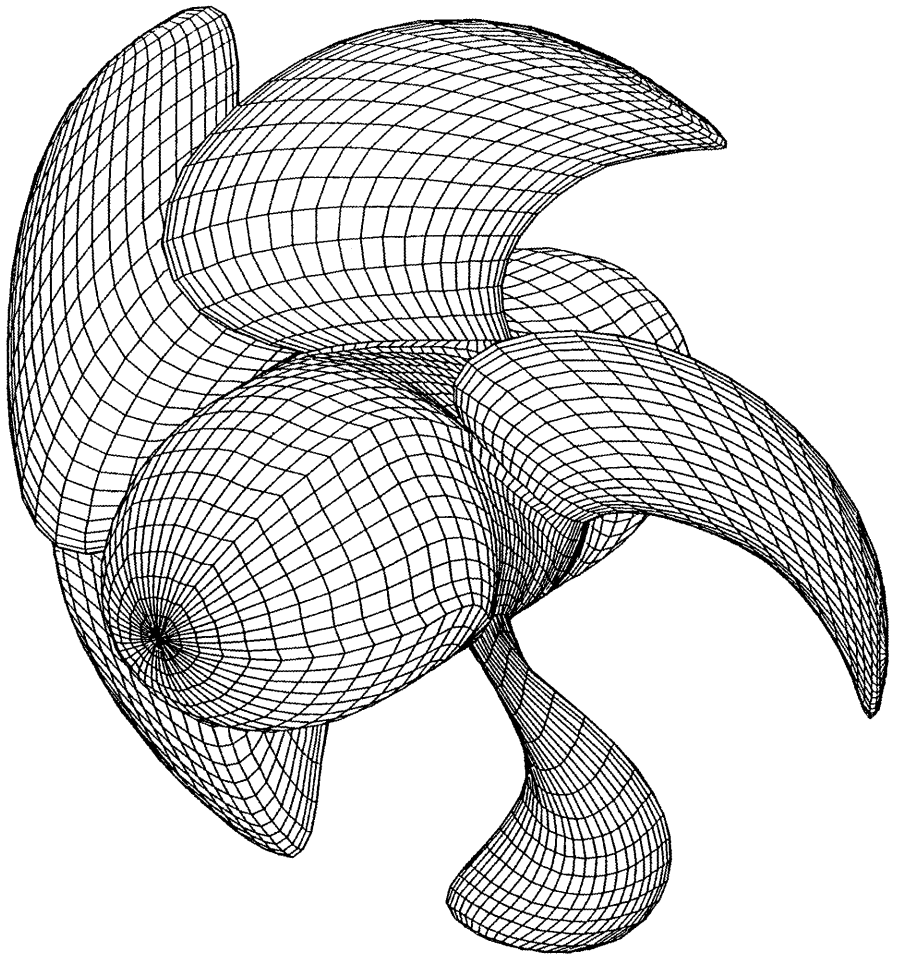

5 BLADE OPEN PROP, DTRC 4842

Fig. 4.8. General View of Panelling

Fig. 4.9. Calculated Pressure Contours at J = 0.905
(a) VSAERO/MPROP

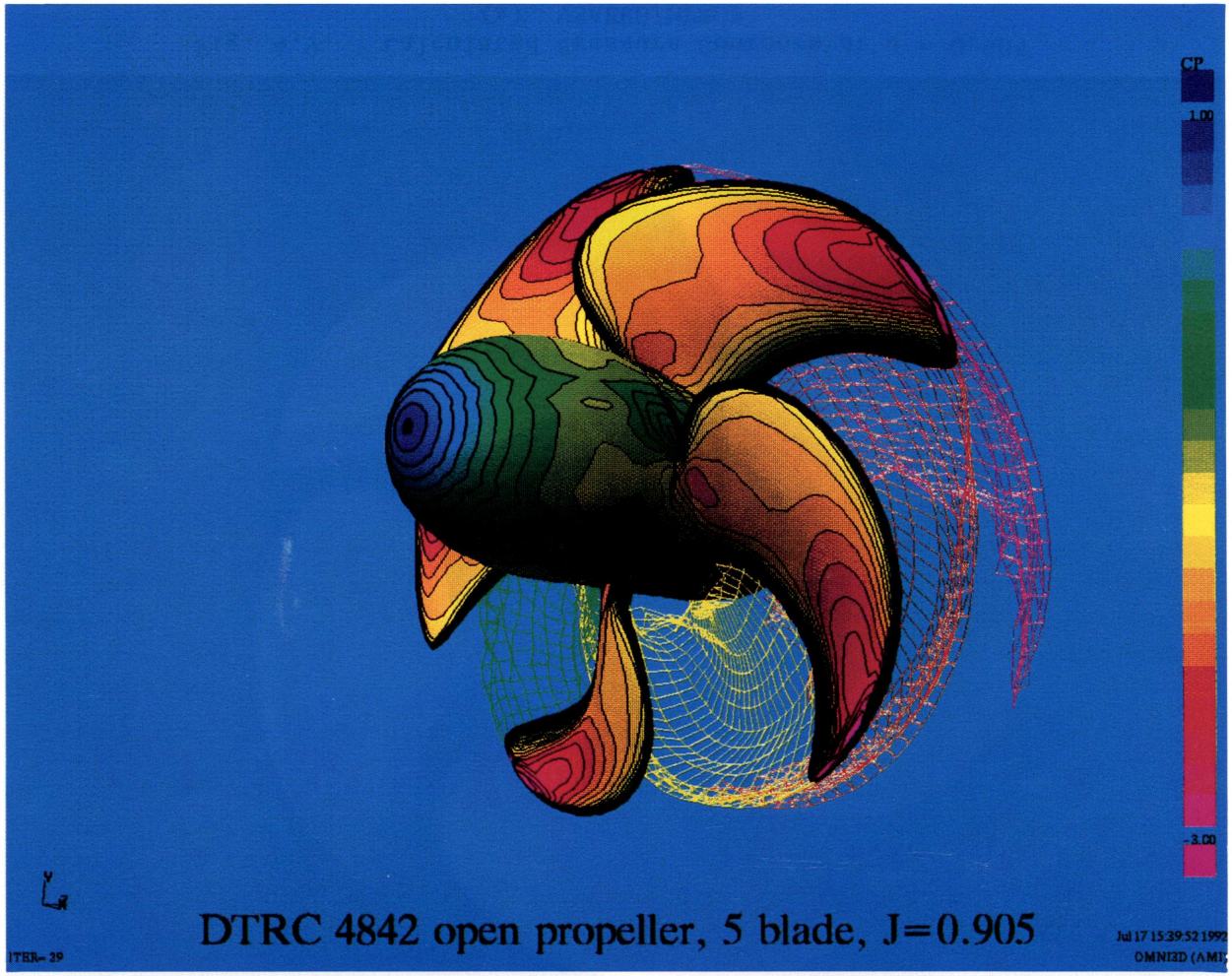

Fig. 4.9. Concluded.
(b) USAERO

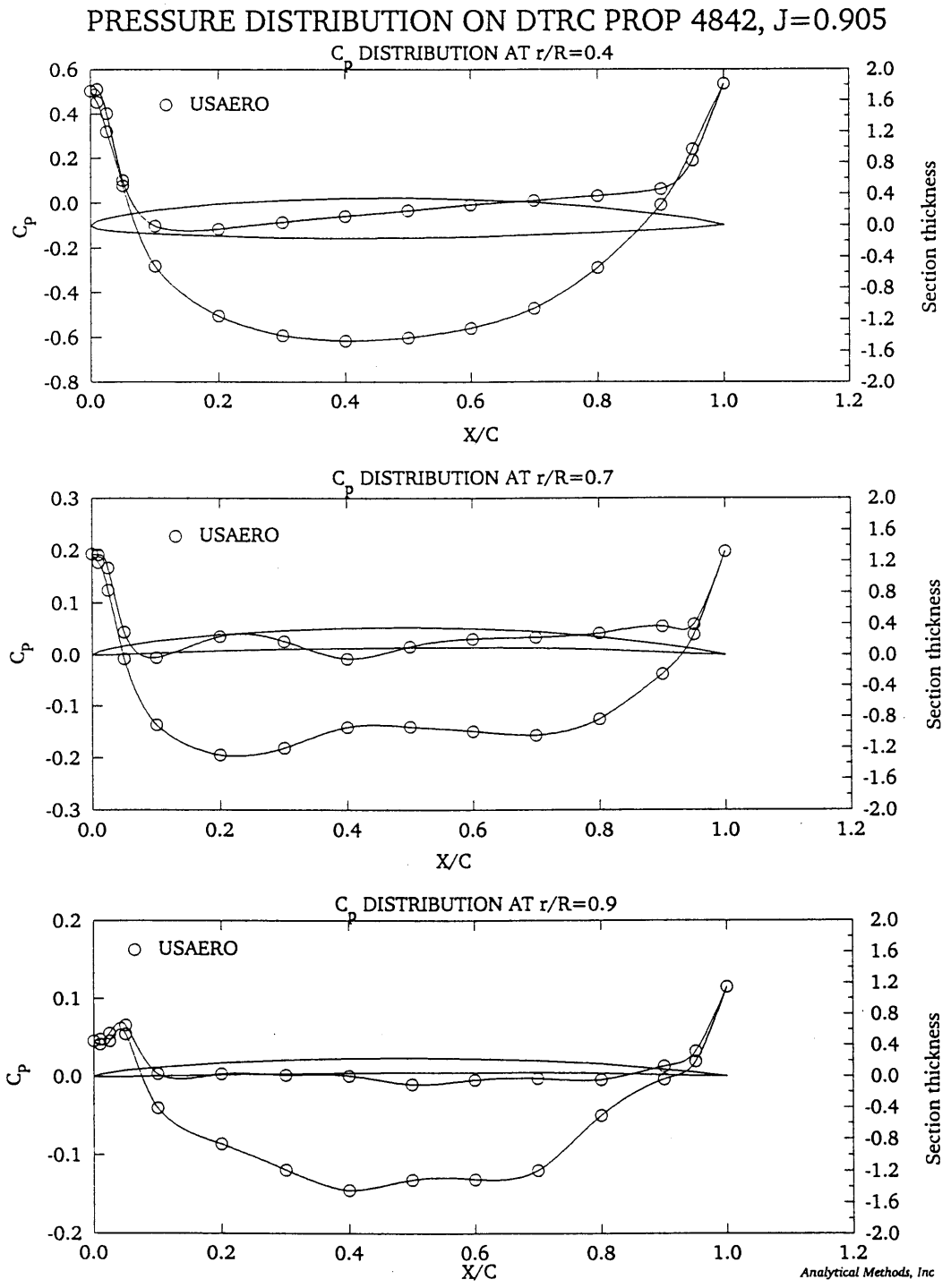

Fig. 4.10. Calculated Chordwise Pressure Distributions by USAERO at Three Radial Stations at J = 0.905.

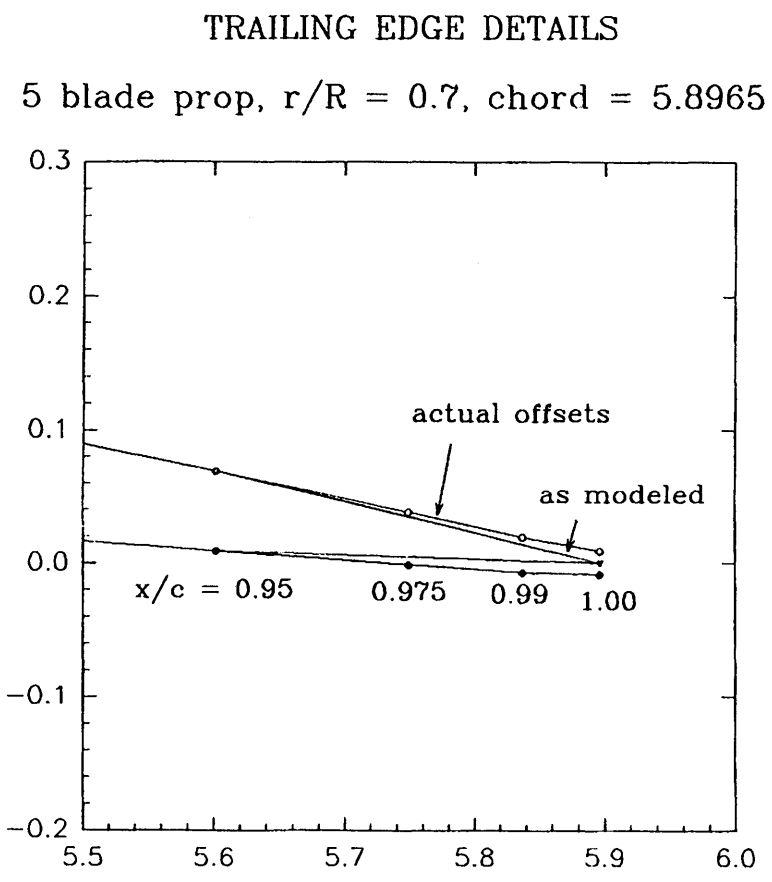

Fig. 4.11. Details of Trailing Edge Modification for Sharp Edge.

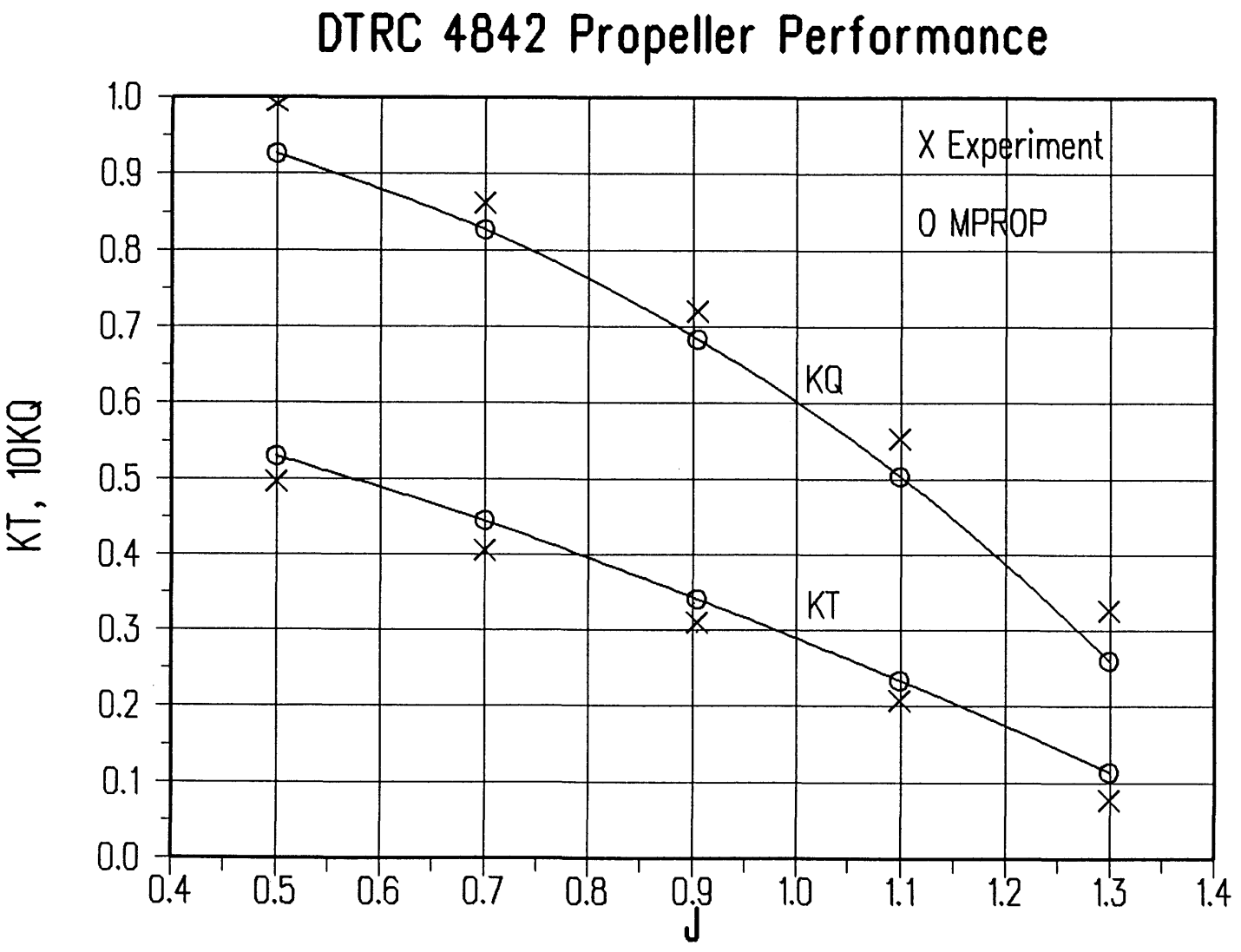

Fig. 4.12. Comparison of Calculated and Experimental KT, KQ Characteristics Using VSAERO/MPROP.

Fig. 4.13. Calculated Skin Friction Distribution at J = 0.905
(a) Along Streamlines in VSAERO/MPROP.

Fig. 4.13 Continued.
(b) Along Streamlines in USAERO.

Fig. 4.13. Concluded.
(c) As Surface Contours in USAERO

APPENDIX E

Calculations by YNU

Calculation by Surface Vortex Lattice Method

H.Yamasaki Yokohama National University, Japan

Aug. 23, 1992

1 Numerical Computing Procedure of Surface Vortex Lattice Method

When a propeller rotates in steady condition, there are generated spanwise and chordwise vortices on the real blade surface and trailing vortices in wake.
By applying Kerwin's formula(1) based on the principle of conservation of circulation, we can replace chordwise vortex and trailing vortex in terms with only discrete spanwise vortices.
In the vortex lattice method, the lifting surface on the mean camber surface of each blade is represented by horse-shoe vortices and the effects of thickness are done by sources. The strength of sources is determined by thin thickness assumption.
Now, in the surface vortex lattice method, the vortex lattice is placed just on the blade surface, and these vortices on the body surface play a part of not only the effect of camber but thickness. Consequently, only the strengths of spanwise vortices on the surface are unkown variables.
A blade surface is divided into several discrete elements, each of which is represented by a horse-shoe vortex.
Analytical expressions are derived for the perturbation velocity field induced by each horse- shoe vortex (vortex lattice). These are deduced to calculate the coefficients of a system of linear equations relating the magnitude of the normal velocity at each control point on the blade surface to the unknown spanwise vortex strength. So as to satisfy the boundary condition at the control points the spanwise vortex strengths are determined by solving this system of equations by an iterative procedure.
The boundary condition is given by the equation

$$\boldsymbol{V}_i \cdot \boldsymbol{n}_i = 0 \tag{1}$$

,where $\boldsymbol{V}_i$ is the resultant velocity vector and $\boldsymbol{n}_i$ is the normal vector to the blade surface at the i-th control point. The resultant velocity $\boldsymbol{V}_i$ at the i-th control point is summation of induced velocities by the vortex lattices, and undisturbed inflow velocity.
Specifically,

$$\boldsymbol{V}_i = \boldsymbol{V}_{iG} + \boldsymbol{V}_{iu} \tag{2}$$

,where $\boldsymbol{V}_{iG}$ is the velocity induced by the votrices relating the propeller, $\boldsymbol{V}_{iu}$ is the undisturbed inflow at i-th control point.

Considering this fact and equation (2), equation (1) becomes the following equation.

$$\boldsymbol{V}_{iG}\cdot\boldsymbol{n}_i = -\boldsymbol{n}_i\cdot\boldsymbol{V}_{iu} \tag{3}$$

We can transform equation (3) with respect to the strengths of spanwise vortices as unknown variables.

$$\sum_{k=1}^{K}\left[\sum_{m=1}^{M}\sum_{n=1}^{N}\Gamma_{nm}^{B}\cdot\left\{u_{inm}^{B\square}(k)+\sum_{n_w=2}^{N_w}u_{inm}^{Bw}(k)\right\}\right.$$
$$\left.+\sum_{m=1}^{M}\sum_{n=1}^{N}\Gamma_{nm}^{F}\cdot\left\{u_{inm}^{F\square}(k)+\sum_{n_w=2}^{N_w}u_{inm}^{Fw}(k)\right\}\right]=d_i \tag{4}$$

,where

$$d_i = -\boldsymbol{n}_i\cdot\boldsymbol{V}_{iu} \tag{5}$$

K	:	number of propeller blades
M	:	number of spanwise vortex elements of a propeller blade
N	:	number of chordwise vortex elements of a propeller blade
N_w	:	number of trailing vortex elements of propeller wake
Γ_{nm}	:	strength of spanwise vortex at n-th chordwise and m-th spanwise
$u_i^{\square}$	:	normal component of the velocity at the i-th control point induced by unit ring vortex on propeller blade
u_i^{w}	:	normal component of the velocity at the i-th control point induced by unit trailing vortex in propeller wake
B, F	:	index of back side or face side of blade

The $u_{inm}^{B\square}$ in the equation (4) means normal induced velocity at the i-th control point by a ring vortex at n-th chordwise and m-th spanwise on the back side surface having unit strength.
The velocity induced by a ring vortex can be calculated by Biot - Savart law.
The continuous vortex distribution representing the blade element is replaced with discrete one, which is placed at the front edge of the small panel and the control point is taken at the point of half chord as shown Fig.1 .
The two vortices on the back and face surfaces which are the closest to the leading edge are placed at a distance of $\alpha \cdot C$. The C is a chord length and α is 0.01 in this calculation.
We obtained the fact that the singularity between vortices near the sharp trailing edge as propeller blade is too strong to get good accuracy solutions.
In the present method, to avoid this the real surface panels satisfying the following expression are replaced by lifting surface panels.

$$\frac{b}{a} < \beta \tag{6}$$

The a means distance from spanwise vortex to control point on the back side and the b is distance from spanwise vortex on the opposite face side to control point on the back side, the β is a constant value and it is taken 1.025.

2 Division of Propeller Blade and Wake Model

2.1 Propeller Blade

The back and face surface of a propeller blade are divided into $N \times M$ panels.
In the chordwise spacing, same spacing is selected and in the spanwise spacing, cosine spacing used by Hoshino(2) is adopted.

$$r_m = \frac{1}{2}(r_t + r_h) - \frac{1}{2}(r_t - r_h)cos\alpha_m \tag{7}$$

$$\alpha_m = \begin{cases} 0 & for \quad m = 1 \\ \frac{(2m-1)\pi}{2(M+1)} & for \quad m = 2, 3, \ldots, M+1 \end{cases} \tag{8}$$

,where r_m are radial positions of the corner points of each panels and r_h is the radius of the boss, the r_t are radial distances represented by following expression.

$$r_t = \frac{(r - r_h)(4M+1)}{4M+2} \tag{9}$$

2.2 Propeller Wake Model

Fig.2 shows that the geometry of the propeller wake was simulated by iterative procedure. In the first step, we calculated the strengths of the vortices in the whole system including classical wake whose pitch distribution is equal to propeller's and which is not considered contraction and computed the induced velocity at each end of the segments of the discrete propeller wake, made them move to new position by using following expressions.

$$P_W^{(N+1)} = P_W^N + \boldsymbol{V}_W \cdot \Delta t \tag{10}$$

$$\boldsymbol{V}_W = (V_a + V_x, V_r, 2\pi nr + V_\theta) \tag{11}$$

,where $P_W^{(N)}$ are the coordinates of the ends of the discrete wake segments at N time step and each components of the V_x, V_r, V_θ are the axis, radial and circumferential induced velocity by vortex distribution respectively.
Moreover, the Δt in the expression (10) is determined by the following expression

$$\Delta t = \frac{1}{n \cdot N_W} \tag{12}$$

,where the n means the number of propeller revolution. After the second step, simulations are continued by the process as mentioned above untill thrust coefficients at each time step converge.

3 Calculation of Hydrodynamic Forces, Thrust and Torque

The hydrodynamic force acting on each discrete element has been composed of the following terms.

1. Kutta - Joukowski force acting on a ring vortex on the surface
2. Viscous drag at each blade element.

We can get the viscous drag working at each blade element by following equation

$$C_F = \left(1 + \frac{t_{max}}{C}\right) \cdot \frac{0.455}{(\log_{10} R_e)^{2.58}} \tag{13}$$

,where t_{max} is maximum thickness of the each blade section and R_e is the Reynolds number. The thrust and the torque of the propeller have been calculated by the summation of each components of the above terms.

4 Calculation of the Density of Circulation Distribution and the Pressure Distribution on the Blade

By applying Kerwin's formula, we have obtained the density of circulation distribution on i-th control point

$$\gamma_i = \frac{\Gamma^b_{nm} + \Gamma^b_{n+1,m}}{2\delta s} \tag{14}$$

,where γ_i is the density of circulation distribution, Γ^b_{nm} is the bound vortex at (n,m)-th panel, and δs is the spanwise length of the panel.
According to Yuasa(3), the pressure at i-th control point has been calculated by using Bernoulli's equation.

$$C_{PB} = 1 - \frac{V_i^{B2}}{V_{iu}^2} \tag{15}$$

$$C_{PF} = 1 - \frac{V_i^{F2}}{V_{iu}^2} \tag{16}$$

$$V_i^B = \mid \boldsymbol{V}_i^B \mid + \left\{(\Gamma^{Bb}_{nm} + \Gamma^{Bb}_{n+1,m})/(4 \cdot \delta s)\right\} \tag{17}$$

$$V_i^F = \mid \boldsymbol{V}_i^F \mid - \left\{(\Gamma^{Fb}_{nm} + \Gamma^{Fb}_{n+1,m})/(4 \cdot \delta s)\right\} \tag{18}$$

5 Results and Discussions

In the present method, DTRC4119 propeller condition without hub and with devised wake as mentioned previously was selected.

5.1 Open Water Characteristics

Fig.3 shows comparison of experiments and calculations. The calculations were both with and without viscous.
The thrust coefficients of the calculations with viscous are in good agreements with the experimental results, but with respect to the torque coefficients, the lower advance coefficients are, the larger differences between them are. They were caused by lack of friction resistance which were calculated by the expression using in flat plate and no taking separation of the tip vortex into consideration.

5.2 Pressure Distribution

Fig.4,5,6 show pressure distribution on blade at 0.3, 0.7 and 0.9 radius respectively.
Fig.4 shows that the calculations are smaller than the experimental results on the whole chord, especialy the differences between them are remarkable at leading edge like other radial positions (Fig.5 and Fig.6). We suppose that the diffrences of estimations on the whole chord depend on the calculation condition without hub and the differences at leading edge were caused by great influence of the closest vortices to the leading edge and discontinuous panel arrangement.
Fig.5 shows that the calculations are in good agreements with the experimental results except for the neighborhood of the leading edge. The differences are caused by the reason as mentioned previously.
Fig.6 show that the calculations are not agree to the experimental results on the whole chord and they are unreal distribution. We think that the unreality of this distribution were induced by the singularity of the close vortices on opposite sides.

5.3 Pitch Distribution of Propeller Wake

Fig.7 shows pitch distribution of the propeller wake calculated by the iterative procedure. The distances from the center line are 0.328 and 0.95 radius.
Both of the calculation distributions are similar to the experimental results but they are not in good agreement. We think that the strengths of the innermost vortex and tip vortex are not calculated correctly.

6 References

1. Kerwin, J.E. and Lee, C. -S.:"Prediction of Steady and Unsteady Marine Propeller Performance by Numerical Lifting Surface Theory", Transactions of the Society of Naval Architects and Marine Engineers, Vol.86, 1978 pp.218-253

2. Hoshino, T.:Hydrodynamic Analysis of Propellers in Steady Flow Using a Sureface Panel Method, Journal of the Society of Naval Architects of Japan, Vol.165, 1989 pp.55-70

3. Yuasa, H.:"Application of Numerical Lifting-Surface Theory on Steady Performance of Propeller/Duct System", Journal of the Society of Naval Architects of Japan, Vol.147, 1980 pp.53-70

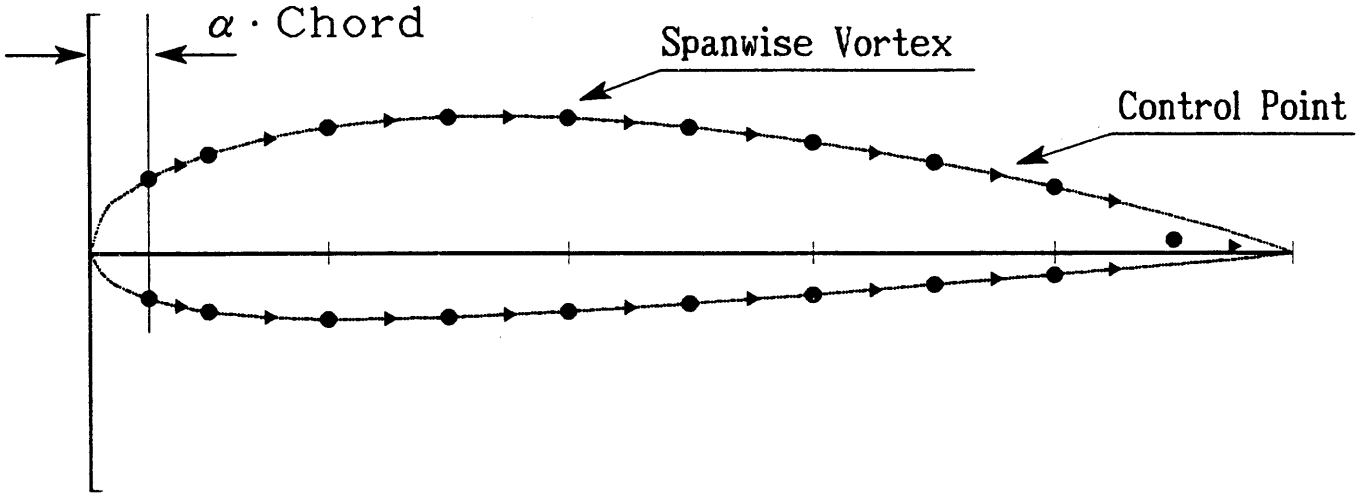

Fig. 1 Arrangement of Surface Vortex Lattice Model

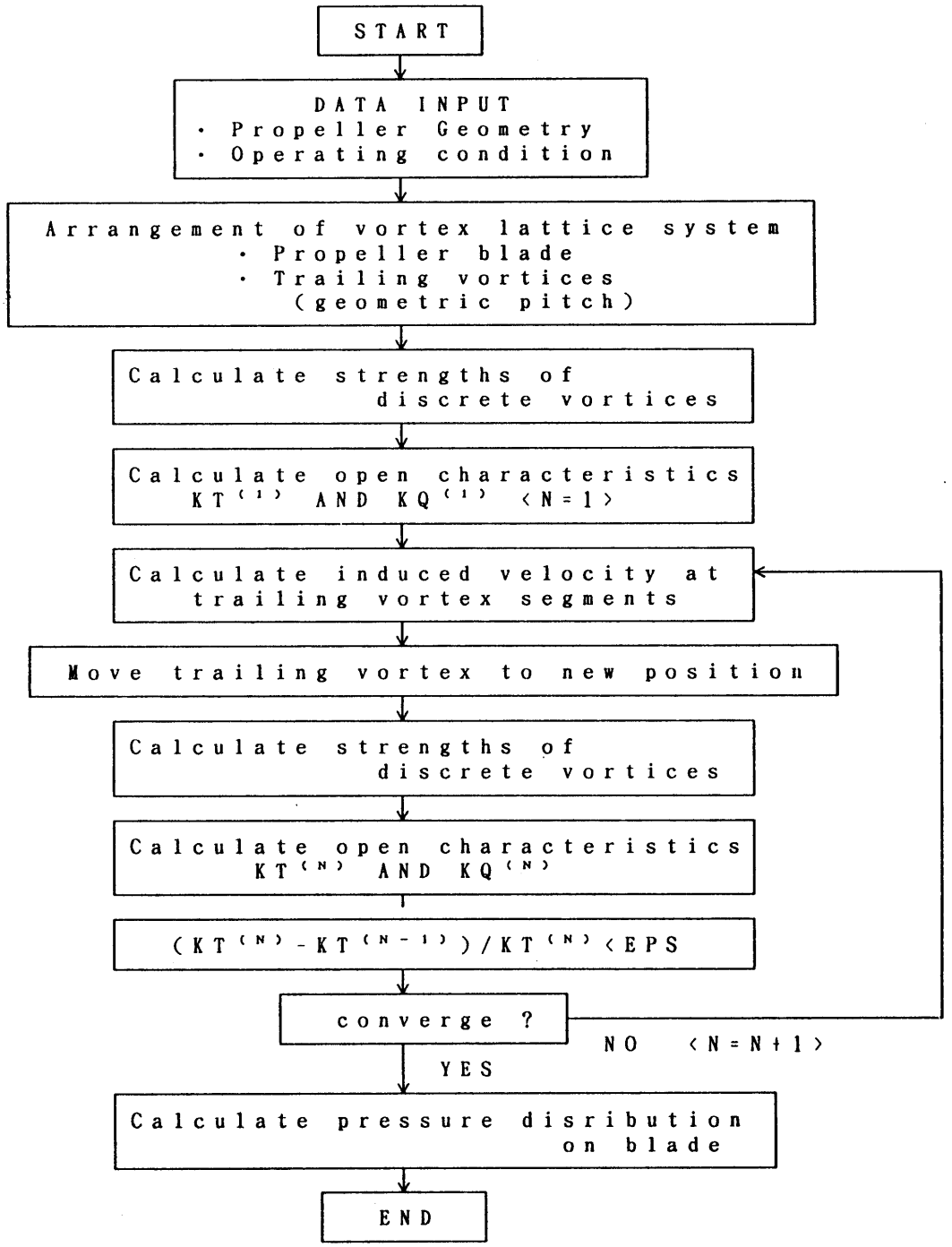

Fig. 2 Flow Chart of Present Calculation

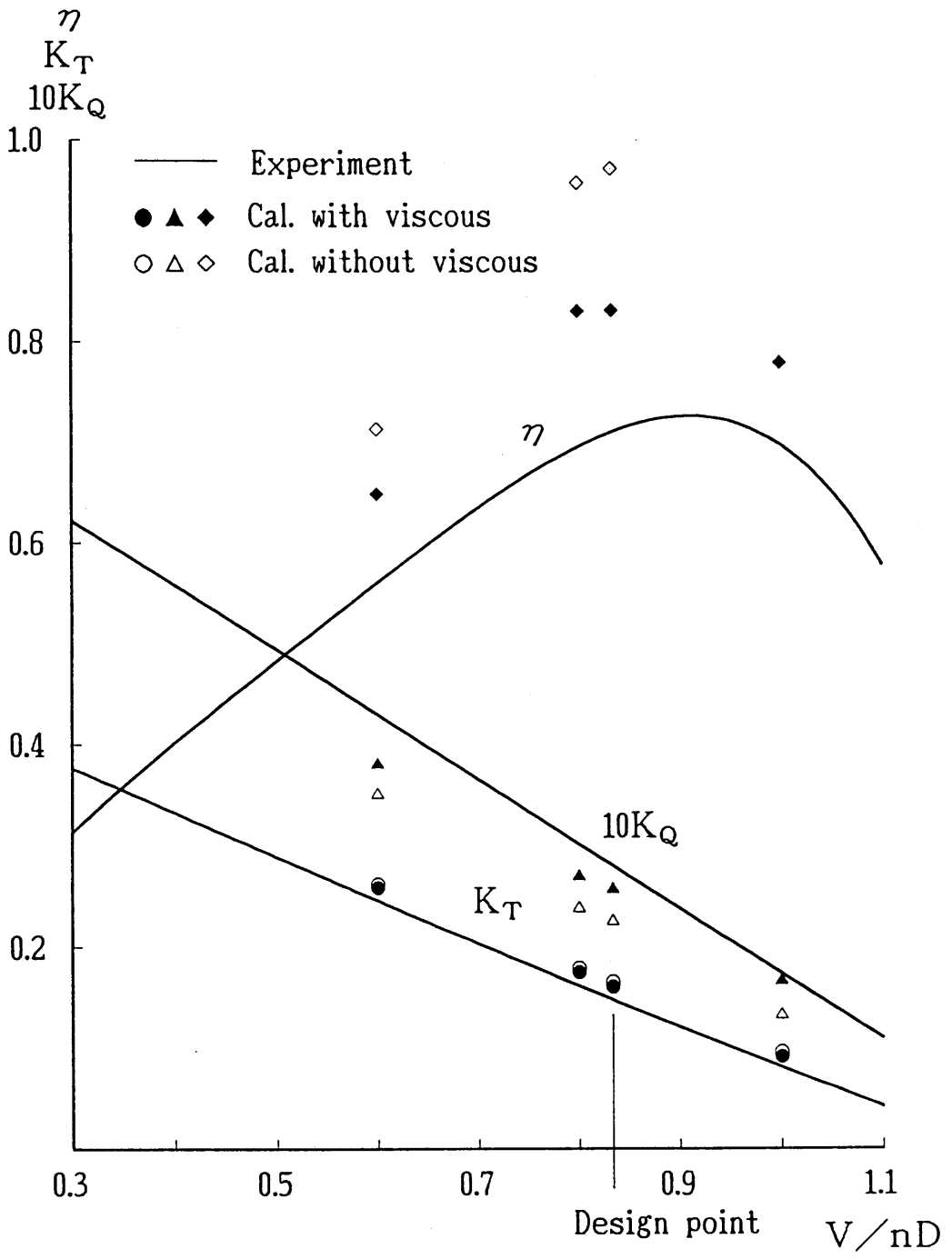

Fig. 3 Open Water Characteristics for Propeller(DTRC4119)
(Devised Wake)

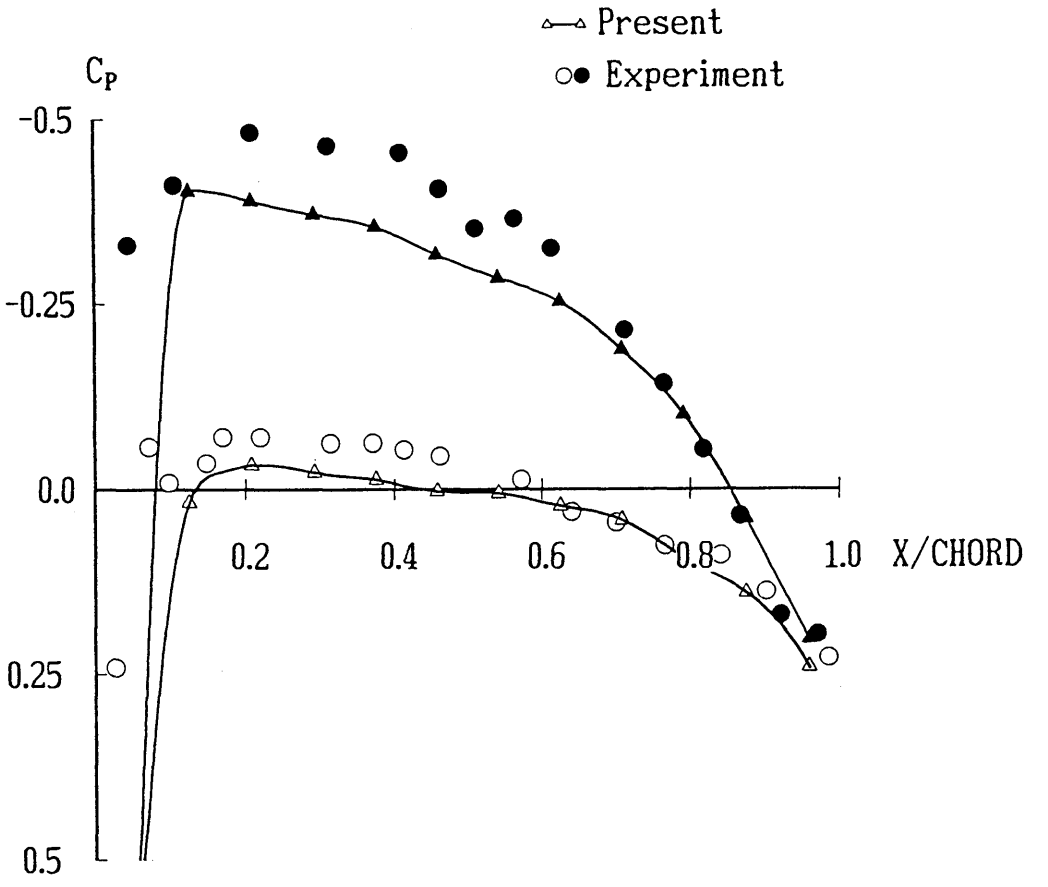

Fig. 4 Pressure distribution on DTRC4119
(Devised Wake, 0.3 Radius)

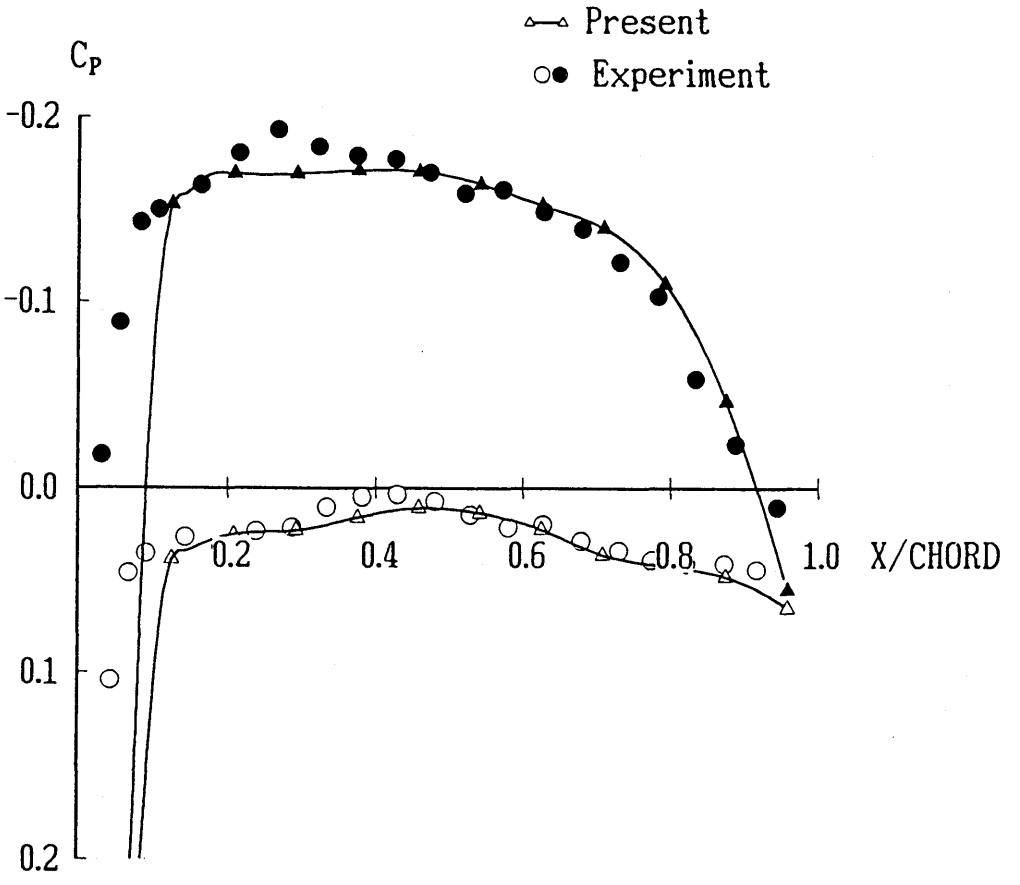

Fig. 5 Pressure distribution on DTRC4119
(Devised Wake, 0.7 Radius)

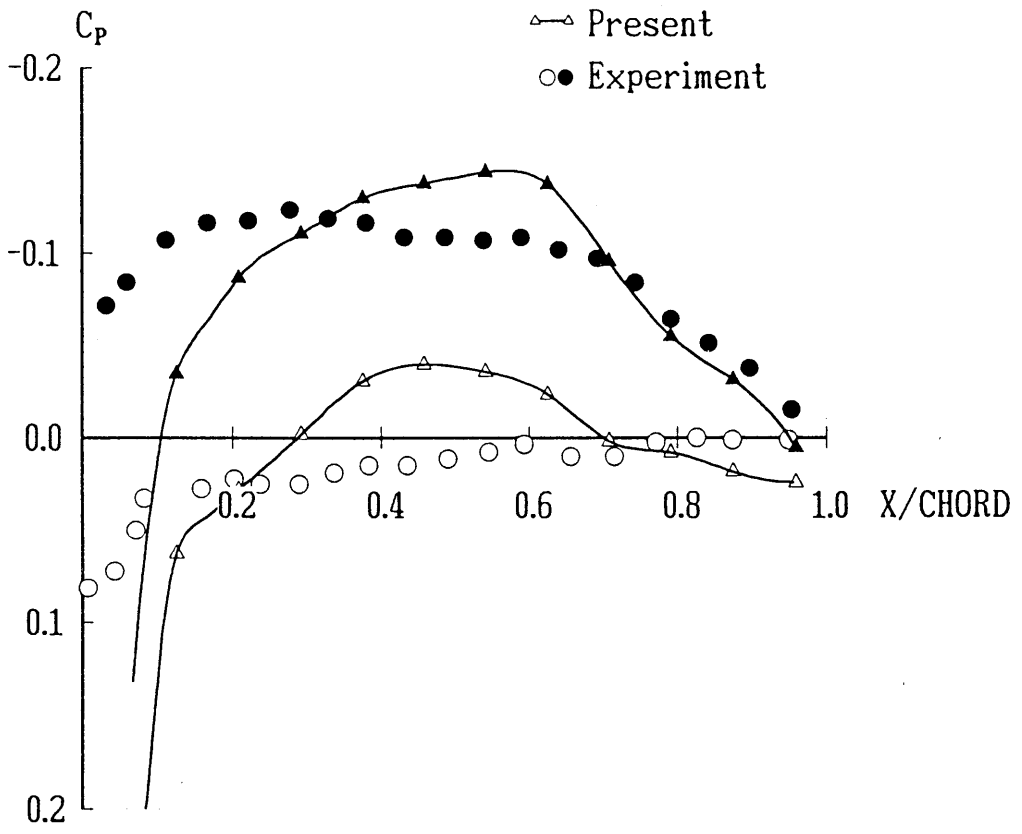

Fig. 6 Pressure distribution on DTRC4119
(Devised Wake, 0.9 Radius)

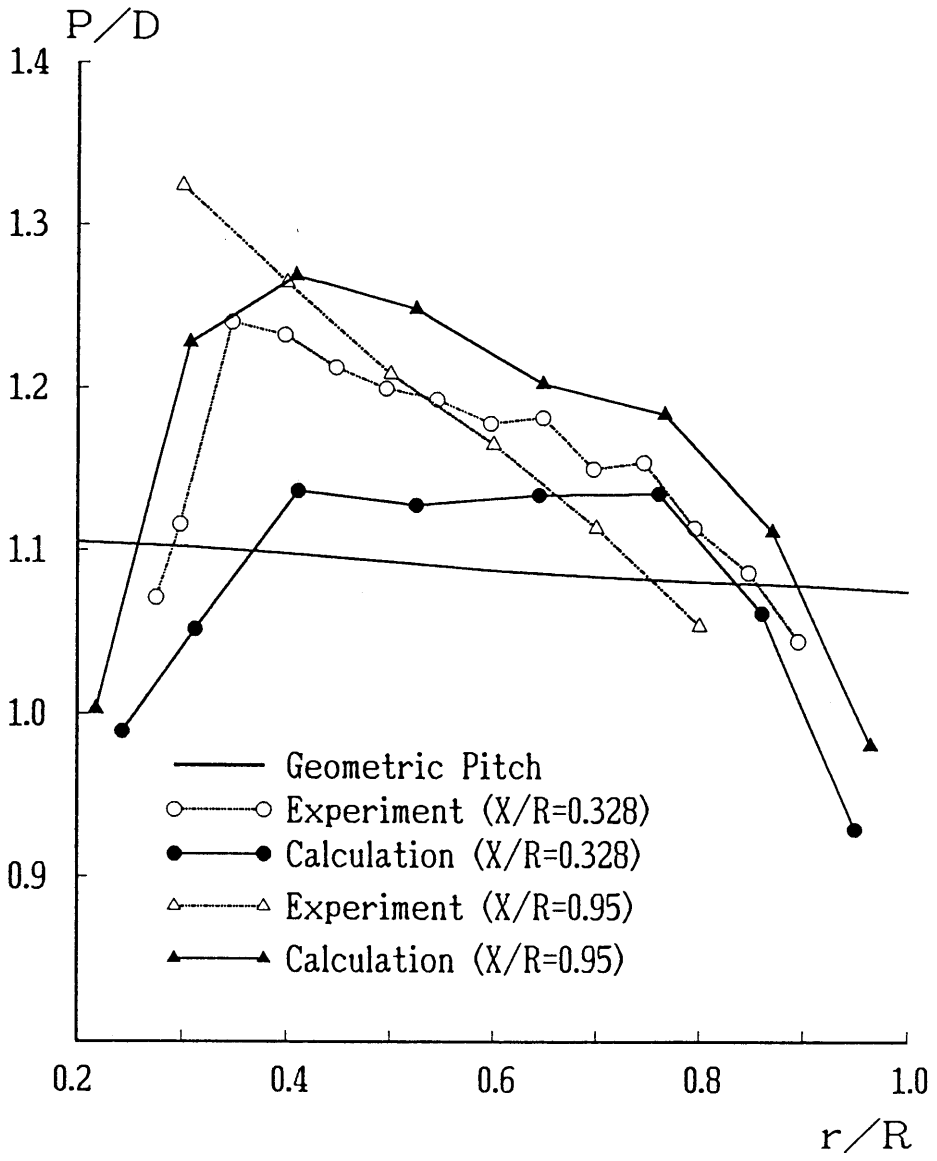

Fig. 7 Distribution of Blade Wake Pitch for DTRC4119

APPENDIX F

Calculations by CETENA

Propanel: A Surface Panel Method for the Steady Analysis of Naval Propellers.

Giovanni Caprino[1] , Luca Sebastiani[1] , Mario Caponnetto[2] , Massimo De Benedetti[3]

[1]CE.TE.NA, Centro di studi di Tecnica Navale, Genova, Italy.
[2]CE.TE.NA Consultant, Genova, Italy.
[3]Physics Department, University of Genova, Italy.

1. Introduction

The present method, devoted to the steady analysis of naval screw propeller, is based on a low-order potential field formulation of the problem: constant distribution of sources and dipoles are placed on flat quadrilateral panels, so that the integral equation of the boundary value problem is transformed in an algebraic linear system. This system is solved numerically with the Gauss-Siedel method. At this step of development, no wake-relaxation is performed.

The Kutta condition is implemented by a linear interpolation between two values, one of which is that of Morino approximation [1]. The improvement of the results, compared with those of the Morino approximation, are quite satisfactory, maintaining on the other hand the same advantages in terms of calculation speed and implementation simplicity.

The calculation of the velocities is performed by numerical differentiation of the perturbation potential on the surface of the blades, through quadratic interpolation of the perturbation potential.

The results of the analysis for two test cases, a non-skewed three-bladed propeller and a highly-skewed five-bladed propeller, are given for the design condition.

For the first propeller we have chosen uniform radial and chordwise spacing, while for the second one a cosine spacing in the chordwise direction and a sine spacing for the radial direction have been selected [2].

2. Basic theory.

The computational procedure is based on a low-order lifting-potential panel method, which consists in discretizing the relevant boundaries with flat quadrilateral elements on which a constant singularities distribution is placed. The boundary value problem is solved numerically at the control point of each panel.

The calculation of the influence matrix is based on the standard formulas for the potential field due to a constant distribution of source and dipoles on a quadrilateral panel [3]. The lowest-order far-field approximation is used when the distance between two control points is greater than 0.2 times the diameter of the propeller. This way a considerable saving in the computational time is achieved without any significant loss in the solution accuracy.

The system of linear equations for the perturbation potential is solved using iterative Gauss-Siedel method.

The surface velocities are obtained by numerical differentiation of the perturbation potential. The direct numerical calculation has been preferred to the analytical approach, based on the velocity influence coefficients, because it is more efficient from the CPU-time

point of view, and it seems also to be more accurate [2].

As a results of the numerical procedure, the C_p distribution on the blades and the torque and thrust coefficients are calculated.

The basic theory is inherently inviscid. Anyway a viscous correction to the inviscid thrust and torque coefficients is provided, taking into accounts the viscous effects on the blades surface on the basis of the two dimensional approach originally formulated by Van Oossanen [4].

A resistance coefficient Cr for each blade section is derived from the flat plank resistance coefficient Cf on the basis of the thickness-over-chord ratio t/c:

$$C_r = C_f\left(1+1.2\,t/c+70(t/c)^4\right)$$

The corresponding contribution in terms of thrust and torque is thence evaluated.

It should be stressed that this technique generally underestimates the viscous correction.

No wake relaxation is provided and a rigid helycoidal wake is adopted, with the pitch linearly varying from the corresponding value of the interested section to the mean value of the blade.

3. Panelling features.

For the non-skewed propeller, a coarser uniform spacing is used in the middle of the blade, while a finer uniform spacing is adopted near the tip, for the radial direction, and near the trailing and leading edges, for the chordwise direction.

Radial spacing is 0.05 r/R up to 0.9 r/R and 0.025 otherwise, chordwise spacing is 0.1 x/c from 0.1 x/c to 0.9 x/c and 0.025 otherwise.

The basic grid adopted for this propeller consists of 408 panels on each blade (see Fig. 1). An additional coarser grid with 260 panels has been analysed to assess the panelling sensitivity. The coarser grid has been obtained from the finer one using a larger radial spacing , namely 0.1 r/R , from 0.2 r/R to 0.9 r/R.

In the case of the highly-skewed propeller a cosine spacing for the chordwise direction:

$$x_c = \frac{1}{2}\left(1-\cos\left(\left(\frac{2\pi}{N}\right)(j-1)\right)\right) \quad j=1,\cdots,N/2+1$$

N = total number of the panels on the section

and a sine spacing:

$$x_r = \frac{R_h}{R}+\frac{R-R_h}{R}\sin\left(\frac{\pi}{2M}(m-1)\right) \quad m=1,\cdots,M+1$$

M(N/2+1) = total number of the panels on the blade

for the radial direction, have been considered to be more suitable to the complex blades geometry.

The basic grid adopted for this propeller consists of 728 panels for each blade (see Fig. 2).

The information on the blades geometry for both propellers has been derived from [5]. The features of blade stations and sections not reported in [5] are obtained by interpolation.

Hub is equally divided into Z portions, each further subdivided into six regions (see Fig. 3): the aft and forward ends, the intermediate region between trailing and leading edges, the portion at the intersection of the blade with the hub and two cylindrical portions between the ends and the intermediate region .

The panelling is helycoidal in the after part and cylindrical in the forward part. In the the intersection portion the grid consists of only one strip of panels, which match the corresponding panels on the blade.

The basic hub grid consists of 132 panels for the non-skewed propeller and

of 164 panels for the skewed one, for each blade portion.

4. Kutta condition.

The first step has been the implementation of the approximate Morino Kutta condition [1], imposing the equality of the strength of the dipole sheet on each strip of the vortex wake with the dipole jump on the corresponding panels adjacent to the trailing edge.

This way Kutta condition resulted generally not exactly satisfied at the trailing edge. On the hypothesis that the dipole sheet on the wake was underestimated, a correction of the original Morino condition was implemented consisting of a trial-and-error technique based on linear interpolation.

The technique starts with Morino approximation. Then Morino estimation for the dipole strength of the strips of the wake is multiplied by a guess coefficient, a value slightly larger than unity being sufficient. Finally the coefficient which makes the pressure jump at the trailing edge be zero, ensuring the satisfaction of Kutta condition, is found through linear interpolation between the two values.

Nevertheless its simplicity the method provided quite satisfactory (see Fig. 4).

5. Numerical procedures.

The features which mostly affect the results are the solution of the system of linear equations for the unknown dipoles distribution and the calculation of fluid velocities on the propeller surface.

The present linear equation solver is based on the Gauss-Siedel iterative method, which is felt to be more efficient than Gauss reduction especially for fine grid. The average iterations number needed for the solution of a linear system with 540 unknowns is 135.

Calculation of surface velocities distribution is performed by numerical differentiation of the potential on the basis of the panel control points on the propeller surface.

Differentiation is performed along two directions on the plane of the panel. To this purpose use is made of local non-orthogonal co-ordinates on the panel, which approximate the curvilinear abscissa on the propeller surface and are obtained joining each panel centroid with the mean point of the two adjacent panel sides. The projection on the local orthogonal co-ordinate system of the panel is performed at the initialisation stage during panelling procedure (see Figs. 5, 6).

fig. 5

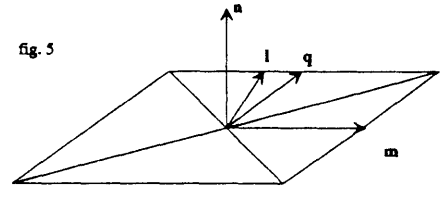

n, l, m, are the local orthogonal axes; q is the unit vector from centroid to mean point of the side

The differentiation algorithm consists in calculating the derivatives of the quadratic fit of the fluid potential through the adjacent panel control points expressed in terms of the curvilinear abscissa.

fig. 6

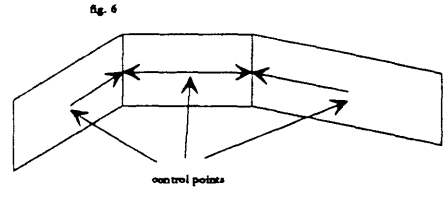

The quadratic fit of the potential is expressed by the parabola :

$$y^2 = as^2 + bs + c$$

The derivative along the directions m and q are thence found through the expression:

$$y'(s) = 2as + b$$

Choosing the origin of the curvilinear co-ordinates at the panel centroid, the derivative is simply equal to the coefficient b of the parabola .

To give an idea of the computational speed of the complete procedure, the solution for the non-skewed propeller with the recomended panelling with 408 panels required one hour of CPU-time on a DEC Micro VAX 4000-200 for one calculation condition.

6. Results and discussion

The computational procedure has been applied to a three-bladed non-skewed propeller and a five-bladed skewed propeller.

The calculations have been performed at the design condition for both propellers, J = 0.833 and J = 0.905 respectively.

The viscous correction, described in paragraph 2, has been applied in the determination of the thrust and torque coefficients.

In the case of the non-skewed propeller the numerical results are compared with published data [5].

The results for the non-skewed propeller are illustrated in the figures from 7 to 10.

In Fig. 7 the C_p distribution on the blade, obtained for the basic panelling with 408 panels, is presented at three r/R values (namely 0.3, 0.7 and 0.9) and compared with the experimental data. The agreement between numerical results and experimental data is generally good except at 0.3 r/R. The observed discrepancy is attributable to the blade-hub interference.

In Fig. 8 the corresponding results for the coarser grid with 260 panels are compared with the previous ones and the experimental data. It can be observed that there is no sensible difference between the two grids.

In Fig. 9 the results with and without hub are compared in terms of C_p distribution on the blade to investigate hub influence. As expected the results are significatively different only for the section nearest to the hub, namely at r/R = 0.3.

In Fig. 10 K_t and K_q values are presented for J from 0.5 to 0.9, with and without viscous correction. It can be noted that the influence of viscous effects on Kt is quite small and the numerical results are in very good agreement with the experimental ones. The discrepancy between the calculated and measured K_q is attributable to the presence of viscous effects, which are underestimated by the present correction technique.

In Fig. 11 the results for the case of the skewed propeller are presented in terms of Cp distribution on the blade at r/R = 0.4, 0.7 and 0.9 for the recommended panelling with 728 panels.

Nevertheless the satisfactory results of this preliminary correlation , further comparison of the numerical results with experimental data for other kinds of propellers is needed to completely validate the procedure and to assess its effectiveness from the propeller designer point of view. The present completion of the Cavitation Tunnel of Genova University seems to be a good basis for future work in this direction.

Finally it must be stressed that the present procedure is not the ultimate product of our research program but the first step towards the development of a complete panel method for propeller analysis.

7. Acknowledgement

The authors wish to thank the Department of Physics of Genova University for the co-operation in the theoretical and numerical formulation.

The appreciation of the authors is extended to the Institute of Naval Architecture of Genova University for the active interest in the development and application of the procedure.

8. List of references

[1] Morino, L. and Kuo, C.-C., "Subsonic Potential Aerodynamics for Complex Configurations: A General Theory," *AIAA Journal*, Vol. 12, No. 2, Feb. 1974.

[2] Kerwin E. J. et al., "A Surface Panel Method for the Hydrodynamic Analysis of Ducted Propellers," *SNAME Trans.*, Vol. 95, 1987.

[3] Hess, J. L., "The Problem of Three-Dimensional Lifting Flow and Its Solution by Means of Surface Singularity Distribution," *Computer Methods in Applied Mechanics and Engineering*, Vol. 4, Nov. 1974.

[4] Van Oossanen, P., "Calculation of Performance and Cavitation Characteristics of Propellers Including Effects of Non-uniform Flow and Viscosity", *NSMB* Publ. N. 457.

[5] Yessup, S. D., "An experimental Investigation of Viscous Aspects of Propeller Blade Flow," Ph.D. thesis, The Catholic University of America, 1989.

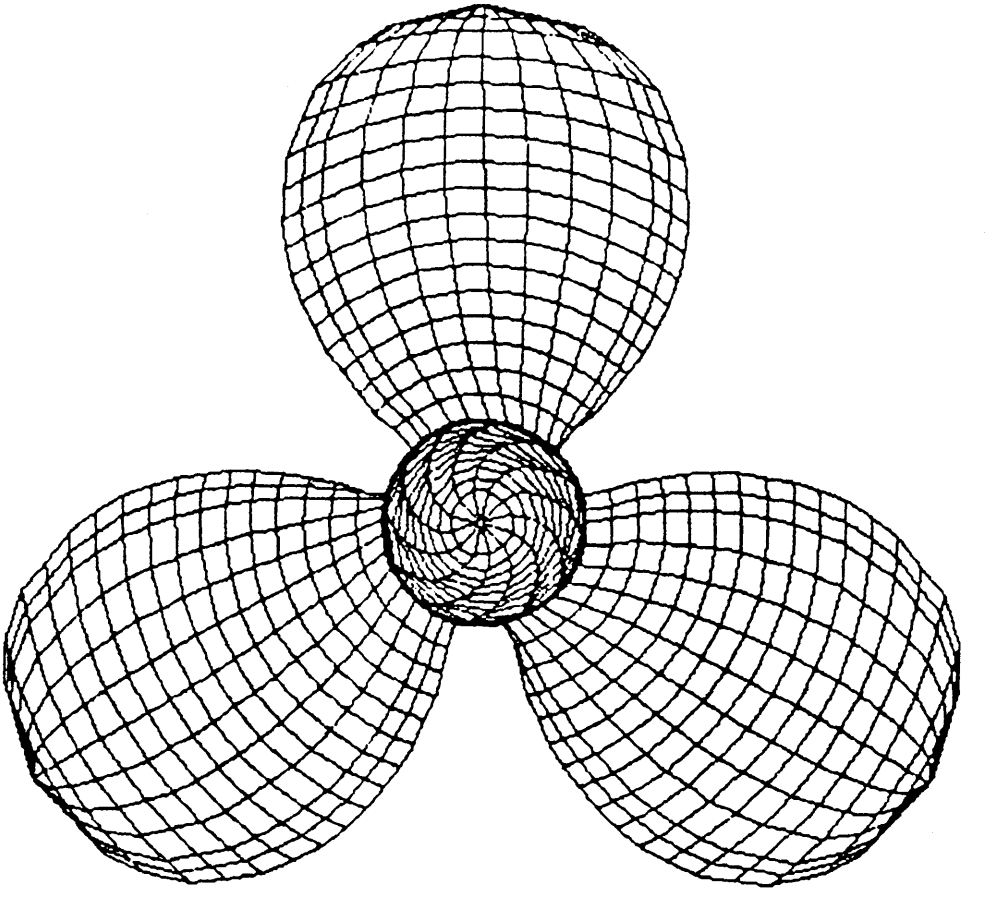

fig. 1. Basic grid for non-skewed propeller.

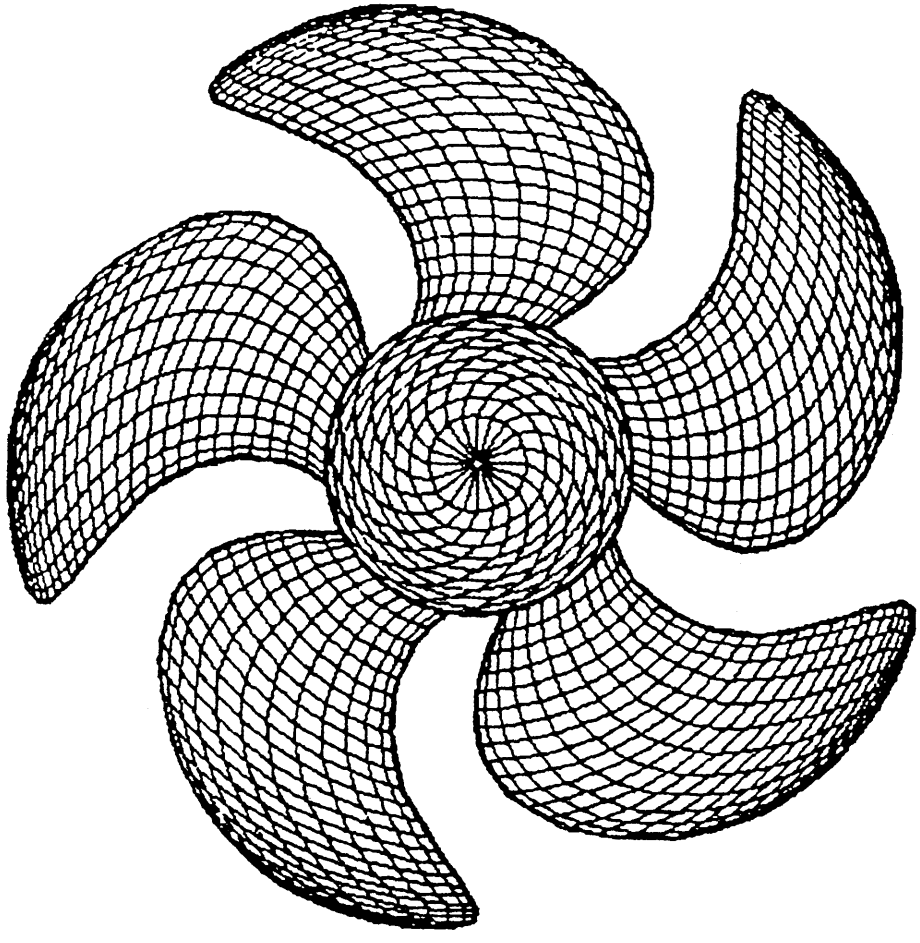

fig. 2 Basic grid for skewed propeller.

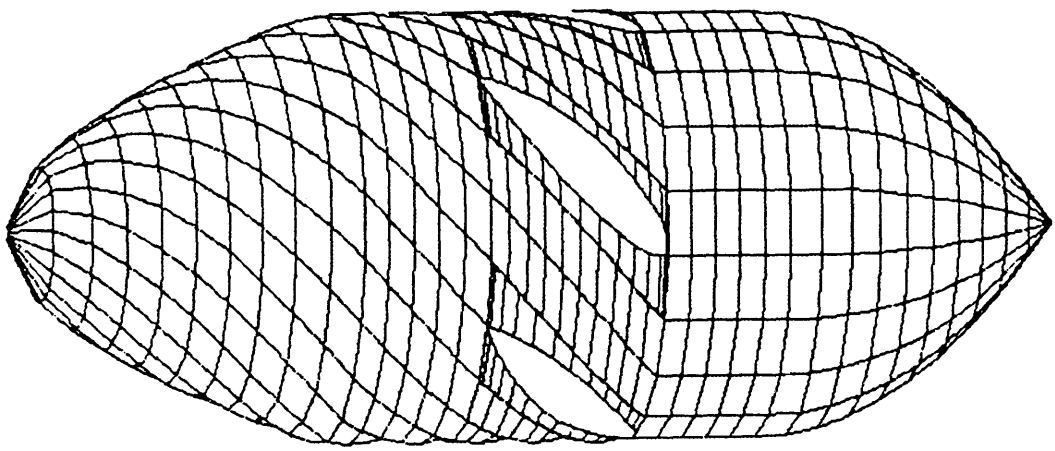

fig. 3 Hub grid

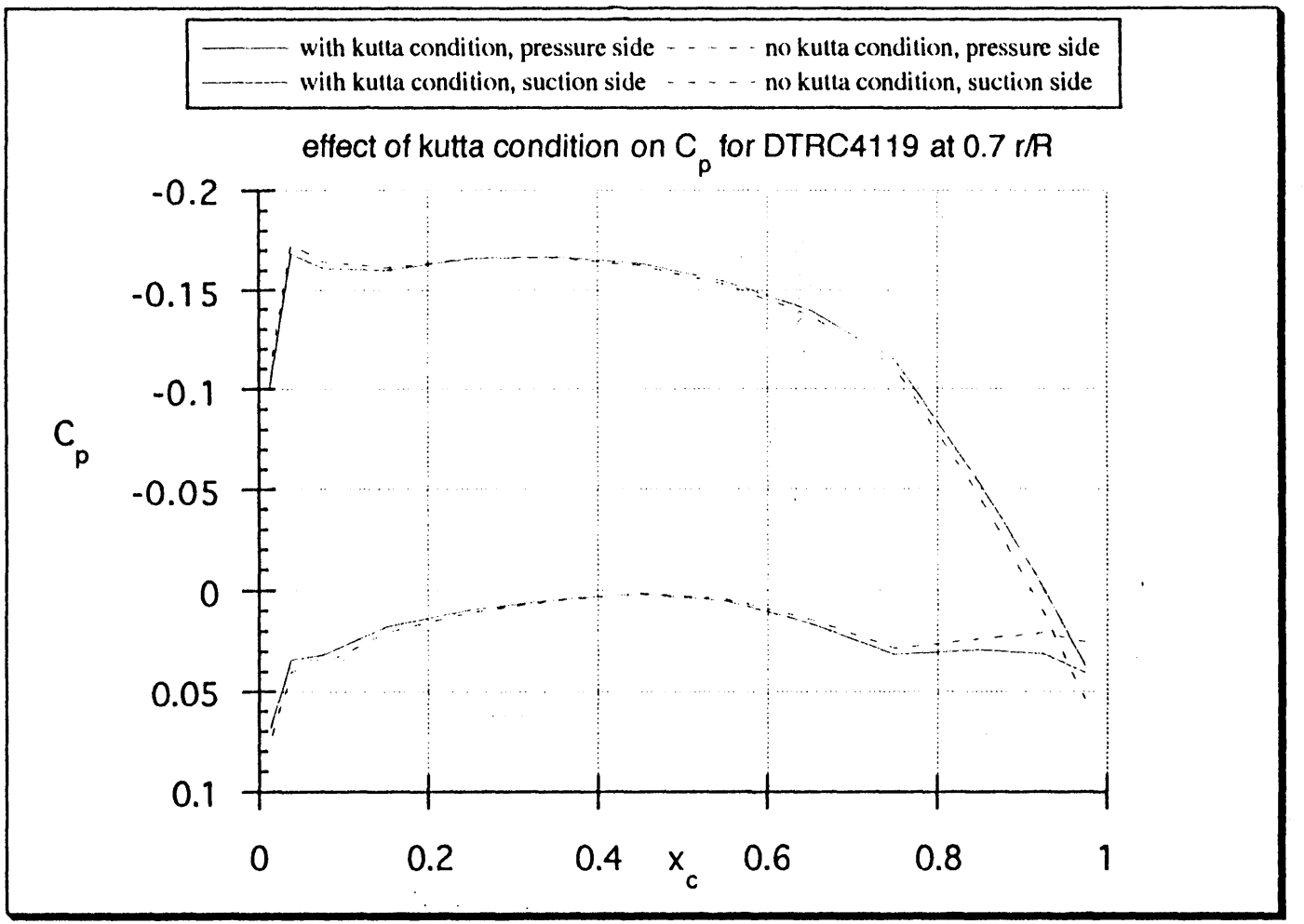
with kutta condition, pressure side
no kutta condition, pressure side
with kutta condition, suction side
no kutta condition, suction side
effect of kutta condition on C_p for DTRC4119 at 0.7 r/R
C_p
-0.2
-0.15
-0.1
-0.05
0
0.05
0.1
0
0.2
0.4
x_c
0.6
0.8
1

fig.4

C_p distributions for propeller DTRC4119 at various values of r/R for J=0.833

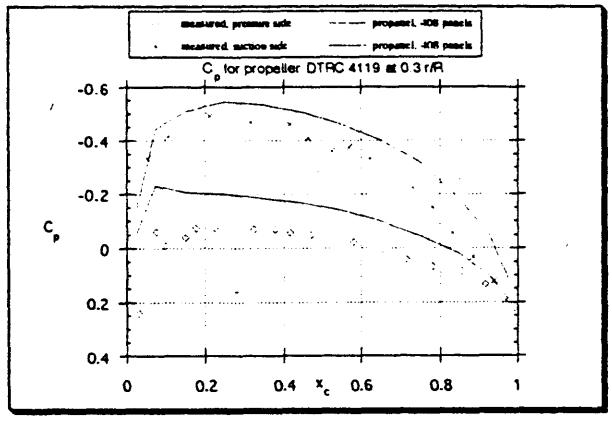

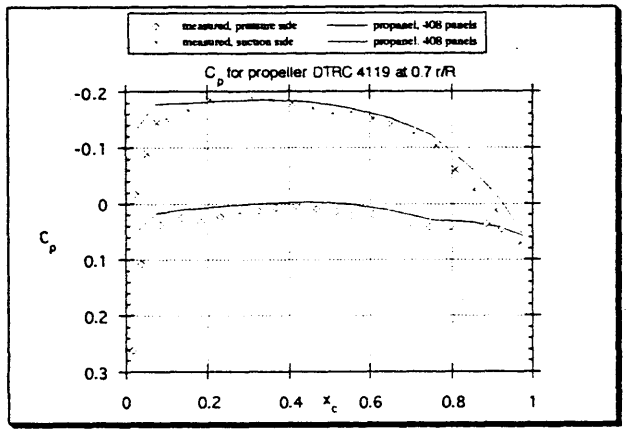

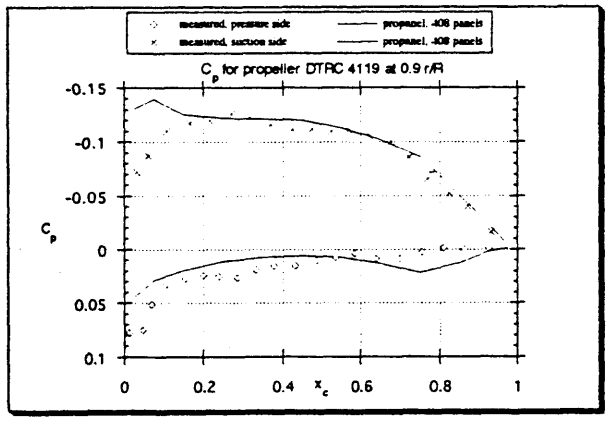

fig.7

C_p distributions for propeller DTRC4119 at various values of r/R for J=0.833

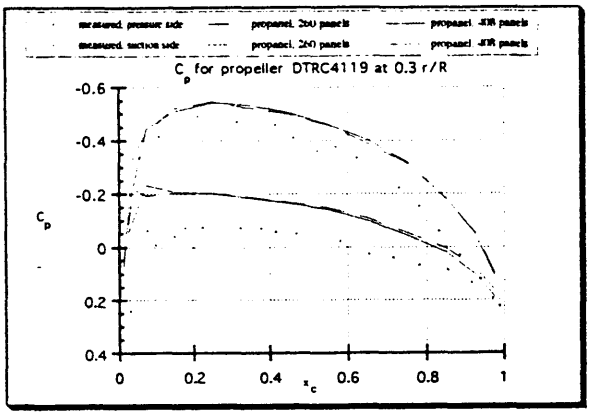

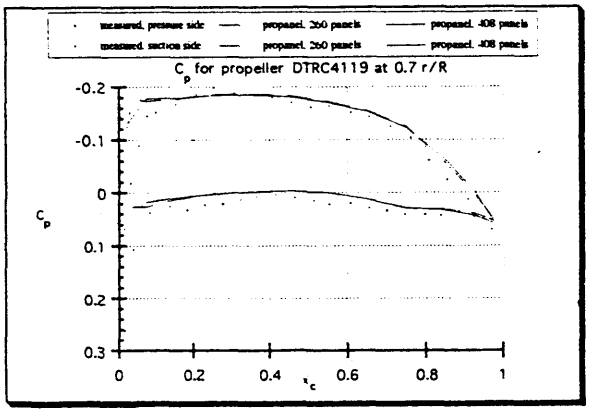

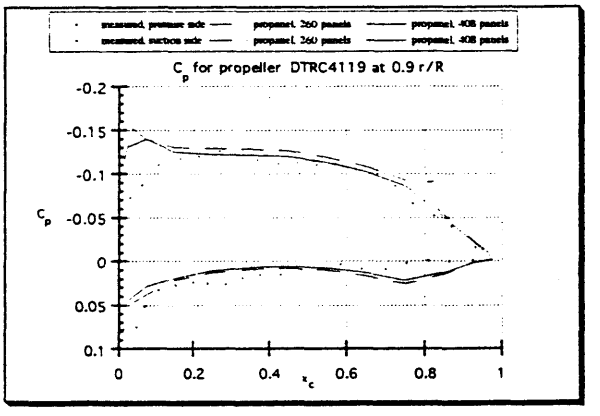

fig.8

C_p distributions for propeller DTRC4119 at various values of r/R for J=0.833 with and without hub

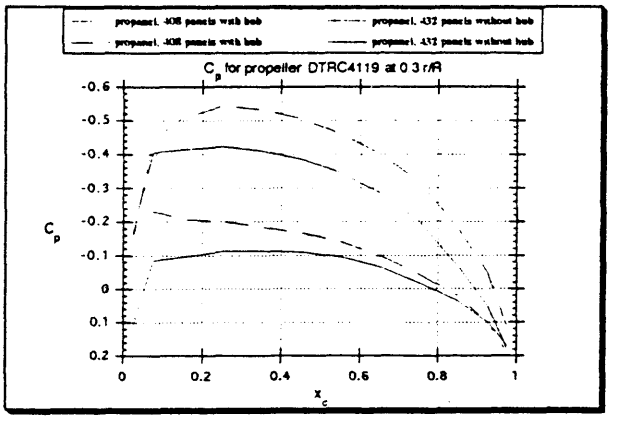

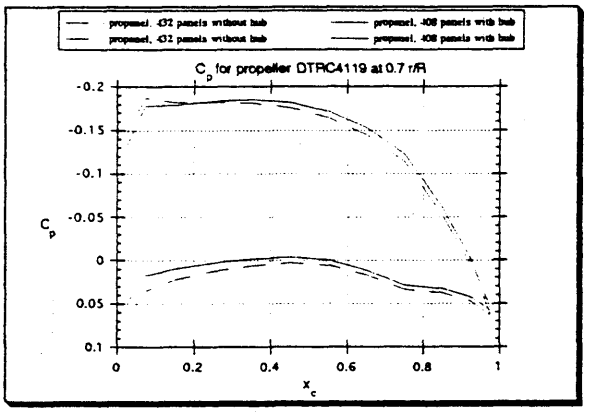

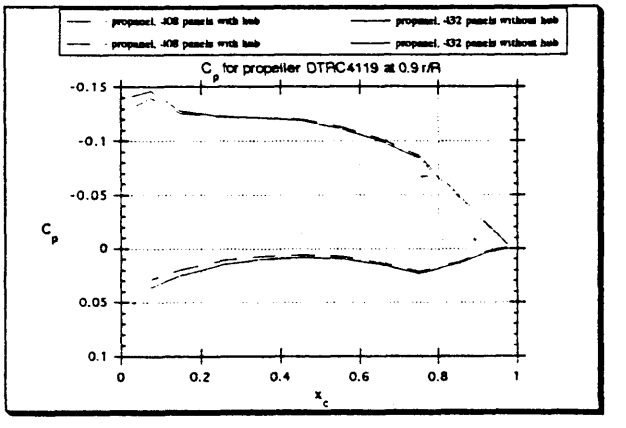

fig.9

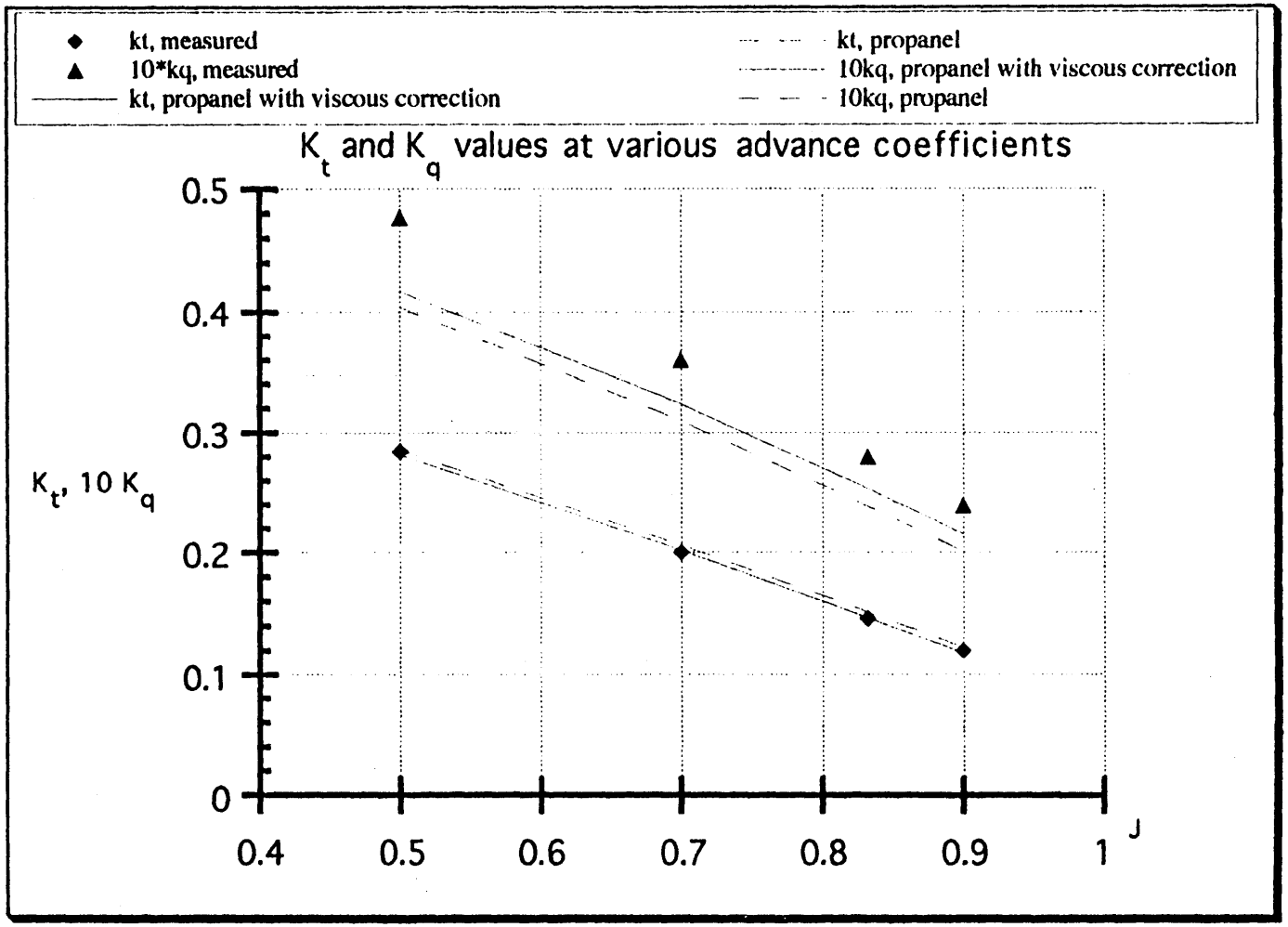
kt, measured
10*kq, measured
kt, propanel with viscous correction
kt, propanel
10kq, propanel with viscous correction
10kq, propanel
K_t and K_q values at various advance coefficients
K_t, 10 K_q
0.5
0.4
0.3
0.2
0.1
0
0.4
0.5
0.6
0.7
0.8
0.9
1
J

fig.10

C_p distributions for propeller DTRC4842 at various values of r/R for J=0.905

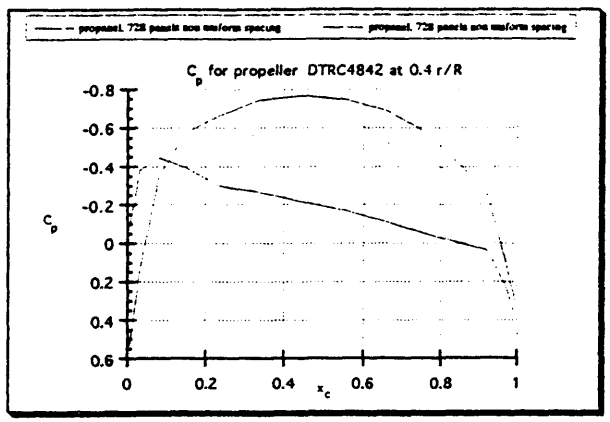

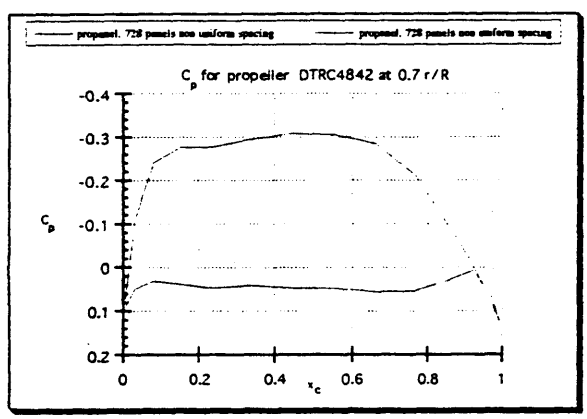

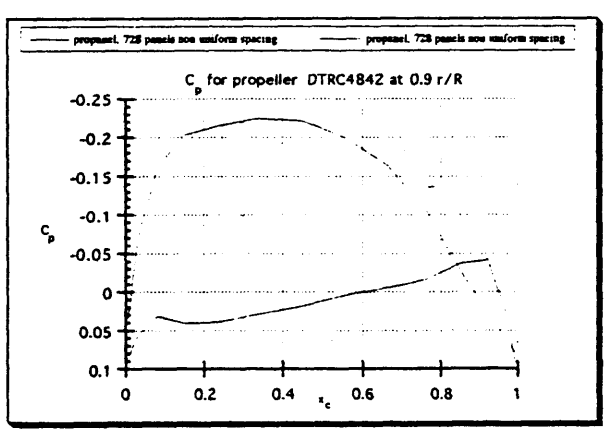

fig.11